THE UNIVERSITY
of EDINBURGH

Monocyte dynamics in breast cancer

Miss Amy Clare Robinson

Doctor of Philosophy

The University of Edinburgh

2019

Declaration

This body of work has been composed by Amy Clare Robinson. Unless otherwise stated, all work has been undertaken by Amy Clare Robinson. The work has not been submitted for any other degree or professional qualification.

Abstract

Work in mouse models has highlighted a role for classical monocytes in promoting cancer. Furthermore, recent human studies show that blood monocytes in a variety of cancers exhibit transcriptional shifts from steady-state. However, it remains unclear exactly how cancer affects monocyte homeostasis and function.

To study monocyte regulation in cancer, blood was analysed over the course of tumour progression in mice that develop spontaneous mammary cancers (MMTV-PyMT). Monocyte production, release and turnover were investigated by colony forming unit assays and BrdU tracing. RNA extracted from blood and bone marrow (BM) monocytes was sequenced. Next, gene expression was compared with monocytes in human breast cancer patients. Finally, Accessibility of Transposase Assay (ATAC) sequencing was used to investigate chromatin conformation of monocytes in human breast cancer.

In mice, blood monocyte numbers were significantly increased in late cancer compared with controls. This increase was equivalent in both classical and non-classical monocytic populations. The proliferation of classical monocytes in the BM was increased in cancer, whereas monocyte release and half-life in the circulation were unaltered. Classical monocytes in mice with late stage cancer featured down-regulation of genes involved in interferon response, cytokine stimulus, and antigen-cross-presentation. These changes were conserved across cells in the BM and blood and across two mice strains. There

were no orthologous genes or functional pathways with humans whom had early stage cancer. In patients with early breast cancer, there was an up-regulation of NFKB pathway signalling in circulating monocytes. Findings by ATACseq were inconclusive but established the use of this technique in this context.

This study suggests that the cancer manipulates the transcriptional landscape of monocytes. The effects in mice may be secondary to haematopoietic stress. This contrasts with humans, where it seems that conditioning of circulating monocytes results in a pro-tumoural phenotype. Due to the lack of orthologous changes in mice, further work needs to be undertaken in humans. To this end, the use of ATAC sequencing of human circulating monocytes has been optimised. These findings lay the foundation from which to understand the transcriptional regulation of monocytes in breast cancer.

Lay Summary

Breast cancer is the most common cancer affecting females. 1 in 5 women with breast cancer that has spread will not survive longer than 5 years. Cancer cannot grow and spread on its own. Instead, it requires cells of the immune system to help it. One of the cells in our blood is a white blood cell called the monocyte. Monocytes can travel to the tumour where they can then be turned into cells that help cancer. The behaviour of these cells is determined, in part, by the genetic code that they have in their DNA. Studies have shown that the DNA of blood monocytes is changed in cancer patients. We do not know when or how this occurs. The DNA can be tightly folded or unfolded and this also changes the way the cell behaves. We do not know if this may be a way that monocytes are changed in cancer. If we understand this, we can try to develop treatments to change monocytes so that they fight rather than help the cancer.

The purpose of this study was to understand how monocytes change during the growth of breast cancer. We also wanted to understand if the changes are the same in mice as they are in humans. This is because it would allow us to do experiments that are not possible in humans that would help us to understand the changes that occur to the DNA. We also wanted to check if the folding or unfolding of the DNA of monocytes is changed in patients with cancer.

Blood cells were studied during the growth of breast cancer in mice. The production of monocytes in the bone and their movement from the bone into

the blood was also studied. We then compared the DNA in monocytes from mice with cancer with the DNA in monocytes from human breast cancer patients. Finally, we checked the folding or unfolding of the DNA in monocytes from patients with breast cancer.

We found that there are more monocytes in the bone and the blood of mice with cancer. To our surprise, the DNA changes in mice were not very obvious. There were no similarities found between mice and humans. This means that the mice that we used are not useful to study the DNA changes that we see in humans. It may be that a different mouse may be useful, but this will need to be checked. We confirmed that there are changes to the DNA of monocytes in patients with breast cancer. We were able to assess the folding of DNA in patient monocytes. In the future, we can use this to understand changes to monocyte DNA in cancer.

Acknowledgements

I would sincerely like to thank the Edinburgh Clinical Academic Track (ECAT) and Cancer Research UK (CRUK) for the opportunity to study my PhD in such a thriving academic environment. With special thanks to my CRUK mentor, Charlie Gourley and my clinical mentor, Mike Dixon, whom have been supportive of my career progress throughout.

I would like to thank my supervisors Prof. Jeff Pollard and Dr. Steve Jenkins for their excellent guidance, support, and advice. I would also like to thank Prof. Chris Glass for hosting me at the University of California San Diego and providing a career-defining period of learning. With special thanks to Claudia Han, Dylan Skola, Zhengyu O'Young and Jana Collier for their enthusiasm and expertise in transcriptomics and epigenetics, and above all kindness.

I would like to thank Will Mungall for all the mouse work undertaken; not only did he help considerably with experiments, but he also provided support, friendship and laughter. I am also extremely grateful for all the help, support and laughs from members within the both the Pollard and the Jenkins Group, in particular Calum Bain, Pieter Louwe and Luca Cassetta. I would also like to thank the Flow Cytometry department within the University of Edinburgh for their dedication and support.

A special thanks must be given to Dr. Sheila Webb without whom my PhD would not have been possible. She not only co-ordinated all the mouse breeding and monitored the mice during cancer development but additionally,

collected all the human samples and transported them in the early morning to allow prompt processing of samples. She has been very kind to me throughout and is an unwavering pillar of support to all in the Pollard lab.

I would like to acknowledge both patients and healthy volunteers for providing samples to allow this work to be undertaken. Thank you to the Centre for Inflammation Research Blood Resource for the provision of volunteers and the team at the Western General Hospital Breast Unit for the provision of patient samples. With a special thanks to Jane Keys whom took all patient samples.

Lastly but most importantly I would like to thank my family and friends for their inspiration, support and patience. I cannot express how indebted I am to you.

Contents

Tables

Figures

Abbreviations

Abbrev.	Meaning (alternative nomenclature)
AML	Amyotrophic Lateral Sclerosis
ATAC	Accessibility of Transposase Assay
BCSS	Breast Cancer Specific Survival
BFU-E	Blast forming Unit Erythroblast
BFU-E	Erythroid Burst Forming Units
BrdU	5-bromo-2'-deoxyuridine
c-Kit	Tyrosine-protein kinase Kit. Used interchangeably with CD117 (stem cell growth factor receptor (SCFR))
CAR	Chimeric antigen receptor
C57BL/6	In-bred mouse strain C57 with Bl6 sub-strain
CCL2	C-C Chemokine Ligand 2 (MCP-1)
CCL3	C-C Chemokine Ligand 3 (MIP-1-α)
CCL4	C-C chemokine Ligand 4 (MIP-1-β)
CCL5	C-C Chemokine Ligand 5 (RANTES)
CCL7	C-C Chemokine Ligand 7 (MCP-3)
CCL8	C-C Chemokine Ligand 8 (MCP-2)
CCR2	C-C Chemokine Receptor type 2 (CD192)
CCR5	C-C Chemokine Receptor type 5 (CD195)
CD	Cluster differentiation, a term used as a prefix for cell surface antigens
CD115	see CSF1R
CD117	see cKit
CD127	CD nomenclature for Interluekin-7-rceptor-alpha (IL-7rα)
CD135	see Flt3
CD14	CD14 receptor Also used to indicate $CD14^{high}$, $CD16^{low}$ classical human monocytes
CD16	CD nomenclature of the FcγRIII Also used to indicate $CD16^{high}$, $CD14^{low}$ non-classical human monocytes
CFU	Colony forming unit
CFU-G	Colony forming unit of Granulocyte type
CFU-GEMM	Colony forming unit of Granulocyte Erythroid Macrophage Megakaryocyte type
CFU-GM	Colony forming unit of Granulocyte Macrophage type
CFU-M	Colony forming unit of Macrophage type
ChIP	Chromatin immunoprecipitation
cMoP	Common Monocyte Progenitor
CMP	Common Myeloid Progenitor
CSF1	Colony stimulating factor 1
CSF1-R	Colony Stimulating Factor 1 Receptor (Used interchangeably with CD115)
CTC	Circulating tumour cell
CTF	Collaborating Transcription Factors
CTs	Cycle threshold (for qPCR)

CX3CR1	C-X3-C Motif Chemokine Receptor 1
CXCL1	Chemokine (C-X-C) ligand 1
CXCL8	Chemokine (C-X-C) ligand 8 (IL-8)
CXCR1	C-X-C Motif Chemokine Receptor 1 (IL-8rα)
CXCR2	C-X-C Motif Chemokine Receptor 2 (IL-8rβ)
DCs	Dendritic cells
DCIS	Ductal carcinoma in-situ
DE	Differential expression
DEGs	Differential expressed genes
DFS	Disease Free Survival
ECM	Extracellular Matrix
EDTA	Ethylenediaminetetraacetic acid
EdU	5-ethynyl-2′-deoxyuridine
ER	Oestrogen receptor
EZH2	Functional enzymatic component of the Polycomb Repressive Complex 2
FDR	False discovery rate
Flt3	Fms like tyrosine kinase 3
FSC-A	Forward scatter-area
FSC-H	Forward scatter-height
FVB	Mouse strain named after sucseptiblity to Friend leukemia virus B
GEMMs	Genetically engineered mouse models
GM-CSF	Granulocyte–Macrophage Colony Stimulating Factor
GMP	Granulocytic Myeloid Progenitor
H3K27ac	Acetylated Histone3 Lysine27
H3K4me3	Histone3 Lysine4 tri-methyl
HAT	Histone Acetyltransferase
HDAC	Histone Deacetylase
HER2	Herceptin 2 Receptor
HLA-DR	Human Leukocyte Antigen –DR isotype (a form of MHCII in humans)
HSC	Haematopoietic Stem Cell
HSPC	Haematopoietic Stem Progenitor Cells
IDR	Irreproducible discovery rate
IFN	Interferon
IL-	Interleukin
ISG	Interferon Stimulated Gene
LDTF	Lineage Determining Transcription Factor
LK	Lineage negative, cKit positive cells. Used interchangeably with CD117 or c-Kit+
LSK	Lineage negative, Sca1 positive, cKit positive cells
LTR	Long terminal repeat
MAMs	Metastatic Associated Macrophages
MC	Mononuclear cell
MCP	Monocyte chemotactic protein
MDP	Macrophage Dendritic Cell Progenitor
MDSCs	Myeloid Derived Suppressor Cells
MEK	Megakaryocyte-Erythrocyte Progenitor

MHCI	Major histone compatibility complex I
MHCII	Major histone compatibility complex II
MIF	Macrophage Migration Inhibitory Factor
MIN	Mammary Intraepithelial Neoplasia. American terminolgy of DCIS
MIP	Monocyte inflammatory protein
MMTV	Mouse Mammary Tumour Virus
Mo	Monocyte or pleural Monocytes
MPP	Multipotent progenitor
Mrc1	Mannose receptor 1
MSP	Macrophage-stimulating protein
MT	Methyltransfersase
Neut	Neutrophil
NGS	Next generation sequencing
N	Natural Killer cells
NPI	Nottingham Prognostic Indicator
NST	No Special Type
PBS	Phosphate buffered saline
PCA	Principle component analysis
PD-L1	Programmed death ligand 1
PDX	Patient derived xenografts
PR	Progesterone Receptor
PTEN	Phosphatase and tensin homolog
PyMT	Polyoma Middle Tumour Antigen
q value	The adjusted p value
qPCR	Quantitative polymerase chain reaction
RNA	Ribonucleic acid
RNAseq	Next-Generation Sequencing of RNA
Sca1	Stem cells antigen-1
scRNAseq	Single cell RNAseq
SDTF	Signal Dependent Transcription Factor
SE	Super enhancers
SETD7/9	SET Domain Containing 7, Histone Lysine. A MT
SIRS	Systemic Inflammatory Response Syndrome
SLE	Systemic Lupus Erythematosus
SSC-A	Side scatter-area
SSC-H	Side scatter-height
TAMs	Tumour Associated Macrophages
TANs	Tumour Associated Neutrophils
TeMO	Tumour Educated Monocytes
TEMs	Tie-2 expressing monocytes
TF	Transcription factor
TGF	Transforming growth factor
Th	T helper
TLR	Toll-like receptor
TME	Tumour microenvironment

TN	Triple Negative
TNF	Tumour necrosis factor
TNM	Tumour Node Metastasis staging system
TPM	Transcripts per million
Treml4	Triggering Receptor Expressed On Myeloid Cells Like 4
WAP	Whey acid protein promoter

Chapter 1 Introduction

1.1 Breast cancer

1.1.1 Breast cancer background

Breast cancer is the most common cancer in women worldwide (25%) and the second most common cancer overall (Antoni et al. 2016). In the UK, breast cancer accounted for 15% of all new cases of cancer in 2014 and this is predicted to rise to 20% by 2035. In the UK a national screening programme has led to a dramatic increase in cases detected early and has contributed to increased survival. The lifetime risk for females in the UK is 1 in 8, with survival being lowest in the younger non-screening population (<50 years old) (C.R.U.K. n.d.). While survival has greatly improved, this has been amongst patients diagnosed with primary disease where survival has increased to nearly 90% (Hayat et al. 2007). Conversely, just 1 of every 5 patients diagnosed with metastases will survive (Hayat et al. 2007). Thus, metastatic disease still poses a great challenge. Overcoming this involves developing better detection techniques to diagnose disease earlier and more effective personalised therapies where diagnosis is made late or disease is of an aggressive subtype.

1.1.2 Breast cancer histological subtypes

Breast cancer, like most solid cancers, develops via a number of stages which were first introduced by Foulds in 1954 (Foulds 1954) and observed in breast lesions by Wellings and Jenson in 1973 (Wellings & Jensen 1973). The first step is considered pre-invasive as proliferating cells are contained by the myoepithelial layer which acts as a gate keeper. The second stage occurs when tumour cells break through this layer and at this point are considered as invasive but are still confined to the primary site. Within the breast, while this may cause morbidity, it is not until the cancer cells are able to disseminate to other organs, to form metastases, that the cancer can be fatal.

Invasive breast cancer is traditionally divided into histological subtypes as standardised by the World Health Organisation (Sinn et al. 2013). The most common subtype, accounting for up to 80% of all cancers is invasive ductal cancer of no special type (NST) (Hayat et al. 2007), termed NST as they cannot be ascribed to any particular growth pattern but used synonymously with the term ductal. The next most common are lobular cancers, termed so as they develop in the lobular aspect of the breast. Other subtypes include mucinous, cribriform, apocrine and medullary. While some subtypes have particularly distinct prognostic outcomes, more important aspects of breast cancer subtypes are the stage, grade and receptor status.

1.1.3 Breast cancer staging, grade and receptor status

The Tumour Node Metastasis (TNM) classification system based on tumour size (T), nodal status (N) and presence of any metastasis (M) (Singletary et al. 2003), is used for many cancers to stage disease and guide treatment. The grading system by Bloom and Richardson and later refined by Elston and Ellis gives a grade from 1 to 3 based on the proportion of tubule formation, the mitotic count, and the degree of nuclear pleomorphism of cancer cells (Elston & Ellis 1991). The grade of breast cancer is in itself a predictor of outcome both for Disease Free Survival (DFS) and breast cancer specific survival (BCSS) (Rakha et al. 2008). The receptor status is defined primarily by oestrogen, progesterone and Herceptin receptor positivity. The worst prognosis is in breast cancers that lack any of these receptors, termed triple negative (TN). Roles of additional receptors such as androgen receptors are also considered important (Hon et al. 2016).

1.1.4 Prognostic indicators of breast cancer

Traditionally, the Nottingham Prognostic Indicator (NPI) was used to calculate the 5-year DFS (Todd et al. 1987). This takes into account the size, grade and nodal status of the cancer. Updates to this model have included the widely used neoadjuvant online tool which additionally includes patient age, hormone receptor status and co-morbidity level (Ravdin et al. 2001). However, these tools fail to recognise the importance of molecular subtypes of breast cancer

which are now recognised to be highly relevant in predicting response to treatment regimens and outcome, essential when planning treatment.

1.1.5 Molecular subtypes of breast cancer

Molecular subtyping of breast cancer can distinguish cancers that are highly aggressive from those that are more indolent. This is due to intrinsic genetic differences in the cells that are overlooked when looking at histological subtype alone. This paradigm shift in breast cancer classification was initiated by a seminal study undertaken by Perou et al in 2000 in which 42 breast cancers were genetically profiled using cDNA microarray to identify 8,103 genes. Using hierarchical clustering methods on defined gene lists, they were able to identify distinct molecular subtypes of breast cancer (Perou et al. 2000). This was later extended to larger cohorts and further validated to produce a classification that is now widely used (Sørlie et al. 2001; Hu et al. 2006; Dai et al. 2015). The principal 4 molecular subtypes of breast cancer are luminal type A, luminal type B, Her2-enriched and basal, with a 5th subtype termed normal-like (Dai et al. 2015). A summary of these subtypes is presented in Table 1. Over time, additional molecular subtypes have been identified, with as many as 10 now being considered (Curtis et al. 2012; Ali et al. 2014). These subtypes correlate with DFS and chemo-sensitivity and therefore can be used to guide treatment decisions (Curtis et al. 2012; Ali et al. 2014).

Subtype	IHC status	Grade	Prog.	Prev.
Luminal A	[ER+|PR+] HER2-KI67-	1|2	Good	23.7%
Luminal B	[ER+|PR+] HER2-KI67+	2|3	Int	38.8%
Luminal B	[ER+|PR+] HER2+KI67+		Poor	14%
HER2 over-expression	[ER-PR-] HER2+	2|3	Poor	11.2%
Basal	[ER-PR-] HER2-, basal+	3	Poor	12.3%
Normal-like	[ER+|PR+] HER2-KI67-	1|2|3	Int	7.8%

Table 1 Molecular subtypes of breast cancer and correlation with immunohistochemistry (IHC) status, grade, outcome and prevalence. *Adapted from Dai et al. 2015.*

1.2 **A shift away from a cancer centric view**

In addition to the histological and molecular subtype of breast cancer discussed, other cancer-intrinsic factors are emerging that explain the extensive heterogeneity that exists in individual patient responses to treatment. These include factors such as the mutational burden and the clonal evolution of cancer cells (Greaves & Maley 2012; Shah et al. 2012; Cowell et al. 2013). While there is no debate that all these intrinsic features of the cancer cells themselves are important in determining the progression of disease, they do not alone account for the full spectrum of disease severity that is observed.

In a seminal review on cancer in 2000, Hanahan and Weinberg defined the common hallmarks of all cancers as their: self-sufficiency in growth signals, insensitivity to growth-inhibitory signals, evasion of programmed cell death, limitless replicative potential, sustained angiogenesis, and tissue invasion and metastasis (Hanahan & Weinberg 2000). Eleven years later they moved away from a reductionist view, and highlighted the role of the tumour microenvironment (TME) and cellular interactions in cancer (Hanahan & Weinberg 2011). It is now well recognised that it is not only factors intrinsic to the cancer itself, but also the microenvironment in which the cancer resides and the other cells within that environment that determine cancer fate. This holistic view of cancer biology has paved the way for many new approaches both in terms of developing prognostic tools and new treatment strategies.

1.2.1 The tumour microenvironment in breast cancer

Any solid tissue is made up of a scaffold in which the cells exist. The components that make up the scaffolding, such as laminins and collagens, and the components that form a mesh-like structure over the scaffolding in which the cells are held is termed the extracellular matrix (ECM). The ECM of any tissue is altered by the components laid down by the cells within the matrix. This is very relevant in cancer whereby the ECM needs to be remodelled to allow tumour cell survival, proliferation and dissemination. In the breast, as with many other tissues, ECM scaffolding is usually held tightly together by

adhering factors such as E-cadherin and integrins (Nelson & Bissell 2006). In breast cancer, loss of these adhesion factors along with proteolytic enzymes leads to the breakdown of the ECM. As the ECM is remodelled and the cell composition changes, growth factors are released resulting in the growth and proliferation of cancer cells. The remodelling of the ECM also permits an environment in which cancer cells can invade beyond the basement membrane and disseminate (Nelson et al. 2018; Nelson & Bissell 2006). It is estimated that only around 0.02% of circulating tumour cells (CTCs) actually go on to form metastases (Micalizzi et al. 2017). This is not just because they are exposed to numerous stresses and immunosurveillance, but also because CTCs lack the means by themselves to intravasate the tissue and establish the necessary microenvironment to survive. Hence, at the site of metastasis the ECM is again modified to form the pre-metastatic niche required for the establishment of metastasis (Joyce & Pollard 2008). The ECM, and ultimately the TME, is determined by the milieu of cells that exists held within the tissue, all of which have important roles in breast cancer evolution and progression (Joyce & Pollard 2008; Tlsty & Coussens 2006; Nelson & Bissell 2006).

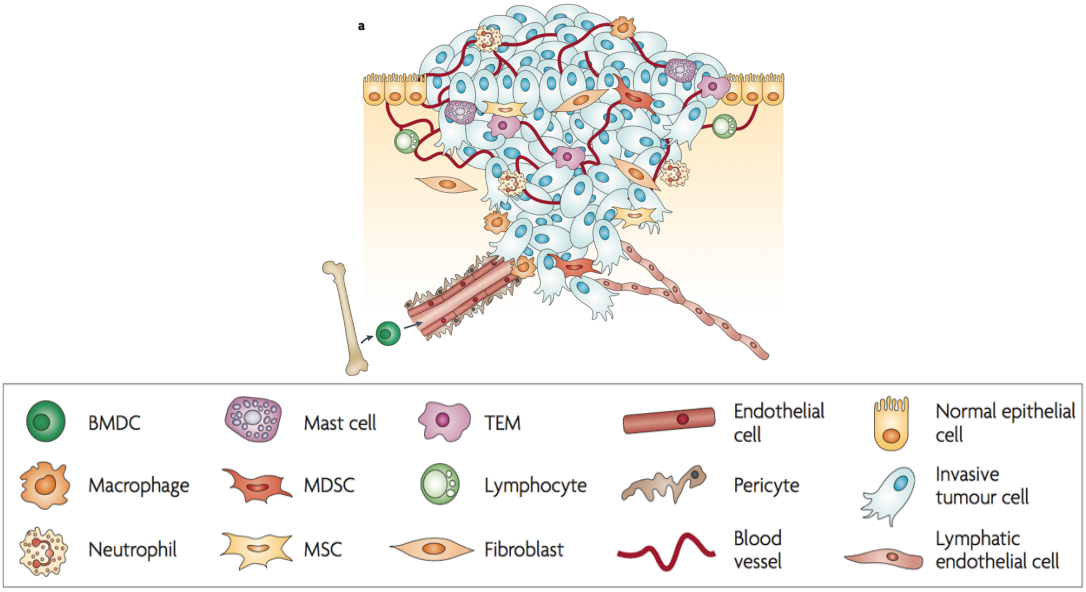

Figure 1 Tumour microenvironment. *Many cells contribute to the microenvironment, including fibroblasts, endothelial cells, bone marrow derived cells (BMDC), mesenchymal stem cells (MSC), Myeloid derived suppressor cells (MDSCs), Tie2 expressing monocytes (TEM) and Macrophages. Adapted from Joyce & Pollard 2008.*

Some of these cells are pre-existing within the tissue, for example fibroblasts, myoepithelial cells and endothelial cells. However, many cells, in particular immune cells, are recruited to the tissue to fulfil a multitude of roles. It is generally accepted that both CD8+ T cells and NK cells kill cancer cells through perforin and granzyme-mediated apoptotic pathways, and thus are anti-tumoural (Ostrand-Rosenberg 2008). The role CD4+ T cells in cancer is more complex, but to briefly summarise: Type I CD4+ T helper cells (Th1) aid CD8+ T cell tumoricidal action and thus are anti-tumoural. Whereas, by potentiating antibody production by B cells, Type II CD4+ T helper cells (Th2) indirectly inhibit anti-tumour immunity (Ostrand-Rosenberg 2008). The CD4+

T regulatory cells (Tregs) both inhibit CD8+ T cells and NK cells and are therefore pro-tumoural (Ostrand-Rosenberg 2008). Another type of T helper cell, which derives its name from the production of IL-17 (Th17) was defined as distinct from the Th2 and Th1 cell lineages in 2005 (Harrington et al. 2005; Park et al. 2005). While initially thought to be pro-tumoural, the roles of the Th17 cell (and IL-17) in cancer are diverse and can be anti-tumoural (Ostrand-Rosenberg 2008; Asadzadeh et al. 2017). Adding further complexity to the role of T cells in cancer is the distinct family of γδT cells, which can be considered to have both innate and adaptive immune functions. This group of T cells can have both pro or anti-tumoural actions (Morita et al. 1995; Morrow et al. 2019; Lafont 2014). Of note, IL-17 production by γδT cells can recruit pro-tumoural cells of the adaptive immune system (Coffelt et al. 2015; Kersten et al. 2017).

The innate immune response can be modulated by cells of the adaptive immune system and, in the case of Myeloid Derived Suppressor Cells (MDSCs), is used to define them. The complexity of MDSCs is discussed latterly but in brief and as their name suggests, these are cells of myeloid lineage that are defined by their ability to suppress T cell cytotoxicity and thus promote cancer cell survival. While MDSCs cells are uniform in their definition, cells such as macrophages are less so: macrophages can reject cancer cells via a type I interferon (IFN) response. However, they may be polarised to a pro-cancerous phenotype known as the Tumour Associated Macrophages (TAMs) and Metastatic Associated Macrophage (MAMs) at the primary the

metastatic site respectively. At the primary site, TAMs are essential in many aspects of tumour progression, including invasion and intravasation (Wyckoff et al. 2007), angiogenesis (Lin et al. 2006), and extravasation to allow metastatic spread (Qian et al. 2009). Furthermore, TAMs at the primary site release pro-survival factors supporting cell establishment and survival at the metastatic site (Qian et al. 2009). Within metastasis, MAMs promote tumour cell survival, growth and angiogenesis (Qian et al. 2009; Kitamura et al. 2017; Valls et al. 2019). In humans the correlation of high TAM infiltrate with poor prognosis in a variety of cancers is a demonstration of the importance of these cells (Zhao et al. 2017).

The cross-talk between recruited immune cells is highly complex and it is the balance between all of these cells that needs to be considered. A study by Azizi et al, using scRNAseq, confirms the complexity of the immune infiltrate in breast cancer. They showed increased phenotypic heterogeneity and expansion of cell populations in tumours, with a two-fold increase in cell total clusters in both T cells and myeloid cells in cancer when compared with benign breast tissue (Azizi et al. 2018). This complex immune environment has created a multitude of cancer immune therapeutic targets, aiming at enhancing tumoricidal cells such as NK and CD8+ T cells or inhibiting tumour promoting cells such as TAMs. A paradigm shift has been in the realisation that a holistic approach in treatments is needed; concurrently using reagents that target

cancer cells directly for example with chemotherapy, enhance cancer killing cells and block or diminish cancer supporting cells. For example, T cell therapies, such as chimeric antigen receptor (CAR) T cells, are effective in some cases (Martinez & Moon 2019). But efficacy is limited by the presence of other immune infiltrates that are able to suppress their action; both MDSCs and TAMs protect cancer cells supress T-cell-tumour interactions (Martinez & Moon 2019). Studies have confirmed that TAMs express high levels of immune checkpoint receptors such as programmed death-ligand 1 (PD-L1), which act to restrict CD8+ T cell function (Noy & Pollard 2014; Mantovani et al. 2017). It is thought that this enables TAMs to intercept the cancer-T cell cross talk and therefore protect cancer cells. This mechanism is supported by studies in mouse models of pancreatic cancer in mice showing the enhanced efficacy of checkpoint inhibitors with CSF1-R targeting of TAMs (Zhu et al. 2014).

In the context of breast cancer, in a mouse model, CSF1-R antagonists improved chemotherapy induced T cell killing of cancer cells (DeNardo et al. 2011). So, while cancer killing therapies using T cells, DC cells and NK cells evolve there is a need to target the immunosuppressive cells. Of key importance for the studies reported in this thesis is to consider that monocytes (Mo) are the source of immature Mo immune-suppressive cells, TAMs and MAMs (Kitamura et al. 2018; Kitamura, Qian & Pollard 2015; Qian et al. 2011).

1.2.2 Nomenclature in tumour immunology

The nomenclature of immune cells within both the TME and the circulation is both confusing and heavily debated. Therefore, this will very briefly be discussed. Hierarchical classification of the immune infiltrate could start with the division of cells into pro or anti-tumoural categories. For the focus of the work in this thesis, the general term myeloid can then be used. Myeloid cells include DCs, Mo, neutrophils (Neut), NK cells, MDSCs and the Mo or Neut derivatives such as TAMs and Tumour Associated Neutrophils (TANs).

A particularly confusing area is with regards to MDSCs. MDSCs are subdivided into polymorphonuclear (PMN-MDSCs), otherwise known as G-MDSCs and mononuclear (M-MDSCs) (Bronte et al. 2016; Brandau et al. 2016). The use of these terms can only be assigned by proving immune-suppressive action. While the G-MDSC is fairly well established, the presence of a distinct M-MDSC and whether it originates from a Mo or from progenitors directly in the bone marrow (BM) is heavily debated (Marvel & Gabrilovich 2015; Veglia et al. 2018; De Vlaeminck et al. 2016; Brandau et al. 2016). Unfortunately, in many papers no distinction is made between the two types of MDSCs as the general marker Gr1, which binds both Ly6c and Ly6g and is expressed upon both Mo and Neuts, is used and no morphological assessment is made (Richards et al. 2012). Even when both Ly6c and Ly6g markers are used, it is not always clear that MDSCs are distinct from Neuts and Mo by common methods such as flow cytometry, where the distinction is simply just that they are in tumour bearing

rather than healthy mice and no immune-suppressive function is proven (Bronte et al. 2016). Here, the distinction will be made between M-MDSCs and PMN-MDCSs and additionally the terms will be avoided in the discussion of cell phenotype where immune-suppressive ability is not proven.

Within Mo nomenclature, another term has arisen due to the presence of Mo expressing the receptor for Tie-2, Tie-2 Mo (TEM) (Murdoch et al. 2007; De Palma et al. 2007; Venneri et al. 2007). The abbreviation TEM should not be confused with that for the tumour microenvironment (TME), nor abbreviations for Mo such as tumour-educated Mo (TeMo). To distinguish between circulating and tissue residing cells the term Tie-2 Mo (Tie-2 Mo) will be adopted when referring to circulating and TEM when referring to Tie-2 expressing Mo in the tissue.

Lastly, the status of macrophages is often described as classically or alternatively activated, and M1 or M2 polarised. The activation of macrophages was first described in 1962 when Mackaness demonstrated phenotypes acquired in response to Listeria monocytogenes infection (Mackaness et al. 1962). This evolved over time, and the terms classical activation referred to the response of macrophages to IFNγ, whereas responses to IL-4 and IL-13 were termed alternative activation (Stein et al. 1992; Doyle et al. 1994). In 2000, Mills and colleagues used the difference in Th1 (IFNγ) and Th2 (IL-4) responses in different mouse strains to show that macrophages, independent

of T cells, could influence different immune responses (Mills et al. 2000). While acknowledging that it may be an oversimplification, Mills introduced the terms M-1 and M-2 in relation to a Th1 or Th2 like response (Mills et al. 2000). As understanding of macrophage plasticity broadened, Mantovani and colleagues further classified macrophages according to the stimuli which induced a given phenotype; M1 (IFNγ + LPS/TNF), M2a (IL-4 and IL-13), M2b (Immune complexes and TLR or IL-1R) and M2c (IL-10) (Mantovani et al. 2004). These subtypes were assigned names according to activation; M1 (Classical), M2a (Alternative), M2b (Type II), and M2c (Deactivated) (Mantovani et al. 2004). This dismissed a paper published in the same year that had confusingly assigned M1 as pro-inflammatory and M2 as anti-inflammatory (Verreck et al. 2004). Inflammatory or anti-inflammatory macrophages were produced when blood Mo were differentiated using G-CSF or GM-CSF respectively (Verreck et al. 2004). Thus, the definition of all of these macrophage types varies throughout the literature and there is still no real consensus or shared understanding when using these terms (Murray et al. 2014). Furthermore, TAMs are sometimes referred to a M2 or as “M1 like TAMs” and “M2 like TAMs” (Clappaert et al. 2018; Murray et al. 2014). The former of these is anti-tumoural and the latter is pro-tumoural.

For the purposes here, the terms M1 and M2 will be avoided. Macrophages may more accurately be described by their specific action for example immune-suppressive or angiogenic. However, for simplicity the term TAM will

herein refer broadly to a pro-tumoural macrophage that can act in immunosuppression (e.g. T cell via PD-L1), angiogenesis (e.g. secrete VEGFα), matrix remodeling (e.g. secrete MMPs), and secretion of factors that promote pro-tumoural inflammation but additionally recruitment of other cells (Movahedi et al. 2010; Joyce & Pollard 2008; Qian et al. 2009; Noy & Pollard 2014; Bonapace et al. 2014). The term TAM and MAM will be used to distinguish the site as the primary or metastatic site respectively (Kitamura et al. 2018).

1.3 **Monocytes and cancer**

1.3.1 Monocyte subset and functions

Mo are key cells in the innate immune system, they are phagocytotic, are recruited in inflammation to form macrophages or DCs and undertake surveillance of the vasculature in steady state (Geissmann et al. 2003). Seminal work by Paslick in the 1980s revealed that there were two populations of Mo (Passlick et al. 1989). The presence of two populations with distinct functions was later confirmed in mice (Geissmann et al. 2003) and microarray demonstrated orthologs with the human classical $CD14^{high}CD16^{low}$ and non-classical $CD14^{int}CD16^{high}$, corresponding to mice $Ly6c^{high}$ and $Ly6c^{low}$ expression respectively (Ingersoll et al. 2010). Further profiling by microarray (Ancuta et al. 2009), RNAseq (Zawada et al. 2011), CAGEseq (Schmidl et al.

2014) and scRNAseq (Villani et al. 2017) has highlighted the differences in the transcriptional profile of these Mo subsets. The distribution of these Mo populations is approximately equal in mice, but in healthy humans only 5-10% of Mo are $CD14^{int}CD16^{high}$ (Passlick et al. 1989). The frequency and distribution of Mo populations has been linked to many diseases including autoimmunity, chronic inflammation, cardiovascular disease, and cancer (Stansfield & Ingram 2015; Joyce & Pollard 2008). The main characteristics and functions of these two distinct Mo population are summarised in Table 2.

It is the classical or inflammatory Mo that are thought to be the source of Mo-derived macrophages and DCs. In mice, it has been shown that $Ly6c^{high}$ Mo infiltrate tissues within hours and differentiate into macrophages in response to inflammation (Geissmann et al. 2003). They are released from the BM into the circulation via the chemokine-receptors action of CCL2-CCR2 (Serbina & Pamer 2006). CCR2 is also highly expressed on human classical Mo (Wong et al. 2011; Ingersoll et al. 2010). Classical Mo are highly phagocytic and secrete a variety of cytokines including IL-6 and IL-8 (Schmidl et al. 2014; Boyette et al. 2017; Cros et al. 2010). Their distinct phagocytic properties are reflected by their increased glucose and nucleotide metabolic pathways demonstrated by transcriptomic and proteomic datasets (Schmidl et al. 2014; Vogel et al. 2018). While the predominant fate of classical Mo is homing to tissues and differentiation into macrophages and DCs, a number of studies

have suggested that they may also remain in a marginated BM pool via the use of CX3CR1 anchoring and may also remain as Mo in lymph nodes rather than differentiating into macrophages (Hamon et al. 2017).

As their name suggests, Ly6c^{low} patrolling Mo crawl along the endothelium, tending not to extravasate (C. Shi & Pamer 2011; Carlin et al. 2013; Biburger et al. 2011; Sumagin et al. 2010; Auffray et al. 2007). Their expression of CX3CR1 enables adherence to the vasculature and characteristic “crawling” along the endothelium can be observed. This characteristic is reflected by the strong expression of migratory and cytoskeleton at both a transcriptional and protein level in these cells (Schmidl et al. 2014; Vogel et al. 2018; Villani et al. 2017). While initially demonstrated in mice, human non-classical Mo were subsequently shown to adhere to the endothelium (Cros et al. 2010). In contrast to the classical Mo, non-classical Mo have minimal phagocytic activity (Cros et al. 2010). However, they produce much higher quantities of TNFα and IL-1 via toll-like receptor (TLR) signalling (Boyette et al. 2017; Cros et al. 2010; Belge et al. 2002). Their production of the anti-inflammatory cytokine IL-10 is debated to be either equal (Cros et al. 2010) or higher (Skrzeczyńska-Moncznik et al. 2008) than in classical Mo. On a metabolic level, non-classical Mo have been described as using oxidative phosphorylation (Schmidl et al. 2014).

While the two Mo populations are distinct, there are Mo that express intermediate levels of either Ly6c in mice or CD16 in humans. Some consider these to be a distinct population, however scRNAseq studies in humans would suggest that this is a heterogeneous population, with genes in common with both distinct Mo populations (Villani et al. 2017). While some of this may have been due to DC contamination, the heterogeneity supports the concept that the intermediate population represent cells in transition from classical to non-classical Mo. A view supported by recent tracking experiments demonstrating this transition in human Mo (Patel et al. 2017).

As technologies advance it is likely that the understanding of Mo populations will alter. For example, using mass cytometry, it was recently suggested that in patients with Coronary Artery Disease there may be up to 8 subpopulations of Mo (Hamers et al. 2018).

	Classical Inflammatory	**Non-Classical Patrolling**
Morphology	Large, low granularity	Smaller, more granular
Human antigen	$CD14^{high}$, $CD16^{low}$ $CCR2^{high}$, $Cd11b^{high}$, $CD163^{high}$, CD62L+	$CD14^{int}$, $CD16^{high}$ $CX3CR1^{high}$, $CCR2^{lo}$, Cd11b+, CD163-
Mouse antigen	$Ly6c^{high}$ Treml4-	$Ly6c^{low}$ $Treml4^{high}$
Recruitment and function	Recruited from bone by CCL2 release Highly phagocytic	Migrate in response to CX3CL1 T cell stimulation, patrolling
Genes up-regulated	*VCAM, CD163, CD63 S100A12, S100A8*	*FCGR3A, IFITM1-3, CDKN1C, MTSS1*
Pathways up-regulated	Immune response, Defense response, inflammatory response, chemotaxis, TLR, Lysosome	Immune system process, leucocyte migration, cytoskeleton rearrangement
Metabolic profile	Carbohydrate Nucleotide production ROS production	Oxidative phosphorylation
Cytokines	IL-6, IL-8, TNFα, IL-10	TNFα, Il-1β, IL-10 (higher than classical)

Table 2 Characteristics of Mo subsets in human and mouse.

1.3.2 The role of monocytes in cancer

In recent years, Mo have emerged as having an important role in a number of pro-cancer and anti-cancer mechanisms. The initial interest into blood Mo came from the perceived origin of TAMs, and more recently MAMs from blood Mo. The majority of functional studies have been undertaken in mouse models of breast cancer. In this context, circulating $Ly6c^{high}$ Mo have been shown to travel to the primary tumour and differentiate into TAMs (Arwert et al. 2018; Movahedi et al 2010; Bonapace et al. 2014). $Ly6c^{high}$ Mo also infiltrate the pre-

metastatic niche prior to other peripheral immune cells (Qian et al. 2011; Movahedi et al. 2010) and form MAMs (Kitamura et al. 2015; Qian et al. 2011). At the metastatic site, elevated levels of Ly6c^{high} Mo correlate with increased metastatic burden (Qian et al. 2011). More recently, it has been shown that this formation of MAMs from circulating Mo occurs via an immunosuppressive precursor which was also able to promote metastasis (Kitamura et al. 2018). The use of nude (immunodeficient) mice into which human Mo can be administered and tracked, enabled confirmation that the corresponding human Mo also travel to the pre-metastatic niche (Qian et al. 2011).

The recruitment and retention of Ly6c^{high} Mo at the metastatic site is under the regulation of CCR2-CCL2 axis (Kitamura et al. 2015; Qian et al. 2011). The role of CCL2 is exemplified in mouse models, whereby anti-CCL2 treatment suppresses metastasis but on termination of anti-CCL2 treatment, Mo are rapidly recruited from BM and metastatic overshoot occurs (Bonapace et al. 2014). Thus, the recruitment and retention of Mo is of great importance in tumour immunology.

Tie-2 Mo are of particular interest because they preferentially home to the tumour (Murdoch et al. 2007; De Palma et al. 2007; Venneri et al. 2007). They are present in both human and mice (Venneri et al 2007). TEMs promote angiogenesis and so are considered to be pro-tumoural (Turrini et al. 2017; Venneri et al. 2007; De Palma et al. 2007). It is not clear which Mo Ly6c subset

the Tie-2 Mo reside within. In humans, Tie-2 is expressed on cells expressing CD14, with or without CD16 expression, though the expression of Tie-2 seems to be highest in $CD14^{high}$, $CD16^{low}$ cells (Venneri et al 2007). TEMs have been shown to be very similar to but distinct from TAMs (Pucci et al. 2009). It is postulated that while TAMs originate from the $Ly6c^{high}$ Mo, TEMs originate from what is termed by the authors as “resident circulating Mo” and reflect $Ly6c^{low}$ Mo (Pucci et al. 2009). But this is based on association and yet to be proven by tracking. This hypothesis is supported by a recent report stating that $Ly6c^{low}$ Mo confer resistance to anti-VEGFR therapy (Jung et al. 2017). The role of $Ly6c^{low}$ Mo is not simple however, and some reports show that they are protective at the metastatic site by activating NK cell killing (Hanna et al. 2015).

It is difficult to discuss the role of Mo in cancer without discussing MDSCs. MDSCs are a key component of immunosuppressive cells contributing to immune evasion by cancer cells (Joyce & Pollard 2008). As discussed, the origin of MDSCs is not clear (Marvel & Gabrilovich 2015; Richards et al. 2012; Kim & Bae 2016). The aforementioned immunosuppressive MAM precursor has been suggested to be equivalent to the M-MDSC population (Kitamura et al. 2018). In this study, they were shown to originate form $Ly6c^{high}$ Mo from the circulation that differentiate in the tissue. However, much of the literature on MDSCs suggests that their phenotype is acquired in the BM due to a combination of stress haematopoiesis, driven by growth factors, and conditioning by cytokines (Marvel & Gabrilovich 2015). In conclusion, while

there is still a lot to be clarified with regards to M-MDSCs, they may have an important role in cancer and may be derived from the Ly6c^{high} Mo.

Thus far, Mo have largely been discussed as a conduit to other cells that have key roles in cancer and in terms of tumour biology. But Mo have also been used as a diagnostic target. In colon cancer, renal cell carcinoma (RCC), breast and endometrial cancer alterations to the transcriptional profile of Mo has been demonstrated (Chittezhath et al. 2014; Hamm et al. 2016; Cassetta et al. 2019). This has subsequently been used to develop diagnostic and prognostic transcriptional signatures. The functional implications of the transcriptional alterations have been investigated to some extent, with Mo from cancer patients producing pro-tumoural factors such as IL-8 (Chittezhath et al. 2014). This suggests that rather than just being a conduit, conditioned on arrival to the TME, that circulating Mo are conditioned within the blood. The susceptibility of Mo to this conditioning relates to their plasticity and complex transcriptional regulation that is necessary in their homeostatic roles but taken advantage of by cancer. To better understand these changes that are observed in circulating Mo in cancer, the general concepts of transcriptional regulation and how these relate to Mo in both steady state and in disease must be understood.

1.4 Transcriptional regulation of monocytes

1.4.1 Promoters, enhancers and histones

Transcriptional regulation is extremely complex and multifaceted but understanding can be gained by looking at how specific regions in the genome and the factors that bind in these regions regulate transcription (Heinz et al. 2013). Two of many of the regulatory regions described are termed promoters and enhancers. Promoters are regions of the genome that occur at the transcriptional start sites of a gene (Heinz et al. 2013). The binding of transcriptional machinery at promoter regions is obligatory for transcription to commence. However, transcriptional activity is greatly influenced by interaction with distal regulatory regions called enhancers. Enhancers confer numerous binding sites for key regulatory transcription factors (TFs) and co-factors which once bound are able to modify transcription by interaction with the promoter (The FANTOM Consortium et al. 2014). While these regions are not defined in absolute terms, regions can be assigned as enhancers and their activity inferred by the status of adjacent histones (Ernst et al. 2011). The enhancer motif accessibility, binding strength and interaction are modulated in part by the status of adjacent histones. By identifying these marks by using Chromatin Immunoprecipitation and sequencing (ChIPseq), enhancers can be putatively classified as inactive, poised or active. While the promoter regions may differ considerably, the enhancer landscape seems to be largely

conserved across species (Donnard et al. 2018). Enhancers are also more cell-type specific than promoters (Lavin et al. 2014) especially in areas where many factors are bound, termed super enhancers (SE) (Hnisz et al. 2013). Identifying both enhancers (or SE) and their surrounding histone status has been shown to identify enhancer-gene interactions that are highly specific to cell-type and likely driving cell identity and function (Chen et al. 2016; Hnisz et al. 2013).

1.4.2 Ontogeny and lineage determining transcription factors

Mo are formed from the differentiation of Haematopoietic Stem Cells (HSCs) via Common Myeloid Progenitor (CMP) and Granulocytic Myeloid Progenitor (GMP) cells into the oligopotent Macrophage Dendritic Cell Progenitor (MDP) (Figure 2) (Gabrilovich et al. 2012; Hettinger et al. 2013; Fogg 2006; Akashi et al. 2000). Mo are subsequently formed from the unipotent Common Monocyte Progenitor (cMoP), which is thought to originate from the MDP (Hettinger et al. 2013; Fogg 2006). Though originally identified in mice, these cells are also found in humans and are transcriptionally similar between both species (Breton et al. 2015; Kawamura et al. 2017).

The development of Mo in the BM via their progenitors requires *de novo* gain of Lineage Determining Transcription Factors (LDTFs), likely at the CMP stage, that commit to a myeloid potential and subsequently determine cell fate

(Naik et al. 2013; Notta et al. 2016). Binding of LDTFs along with Collaborating Transcription Factors (CTFs) at enhancer regions greatly influences the transcriptional activity and identity of cells (Hnisz et al. 2013). This is because LDTFs are distinct in their ability to bind to inaccessible motifs, selecting enhancers and therefore re-modelling chromatin (Heinz et al. 2015). Despite the presence of hundreds of TFs, the combinatorial binding of a very small number of LDTFs leads to the specific selection of a cell's transcriptionally regulatory elements (Heinz et al. 2010).

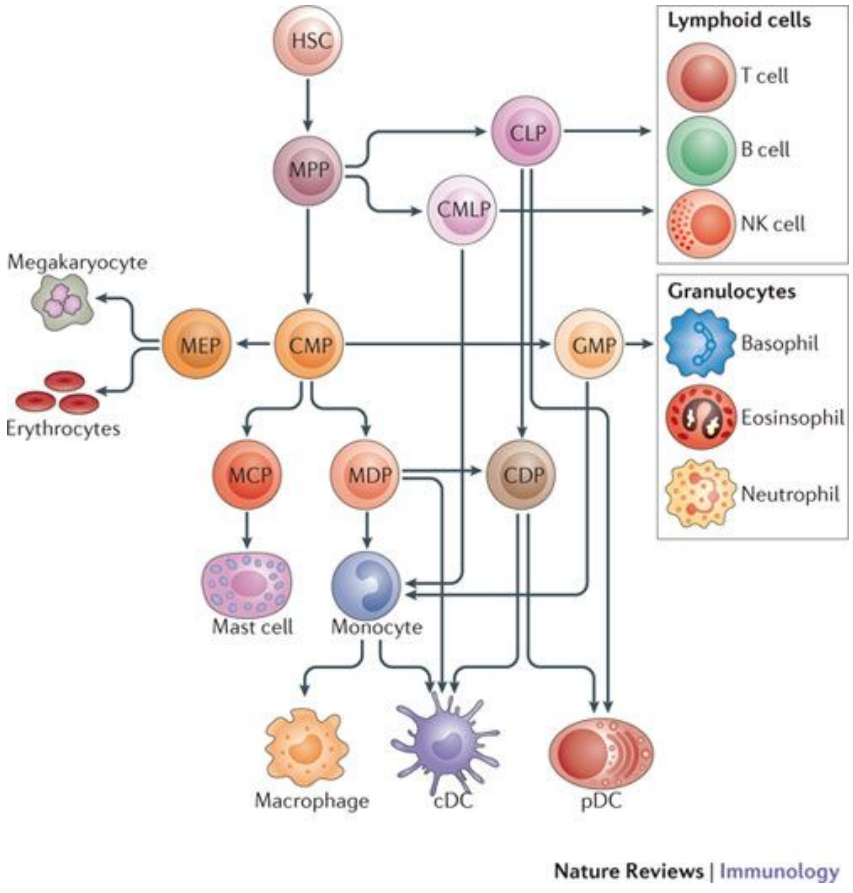

Figure 2 The haematopoetic tree and Mo ontogeny. *Image used with permission from Gabrilovich et al. 2012.*

The key LDTF in Mo is PU.1 whose levels increase during transition from the CMP to the GMP (Notta et al. 2016). This is accompanied by a large decrease in GATA2, which is inhibited by PU.1 at the GMP stage (Notta et al. 2016; Walsh et al. 2002). The accessibility of binding motifs are also switched (Corces et al. 2016; Buenrostro et al. 2018) and repressive histone marks at GATA2 motifs, coupled with up-regulation of PU.1 is observed when HSPCs differentiate into Mo (Wiśnik et al. 2017). As discussed, LTDFs require collaborative LDTFs and the collaborative binding of PU.1 with the LDTF C/EBPα is essential for HSC commitment to the CMP (Lara-Astiaso et al. 2014). Yet, subsequently much higher levels of the PU.1 potentiates IRF8 and collaborative binding of these two TFs temporarily blocks the binding of C/EBPα ensuring Mo/DC rather than Neut lineage in the MDP (Schönheit et al. 2013; Kurotaki et al. 2014). This is exemplified by the finding that there is a significant reduction in enhancer binding in MDPs from IRF8$^{-/-}$ mice coupled with the finding that MDPs isolated from IRF8$^{-/-}$ mice differentiate into Neuts rather than Mo despite similar mRNA expression profiles to WT mice (Kurotaki et al. 2018). The roles are then restored whereby IRF8 levels are reduced and the collaborative binding of PU.1 and C/EPBα are essential for Mo to macrophage differentiation in tissues (Heinz et al. 2013). This system is hierarchical, for example PU.1 expression is obligatory for IRF8 expression whereas the reverse is not true, and both IRF8 and PU.1 seem to be necessary

for the expression of KLF4 which is also essential in Mo formation (Kurotaki et al. 2013).

1.4.3 The collaborative action of transcription factors

Eloquent tracking of blood Mo has confirmed that the non-classical population derive from the classical Mo via a transitional intermediate population (Patel et al. 2017). As expected, Mo share common LDTFS; PU.1 motif and TF expression is enriched across all Mo subpopulations. But the motifs for AP-1 and KLF are enriched in classical and non-classical Mo respectively (Thomas et al. 2016). Their corresponding TFs correlate, with mRNA levels of *Fos* and *Klf2* being highly expressed in classical and non-classical Mo respectively (Thomas et al. 2016).

A more striking difference is seen in the expression of the orphan nuclear receptor NR4A1 which is highly expressed in both human and mouse non-classical Mo (Carlin et al. 2013; Thomas et al. 2016). The specificity of this to non-classical Mo is exemplified by both the preservation of classical Mo and macrophage function but the loss of non-classical Mo in mouse lacking *Nrf4a1* (Thomas et al. 2016). However the control of this is far more complex as can be seen in the role of external drivers to cell transition such as stimulation of the NOD2 receptor. Using three different NOD2 agonists it has been demonstrated that NOD2 prompts the transition of Mo from classical to non-

classical Mo (Lessard et al. 2017). Exposure to a NOD2 agonist resulted in increased expression of *Nrfa1* in classical Mo. A study using *Nrfa1* deficient mice however, reported that a NOD2 agonist was able to drive differentiation of Mo from classical to non-classical. This suggests that *Nr4a1* is not obligatory and its regulatory effects can be bypassed (Lessard et al. 2017).

1.4.4 The hierarchical model of transcription factors

Thus far LDTFs have been discussed as pioneering factors determining cell type. The selection of many enhancers, by LDTFs, confers greater cell plasticity which is essential to Mo given their varied functions (Lavin et al. 2014). Indeed, Mo have a 4-fold higher number of cell-specific enhancer regions than Neuts (Rico et al. 2017). Additionally, the enrichment of motifs such as *MYC* in Mo enhances transcriptional activity, which is essential when mounting an inflammatory response (Rico et al. 2017). Thus, Mo are “primed” to respond to external and internal cues. Mounting of this actual response, however, requires further modifications and these occur via the binding of so-called Signal Dependent Transcription Factors (SDTFs). The binding of SDTFs may occur in those regions that have already been primed by LDTFs and CTFs or by de novo collaborative binding with LDTFs in response to any given signal (Heinz et al. 2013). An important example of this in Mo are the Signal Transducer and Activator of Transcription (STAT) factors, involved in both IFN and NFκB pathways.

The STATs are a collection 7 TFs that interact as dimers or trimers in cell signalling and transcriptional regulation. A key mechanism in Mo is the activation of the IFNγ–JAK–STAT1 pathway (Stark & Darnell 2012; Villarino et al. 2017). The binding of IFNγ to transmembrane receptors on Mo activates Janus kinase (JAK) and phosphorylation of STAT1 leading to STAT1 translocation to the nucleus. STAT1 can act directly by binding GAS motifs or indirectly via collaborative binding (Villarino et al. 2017). Binding of STAT1 to the GAS motif leads to increased transcription of Interferon Stimulated Genes (ISGs), inducing an inflammatory response. As discussed, the binding of this SDTF is reliant on the LDTF PU.1 and also other SDTFs such as IRF8 (Villarino et al. 2017) thus meaning that the response to IFNγ can be varied dependent on the LDTF-SDTF landscape of the cell. This is an oversimplification however as STATs do not only act as TFs but can also recruit molecules capable of chromatin re-modelling and as this re-modelling occurs, the binding activity of STAT1 can shift, leading to altered activity. An example of this is the immediate induction of ISGs and the delayed induction of IRF genes. As mentioned, IRFs such as IRF8 can further act to alter the binding activity of STAT1 and so continues the highly dynamic yet co-ordinated response of Mo to IFNγ. Importantly, both the STAT1-JAK and NFkB pathways lead to STAT3 signalling which in turn acts to regulate inflammatory response and prevent excessive inflammatory response. It is not clear exactly how STAT3 reduces inflammatory response in this context. Two proposed

mechanisms are competition for binding motifs and the formation of STAT1-STAT3 heterodimers (Roca Suarez et al. 2018).

As alluded to, the signal that the cell receives is key in determining response and this is not only in the particular SDTF that is prompted but can also differ in how that SDTF responds. This is particularly true for STAT3. The above role of STAT3 would suggest that this is an anti-inflammatory TF. However, the action of STAT3 can also be pro-inflammatory. IL-6, produced in response for example to SDTF activity of NFkB, acts through binding to the gp130 subunit of its receptor, activating downstream JAK-STAT3 (and SHP-2-Ras-ERK1/2) signalling (Hirano et al. 2000). It is thought that STAT3 then initiates an inflammatory response by inducing gene expression; altering cell survival, proliferation and the differentiation of Mo into macrophages (Hirano et al. 2000). This feedback loop is further enhanced by STAT3-induced expression of NOTCH receptor antagonists, NOTCH receptor activation and enhanced NFkB production, increased IL-6 production and hence the cycle continues (Hildebrand et al. 2018). Conversely, IL-10 also induces STAT3 but results in a longer-lived anti-inflammatory response. The mystery of why the same SDTF leads to such different responses is explained by the importance of the combinatorial binding of SDTFs in response to each signal. In both the STAT1-IFNγ and the IL-6 responses, SOCS3, which is part of the suppressor of cytokine signalling (SOC) family, is able to repress STAT action through binding to the JAK (Villarino et al. 2017; Roca Suarez et al. 2018). The SOCs

proteins are both induced and have different effector STATs depending on the cell type and the signal received (reviewed in Duncan et al. 2017). The SOC3 is able to block the action of IL-6 but not IL-10, thus dampening the inflammatory response and enabling a longer-term anti-inflammatory effect.

1.4.5 Refined responses by histone modifications

The histone status modifies promoter and enhancer activity (Chen & Dent 2013). Post-transcriptional modification of histone status is a key mechanism by which TFs initiate feedback. Recruitment of transcription co-regulators modifies the histone environment, enhancing, activating or repressing transcription. For example, IFNγ primes Mo, resulting in an enhanced inflammatory response on exposure to inflammatory stimuli such as LPS. It has been shown that IFNγ increases the density of H3K27ac at enhancers for key genes in this response. Via this process, active enhancers are increased and therefore subsequent SDTF binding and effects are enhanced. However, IFNγ also recruits the methyltransfersase (MT) enzyme, EHZ, at promoters for MERTK, PPARγ and RANK (TNFSF11) resulting in methyl deposition at H3K27 and silencing, thus stabilising gene expression and regulating the intensity of inflammation (Qiao et al. 2016). This is in part explained by the ability of STATs to alter histones via recruitment of co-regulators such as the Histone Acetyltransferases (HATs), p300 and MTs, such as EZH2. In addition, the regulation of STAT1/3 in IFNγ response is partly co-ordinated by the

HDAC1/2 complex SIN3a which ensures the initial repression of STAT3, allowing a dominant STAT1 response which is later altered (though this is not well understood) (Roca Suarez et al. 2018).

1.4.6 Transcriptional regulation of monocytes in disease

To date, there is very little detailed evidence with regards to the transcriptional regulation of Mo in cancer. It has been suggested that the NFκB pathway is up-regulated in circulating cancer Mo, but it is unclear as to what factors drive this process (Chittezhath et al. 2014).

The role of some chemokines in this respect have been explored. For example, the chemokine CCL5 is released from T cells and acts on the myeloid population. In the context of metastatic colorectal cancer, blocking CCR5 leads to STAT3 activation and tumour killing due to re-polarization of the Mo-derived TAM (Halama et al. 2016). The CCR5 promoter usually features a high density of the H3K27me3 (Wierda et al. 2012). Using T cell cultures, it has been shown that drugs targeting co-regulatory factors such as DNA MTs or HDACs modulate CCR5 expression (Wierda et al. 2012). This is yet to be explored specifically in the context of cancer.

The role of HDACs in the regulation of Mo also points to possible mechanisms. The use of HDAC inhibitors results in altered production of pro-inflammatory cytokines by Mo and thus can be used as an anti-inflammatory therapy (Leoni

& Fossati 2005; Anon 2002; Leoni et al. 2002). In the context of breast cancer, Guerriero and colleagues demonstrated that use of a HDACII inhibitor resulted in altered macrophage signatures and phenotype within the tumour (Guerriero et al. 2017). There was increased tumoricidal activity of macrophages and concurrent reduction in solid tumour primary burden and pulmonary metastasis (Guerriero et al. 2017). The data suggests that this occurs via recruitment of Mo that subsequently differentiate into anti-tumoural rather than pro-tumoural TAMs (Guerriero et al. 2017). Therapeutically, this enhanced the efficacy of chemotherapy and receptor blockade in this mouse model of breast cancer (Guerriero et al. 2017).

Another area of interest is in the role of tumour exosomes. Exposing Mo to tumour-derived exosomes in pancreatic cancer altered the expression profile of CD14 HLADR and also led to altered STAT signalling and an immunosuppressive phenotype (Javeed et al. 2017). Tumour exosomes also seem to enhance survival of Mo (Song et al. 2016). A very interesting study by Plebanek and colleagues on the pre-metastatic environment and the role of exosomes demonstrated that when exosomes from highly metastatic cells were injected in a mouse model, pro-tumoural Mo were recruited to the pre-metastatic niche (Plebanek et al. 2017). Conversely, injecting exosomes isolated from less invasive non-metastatic cancers led to anti-tumoural Mo being recruited (Plebanek et al. 2017). This held true using human exosomes (Plebanek et al. 2017). On a transcriptional level, in the context of exosomes

isolated from less invasive cancer, *Nr4a1* levels were increased and more ly6c^{low} Mo were detected in the BM and lungs where they had a protective effect (Plebanek et al. 2017). This is consistent with the previously discussed protective role of ly6c^{low} Mo (Hanna et al. 2015) in the metastatic setting but for the first time demonstrates the role of exosomes in altering key TFs in Mo.

Given the lack of evidence in the context of cancer, understanding transcriptional regulation in other diseases may be useful when trying to better understand the process underlying transcriptional and functional perturbations to Mo in cancer. There are some parallels with sepsis, circulating immune-suppressive Mo in severe sepsis and Mo in breast cancer share common trasncriptional profiles when compared with age-matched controls (Bergenfelz et al. 2015). In severe sepsis Mo fail to phagocytose and present material to T cells because HLA-DR is down-regulated at both a gene and surface marker level (Bergenfelz et al. 2015). Silencing of genes involved in MHCII, antigen presentation and immune response occurs, in part, via a simultaneous loss of active and gain of inactive histone marks at these genes (Bergenfelz et al. 2015). Another aspect is the silencing of NFkB signalling and thus reduction in cytokine production. Recruitment of the CTF RelB in the initial NFkB response initiates silencing via interaction with the co-regulator G9a (MT) (Weiterer et al. 2015). This ultimately leads to chromatin inaccessibility and gene silencing, for example at the Il-1β promoter region (Weiterer et al. 2015).

Transcriptional alterations are observed in a number of autoimmune and inflammatory disorders: In Amyotrophic Lateral Sclerosis (AML), a severe neurodegenerative disease, a pro-inflammatory shift in the transcriptional profile of Mo occurs (Yang et al. 2010). The same shift can be seen in chronic inflammation such as in chronic periodontitis (Liu et al. 2016). In sarcoidosis patients, Mo show an enrichment for genes associated with phagocytosis and lysosomal processes and a down-regulation of proteasome degradation and ribosome pathways (Liu et al. 2016). Metabolic pathways and oxidative phosphorylation are also significantly altered (Talreja et al. 2017).

Autoimmune disease is characterised by a loss of homeostasis and tolerance resulting in inappropriate immunogenic responses and ultimately tissue damage. In the intestines, Mo and macrophages are constantly exposed to microbiota. Both in terms of mRNA and cell surface expression, CD16 and CD14 are down-regulated on intestinal Mo, leading to a downregulation in immune response and allowing for microbiota to exist without causing inadvertent inflammation (Cole et al. 2016). It has been found that microbial metabolites, produced in the gut, may modulate co-regulatory activity by HDACs and the levels of active PU.1 leading to the dampening of immune responses (Lasitschka et al. 2017). In the inflammatory bowel disorder Chrohn's disease, PU.1 levels are overexpressed in Mo and an inflammatory phenotype observed (Lasitschka et al. 2017).

Systemic Lupus Erythematosus (SLE) is an autoimmune disease characterised by abnormal Type I IFN responses. Microarray of blood Mo could not only distinguish SLE patients from immunised or healthy controls, but could also be used as a biosensor to monitor Type I IFN response and predict prognosis (Lasitschka et al. 2017). Another study on SLE showed that Mo isolated from patients had an altered histone landscape with K3K4me3 increased at promoter regions and K3K27ac at the enhancer regions of Mo. Increased levels of the demethylase enzyme, JMD3 in combination with reduced EHZ2 were found and point to the role of these enzymes in this disease process and potential for therapeutic targets (Shi et al. 2015).

In chronic inflammation associated with cardiovascular disease and diabetes, Mo are clearly implicated. Pro-inflammatory and atherosclerotic factors in diabetic Mo are driven in part by the sustained activation of the co-transcriptional regulators SETD7/9 (a MT enzyme) and EHZ (Li et al. 2008). Enhanced TNFα responses occur as excessive SETD7/9 both stabilises the binding of NFkB while simultaneously methylating adjacent H3K4 (Li et al. 2008). The simultaneous recruitment of JMD3 further potentiates this response via removing repressive marks at other relevant promoters (Li et al. 2008). The attenuation of this effect when knocking out SETD7/9 clearly demonstrates a relevance to potential therapies (Li et al. 2008). Though not linked to cardiovascular diseases, SETD7/9 is also known to act on STAT3 binding

sites, impairing its action and therefore potentiating inflammation (Li et al. 2008).

In summary, the transcriptional regulation of Mo is dependent on complex interactions between LDTFs, CTFs, SDTFs and co-transcriptional regulators. The multiple combinations possible among these factors allow for the plasticity essential to Mo function but also the susceptibility to alterations in the context of cancer. Understanding of this regulation would confer potential benefits to manipulating Mo in cancer.

1.5 **Mouse models of breast cancer**

Mouse models of breast cancer provide a means to deconvolute mechanisms of disease and develop potential therapies in what is hoped to be a clinically relevant context. The simplest, cheapest and quickest strategies are intravenous injection of metastatic cell lines or orthotopic injection of cancer cell lines subcutaneously or directly into the mammary fat pad. However, these models lack the establishment of cancer from pre-invasive to invasive stages and therefore do not fully recapitulate the tumour-host interactions. This can lead to misleading findings (Ciampricotti et al. 2012). Additionally, if the focus of the research of the immune environment, then the use of immunocompetent mice is essential. This precludes the use of mouse models using patient derived xenografts (PDX), though this is not to say that these cannot be very useful in other contexts. To overcome this aspect, humanised mouse models have been developed whereby human haematopoietic stem and precursor cells can be engrafted into sublethal irradiated immunodeficient mice (Shultz et al. 2005). The use of PDX models in these mice presents the potential to explore the human immune system response to a human tumour within the benefits of a mouse model. However, these mice lack both T and B cells and thus their utility is limited. Thus while it may be that with further development humanised mouse models become the gold standard (de Ruiter et al. 2018), currently the most well-established system to study the tumour-immune

environment remains the use of genetically engineered mouse models (GEMMs).

As GEMMs are a well-established way of studying immuno-oncology, many different options exist (de Ruiter et al. 2018). The first breast cancer GEMM to be developed made use of a naturally occurring virus termed mouse mammary tumour virus (MMTV, also known as Bittner virus), which was discovered by Bittner in 1936 (Bittner 1936). This viral RNA oncogene encodes for super-antigens which stimulate T cell and B cell proliferation (Reuss & Coffin 1995). In natural conditions, it is during puberty that the virus enters the mammary glands with migrating lymphocytes and infects proliferating mammary gland epithelial cells (Golovkina et al. 1998). As the RNA is reverse transcribed, the virus incorporates into the DNA. Inevitably, when this viral DNA is inserted in proximity to any gene, it will drive expression within the mammary epithelium. The long terminal repeat of the MMTV contains a glucocorticoid hormone response element that acts as a promoter to drive the adjacent gene. This is potentiated by oestrogen and other steroid hormones. To this end, the MMTV alone can lead to mammary cancer through insertional mutagenesis. However, when the MMTV LTR is coupled with the highly oncogenic Middle T antigen protein of the polyoma virus, this is very effective in inducing mammary cancer. This model, developed by Muller and colleagues in the late 1980s (Muller et al. 1988) and termed the MMTV-PyMT, is the one of the most well established GEMMs of breast cancer. It is a favoured model for studying ductal cancer as

tumours develop spontaneously in the mammary and salivary glands and evolve in a manner that reflects stages of human ductal cancer (Figure 3) (Lin et al. 2003, Muller et al. 1988). Tumour dissemination is haematogenous rather than lymphatic and mice develop lung metastasis (Lin et al. 2003).

The MMTV promoter can also be coupled with other oncogenes, such as in the MMTV-Wnt1 model, or other combinations of localised promoter-oncogene can be used, such as the whey acid protein promoter (WAP) and Myc oncogene in the WAP-Myc model. The exact promoter used is important, as models have been replicated and modified. For example, the original MMTV-PyMT developed by Muller was also developed by Hennighausen and colleagues (Wagner et al. 1997). While the promoter used in both models are very similar, they are not the same and the latter is more promiscuous. Thus, despite having the same name, the phenotype of the models differ.

A more complex approach can be to use the cre-lox system in which target genes are flanked by loxP which is recognisable by cre recombinase. Cre expression is restricted to the mammary gland. Using this, oncogenes can be activated by removing genetically engineered stop codons or tumour repressor genes can be deleted by targeting their functional exons. This can be used to manipulate the model to reflect molecular or genetic mutational types of breast cancer. An example of this is the MMTV-Cre/PTEN$^{flox/flox}$ mouse model which deletes the tumour suppressor gene *Pten* within the mammary gland (Schade

et al. 2009). This can additionally become more complex by, for example, adding in an allele for a chosen gene of interest to investigate how this gene is involved in any given mechanism. A limitation that should be noted with all the GEMMs discussed is that every cell in the mammary gland has the same mutation. Thus, while GEMMs partly recapitulate the natural evolution of cancer and the accompanying changed to the TME, they lack the accumulation of mutational burden within a single cell that occurs in naturally evolving cancer (de Ruiter et al. 2018).

An important consideration when using GEMMs is the strain and background of the mouse used. For example, the well-established MMTV-PyMT model is available in many different strains. In each strain the time to onset of tumour, tumour burden and metastatic burden varies (Lifsted et al. 1998). Two commonly used strains are the FVB and C57BL/6 mice. The former is advantageous as tumours develop by 8 weeks and tumour development is relatively homogeneous. However, if more complex questions are to be explored, requiring further crosses, many targeted alleles are not available on an FVB strain. For this reason, the C57BL/6 strain can be more useful. An explanation for the variation in tumour development is in part due to the differences in immune responses between strains, an important consideration when studying tumour-immune interactions (Lifsted et al. 1998, Davie et al. 2007; Mills et al. 2000).

Traditional GEMMs have many benefits. However, the spontaneous and sporadic nature of tumour development causes heterogeneity and can hinder the planning of experiments. Adding in an “on-off” system, such as the doxycycline inducible tetracycline system or tamoxifen inducible system can improve this. However, the breeding time and time for tumours to develop can still lead to heavy financial burdens and extensive time-delays. To counteract this, mammary tumours at the same stage can be frozen down, segmented and then re-implanted into a group of mice (Casbon et al. 2015). To further this, tumours can be grafted into mice of a genetically modified background of any gene of interest to preclude the use of more complex cre-lox breeding. This model system can be referred to as an allograft. When studying metastatic progression, the presence of large primary tumours can be a limiting factor. Therefore, another approach can be to resect the primary allograft tumour once metastasis are established, and monitor metastatic disease thereafter (Doornebal et al. 2013).

The complexity of which exact model to choose was highlighted by a recent paper which assessed 16 different GEMMs (Wellenstein et al. 2019). The immune response (assessed in terms of neutrophilia) varied across all 16 GEMMs, dependent of the loss of *p53* (Wellenstein et al. 2019). The combinations of specific promoter(s), oncogene(s) and mutation(s), the strain and background, and the exact system to use means that many options are available to study Mo in breast cancer.

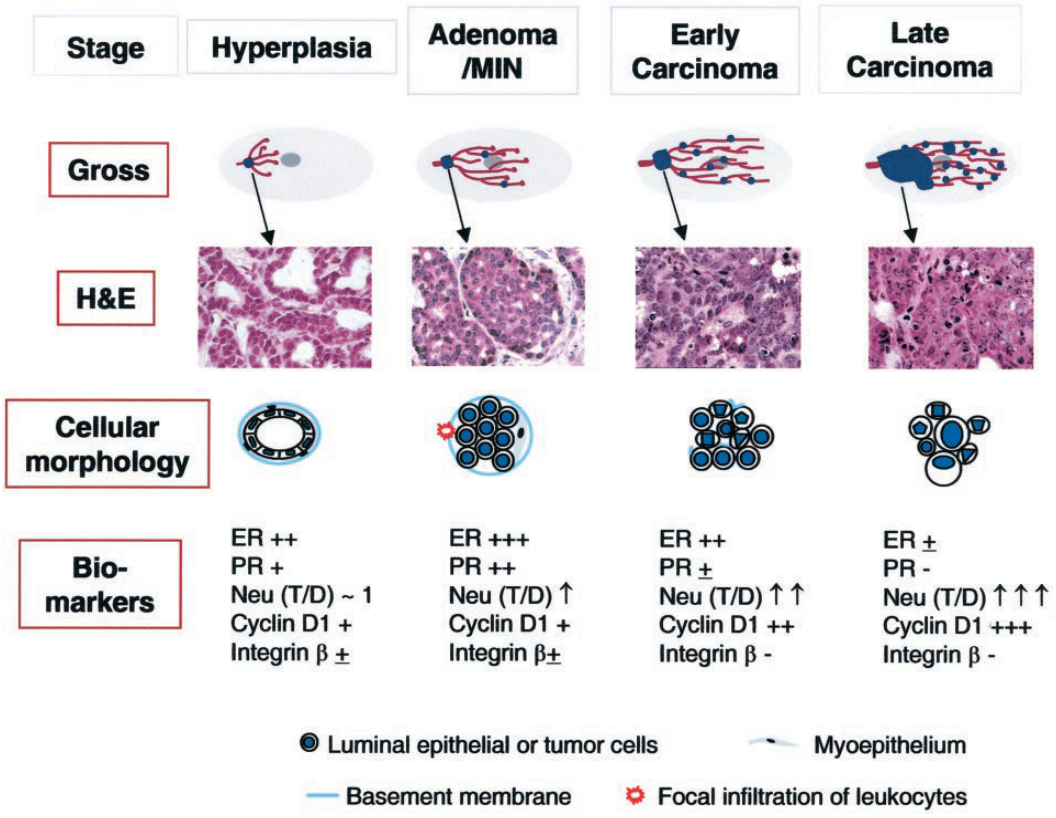

Figure 3 Summary of tumour progression and biomarker expression in PyMT mouse model of breast cancer. *Top: Gross, displays the overall development of lesions in mammary glands of PyMT mice. Tumour lesions are indicated by blue dots. The H&E panel displays the corresponding histology of primary lesions at different stages of tumour progression. The cellular morphology panel schematically illustrates changes in the cytology of the cells as well as the integrity of the basement membrane and the presence or absence of myoepithelial and focal inflammation. Moreover, the changes in biomarkers during tumour progression is summarised in the panel of biomarkers. T/D, the ratio of Neu expression between lesions and normal ducts in age-matched mammary glands. Figure and caption used with permission from Lin et al. 2003.*

Chapter 2 Hypothesis and Aims

2.1 Hypothesis

It is proposed that in breast cancer, epigenetic and transcriptional modifications occur in Mo. If this occurs, it may involve alterations at the progenitor stage in the BM, within the blood, within the tumour or a combination of these. There are aspects common to human and mouse, both in the alterations to Mo and the mechanisms by which this occurs.

2.2 Aims

1. Establish if changes in Mo populations occur in MMTV-PyMT mouse models of breast cancer and if so, what the role of Mo progenitors are in this process.
2. Transcriptionally profile Mo in MMTV-PyMT mouse models of breast cancer and determine, if changes occur, where conditioning occurs and if orthologous differentially expressed genes exist when compared with a human breast cancer Mo dataset.
3. Establish potential mechanisms by which Mo transcriptional regulation is altered in cancer by assessing the epigenetic landscape of Mo and investigating targets common to both the human and mouse datasets.

Chapter 3 Methods

3.1 Mouse models

Male Tg(MMTV-PyMT)$^{634Mul/Lellj}$ were bred with female WT or PyMT$^{-/-}$ female mice from within the existing GEM colony. The MMTV-PyMT GEM lines were on two different background strains; C57BL/6 PyMT GEM lines were on C57BL/6JCrl and FVB PyMT lines were on FVB/NHanHsd. 8-week old C57BL/6JCrl mice were purchased from Charles River Laboratories. 8-week old FVB/NHanHsd mice were purchased from Harlan Olac, now Envigo. PyMT+ve mice were PYMT$^{+/-}$ and controls were PyMT$^{-/-}$ littermates. For allograft models, tumours were harvested from PYMT$^{+/-}$ tumour bearing females and recipients were 10-16 week old female C57Bl/6JCrl mice.

All 10 mammary glands were palpated weekly from 8 weeks of age (see Figure 4 for mouse mammary anatomy). Once tumours were first detected, they were monitored and measured bi-weekly. Tumours in the spontaneous model were permitted to a maximum size of 20mm. Tumours for the allograft model were permitted to a maximum size of 12mm. Consistency of tumours was monitored for the formation of cysts by palpating tumours and the skin was monitored for any signs of ulceration. The general health of mice, including weekly weighing of mice, was also monitored to comply with animal use protocols.

For allografts, tumours were harvested immediately after culling by using a rising concentration of CO_2. Tumour segments were cut into standard sizes, 4x2mm and placed in a petri dish with PBS on ice. Under general anaesthetic, a right sided 1cm medio-lateral incision was made and the skin flap raised to allow direct visualisation of the right inguinal mammary gland. The tumour segment was then inserted using a coring needle and the site of entry sealed with tissue glue. Once homeostasis was confirmed, the skin was closed with 2 skin clips. Skin clips were removed at 10-14 days and mice were monitored for tumour development. For sham procedures, the same procedure was carried out, but the coring needle contained no tissue.

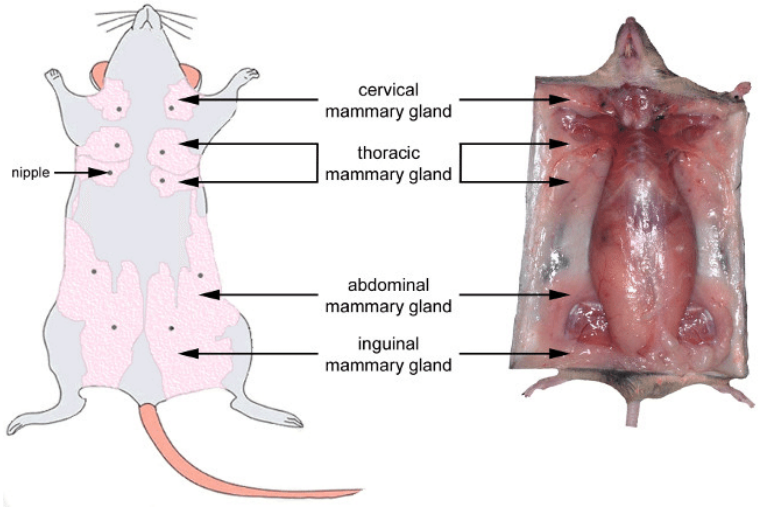

Figure 4 Anatomical location of the mouse mammary glands. *Left: ventral view of the mouse mammary system at the late gestation stage. Right: localization and aspect of the mammary gland at the late gestation stage in the mouse. Open access article Honvo-Houeto & Truchet 2015.*

3.2 **Tissue collection**

For blood kinetic experiments, 50µl of blood was obtained every 14 days by tail vein bleed. Blood was taken up using a P100 containing 10µl 0.5MM EDTA. A cumulative record of blood collection was maintained to ensure that total did not exceed recommended allowances (10.8 x weight, over 30 days). The endpoint for this kinetic was once the tumours reached 20mm.

For terminal experiments, mice were culled using a rising concentration of CO_2. A thoracotomy was then performed, and cardiac puncture performed using a 23G needle and 1ml syringe primed with 100µl EDTA. BM, spleen and tumours were harvested and placed in PBS on ice if being processed for flow cytometry or into 4% paraformaldehyde. Tissues placed in 4% paraformaldehyde were washed at 48 hrs and stored in 70% ethanol.

3.3 **Flow cytometry analysis for mouse**

For all antibodies see Appendix section 9.1.1 Flow cytometry antibodies. Detailed sample preparation methods for all methods in this section can be found in the Appendix section 9.2 Detailed protocols. For all flow cytometry experiments initial panels were optimised, and FMOs were used to define gates, with use of isotype controls where necessary. For compensation OneComp eBeads™ Compensation Beads (ThermoFisherScientifc, Cat No 01-1111-42) were used.

All gating strategies initially selected cells (SSC-A against FSC-A), excluded doublets (SSC-A against SSC-H), and live cells using live/dead as specified.

3.3.1 Flow cytometry of mouse blood cells

Blood Mo were defined as dump- (CD3, CD19, NK1.1), CD11b+, CD115^{high} and then assessed using both Ly6c and Treml4 to separate out Ly6c^{high} (Ly6c^{high}/Treml4-), Ly6c^{low} (Ly6c^{low}/Treml4^{high}), and Ly6c^{int} populations. The gating strategy is as for BrdU analysis in Figure 10 with the exception of the appearance of cells on SSC-A versus FSC-A being different given the fixing process used for BrdU staining. The use of Treml4 in addition to Ly6c helped to separate out the populations as it acts as a positive marker for the Ly6c^{low} population (Briseño et al. 2016). This was validated with scRNAseq data. As shown in Figure 6, F the Ly6c^{int} population appear as a waterfall between the two more distinct populations.

Neuts were defined as dump-, Cd11b+ and CD115^{low}, Ly6g+.

For accurate quantification of cell numbers in the blood, 123count eBeads™ Counting Beads (ThermoFisherScientifc, Cat No 01-1234-42) were used: Cells were suspended in 300µl for flow cytometry. Immediately prior to analysis, 50µl of counting beads were added and the sample vortexed and then acquired. The following calculation was applied:

$$\text{Absolute cell count (cells/µl)} = \frac{(\text{cell count} \times \text{eBead Volume})}{(\text{eBead Count} \times \text{Cell Volume})} \times \text{eBead Concentration}$$

3.3.2 Flow cytometry of mouse bone marrow cells

BM Mo were defined as dump- (CD3, CD19, NK1.1, Ter119), CD11b+, CD115^{high} and then assessed as Ly6c^{high}, or Ly6c^{low} based on Ly6c expression alone. The gating strategy is the same as for BrdU of BM Mo shown in Figure 11. While Treml4 is expressed on Ly6c^{low} Mo, the BM contains only 5-10% of Ly6c^{low} Mo and even less, if any, intermediates (Hamon et al. 2017). As discussed in the introduction, Ly6c^{high} Mo exit the BM and, in the blood, differentiate into the Ly6c^{low} Mo via an intermediate cell. Ly6c^{low} Mo may then re-circulate back to the BM, but they account for very low frequencies in the total BM myeloid pool (Hamon et al. 2017). Given this, it was reasoned that the intermediate population were not relevant within the BM and they were neither gated nor analysed. The use of Treml4 was not necessary for accurate gating of the BM Ly6c^{low} populations. Furthermore, as a direct flow cytometry fluorophore, Treml4 is only available on PE. The panel was initially developed for the analysis and sorting of Mo and progenitors so was a 10-colour panel. Many of the markers used took multiple trials with different fluorophores to get optimal staining of populations. This precluded the use of Treml4 on PE.

For alternative BM data, provided by a colleague in the lab (Dr. Agnieszka Swierckzak) the panel and gating strategy were different (Figure 5). The inclusion of CD45 in the panel did not alter findings and was therfore comparable with other strategies where CD45 had not been used (Fig 5, D).

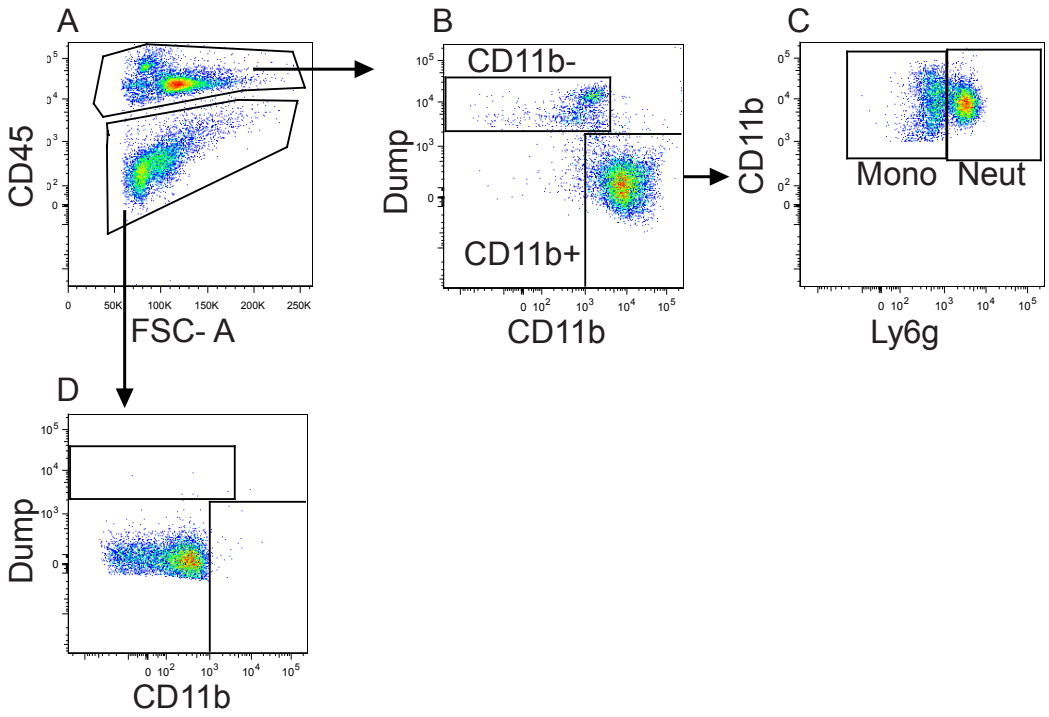

Figure 5 Gating of BM cells using an alternative strategy. *Cells have already been gated for exclusion of debris, doublets and dead cells (A) Selection of CD45+ cells (B) Selection of cells based of expression of dump (Cd3, B220, CD49b) and CD11b (C) Selection of Neuts as Ly6g+ and Mo as Ly6g- (D) Expression of dump and CD11b in the CD45- compartment.*

3.3.3 Flow cytometry of BM progenitors

For analysis and sorting of Macrophage Dendritic Progenitor cells (MDPs) and Common Myeloid Progenitors (cMoPs) a sorting strategy was designed based on the literature (Hettinger et al. 2013). The full gating strategy is shown in Figure 6. Live, $CD115^{high}$ cells were selected as dump- (CD3, Cd19, NK1.1, Ter119) and Ly6g-. Sca1-, CD127- (IL7rα-) cells were gated into three populations based on CD117 (cKit) and CD135 (Flt3) expression and each of these populations assessed for Ly6c and CD11b expression: $CD117^{low}$, CD135-,$Ly6c^{high}$, CD11b+ Mo; $CD117^{high}$, CD135-, $Ly6c^{high}$, CD11b- cMoPs; $CD117^{high}$, CD135+, Ly6c-, CD11b- MDPs. To validate this, sorted MDPs and cMoPs were cultured in, picked and Giemsa stained (Figure 7).

For sorting of Lin- Sca- c-Kit+ (LK) cells the gating strategy was altered (Figure 8): Live cells were selected as dump- (CD3, Cd19, NK1.1, Ter119) and Ly6g-. LK cells were gated as Ly6c-, CD11b-. The observation of all types of colonies in CFU assays from these cells confirmed their multipotency, particularly the red tinged BFU-E colonies.

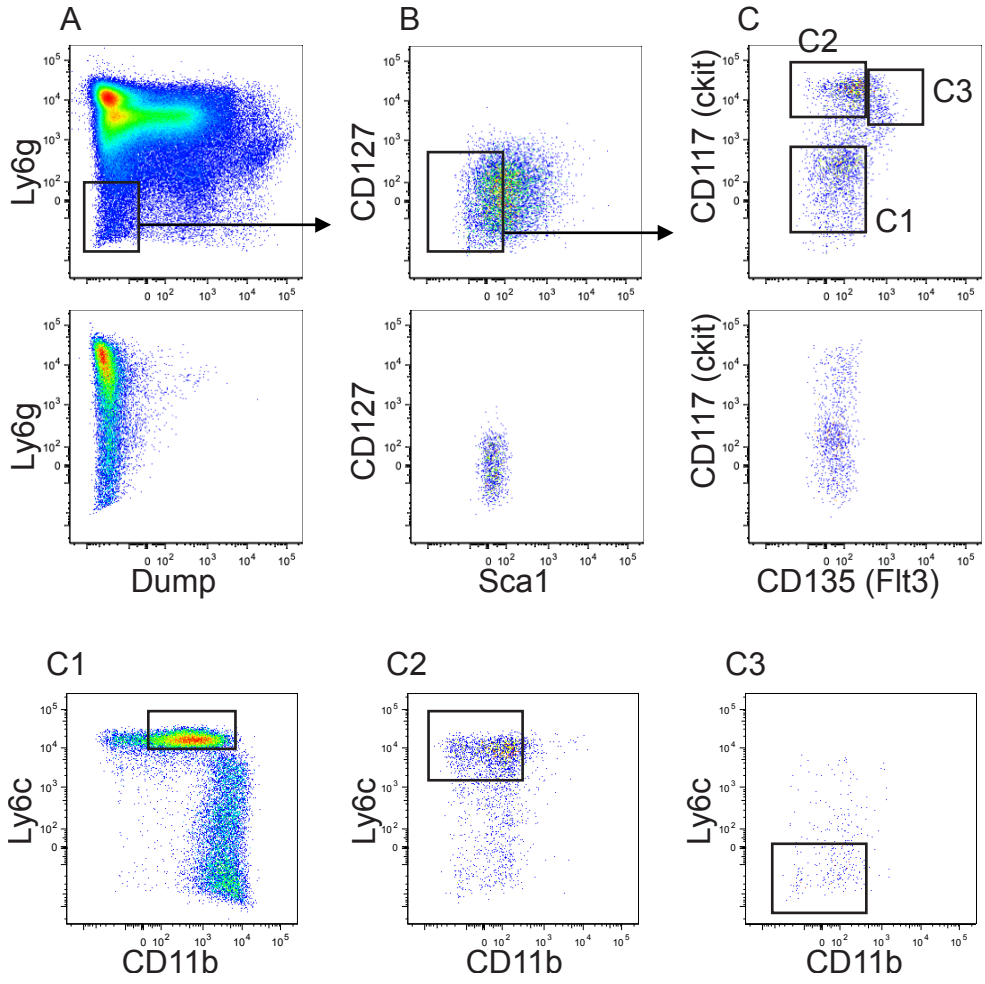

Figure 6 Gating strategy for sorting of MDPs and cMoPs. *Following selection of live and CD115^{high} cells (A) dump- (CD3, CD19, NK1.1, Ter119), Ly6g- cells selected (B) Selection of Sca1-, CD127- cells (C) Selection of CD117^{low}, CD135- cells (C1); CD117^{high}, CD135- cells (C2); CD117^{high}, CD135+ cells (C3). For (A-C) Top; full stain, bottom; FMO for antibody on each x-axis. (C1-C3) Further selection of respective gates using Ly6c and CD11b expression for (C1) Ly6c^{high}, CD11b+ Mo (C2) Ly6c^{high}, CD11b- cMoPs (C3) Ly6c-, CD11b- MDPs.*

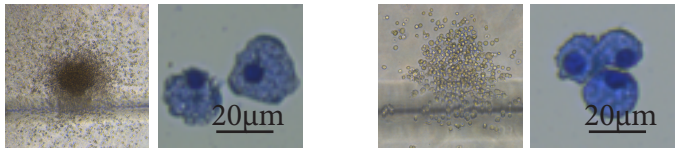

Figure 7 Validation of MDP sorts. *Two examples of colonies with picked, cytospun, Giemsa staining demonstrating macrophage phenotype. For each example the colony is shown on the left and the morphological giemsa staining on the right.*

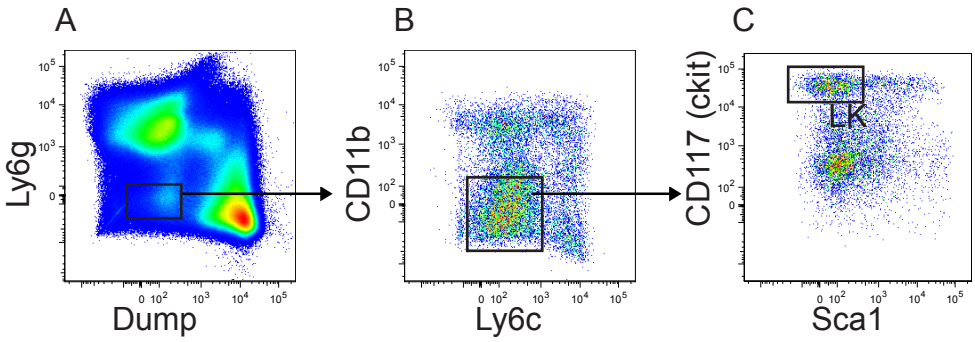

Figure 8 Altered gating to select for LK cells *(A) Live cells gated as dump- (CD3, CD19, NK1.1, Ter119) and Ly6g- (B) Selection of the Lin- population using Ly6c and CD11b (C) Selection of LK as CD117^{high} Sca1-.*

The gating strategy for Primitive BM progenitors is shown in Figure 9. Myeloid progenitors were defined as Lineage- (CD3, Cd19, NK1.1, Cd11b, Ly6g, Ly6c, Ter119) and CD127- and then divided into LK and LSK as $CD117^{high}$, and Sca1- and Sca1+ respectively. The LSK population was divided into CD135+ Multipotent progenitors (Flt3+ MPPs) and CD135- Haematopoietic Stem Progenitor Cells (HSPCs). All CD135- cells were then divided into CD48+ cells, representative of the CD135- MPPs (Flt3- MPPs), and CD48-, CD150+ Haematopoietic Stem Cells (HSCs). The LK population was divided into Megakaryocyte-Erythrocyte Progenitors (MEPs) (CD34-, CD16/32), CMPs (CD34+, CD16/32-) and GMPs (CD34+, CD16/32). This gating was designed to be consistent and therefore comparable with that in the literature (Casbon et al. 2015).

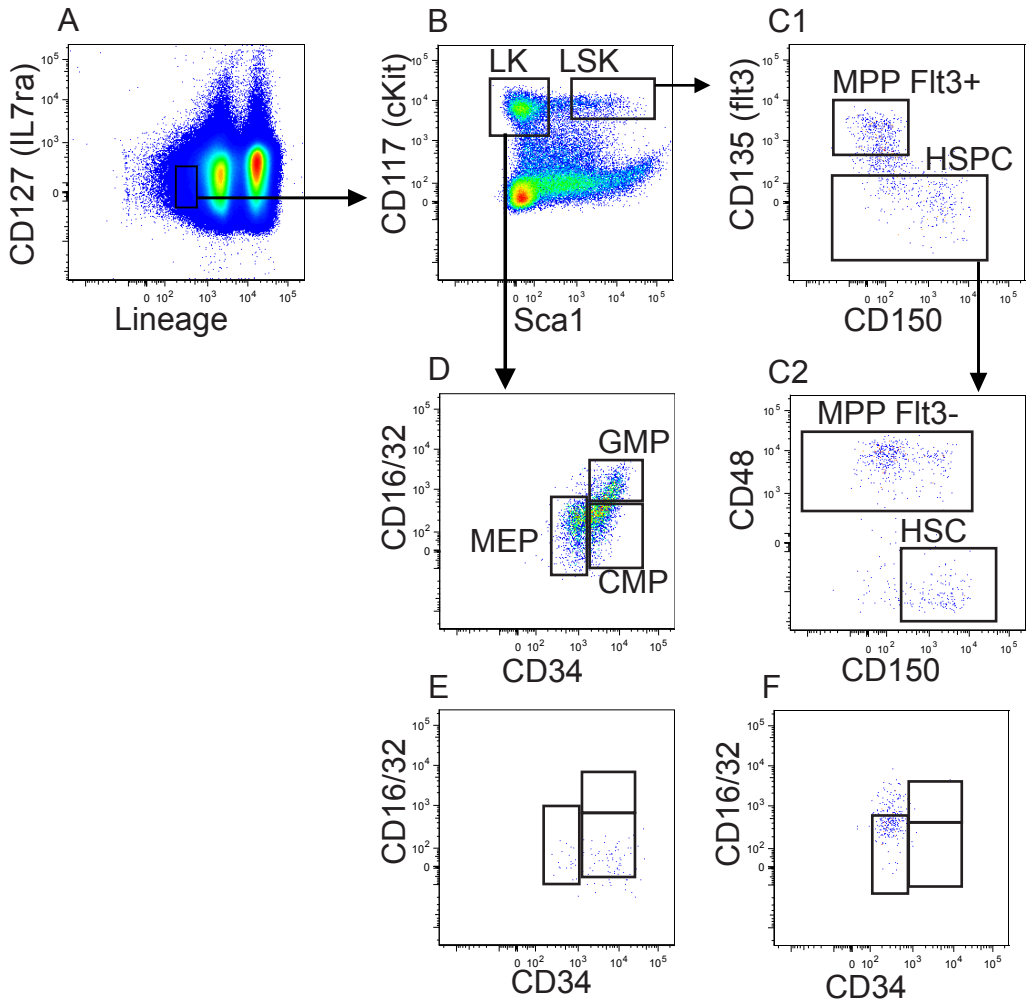

Figure 9 Analysis of BM progenitors *(A) Selection of CD127-, Lineage- (CD3, Cd19, NK1.1, Cd11b, Ly6g, Ly6c, Ter119) cells (B) Selection of LK as CD117^{high} Sca1- and LSK as CD117^{high} Sca1+ (C1) LSK population gated as CD135+ MPPs (termed Flt3+ LMPPs); and CD135- HSPC cells (C2) HSPC gated in C1 further gated as Flt3- MPPs (CD48+, Cd150-) and HSCs (CD48-, Cd150+) (D) LK population divided into MEP (CD34-, CD16/32-), CMP (CD34+, CD16/32-) and GMP (CD34+, CD16/32+). (E) FMO for CD16/32 staining (F) FMO for CD34 staining.*

3.3.4 BrdU

Mice were injected intraperitoneally with 100ul BrdU-stock (10mg/ml in D-PBS of BrdU, Sigma Aldrich, cat.no. B9285. 100µl is equivalent to 1mg per mouse). For tracking, a 40µl tail vein bleed was taken at the specified time point. For the BM, blood and spleen, mice were culled by rising CO_2 at 1hr after injection of BrdU and tissue harvested. Differing from previous experiments, a fixable live/dead stain was used and after the primary staining, cells were fixed for 1hr at RT and then permeabilised and incubated with DNase at 37˚C for 30 mins. Cells were then washed with permeabilisation/fixation wash and stained with Anti-BrdU-antibody (Alexa Fluor® 488 anti-BrdU Antibody, EBioScience, Cat No 364106) for 30 mins at RT. For each group and in all experiments, background BrdU levels were set using a control in which cells were processed identically but instead of DNase, PBS was applied. The control was used to determine the BrdU+ gate and the percentage of BrdU+ cells per cell type was calculated. Examples of gating for the blood and BM at 24 hrs can be seen in Figure 10 and 11 respectively.

For the spleen, following selection of live single cell populations, Dump- (CD3, CD19, NK1.1, Ter119, Ly6g) and $CD115^{high}$ cells were gated and then divided according to expression of CD135 and CD117 with the Mo defined as double negative and MDPs as double positive. Mo were gated as CD11b+, $Ly6c^{high}$ and MDPs as CD11b-, Ly6c-. The gating strategy is shown in Figure 12.

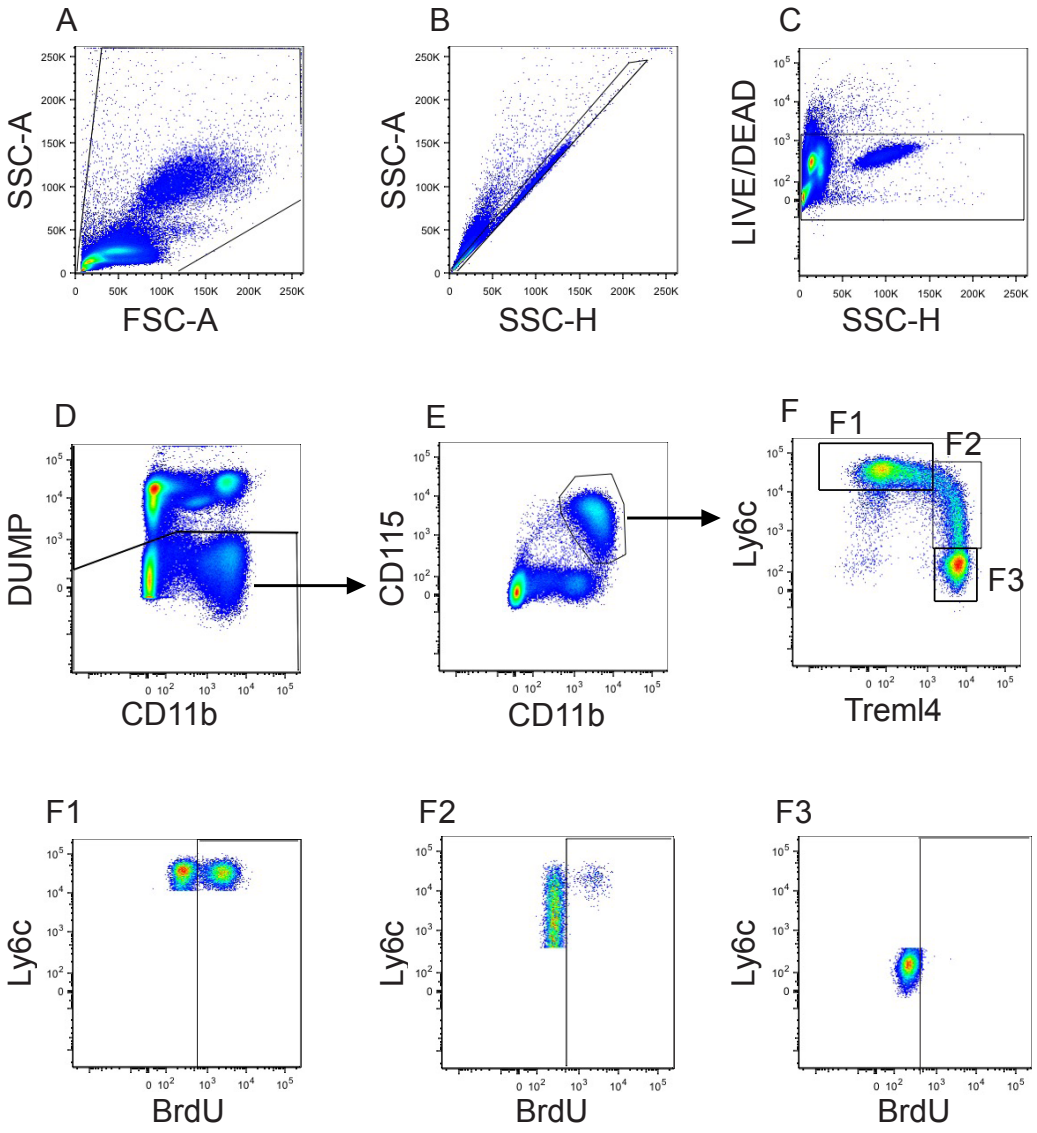

Figure 10 Gating of blood Mo for BrdU levels at 24 hrs *(A) Exclusion of debris (B) Exclusion of doublets (C) Exclusion of dead cells (D) Selection of dump- (CD3, CD19, NK1.1, siglecF, Ly6g) cells (E) Selection of CD115^{high} and CD11b+ cells (F) Gating of Mo into F1:Ly6c^{high} (Ly6c^{high}, Treml4^{high}), F2:Ly6c^{int} (Ly6c^{int}, Treml4^{int}), F3:Ly6c^{low} (Ly6c^{low}, Treml4^{high}) (F1-3) Gating of BrdU+ cells in respective Mo populations.*

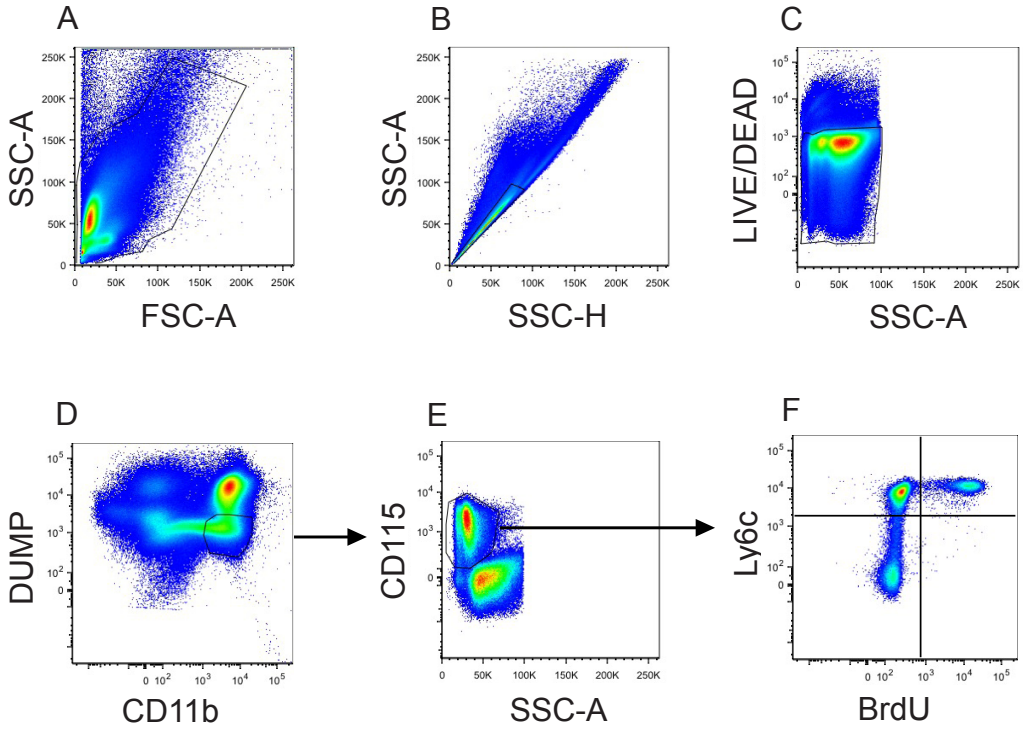

Figure 11 Gating of BM Mo for BrdU levels at 1hr *(A) Exclusion of debris (B) Exclusion of doublets (C) Exclusion of dead cells (D) Selection of Dump- (CD3, CD19, NK1.1, Ter119, Ly6g) and CD11b+ cells (E) CD115^{high} cells (F) Top quadrants Ly6c^{high} Mo, top right Ly6c^{high} BrdU+ cells.*

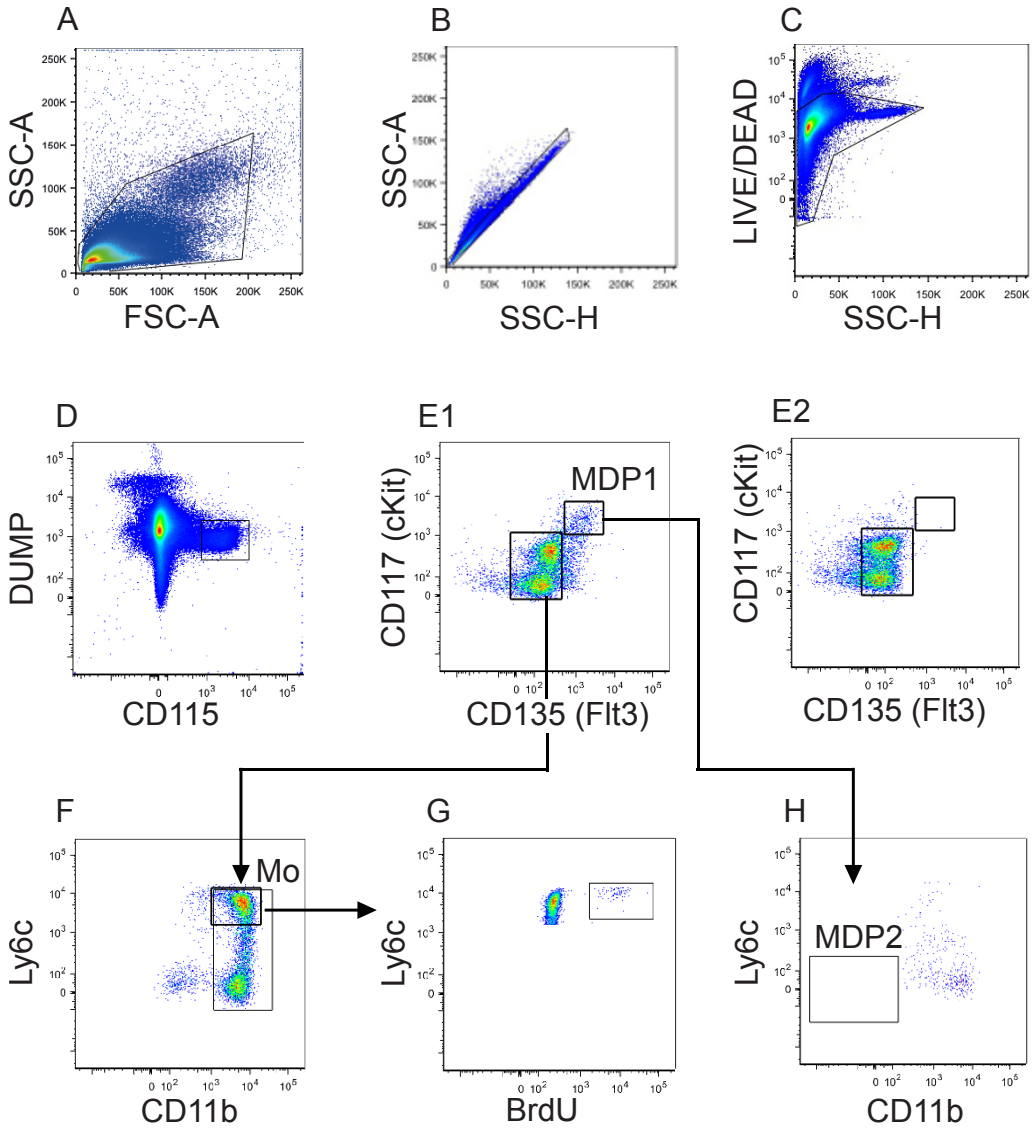

Figure 12 Gating of Mo and MDP populations in the spleen *(A) Exclusion of debris (B) Exclusion of doublets (C) Exclusion of dead cells (D) Selection of Dump- (CD3, CD19, NK1.1, Ter119, Ly6g) and CD115^{high} cells (E1-2) Full stained sample and FMO for CD135 to show the positive staining of CD135. Gates shown for myeloid cells (CD117^{low}, CD135-) and MDP1 (CD117^{high}, CD135+) (F) selection of Mo as CD11b+ and Ly6c^{high} (G) Ly6c^{high} BrdU+ cells (H) Stringent gating of MDPs as CD11b- and Ly6c^{low}.*

3.3.5 Phosphorylated Stat1 Flow cytometry

Sorted BM Ly6c^{high} Mo were centrifuged at 400g for 5 mins and re-suspended in medium (Dulbecco's Modified Eagle Medium + L/Glutamax + 10% FCS) prewarmed to 37˚C. Pre-warmed 50µl aliquots of either medium or medium supplemented with INFγ (at a concentration of 10 or 20ng/ml) was added to each well and samples were incubated at 37 ˚C for 15 mins. Samples were transferred to a V bottom 96 well plate and centrifuged at 400g for 5 mins. Samples were washed twice with wash buffer (centrifuged at 400g for 5 mins). Pre-chilled True-Phos™ Perm Buffer (Biolgened, Cat No 425401) (100µl) was added to each sample and pipetted up and down to ensure all cells were in suspension. Cells were left overnight in the fridge at 4˚C.

The following morning, plates were centrifuged at 1000g for 5 mins, washed with specialised cell staining buffer (Biolegend, Cat No 420201) and centrifuged at 1000g for 5 mins. Cells were re-suspended in 19µl of staining buffer + 1µl of Alexa Fluor® 488 anti-STAT1 Phospho (Ser727) Antibody (Biolegend, Cat No 686409), covered with foil and left at RT for 30 mins. Cells were washed twice with staining buffer (centrifuged at 1000g for 5 mins) and re-suspended in staining buffer for sample acquisition.

3.4 **CFU assays**

Detailed sample preparation methods for all methods can be found in the Appendix section 9.2 Detailed protocols. Progenitor cells were sorted into 1.5ml Eppendorph tubes containing Iscove's Modified Dulbecco's Medium (IMDM) medium and centrifuged at 400g and re-suspended in IMDM medium to ensure a concentration of 600cells/300µl for MDPs or 800cells/300µl for LK cells. 300µl of cell suspension was added to 3ml aliquots of MethocultTM M3534 (STEMCELL Technologies, Cat No #03534) in Falcon™ Round-Bottom Polystyrene Tubes (Falcon 352058, product code 10100151) and vortexed. Once samples were settled and free of air bubbles, 1.1ml of medium was plated and carefully spread across a 35mm petri dish. A duplicate was done for each sample. Plates were stored in a 15cm dish with an additional 35mmm petri in the centre of the 15cm dish containing DPBS.

Plates were incubated at 37˚C 5% CO_2 >= 95% humidity and colonies were counted at 7-14 days. An average count was taken for each sample from the duplicate plates. Plates were counted additionally by Dr. Mathew Burgess, Centre for Inflammation Research, University of Edinburgh who was blinded from the cancer status of the mouse.

For assessment of morphology by cytospin, colonies were lifted from the plate using a P200 and placed into a 1.5ml Eppendorph, washed with PBS and

centrifuged at 500g for 5 mins and re-suspended in 100µl of FACS buffer. Slides were labelled, filter papers placed and cyto-funnels secured. Slides were primed with 50ul of PBS and centrifuged for 1min at 500rpm (50x10) using the Shandon Cytospin II. Cells were loaded (100ul volumes only) and centrifuged for 5mins at 500rpm. The Rapid Romanowsky Stain Solutions A, B, C, (TCS Biosciences Ltd; Cat#HS705) were used: slides were immersed for 30 secs, 15 secs and 2 mins into solutions A, B and C respectively and left to dry overnight.

3.5 **Flow cytometry sorting of human cells**

Detailed sample preparation methods for all methods can be found in the Appendix section 9.2 Detailed protocols. Cancer patients were consented, and samples obtained by a trained research nurse (Jane Keys) on the morning prior to surgery. Samples were transported to the Queen's Medical Research Institute (QMRI) on ice. Samples were immediately processed as detailed below. All data was anonymised; a unique patient identifier was generated. Ethical permission was granted prior to commencing the project (code SR390). Control samples were obtained from volunteers enlisted in the Centre for Inflammation Research Blood Resource (AMREC Reference number 15-HV-013). Controls were all female and age-matched to cancer patients. All donors had no history of cancer or auto-immune disease and were not on any medication, such as steroids or antibiotics. Donors were fasted and samples

collected at 08:30-09:00 to reflect the cancer samples and the metabolic and circadian context to which Mo are extremely sensitive. All data were anonymised.

Blood was lysed using RBC lysis buffer (Biolegend, cat no 420301) at 4˚C for 5-10 mins. Cells were incubated with FcR block for 20 mins (FcR blocking reagent Human, Miltenyi Biotec Cat No 130-059-901) and stained with antibodies for 30 mins in the dark on ice. All staining was undertaken in FACS buffer (0.5% w/vBSA in PBS). Cells were sorted on the BD FACSAria™ Fusion flow cytometer at the QMRI flow cytometry facility. A total of $25x10^3$, $50x10^3$ and $>400x10^3$ cells were sorted into Eppendorph tubes for RNAseq, ATACseq and ChIPseq respectively.

All antibodies are listed in the Appendix section 9.1.1 Flow cytometry antibodies. Single live cells were selected as dump- (CD3, CD19, CD56) and CD45+. HLA-DR^{high} cells were selected to leave Mo and dendritic cells from which Mo were selected as classical ($CD14^{high}$ $CD16^{low}$) or non-classical ($CD14^{low}$, $CD16^{high}$) as described in the literature (Mukherjee et al. 2015). Neuts were principally excluded by size via the SSC-A versus FSC-A initial gating. Any contaminant Neuts could be seen as a population just above the non-classical population of Mo as they express high levels of CD16. An example of the gating strategy is shown in Figure 13.

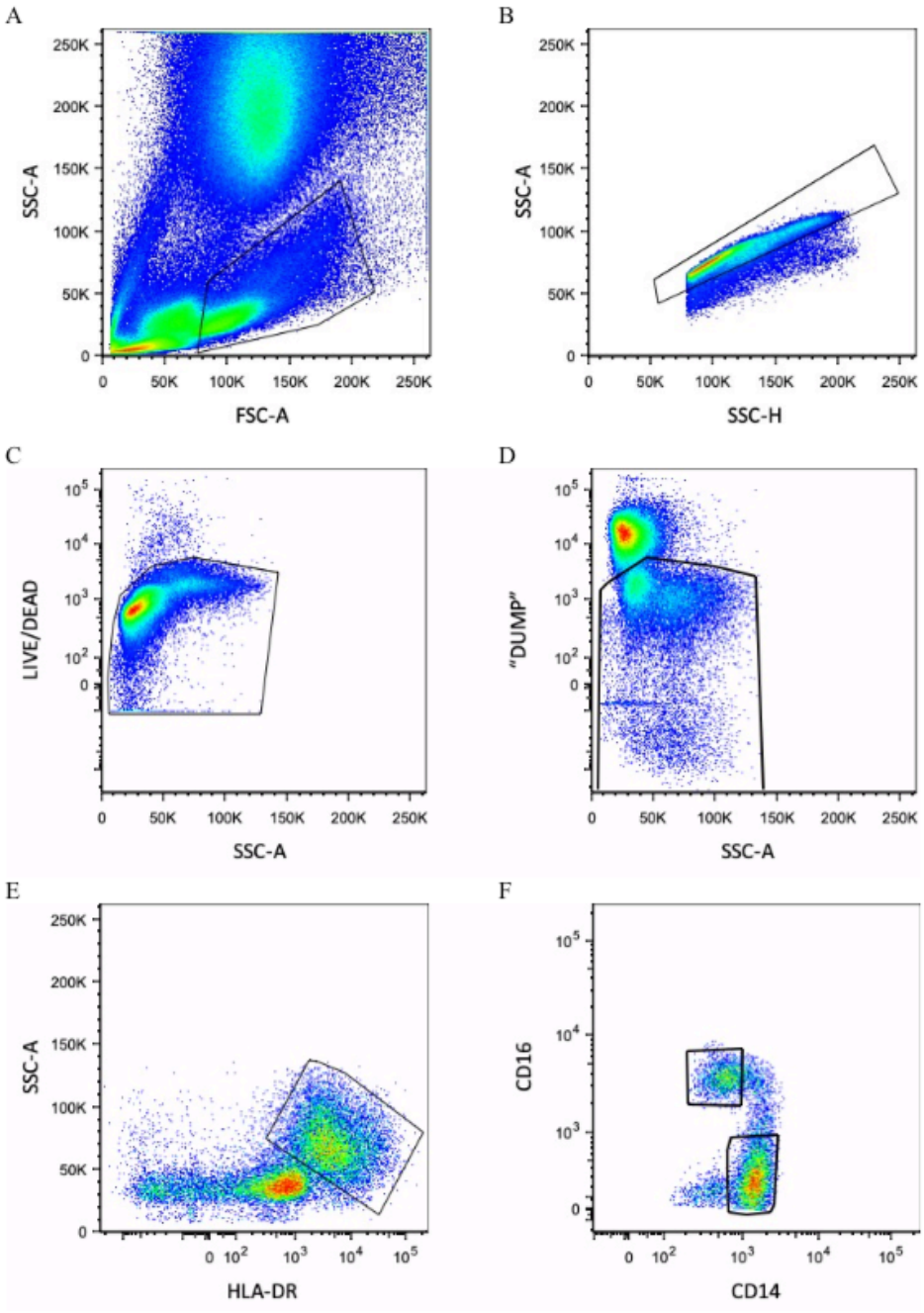

Figure 13 Sorting strategy for human Mo populations *(A) Selection of Mo based on size (FSC) and granularity (SSC) (B) Exclusion of doublets (C) Exclusion of dead cells D) Selection of dump- (CD3, CD19, CD56) cells (E) Selection of HLA-DR+ cells (F) Selection of classical* $CD14^{high}CD16^{low}$ *and non-classical* $CD14^{low}CD16^{high}$ *Mo subsets.*

3.6 **Bead isolation of monocytes**

For optimisation of ATACseq, blood was taken via venepuncture directly into BD Vacutainer® CPT™ Mononuclear Cell Preparation Tubes with Sodium Heparin (16x125 mm / 8ml, cat. no. 362753) which were centrifuged at 1800g for 20 mins at RT (5 brake/acceleration). Using a 5ml pipette, the first half of the plasma was pipetted off and discarded and the remainder gently pipetted up and down against the gel plug to dislodge cells stuck to the top of the gel. Vigorous pipetting was avoided as this would disintegrate the gel plug itself. The sample was transferred to a 50ml conical polypropylene tube and a 10µl aliquot of cell suspension was used for counting while the sample was centrifuged at 400g for 5 mins at 4˚C. Cells were re-suspended to ensure $1x10^7$ cells in 40µl of buffer (PBS, 0.5% w/vBSA) and the Miltenyi Biotec Pan Monocyte Isolation Kit, human (cat. no. 130-096-537) used: FcR receptors on cells were blocked with 10µl of FcR Blocking Reagent (Miltenyi Biotec Cat No 130-059-901), 10µl of Biotin-Antibody Cocktail added and samples incubated in the refrigerator (2−8 °C). After 5 mins, 30µl of buffer was added and the sample mixed prior to adding 20µl of Anti-Biotin MicroBeads, mixing well and incubating for 10 mins in the refrigerator (2−8 °C). Miltenyi MS Columns (cat. no. 130-042-201) were prepared by rinsing with 500µl of buffer and the cell suspension was added to the column with the flow-through of enriched Mo collected below the column. Columns were washed twice with buffer to ensure full yield.

3.7 **RNA**

For scRNAseq, cells were sorted as per protocol for blood sorts. To establish efficiency of single cell deposit into plates, Hoescht stained cells were sorted initially and quantified (See Appendix 9.2.9 Hoescht staining of monocytes) For scRNAseq, total Mo rather than subpopulations were sorted into low binding, conical 96 well non-skirted plates (Sigma, Cat No CLS3474-24EA) containing 2µl of lysis buffer (1.9ul of 0.2% Triton-X l00 vol/vol + 0.1ul of RNasin Plus RNase inhibitor (10,000 U, Promega) per well). Stocks of lysis buffer were made up on the morning of sorting and plates were pre-chilled at 4˚C and sorted at 4˚C. Immediately after sorting, plates were sealed with MicroAmp clear adhesive film and centrifuged at 300g at 4˚C. Plates were immediately transferred on dry ice to the lab of Dr. N Batada, (MRC Institute of Genetics and Molecular Medicine, Edinburgh, UK) for library preparation and sequencing.

For bulk RNAseq, cells were sorted into 1.5ml Eppendorph tubes and pelleted for 10 mins at 500g at 4˚C and re-suspended into 475µl TRIzol™ LS Reagent (Illumina,10296028) and immediately frozen in a dry ice and methanol bath and stored at -80˚C. Detailed methods for RNAseq libraries can be found in the Appendix section 9.2.10 Preparing dUTP RNA-seq libraries. Samples were sequenced on Next Seq 500 to a desired read depth of $10x10^6$ initially and $60x10^6$ for deeper sequencing.

3.8 **RT-qPCR**

Samples were sorted as per blood sorting protocol and gating strategy. Cells were pelleted at 500g and re-suspended in 350µl RNA Later (RLT) plus (Qiagen, Cat No 74004). For blood Mo, RNA was extracted using the RNeasy Micro Kit (Qiagen, Cat No 74004) and quantified on the NanoDrop™ One/OneC Microvolume UV-Vis Spectrophotometer. To make cDNA the Superscript VILO cDNA Synthesis Kit (Invitrogen, Cat No11754-050) was used. A list of primers is provided in the Appendix section 9.1.3. Primers for qPCR. qPCR was undertaken using a non-skirted 96 well plate (ThermoFisherScientifc, Cat No AB0600) on the ThermoFisherScientifc QuantStudio5 PCR machine. Detailed sample preparation methods for all methods can be found in the Appendix section 9.2 Detailed protocols.

For all primers, Bone Marrow Derived Macrophages (BMDMs) were used to assess the melting curve. At first triplicates were used for all experiments in case of pipetting error but CTs were either identical or differed by no more than 0.05CTs between all triplicates and so it was decided that duplicates were adequate. Duplicate H_2O controls were added to every experiment for each gene to ensure no contamination was present. BMDMs for these methods were provided by Demi Brownlie of the Pollard Laboratory. Cultured BMDMs were washed and placed in RLT and RNA was extracted using the RNeasy Mini Kit (Qiagen, Cat No74104).

Initially, GAPDH was used as the reference gene. However, on further investigation and reviewing the literature, this was found not to be the best reference for Mo as it was reported that the levels are not stable in Mo (Piehler et al. 2010). This was confirmed on reviewing the RNAseq data and observing that levels of GAPDH were not uniform across the cancer nor control samples. Therefore, SDHA was used as the reference gene for all quantifications shown. The delta-delta CT method was used to calculate relative expression of genes.

3.9 **ATACseq**

A total of $50x10^3$ Mo were sorted. Samples were washed with PBS and centrifuged at 500g at 4˚C for 5 mins. All supernatant was removed, and samples were re-suspended in 47.5µl of lysis buffer and 2.5µl of Tn5 enzyme (in NEXTERA DNA Sample Prep Kit, Illumina, Cat No FC-121-1030) was added. Samples were incubated at 37˚C and agitated at 600 rpm for 30 mins. To stop the reaction and purify the DNA, the ChIP DNA Clean and Concentrator capped Zymo-Spin kt was used (Cambridge Scientific, Cat No D5205). DNA was amplified using the Nextera Primer Ad1 and a unique Ad2.n barcoding primers using NEBNext High-Fidelity 2X PCR MM for 8-12 cycles. PCR reactions were purified using 1.5 volumes of SpeedBeads in 2.5M NaCl, 20% PEG8000, size selected using TBE gels for 160 – 280bp and DNA eluted. Detailed methods for ATAC libraries can be found in the

Appendix section 9.3.1. Preparation of ATACseq samples and libraries. Samples were sequenced on Next Seq 500 to a desired read depth of $20x10^6$.

3.10 **Statistics**

All analysis was performed on Graph Pad Prism software. The unpaired t-test was used to compare control and cancer groups. For comparison of multiple time points from kinetic data for one animal, a multi paired t-test was applied. To assess for outliers both Grubbs and the modified ROUT algorithm were used (Motulsky & Brown 2006).

3.11 **Bioinformatics**

3.11.1 Mapping

Mapping was undertaken by colleagues Dr. Zhengyu Ouyang and Dylan Skola at University of California San Diego (UCSD). The reference genomes from the UCSC genome browser were used: For C57BL/6J the mm10 and for human samples the hg38 reference genome. Data was mapped to custom genomes using STAR (Dobin et al. 2013) with default parameters. ATAC-seq data was mapped to custom genomes using bowtie2 (Langmead & Salzberg 2012) with default parameters. Data analysis was undertaken on the Epiglass

server, with thanks to Professor Chris Glass at UCSD for continued access. Further analysis was undertaken by Miss Amy Robinson using HOMER (Heinz et al. 2010) available at http://homer.ucsd.edu/homer. Throughout analysis the reference genome for commands was set at mm10 or hg38 for mouse and human samples respectively.

3.11.2 RNAseq

All samples were assessed for quality using the FastQC (Babraham Bioinformatics, 2010) package with MutliQC (Ewels et al. 2016). Unique mapping rates and read depths were checked with a cut-off of 90% minimum uniquely mapped reads and $>20x10^6$ total read depths unless otherwise specified. Additionally, correlation between samples and clonality were checked across all samples and all samples were visually inspected on the UCSC genome browser (Krämer et al. 2013).

Adapter trimming was undertaken using homerTools trim. To generate both raw and normalised count files, HOMER command “analyzeRepeats” with the following parameters was used: -rna, -condenseGenes (only reports one locus per isoform), -count exons -normMatrix (normalises the total of number of reads found in the gene expression matrix i.e. normalise total reads in mRNAs rather than all RNAs) -rpkm (report normalized values as reads per kilobase per million mapped reads). Differential gene expression (DGE) was assessed

with DESeq2 package with False discovery rate <- 0.05 and betaPrior = TRUE. Data visualization was undertaken in R studio. For average expression and log fold change (LFC) visualisation, LFC shrinkage using alpegm method was used. Pathway analysis was undertaken using Metascape (Barter & Bin Yu 2018; Zhou et al. 2019) available at http://metascape.org/gp/index.html. To convert mouse genes to human orthologues the R package g:Orth (Reimand et al. 2007) was used with the following command line:

```
orth=gorth(rownames(mousedf), source_organism = "mmusculus", target_organism = "hsapiens", region_query = F, numeric_ns = "", mthreshold = 1, filter_na = T, df = T)
```

As there are multiple orthologue matches, the genes with the highest variance were selected.

3.11.3 ATAC-seq

All ATACseq samples were trimmed to 35bp. All samples were assessed for quality as for RNAseq with additional steps to quantify the percentage of tags that occurred within peaks as a measure of noise within the sample.

For the optimisation of the lysis buffers analysis carried out using HOMER: To identify open chromatin or peaks the HOMER command “findPeaks” was used with the style set to factor and a size of 200bp. To identify the number of open chromatin peaks, peak files were merged using HOMER command “mergePeaks” with a set distance of 200bp and peaks were then annotated

using the HOMER command “annotatePeaks.pl”. To identify motifs the HOMER command “findMotifsGenome.pl” was used on the peak files. Samples were compared for tag density within peaks and motif enrichment.

For analysis of samples from the cohort of controls and cancer patients, the irreproducible discovery rate (IDR) and DEseq2 methods were used. In brief: samples were grouped into 4 as: CD14 CANCER, CD14 CONTROL, CD16 CANCER, CD16 CONTROL. Within each group all samples were processed as above to find peaks, merge peaks and annotate peaks. The correlation of tags in peaks between all samples in each group was analysed and the two best replicates for each group selected. Replicates were subjected to IDR to define peaks (Li et al. 2011). Each sample in each group was quantified against the respective IDR peaks and differential peaks discovered using DEseq2 (Love et al. 2014). For each group enriched peaks were checked for motifs using HOMER “findMotifsGenome.pl” and comparing against both a genome wide background and the background peaks generated for all the samples included in the DEseq2 analysis.

Chapter 4 Results: Monopoiesis in MMTV-PyMT mouse models of breast cancer

4.1 Introduction

In humans, an increase in non-classical Mo in cancer has been observed (Cassetta et al. 2019). However, the kinetics of this change has not been characterised. Nor is the function of different Mo populations in human cancer clear. It is not feasible to follow Mo dynamics during the natural evolution of breast cancer in patients. In lieu of being able to observe this in humans, mouse models provide an alternative.

An increase in the myeloid populations and the potentiation of BM progenitors in FVB PyMT late tumour bearing mice has been reported (Casbon et al. 2015). It is also known that Mo are mobilised from the BM and recruited to tumours (Qian et al. 2011; Arwert et al. 2018; Franklin et al. 2014). Recruited Mo are a contributor to cancer progression (Qian et al. 2011). It is known that myeloid cells expand in the FVB PyMT mouse model (Casbon et al. 2015). In this model, the expansion of Neuts has been explained by alterations in BM progenitor populations (Casbon et al). But, the release and half-life of Mo was not assessed, and the contribution of this towards Mo kinetics in cancer is not known.

With regards to other myeloid compartments in cancer, following myocardial infarction Mo are rapidly mobilised from the spleen (Swirski et al. 2009; Leuschner et al. 2012). Additionally, Mo progenitors have been reported in the spleen (Leuschner et al. 2012). Yet, the dynamics of splenic Mo in cancer are not known.

An objective of the PhD was to ascertain if, in mice, Mo populations were perturbed during cancer development and if so, when and how this occurs. The timing of any perturbance would then inform when to undertake RNAseq of Mo in mice. Given the advantages of using a spontaneous model which best reflects human cancer evolution and the advantages of the allograft system, both the spontaneous and allograft MMTV-PyMT models were considered.

4.2 **Allograft model of breast cancer**

To establish the allograft technique and to assess tumour engraftment and growth, late stage tumours were transplanted to 4 recipient mice and 1 sham operation was performed. Tumours were palpable by 14 days and at 21 days were growing but regressed by 28 days (Figure 14, A). On palpation of the tumours, a cystic nature was evident. This was confirmed at termination. There was no difference in Mo between cancer and sham mice (Figure 14, B).

Though it was not conclusive why cysts had developed, the advanced nature of the donor tumour was identified as a possible factor, as well as the area of the tumour harvested. To avoid the central necrotic tumour zone, the periphery of the tumour was selected. But this area has a high density of collagen and is relatively fibrous. It was reasoned that by using early stage tumours, engraftment may be better. Thus, to try and achieve better grafting of tumours, the experiment was repeated but tumours were harvested from mice with newly palpated tumours.

A total of 6 mice were allografted with early tumour fragments and 6 mice underwent a sham procedure. Tumours were first palpable by 28 days after the operation and progressed without evidence of any cysts or regression (Figure 14, A). Tumours reached the maximum permitted size of 12mm by day 42 in 5 of the mice and day 35 in 1 mouse. Tumour histology confirmed the presence of invasive disease reflective of the PyMT model.

Quantification of total Mo over the course of tumour development revealed no significant increase in blood Mo over the time course of the experiment (Figure 14, C). On day 28, there was a significant increase in Mo ($p = 0.0275$, unpaired t-test) but this was not sustained once tumours developed further and was not significant when multiple t-test adjustments were made. There was no increase in Neuts (Figure 14, D). There was no alteration to the distribution of Mo

populations at any time point (Figure 14, E). Thus, no perturbations to Mo could be shown in the allograft MMTV-PyMT model on a C57BL/6 background.

An additional model was trialled concurrently using orthotopic injection of the MET1 cell line into the mammary fate pad. Unfortunately, while the injections and tumour development were non-problematic, the data acquired by flow cytometry was of very poor quality and therefore is not presented.

Both the allograft and MET1 models were suspended and it was decided to characterise Mo dynamics during tumour development in the spontaneous MMTV-PyMT model in C57BL/6 mice.

4.3 **Spontaneous MMTV-PyMT model**

There was a gradual increase in Mo numbers as mice aged, but this was more pronounced in PyMT+ve mice (Figure 15, A). As mice developed tumours at variable ages (mean 18, range 16-24 weeks) it is more useful to stratify mice according to tumour stage; early tumour (time at which tumours were first palpable) or late tumour (~20mm). This demonstrated that there was a doubling in Mo numbers by late tumour stage (mean number of Mo in 50µl blood was $18x10^3$ and $38x10^3$ in control and mice with late stage tumours respectively) (Figure 15, B). There was no difference in the ratio of Mo subpopulations (Figure 15, C).

There was a significant increase in blood Neuts (Figure 15, D). This preceded the rise in Mo and was more profound, with a doubling at early stages and a 3.5-fold increase by late stage disease (in control and cancer mice respectively the mean number of Neuts in 50µl blood for early stage tumours was $10x10^3$ and $22x10^3$ and for late stage $24x10^3$ and $84x10^3$). By late stage there was an overall increase in the total number of cells in the blood of tumour bearing mice (Figure 15, E). The increase was restricted to the CD11b+ populations (Figure 15, F).

Both Mo and Neuts increased with age in both the PyMT-ve and PyMT+ve mice. For simplicity the comparison is not shown on Figure 15, but this was significant. For both the Mo and Neuts, the difference between cancer-cancer at each stage was more significant than the difference between control-control at each stage (multiple t-test results: early-to-late for cancer Mo q.value=0.00017, early-to-late for control Mo q.value=0.00193, early-to-late for cancer Neuts q.value=0.00001, early-to-late for control Neuts q.value=0.001005).

While there was a greater change in Neuts, the understanding of Mo in particular was related to the principal aims of the PhD. Additionally, Neut dynamics had been relatively well characterised (Casbon et al. 2015) and therefore was less novel. Hence, the Mo expansion in the spontaneous C57BL/6 PyMT model remained the focus of subsequent work undertaken.

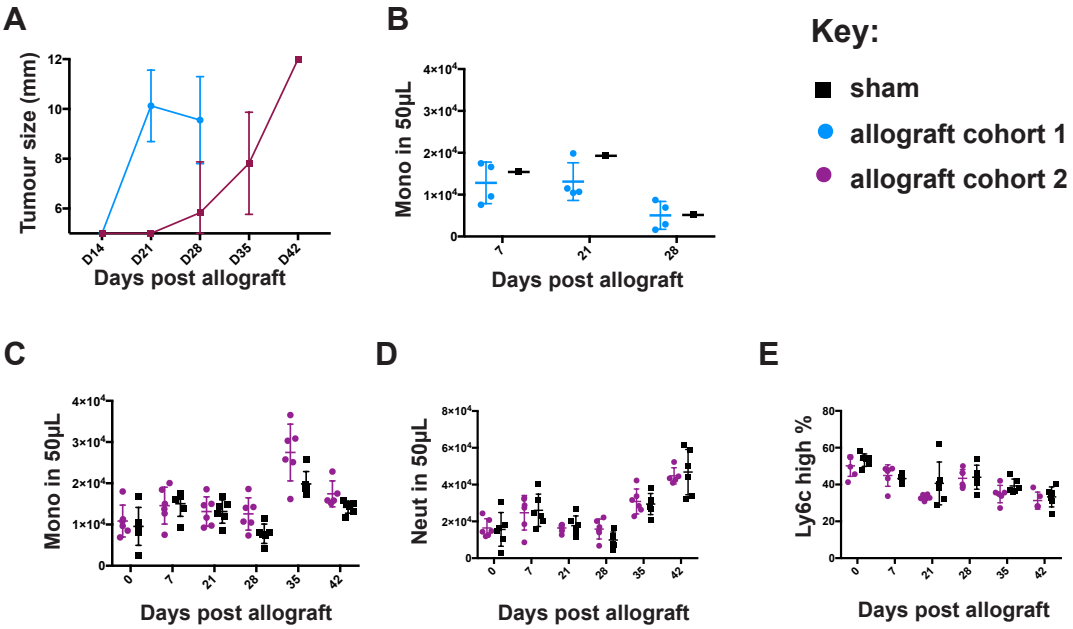

Figure 14 Tumour growth and myeloid populations during tumour development in the allograft PyMT model on C57BL/6 background *(A) Tumour growth in mice transplanted with late stage tumours (n=4, shown in blue) and early stage tumours (n=6, shown in plum) (B) Total blood Mo in mice transplanted with late stage tumours (n=4) or sham (n=1) (C-E) Mice transplanted with early stage tumours or sham (C) Mo in 50µl of blood (D) Neuts in 50µl of blood (E) Ly6c^{high} Mo as % all blood Mo. As detailed in the key, samples in blue were from the first cohort and samples in plum are from the second cohort. All shams are in black. No statistically significant difference between cancer or sham by multiple t-test. Experiments were conducted in co-housed groups of n=5 (4 late tumour fragments, 1 sham) in cancer cohort 1 and n=12 (6 early tumour fragments, 6 sham) in cancer cohort 2. For (C-D) there is no data for one sample at day 42 as the tumour reached the maximal permitted size (12mm) by day 38.*

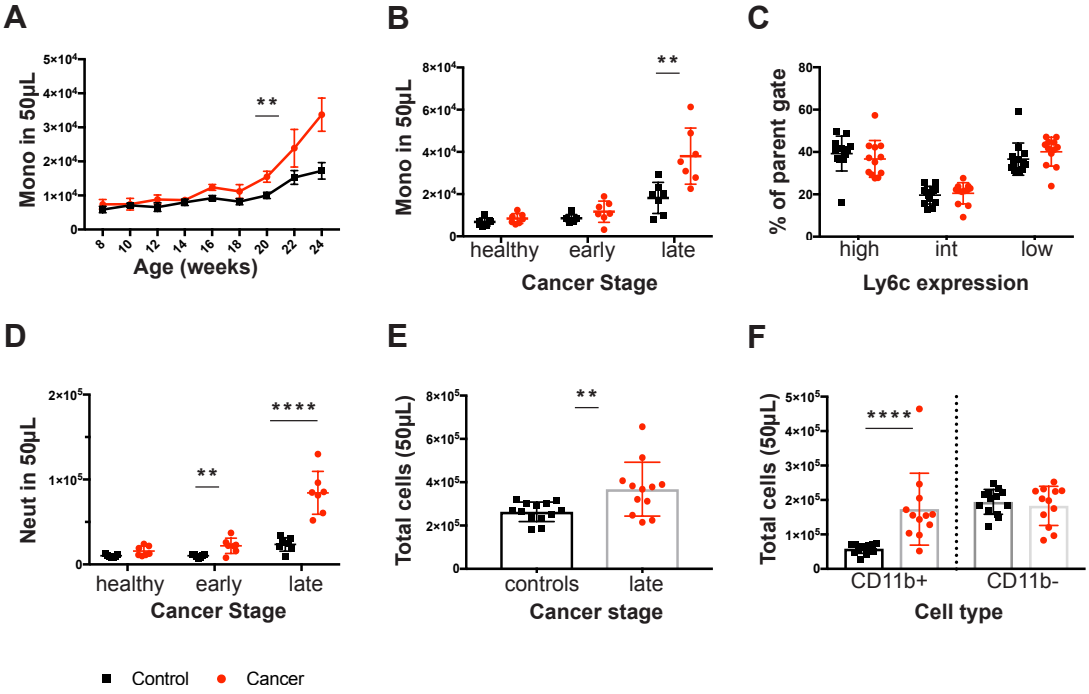

Figure 15 Blood composition in PyMT+ve versus PyMT-ve C57BL/6 mice

*(A) Total blood Mo according to age (weeks) during spontaneous PyMT tumour model. Not significant (multiple t-test) (B) Total circulating Mo prior to tumour development (healthy), at onset of tumours (early) and at late stage ~20mm tumour (late) (C) % of Mo subpopulations comparing at late stage (D) Total Neuts prior to tumour development (healthy), at onset of tumours (early) and at late stage ~20mm tumour (late) (E) Total blood cells in 50µl at late stage (F) Total number of CD11b+ and CD11b- cells at late stage. Cancer samples are shown in red and age-matched controls in black. * p value <0.05, ** p value <0.01, *** p value <0.001, **** p value <0.0001, multiple t-test. Experiments were conducted in duplicates with littermate and co-housed groups of n=6 (3 PyMT+ve) and n=8 (4 PyMT+ve) in each replicate.*

4.4 **Establishing the role of bone marrow progenitors**

To firstly assess if Mo progenitors were altered by cancer, data from sorts for CFU assays was analysed. Mice with late stage tumours were compared with littermate controls. Total BM cell counts were not accurate for all samples and therefore estimated cell numbers are not provided. Results are expressed as the proportion of live cells. CD11b+ cells were increased and there was a reciprocal decrease CD11b- cells in the BM of mice with cancer (Figure 16, A). The ratio of Mo and Neuts remained the same (Figure 16, B), implying an overall increase in BM myeloid populations. There was no difference in cMoPs, MDPs or LK cells (Figure 16, C).

On isolation and culturing of cMoPs, MDPs and LK cells, there was no difference in the total number of colonies formed in cancer (Figure 16, D). The proportion of different types of colonies formed from LK cells was unaltered in cancer (Figure 16, E). To assess this further CMP, GMP and MEP populations were analysed by flow cytometry. There was no evidence of shifts in the distributions of the CMPs, GMPs or MEPs (Figure 16, F).

To explore the most-primitive BM progenitors, the LSK compartment was analysed. For these experiments, total BM cells were quantified and were not increase in cancer (Figure 17, A). There was a 2-fold increase in the LSK fraction of the BM from 2.1% (± 0.4) in control mice to 5.0% (± 0.6) in cancer bearing mice (Figure 17, B). Calculating the actual number of LK and LSK cells

demonstrated that the LK cells were not increased (Figure 17, C). In the LSK fraction there was a trend towards increased actual numbers in cancer, with a mean of 9000 (± 2033) and 15236 (± 3172) in controls and cancer respectively. But this was not statistically significant. Within the LSK fraction of BM the distribution of progenitor subsets was significantly altered (Figure 17, D). Estimating the actual number of cells, both HSPCs and Flt3- LMPP cells were significantly increased in cancer (Figure 17, E).

To be able to estimate the total BM Mo and Neuts, data provided by Dr. Agnieszka Swierckzak (Prof. J Pollard lab, Edinburgh) was analysed. BM samples were compared in C57BL/6 PyMT mice with late stage tumours and age-matched controls. There was no increase in the total number of cells within the BM of late tumour bearing mice (Figure 18, A). Within the CD45+ compartment, as assessed by the proportion of live cells, there was an increase in Mo and Neuts and a reciprocal decrease CD11b- cells in cancer (Figure 18, B-C). But the estimated frequency of Mo or Neuts did not reach statistical significance (Figure 18, D). Applying Grubbs method, 1 control sample was identified as an outlier (Figure 20, E). Using the ROUT algorithm 3 outliers were identified (Figure 18, E). Using either of these methods resulted in significant increases in the estimated number of both Neuts and Mo in the BM in cancer. For transparency all results are reported.

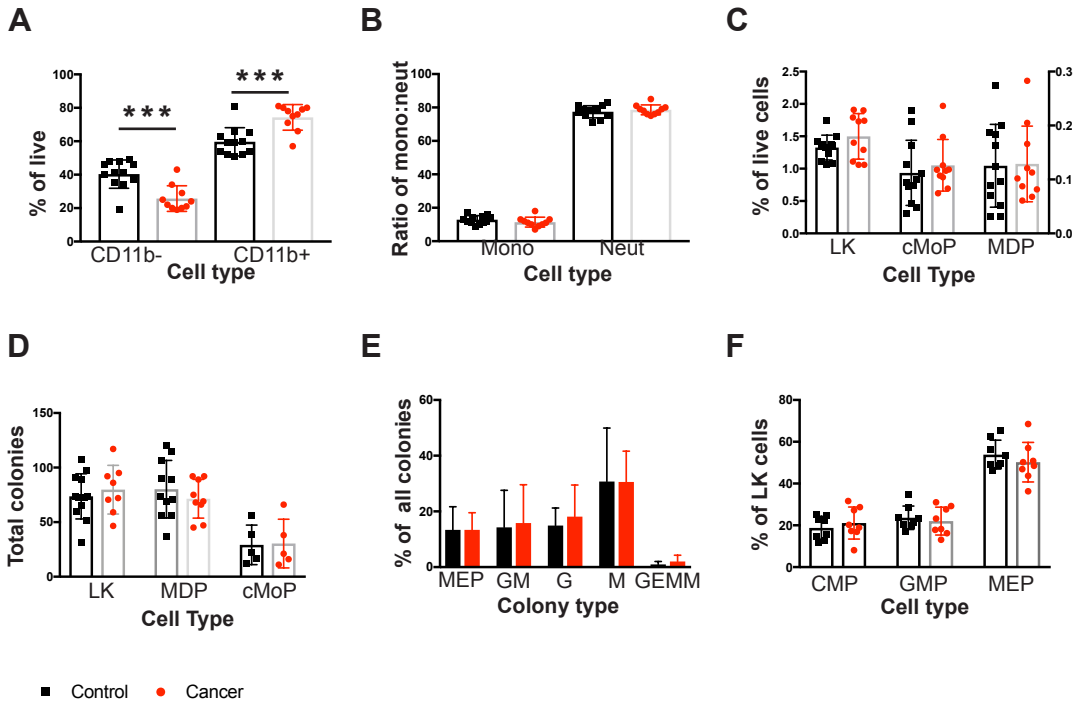

Figure 16 Analysis of BM sorts and CFU assays in C57BL/6 mice with late cancer or age-matched controls *(A) Proportion of CD11b- and CD11b+ cells within the BM shown as a % of live cells (B) Ratio of Mo and Neuts within the BM (C) Proportion of LK, cMoP and MDP cells within the BM shown as a % of live cells (D) Total colonies in CFU assays from LK cells, MDPs, cMoPs (E) Distribution of colony types within the LK CFU assays. (F) Analysis of LK cell progenitors; CMP, GMP and MEP as a % of LK cells. Late cancer samples are shown in red and age-matched controls in black. Isolated progenitors were cultured in methocellulose medium for 12-14 days and the number of colonies present were quantified. *** p value <0.001, unpaired t-test. For LK cells sorts conducted on 3 days in triplicates of co-housed littermate groups of n=4 (2 cancer), n=11 (4 cancer) and n=5 (2 cancer). For MDPs sorts conducted on 3 days with co-housed littermate groups of n=6 (3 cancer), n=4 (2 cancer) and n=10 (5 cancer). For cMoPs sorts were conducted on 1 day with n=10 (5 cancer). For (F) experiments were conducted in triplicates of co-housed littermate groups of n=6 (3 cancer), n=4 (2 cancer) and n=6 (3 cancer).*

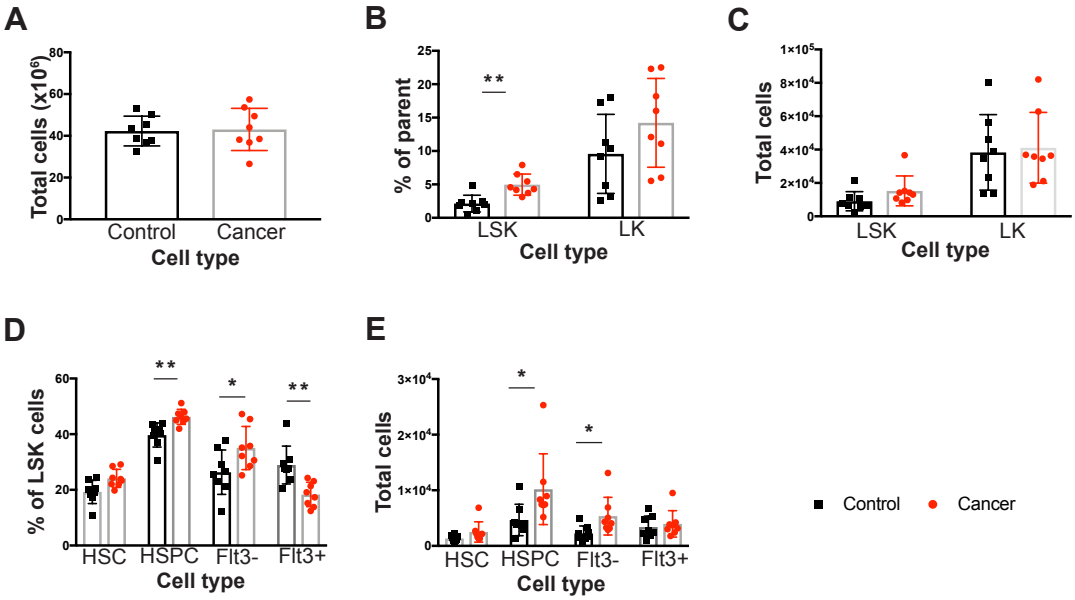

Figure 17 Perturbations to BM progenitors in C57BL/6 mice with late cancer or age-matched controls *(A) Total cells per two femurs (B-C) LK and LSK cells (B) as % of parent (C) estimated total cells (D-E) HSCs, HSPCs, Flt- MPP and Flt3+ MPP (D) as % of parent (E) estimated total cells. Late cancer samples are shown in red and age-matched controls in black. * p value <0.05, ** p value <0.01, unpaired t-test. For (D-F) Experiments were conducted in triplicates of co-housed littermate groups of n=6 (3 cancer), n=4 (2 cancer) and n=6 (3 cancer).*

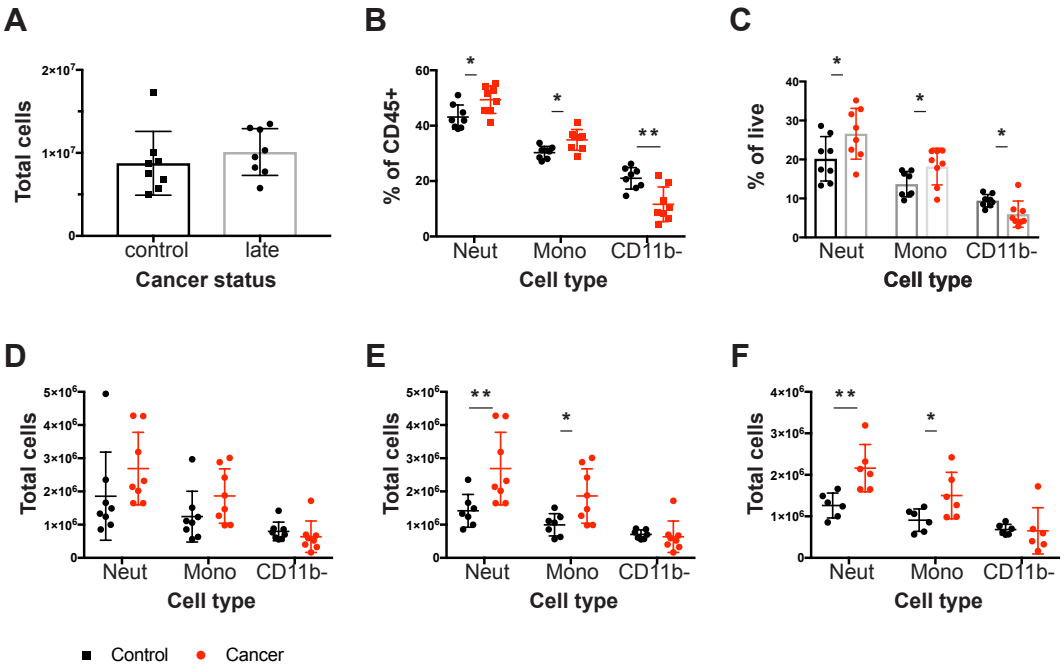

Figure 18 Quantification of BM populations in C57BL/6 mice with late cancer or age-matched controls using alternative data. *Data courtesy of Dr. Agnieszka Swierckzak (A) Total cells flushed from 1 femur (B-C) Neuts, Mo and CD11b- cells as (B) % of CD45+ cells (C) % of live cells (D-F) Estimated total Neuts, Mo and CD11b- cells (D) All data point (E) Outliers removed by Grubb's (F) Outliers removed by ROUT. Late cancer samples are shown in red and age-matched controls in black. * p value <0.05, ** p value <0.01 multiple t-test. Outliers removed using Grubb's and ROUT method in Prism. Experiments were conducted in duplicates of co-housed littermate groups of n=4 (4 cancer).*

4.5 Effects of cancer on monocyte egress, half-life and proliferation

Because the changes observed in BM progenitors were not considered sufficient to explain the increase in blood Mo, it was hypothesised that Mo were being released more rapidly from the BM or that half-life within the blood was increased in the context of cancer.

To test this hypothesis, mice with late stage tumours or age-matched controls were injected with BrdU and blood Mo were tracked by BrdU levels in each population at 1hr, 24hrs, 72hrs, 96hrs, 7 days and 10 days (Figure 19). At 1 hr there were no BrdU+ cells in the blood confirming that proliferation of Mo does not occur in the blood in cancer (or steady-state). There was no difference in the level of BrdU+ Mo between control and caner at any time-point.

Because the altered release and half-life of Mo was not a mechanism whereby Mo were perturbed in this cancer model, it was hypothesised that proliferation of BM Mo may be a contributing factor. To test this, mice with late stage tumours and control mice were injected with BrdU and culled at 1hr to assess BrdU levels in BM Mo.

There was no difference in the incorporation of BrdU between cancer and control in the LSK or LK cells as a whole, the GMPs, MDPs or the cMoPs

(Figure 20, A). However, in cancer there was a significant increase in the frequency of BrdU+ ly6c^{high} Mo in the BM (Figure 20, B).

4.6 **Contribution of the spleen to monopoesis**

It was hypothesised that monopoiesis in the spleen may be contributing towards the increased circulating Mo observed. The observation of splenomegaly in mice with late stage cancer further supported this. There were two principal questions, firstly is the spleen a reservoir for Mo and secondly are there any MDPs as evidence to support a hypothesis that extramedullary splenic monopoiesis contributes to the monopoiesis in late stage cancer.

To address these questions, spleens were harvested 1hr post BrdU injection. Because gradient separation was used to isolate the mononuclear cells (T cells, B cells and Mo), these are termed collectively as splenic Mononuclear Cells (MCs). There was a 1.66-fold increase in the weight of spleens from late tumour bearing mice compared with age-matched controls (Figure 21, A). There was a 2-fold increase in total splenic MCs in cancer with a mean of 52x10^6 (± 7) and 100x10^6 (±11) in control and cancer respectively (Figure 21, B). Adjusting for weight, there was no difference between cancer and controls (Figure 21, C). Ly6c^{high} Mo formed a greater proportion of live cells in cancer versus control (Figure 21, D). Estimating the actual number of Ly6c^{high} Mo indicated that there was a significant increase in splenic Ly6c^{high} Mo in cancer (Figure 21, E).

To assess the splenic MDPs, the criterion previously described by Fogg et al (Fogg 2006) was used. No splenic MDPs were detected in any control mice nor in tumour bearing mice. Returning to the paper by Leuschner et al that had demonstrated splenic MDPs post MI, the gating strategy was more lenient, having CD117 but not CD135, which is crucial to distinguishing cMoPs from MDPs (Fogg 2006). Re-analysing with this less stringent gating, there was a population of $CD117^{high}$ cells present (approximately 0.02% of all live splenic MCs) but they were not significantly altered in cancer.

Finally, to assess if Mo were proliferating in the spleen, BrdU levels were assessed. There was no proliferation of the $Ly6c^{low}$ Mo/macrophage population. There were BrdU+ cells in the spleen, but these were non-myeloid cells (Figure 21, F). There was no difference in the splenic $Ly6c^{high}$ Mo BrdU levels in cancer versus controls, with very low levels overall (1-2% BrdU+).

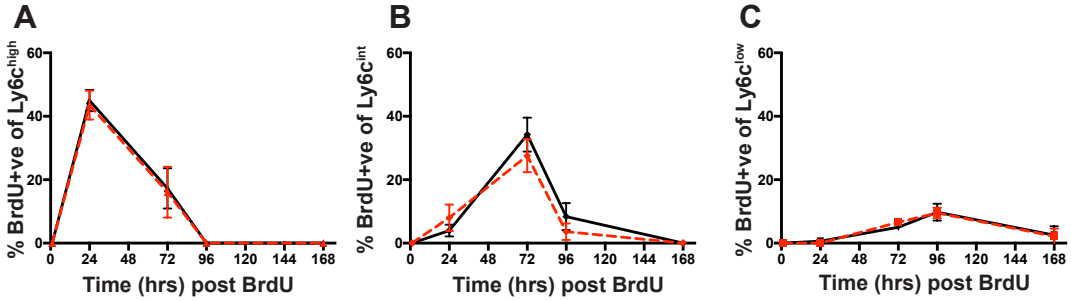

Figure 19 BrdU tracing of blood Mo and level of proliferation in the BM of C57BL/6 mice with late cancer or age-matched controls. *Level of BrdU+ circulating Mo within each population over time (A) Lyc6^{high} (B) Ly6c^{int} (C) Ly6c^{low}. Late cancer samples are shown with a red dashed line and age-matched controls with a solid black line. No significant difference by multiple t-test or by unpaired t-test at each time point. Experiments were conducted in duplicates of co-housed littermate groups of n=6 (3 cancer).*

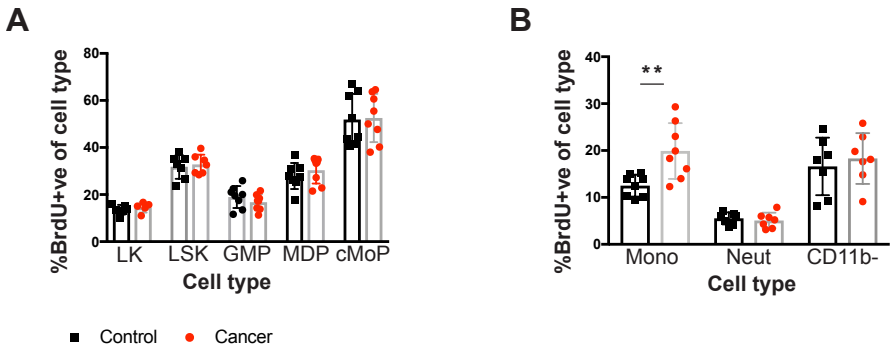

Figure 20 BrdU levels in the BM 1hr post injection in C57BL/6 mice with late cancer or age-matched controls *(A) LK, LSK, GMP (LSK, CD115^{low}), MDPs and cMoPs (B) Mo, Neuts and CD11b- cells. For each value the % of BrdU+ve cells of the stated cell type is given. Late cancer samples are shown in red and age-matched controls in black. ** p value <0.01, unpaired t-test. Experiments were conducted in triplicates of co-housed littermate groups of n=6 (3 cancer), n=6 (3 cancer) and n=4 (2 cancer). In one sample staining for BrdU was not fully saturated and has been excluded.*

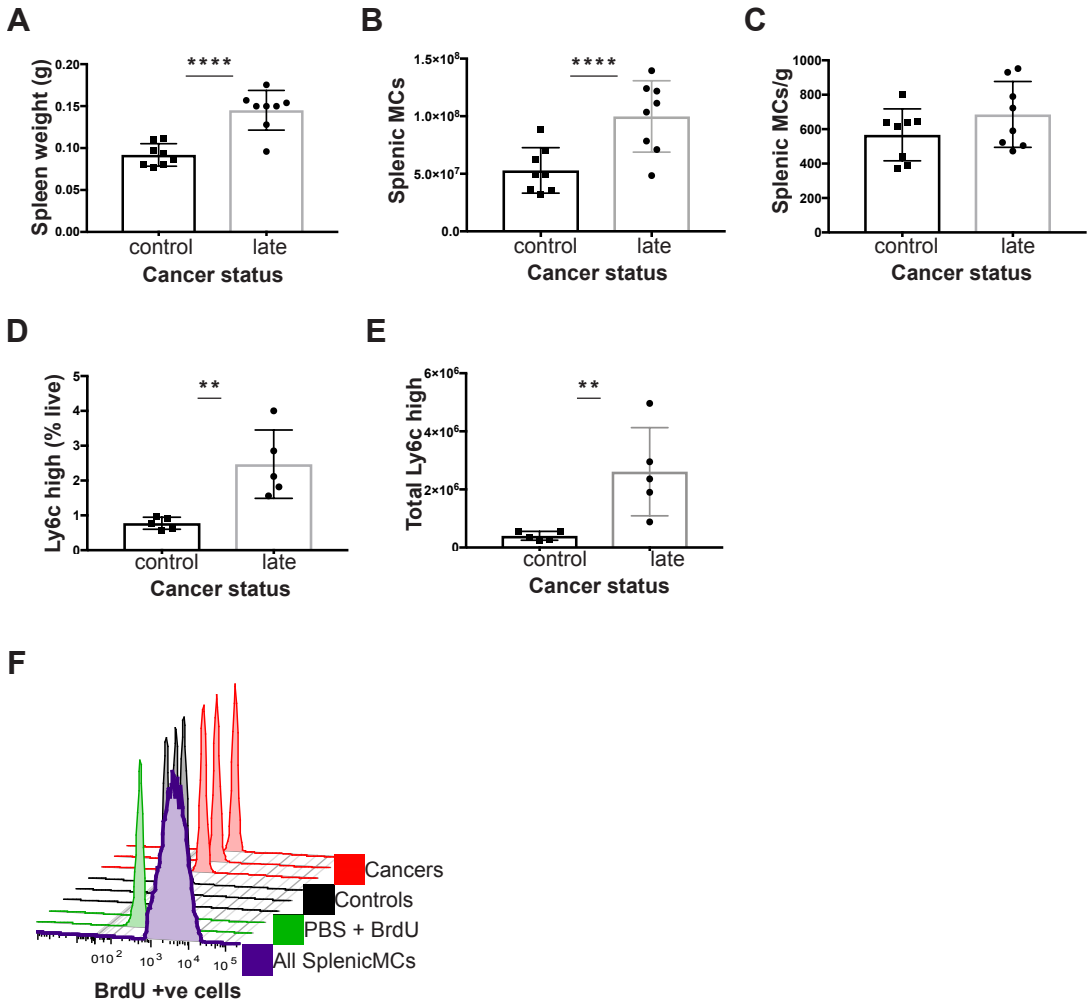

Figure 21 Characterisation of the spleen in C57BL/6 mice with late cancer or age-matched controls *(A) Splenic weight (B) Total splenic MCs (C) Total splenic MCs normalised to splenic weight (D) Ly6c^{high} Mo as % of live cells (E) Total Ly6c^{high} Mo in spleen (F) Histogram of splenic BrdU levels in: all Splenic MCs in spleen (purple), PBS with no DNase control (green), Ly6c^{high} Mo from controls (n=3, black) and Ly6c^{high} Mo from late cancer mice (n=3, red). ** p value <0.01, **** p value <0.0001, unpaired t-test. Experiments were conducted in duplicates of co-housed littermate groups of n=6 (3 cancer) and n=4 (2 cancer). The term Splenic MCs refers to the splenic mononuclear cells (T cells, B cells, Mo) from gradient separation.*

4.7 **Discussion**

The aim of this work was to characterise the Mo kinetics in the context of breast cancer in both the allograft and spontaneous C57BL/6 PyMT-MMTV models. While it was possible to demonstrate a significant monopoiesis in C57BL/6 PyMT mice with late stage tumours, this was not shown in the allograft model. Thus, it was not possible to repeat the findings of Casbon et al, where the allograft model was undertaken using FVB mice (Casbon et al. 2015). While this could be due to strain differences as C57BL/6 are known to be more tumour resistant than FVBs (Lifsted et al. 1998), it could also be due to discrepancies in the methods used.

Casbon et al used an epithelial reporter mouse to enable harvesting of pre-invasive in-situ disease (Casbon et al. 2015). While the late stage tumours in the spontaneous model resulted in monopoesis, this progressed as tumours developed. It may be that the early signals are required to potentiate the myeloid system. The early expansion of Neuts in cancer both here and in the literature would indicate that pro-inflammatory cascades commence early in the evolution of tumours in the MMTV-PyMT model (Casbon et al. 2015).

Because there were no epithelial reporter mice lines available in the breeding stocks and it was estimated that Importing this line would take ~6 months this model was abandoned. With hindsight, the decision to not invest further in the

allograft model was perhaps premature as the project thereafter would have benefited from using this system.

Given that work undertaken in the spontaneous transgenic PyMT FVB mouse model (Casbon et al. 2015), reported an increase in BM progenitors in cancer, it was hypothesised that this might explain the myelopoeisis in the C57BL/6 tumour bearing mice. Casbon et al found increases in the earliest stem cell progenitors, HSCs were less significant than in the downstream Flt3- LMPPs. The latter of which were the most significantly increased BM progenitor population in tumour bearing mice (Casbon et al. 2015). This agrees with the data here in the C57BL/6 mice. However, further downstream, there was no differential increase in the myeloid progenitors in the C57BL/6 mice. Whereas, in the FVB it was shown that the frequency of GMPs was increased, with no change to the frequencies of CMPs or MEPs (Casbon et al. 2015). In the experiments conducted in this PhD, the lack of altered proportions of CMP, GMP and MEPs, when LK cells were cultured using CFU assays, supports the flow cytometric analysis. Therefore, it is likely that the contrasting findings are due to differences between the FVB and C57BL/6 strains. Furthermore, there was no difference in the downstream progenitors of Mo, data not assessed by Casbon et al. It would be useful to repeat this experiment in the FVB strain, to ascertain whether the findings of Casbon et al can be repeated. This would enable conclusions to be drawn as to whether the contrasting findings here are indeed due to differences in the strains.

With regards to the release and survival of Mo, the peak of the Ly6c^{high} Mo in the blood by 48 hrs is consistent with data in steady state and in the context of PyMT tumours (Yona et al. 2013; Arwert et al. 2018). The loss of BrdU+ Ly6c^{high} Mo from the blood by 96 hrs is again consistent with previous published data using either BrdU or EdU tracing (Yona et al. 2013; Arwert et al. 2018). Previously, in steady state it was shown, both in mice and in humans, that Ly6c^{high} Mo differentiate into Ly6c^{low} Mo via an intermediary Mo (classical to non-classical respectively in humans) (Yona et al. 2013; Patel et al. 2017). From the BrdU tracing undertaken here, this transition seems to be unaffected by cancer. It is of note that while there was an increase in BrdU+ Ly6c^{high} Mo in the BM, this was not then reflected in higher levels of BrdU+ Ly6c^{high} Mo in the blood. Discrepancies in this may reflect marginated pools of monocytes that are unaccounted for within the data presented here. One consideration with regards to this conclusion is that Ly6c^{high} Mo recruited to the tumour are not accounted for. Using EdU tracing in PyMT allograft model Arwert et al found that from 72 hrs, EdU+ CD68+ TAMs were increasing and by 10 days ~80% of perivascular TAMs were EdU+ (Arwert et al. 2018). This coincided with the decline of EdU+ Ly6c^{high} blood Mo from their peak at 48 hrs to their disappearance at 96hrs. If the ratio of populations remains the same, then the same proportion of Ly6^{high} must convert to Lyc6^{low} Mo. If concurrently, Ly6^{high} Mo are intravasating from the blood stream into the tumour in the cancer mice only then there must be an excess of Ly6c^{high} Mo to fulfil both these conditions. Without knowing the exact proportions of Ly6c^{high} Mo that are recruited to the

tumour, that differentiate into Lyc6^{low} Mo or that undergo apoptosis, it is not possible to fully assess the effects of recruitment on the ratio of Mo. Furthermore, the marginated pool of Ly6clow Mo that may be attached to the endothelium are not assessed. Adding to the complexity of this, some argue that Lyc6^{low} Mo may be re-absorbed into the BM pool (Hamon et al. 2017). Tracing of Mo to the tumour and also of Ly6c^{low} Mo to the bone is hindered by the very low levels of these cells present in tissues. Without undertaking these tracing experiments, it is impossible to fully deduce the origin and fate of the Ly6c^{high} Mo and it should be noted that this may mask differences in the ratio of subpopulations of Mo presented here. Additionally, the spleen was shown to act as a reservoir for Mo but not to be a site of monopoiesis. The release of Mo from the spleen was not explored and thus how this contributes to circulating Mo populations is not known.

The combined findings of increased BrdU+ Ly6c^{high} Mo in the BM of tumour bearing mice and very little alteration to BM progenitor niches, nor BrdU tracing in the blood, would imply that increased Mo frequency is due to proliferation of Mo themselves rather than increased haematopoiesis or altered release and half-life. While this may be true, there are limitations to this interpretation. In agreement with findings in FVB mice (Casbon et al. 2015), Neuts were increased to a greater extent than the Mo in C57BL/6 mice with cancer. The BrdU results at 1hr for Neuts agree with findings in the FVB mice that show that the Neuts (unlike Mo) do not proliferate at high levels in the BM (Casbon

et al. 2015). However, an explanation for increased Neuts in FVB tumour bearing mice was provided by a corresponding increase in GMPs (Casbon et al. 2015). This was not a finding that was repeated in the work undertaken here in C57BL/6 mice. Nor was it found that there was an increase in total BM cells, again disagreeing with findings in FVB mice (Casbon et al. 2015). The use of outlier algorithms is contentious and thus it may be that the Neut BM frequencies are not actually increased in C57BL/6 mice with late stage tumours. Nonetheless, the blood Neuts are increased and there is currently no explanation for this within the data of this thesis.

Despite the caveats in the data, overall it would seem that there are systemic effects of cancer on Mo production in the BM. Hence, it is likely that the release of systemic growth factors in the context of cancer may explain the monopoiesis observed. The growth factor CSF1, is the main factor responsible for the expansion and survival of Mo (Stanley & Chitu 2014). Breast cancer cells are known to produce CSF1 and this in turn interacts with the CSF1-R on TAMs promoting survival and manipulating macrophage polarisation (Joyce & Pollard 2008). Levels of CSF1 in solid tumours also correlate with survival across a range of cancers, including breast cancer (Lin et al. 2002; Richardsen et al. 2015; Scholl et al. 1994). This has led to many new cancer trials exploring the use of anti CSF1 therapy (Cannarile et al. 2017).

In the MMTV-PyMT model specifically, it is known that CSF1 has a key role in the recruitment of TAMs to mammary tumours. Crossing the MMTV-PyMT with

the CSF1 null mutant ($CSF1^{op}$/ $CSF1^{op}$) mice, it has been shown that the loss of CSF1 does not alter the development of mammary hyperplasia or adenoma (Lin et al. 2001). But it greatly reduces the formation of advanced primary tumours and metastasis (Lin et al. 2001). While the levels of Mo were not measured in the blood of mice in these studies, the macrophage frequency within mammary tumours was greatly reduced (Lin et al. 2001). Additionally, overexpression of CSF1 via a transgene limited to the mammary epithelium, restored the progression of cancer in CSF1 null mutant mice (Lin et al. 2001). Relating this back to findings here, it is interesting that the role of CSF1 seems most relevant in the late stages of cancer as this is when significant perturbations to Mo were observed here.

However, recent research has placed the role of CSF1 directly on the Mo into question. Using both a doxycycline inducible CSF1-R system and a CSF1-R antagonist in a metastatic mouse model it was shown that while MAMs were reduced, circulating Mo and the Mo derived metastatic precursor cell for MAMs were unaffected (Kitamura et al. 2018). However, the treatments were limited to 1-week duration which could underestimate the effects of CSF1. Additionally, in FVB PyMT mice, CSF1 was elevated in mice with late stage tumours (Casbon et al. 2015). Thus, overall, there is a strong body of evidence to highlight CSF1 as a potential growth factor that may be causing the monopoiesis observed.

Expansion was not limited to Mo, but additionally observed in Neuts. GM-CSF, which potentiates generalised myeloid expansion, is known to be secreted by a range of tumours (Dougan et al. 2019). Both GM-CSF and CSF1 have been shown to increase the production of M-MDSCs in the BM of tumour bearing mice. Contradicting this, in the FVB PyMT model, no alteration to the levels of GM-CSF was detected, even in advanced disease (Casbon et al. 2015). Rather, G-CSF was elevated and shown to be responsible for Neut expansion in both the FVB PyMT (Casbon et al. 2015) and alternative models, such as the K14Cre;Cdh1$^{F/F}$;Trp53$^{F/F}$ (KEP) model (Coffelt et al. 2015). Thus, perhaps CSF1 and G-CSF are active in the expansion of the Mo and Neuts respectively. In FVB PyMT mice, G-CSF increases from the early stages of tumour development, but CSF1 is only elevated in late disease (Casbon et al. 2015). This agrees with observations here and in the literature that Neut expansion precedes Mo expansion (Casbon et al. 2015; Coffelt et al. 2015).

As it is known that chemokines regulate both the release of Mo from the BM and their recruitment to tissues it may be that chemokines also play an active role in the monopoiesis observed. Mo are recruited from the BM via the CCR2 (Serbina & Pamer 2006). The levels of expression of the CCR2-ligand, CCL2 within tumours is known to correlate with poor survival (Ueno et al. 2000). Previous work undertaken has demonstrated that the release of Ly6c^{high} Mo from the BM, into the blood and subsequent retention in the tumour is CCL2 dependent; TAMs are formed by CCR2+ Ly6c^{high} Mo recruited from the blood

(Qian et al. 2011; Arwert et al. 2018; Franklin et al. 2014). In these mouse models, either blocking CCL2 or using $CCR2^{-/-}$ mice impaired Mo recruitment and reduced TAM frequency, and ultimately stunted tumour progression (Qian et al. 2011; Arwert et al. 2018; Franklin et al. 2014). However, the effects of CCL2 on cancer is complex and while it is largely pro-metastatic, administration of neo-adjuvant anti-CCL2 can potentiate metastasis due to rebound effects on cessation of treatment (Bonapace et al. 2014; Kersten et al. 2017). Thus, it is important to consider that the effect of CCL2 is dependent on the primary and metastatic disease stage. Elevated levels of serum CCL2 have been found in late but not early tumour bearing FVB PyMT mice (Casbon et al. 2015). Recent evidence in non-metastatic breast cancer patients found that CCL2 is locally elevated in the tumour but is not systemically elevated in the blood (Cassetta et al. 2019). Interestingly, elevation in blood levels of CCL2 in mice seems to precede the elevation of CSF1 (Casbon et al. 2015). This may suggest a feedback loop is at play.

CCR2 can bind a number of other ligands, including CCL7, CCL8, and CCL12. These ligand can also form heterodimers, such as CCL2:CCL8 (Crown et al. 2006). There is evidence for CCL8 being important in tumour biology as it is known to be increased at the periphery of tumours and increases tumour cell intravasation (Farmaki et al. 2016). Again, the levels seem to be acting locally at the tumour site and seem not to be systemically elevated (Cassetta et al. 2019). It has recently been suggested that in breast cancer, TAMs secrete

CCL8 and that this subsequently leads to the recruitment of Mo (Cassetta et al. 2019) (Figure 22).

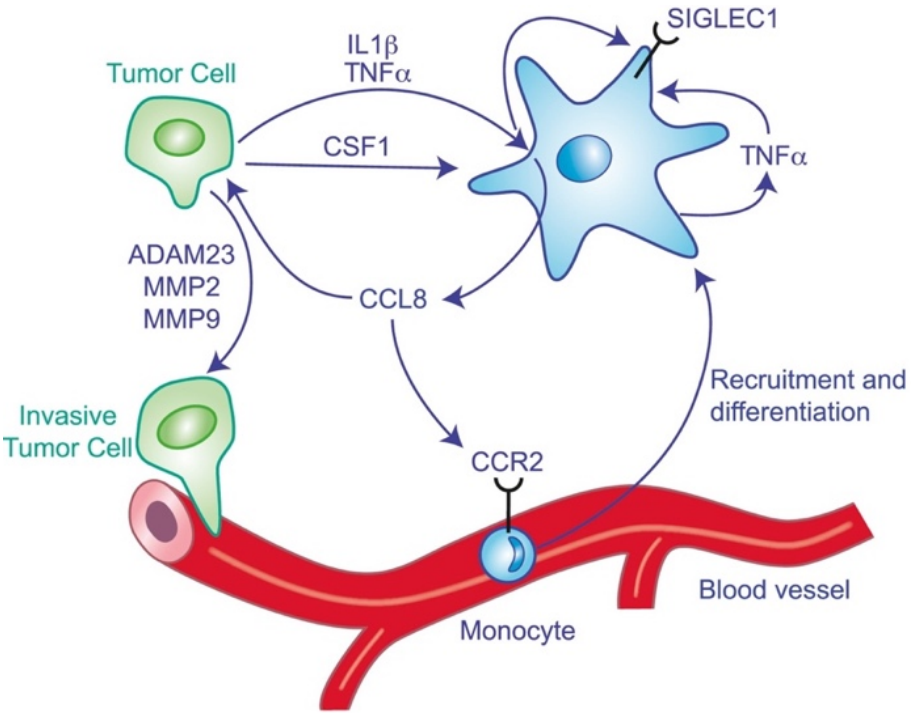

Figure 22 Schematic Representation of the Crosstalk between Br-TAM and Cancer Cells. *Tumor cells upregulate SIGLEC1, TNF-α, and CCL8 expression in Br-TAM. In turn, cancer cells respond to CCL8 stimulation by producing CSF1, IL-1β, and TNF-α, which further contribute to the positive feedback loop. Figure and legend used with permission from Cassetta, L. et al. 2019.*

Another candidate is the CCR1 and related ligands. In liver cancer mouse models using $CCR1^{-/-}$ mice, CCR1 expression on tumour cells was shown to drive Mo recruitment and angiogenesis, promoting metastasis (Rodero et al. 2013). The CCR1 ligands include CCL3, CCL5, CCL7, and CCL23. In relation

to cancer, there is a substantial body of evidence for CCL5 being an important chemokine.

In metastatic colorectal cancer, release of CCL5 from endothelial cells within the tumour, leads to the recruitment of Mo and TAMs (Läubli et al. 2009). Additionally, blocking CCR5 in colon cancer models leads to STAT3 activation and tumour killing via polarization of TAMs (Halama et al. 2016). In triple negative breast cancer models, CCL5 has been shown to modulate the immune-suppressive abilities of Ly6c^{high} derived MDSCs (Zhang et al. 2012). Further studies in mouse models, including the use of patient derived xenografts have demonstrated efficacy of agents blocking the CCL5-CCR5 axis in breast cancer (Ban et al. 2017; Nie et al. 2019). A study using both 4T1 (a triple negative breast cancer cell line) and the spontaneous MMTV-Wnt1 model demonstrated that the expansion of Ly6c^{high} Mo in the BM was attenuated when CCL5 was knocked out (Zhang et al. 2012). These findings were repeated, with the proliferation of Ly6c^{high} Mo in the BM of tumour bearing mice again being attenuated in CCL5$^{-/-}$ mice and furthered by using adoptive transfer to show that locally acting CCL5 in the BM was a key factor in Mo expansion (Ban et al. 2017). Interestingly, it has been shown that the action of CCL5 on the BM was reliant on the growth factors CSF1 and GM-CSF (Zhang et al. 2012).

Hypotheses regarding what may be driving the monopoiesis could be tested by a number of methods. The levels of growth factors and chemokines in either the blood and, or the bone could be assessed. A useful addition to interpreting this data may have been measuring biochemical markers of systemic inflammation which were not measured during the kinetic. More interestingly, perhaps, would be to attempt to show mechanism by manipulating likely candidates. An experiment that has been considered is testing if a CCL2 small molecule inhibitor impedes the increase in BrdU+ Ly6c^{high} BM Mo in late tumour bearing mice. This mechanistic work was not undertaking as it was not a primary focus of the PhD. Rather, the reason to assess Mo kinetics in these models was to justify the use of a given model in investigating transcriptional changes that might be occurring. Having established that Mo kinetics were perturbed in mice with late stage spontaneous MMTV-PyMT tumours the next step was to assess if Mo were transcriptionally altered in this context and compare this with findings in humans. This will therefore be the focus of the next section.

Chapter 5 Transcriptional alterations to mouse monocytes in PyMT mice

5.1 Introduction

As discussed, studies in humans have shown that circulating Mo are transcriptionally altered in a number of epithelial cancers (Cassetta et al. 2019; Chittezhath et al. 2014; Hamm et al. 2016). How conditioning of Mo occurs has yet to be investigated and little is known about Mo transcriptional regulation in the context of cancer.

Having now established Mo kinetics in late stage tumour bearing PyMT mice, transcriptional profiling of mouse Mo would screen for any differential gene expression suggesting altered transcriptional regulation. If present, it may then be possible to decipher whether conditioning occurs in the BM, in the blood or on multiple levels. It would also permit comparison with human data to identify any orthologous genes or pathways.

To this end, this chapter aimed to build a profile of the transcriptional profile of Mo in the C57BL/6 MMTV-PyMT spontaneous mouse model. The ultimate aim was to identify gene, or pathway targets common to both human and mouse. This would confer the benefit of using the mouse to better understand the transcriptional regulation of human Mo in cancer.

5.2 RNAseq of blood monocytes in C57BL/6 PyMT mice

Before proceeding to sorting cells on established gating strategies, it was necessary to ascertain if any novel Mo populations existed in tumour bearing mice. Given this, a collaboration was established with Dr. N Batada (MRC Institute of Genetics and Molecular Medicine, Edinburgh) whom is experienced in data analysis of the scRNAseq method, smartSEQ.

To confirm high efficiency of sorting single cells into a 96 well plate, Hoescht stained Mo were sorted. Imaging of the 96 well plate confirmed that all 96 wells contained a single cell. SmartSEQ of blood Mo in three late stage tumour bearing PyMT+ve C57BL/6 mice and three littermate PyMT-ve control mice was undertaken. By t-distributed stochastic neighbour embedded (t-sne) analysis no distinct novel populations were identified (Figure 23, A). The use of Ly6c and Treml4 to segregate blood Mo was validated on a mRNA level (Figure 23, B-C). Gene coverage was limited to approximately 2000 and analysis of this data is ongoing, thus only the preliminary analysis is shown.

Having established that the two populations of Mo were maintained in both control and tumour bearing mice, blood Ly6c^{high} and Ly6c^{low} Mo were sorted from C57BL/6 mice with late stage PyMT tumours and littermate controls and processed for RNAseq. To screen samples to identify potentially interesting alterations but minimise batch effect, initially all samples were sequenced on

the same lane. Analysing all samples together, Lyc^{high} or Ly6c^{low} cell type accounted for the greatest variance (Figure 24, A). For Ly6c^{low} blood Mo, there was no clear effect of cancer on clustering by principle component analysis (PCA) (Figure 24, B). However, the Euclidean distance between cancer and control Ly6c^{high} blood Mo did suggest that there may be some effects of cancer present in these cells (Figure 24, C).

Further analysis revealed very few DEGs in cancer versus control samples for Ly6c^{low} Mo. This analysis was repeated, modelling for sort date and also by biasing and testing multiple permutations of selected samples. Despite this, for the Ly6c^{low} blood Mo there were just 7 DEGs (q.value<0.05). However, in Ly6c^{high} blood Mo a simple analysis revealed 177 DEGs (q.value<0.05). Initial analysis of these samples indicated DEGs and pathways related to IFN signalling and immune response. Deeper sequencing was undertaken to gain full coverage of genes and detect the maximal number of DEGs for comparison with human data. Given that transcriptional changes were only apparent in the Ly6c^{high} blood Mo, Ly6c^{low} blood Mo samples were not re-sequenced.

A total of six Ly6c^{high} blood Mo were re-sequenced on one lane (60-80x10^6 reads). The six samples were chosen as they had been sorted on the same days, thus minimising batch effects. The clustering of the chosen 6 samples is featured in Figure 24, C. There was a total of 611 DEGs (q.value<0.05) between cancer and control samples (Figure 24, D). There was an almost 2-

fold difference in number of genes down versus up-regulated (393 down, 218 up). Of note, the LFC sizes were minimal and larger LFC tended to occur in some genes that were of lower mean expression (Figure 25).

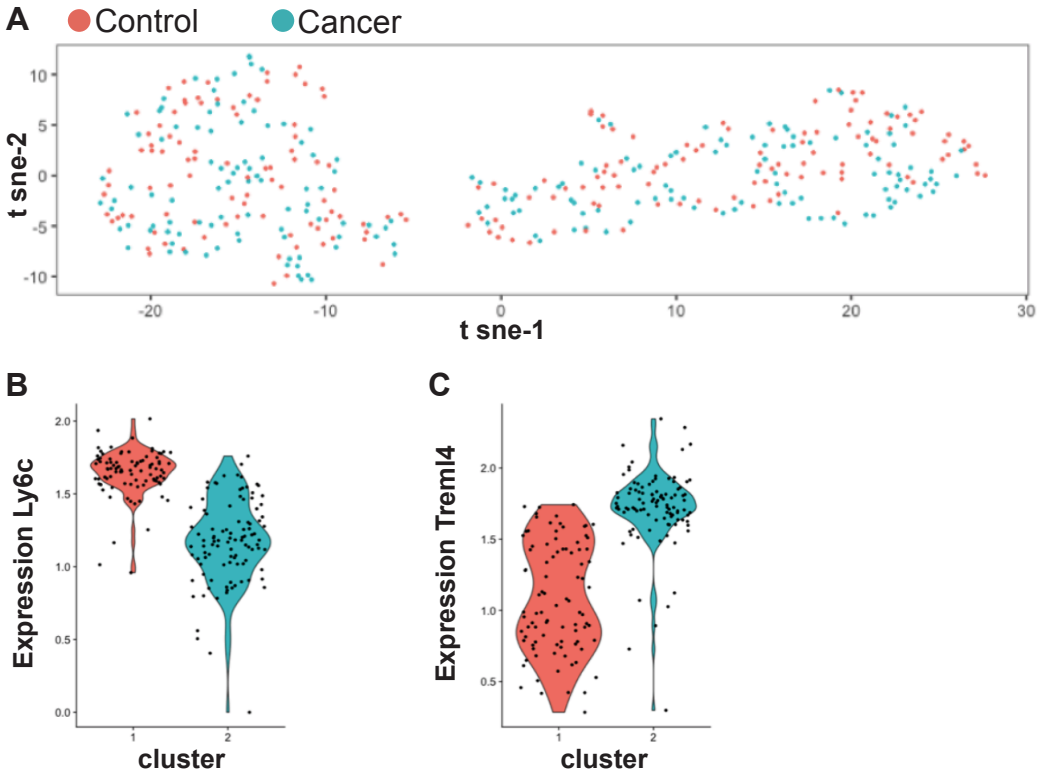

Figure 23 Single cell RNA-seq of Mo in C57BL/6 mice with late cancer and littermate controls *(A) t-sne plot for cells from control (pink) and cancer (turquoise) mouse (B-C) Violin plot taken from n=1, showing expression (z transformed normalised counts) in cluster 1 and 2 of (B) Ly6c (C) Treml4. Experiments were conducted in duplicates of co-housed littermate groups of n=6 (3 cancer) and n=2 (1 cancer).*

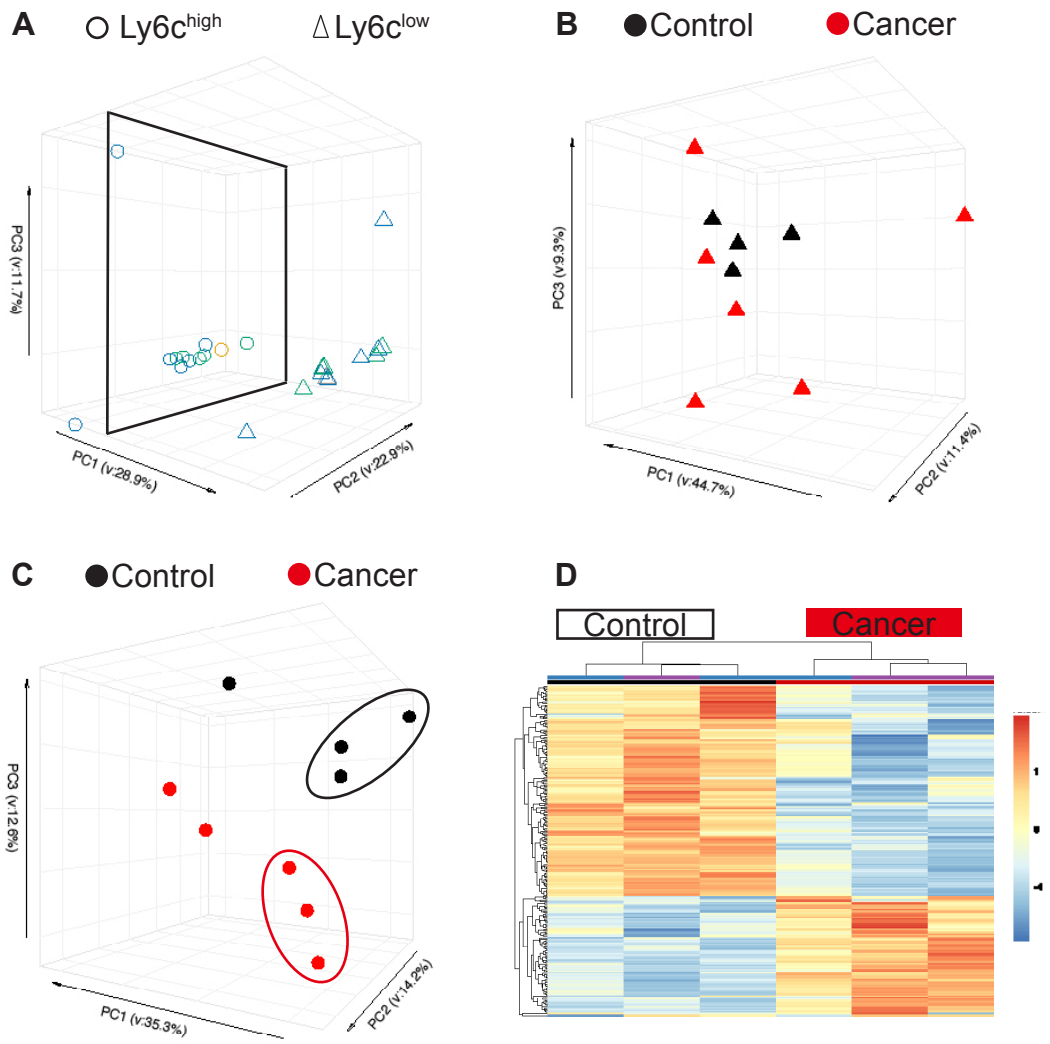

Figure 24 Analysis of RNAseq of blood Mo in C57BL/6 mice with late cancer versus littermate controls *(A) PCA of all samples (B) PCA of Ly6c^{low} Mo. (C) PCA of Ly6c^{high} Mo (D) Gene expression heatmap of Ly6c^{high} blood Mo DEGs between control and cancer samples with a q.value<0.05. Samples are arranged horizontally, and sample characteristics are provided in horizontal bars for each column denoting cancer in red and control in black and the date samples were sorted in purple and blue. Genes are arranged vertically; Red colour within the heatmap indicates up-regulation, and blue colour indicates down regulation based on the tpm z-score (range [-2, 2]). Samples are clustered using complete linkage and Pearson correlation.*

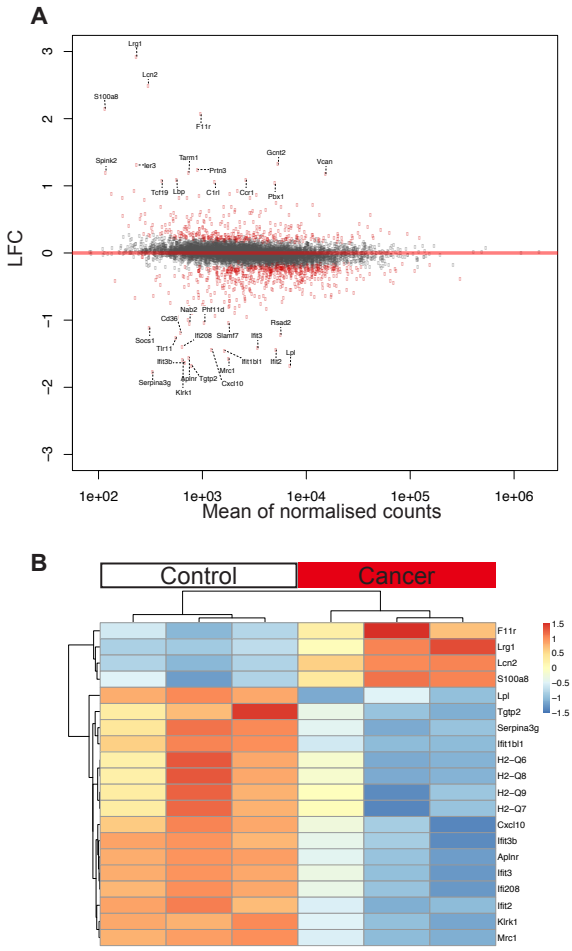

Figure 25 DEGs from Ly6c^{high} blood Mo in C57BL/6 mice with late cancer versus littermate controls. *(A) Mean normalised counts (x axis) and LFC (y-axis) for DEGs. DEGs with absolute LFC>0.5 are in red. DEGs with absolute LFC>1. 5 are labelled. Mean normalised counts are the calculated mean of normalised counts across all samples. (B) Gene expression heatmap of DEGs with highest LFC (Top 20). Samples are arranged horizontally, left 3 columns denoted as control in black and right 3 columns deonoted as cancer in red. Genes are arranged vertically; Red colour within the heatmap indicates up-regulation, and blue colour indicates down regulation based on the tpm z-score (range [-1.5, 1.5]). Samples are clustered using complete linkage and Pearson correlation.*

To explore whether the DEGs may be functionally related, genes were analysed for pathway enrichment. The top 3 pathways enriched in the set of 218 up-regulated genes in Ly6c^{high} cancer Mo were "neutrophil degranulation", "leukocyte migration" and "cytokine response". In the down-regulated list of 393 genes, highly enriched pathways (log q.value>10) were observed in relation to IFN signalling and antigen presentation. While some pathways were shared, there was a predominance of enrichment in the down-regulated pathways (Figure 26).

In order to identify potentially important genes, the chemokines and transmembrane receptors relevant to Mo biology were explored (Figure 27). Furthermore, as the main aim was to identify how the transcriptional regulation was being modulated, ISG genes and relevant TF genes were annotated.

Consistent with the pathway analysis, key genes modulated by IFNs were altered. This included the type II IFN induced chemokine gene, *Cxcl10* and genes for MHCI and MHCII proteins. The mannose receptor gene (*Mrc1*) was also down-regulated. Members of the CD2 Ig superfamily (*Cd2, Ly9 and Cd84*) (de la Fuente et al. 1997) were also altered, but in opposing directions. The gene for the β subunit of the CSF2-R, *Csf2rb*, was up-regulated. The LDTFs, *Fosb* and *Jun,* were down-regulated. SDTFs involved in IFN response, *Stat1* and *Stat2* were down-regulated along with the regulatory TFs *Socs1, Socs3, Socs6*, *Jak2* and *Jak3*.

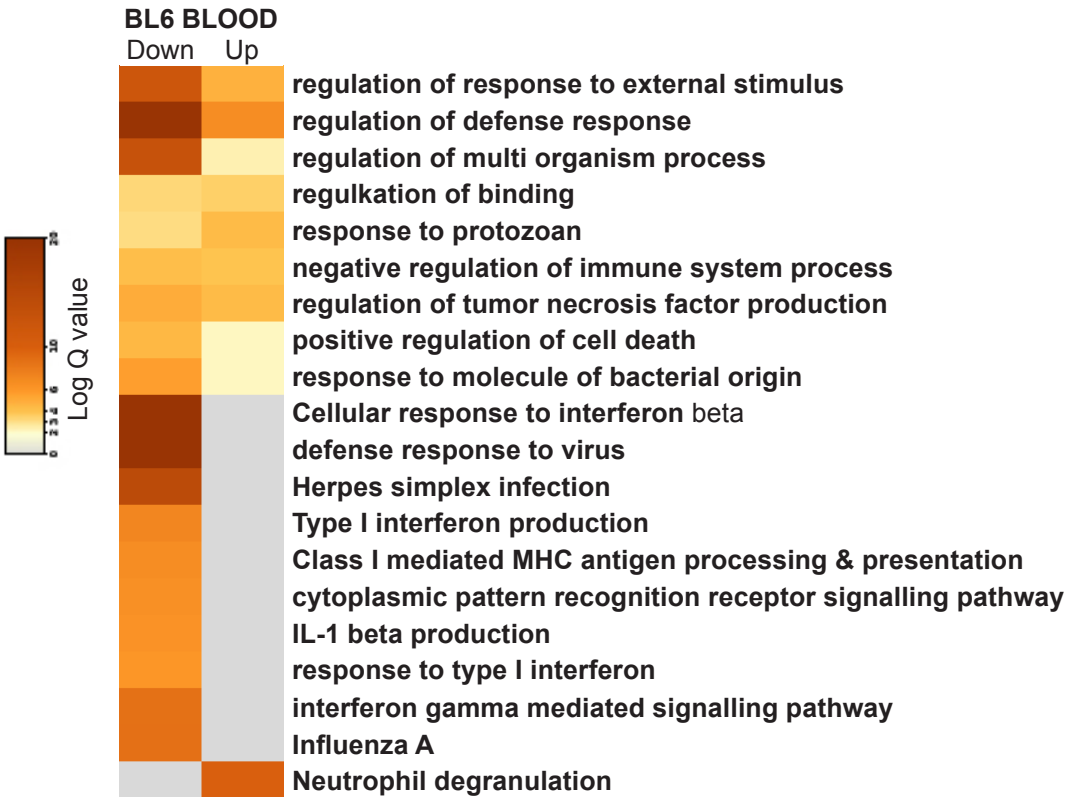

Figure 26 Heatmap of pathway analysis for DEGs between cancer and control samples of Ly6c^{high} blood Mo in C57BL/6 mice with late cancer versus littermate controls. *Each column represents the group of down or up-regulated genes. Each row represents the Gene Ontology or KEGG terms for pathways that are enriched. Pathways are annotated to the right of the heatmap. Log q.values are plotted, and each bar coloured according to the log q.value on a scale of 0 to 20, represented with graduating intensity from cream to dark brown.*

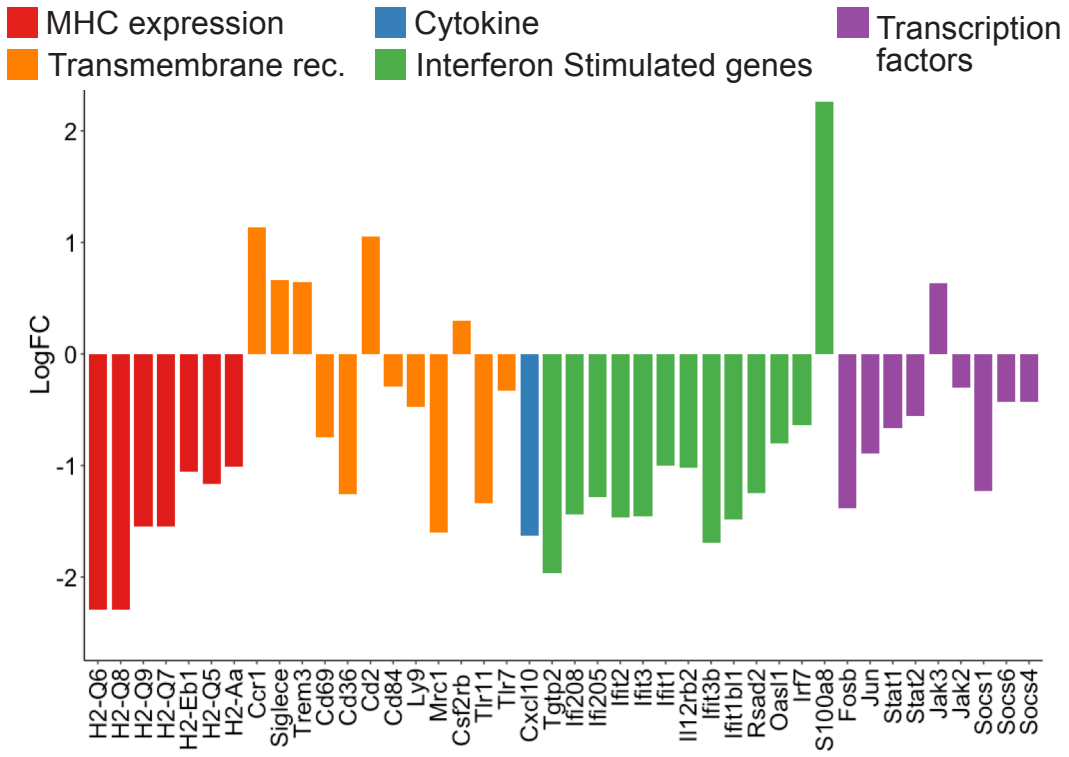

Figure 27 Histogram of LFC in DEGs for blood Mo in C57BL/6 mice with late cancer versus littermate controls. *Genes have been selected and grouped functionally as cytokines (blue), transmembrane receptors related to MHC expression (red) and IFN response (orange), Interferon Stimulated Genes (green), and transcription factors (purple).*

5.3 RNAseq of bone marrow monocytes in C57BL/6 PyMT mice

To determine at what level Mo may be conditioned, six Ly6^{high} BM Mo were sequenced. Contrasting cancer and control samples, there were 158 DEGs (50 up and 108 down-regulated in cancer with a q.value<0.05). Genes associated with proliferation were up-regulated (Figure 28). Just under half of the down-regulated genes in the BM were also down-regulated in Ly6^{high} blood Mo (Figure 29, B). These 47 common genes were highly enriched for type I IFN pathways (Figure 29, C).

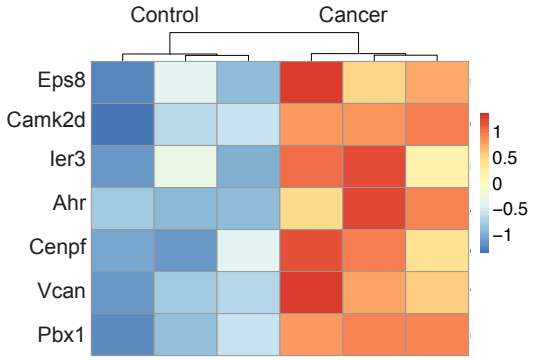

Figure 28 Gene expression heatmap of genes involved in proliferation in Lyc^{high} BM Mo in C57BL/6 mice with late cancer versus littermate controls. *Samples are arranged horizontally. Genes are arranged vertically; Red colour within the heatmap indicates up-regulation, and blue colour indicates down regulation based on the tpm z-score. Samples are clustered using complete linkage and Pearson correlation. The highest two clusters are labelled and cluster on cancer status.*

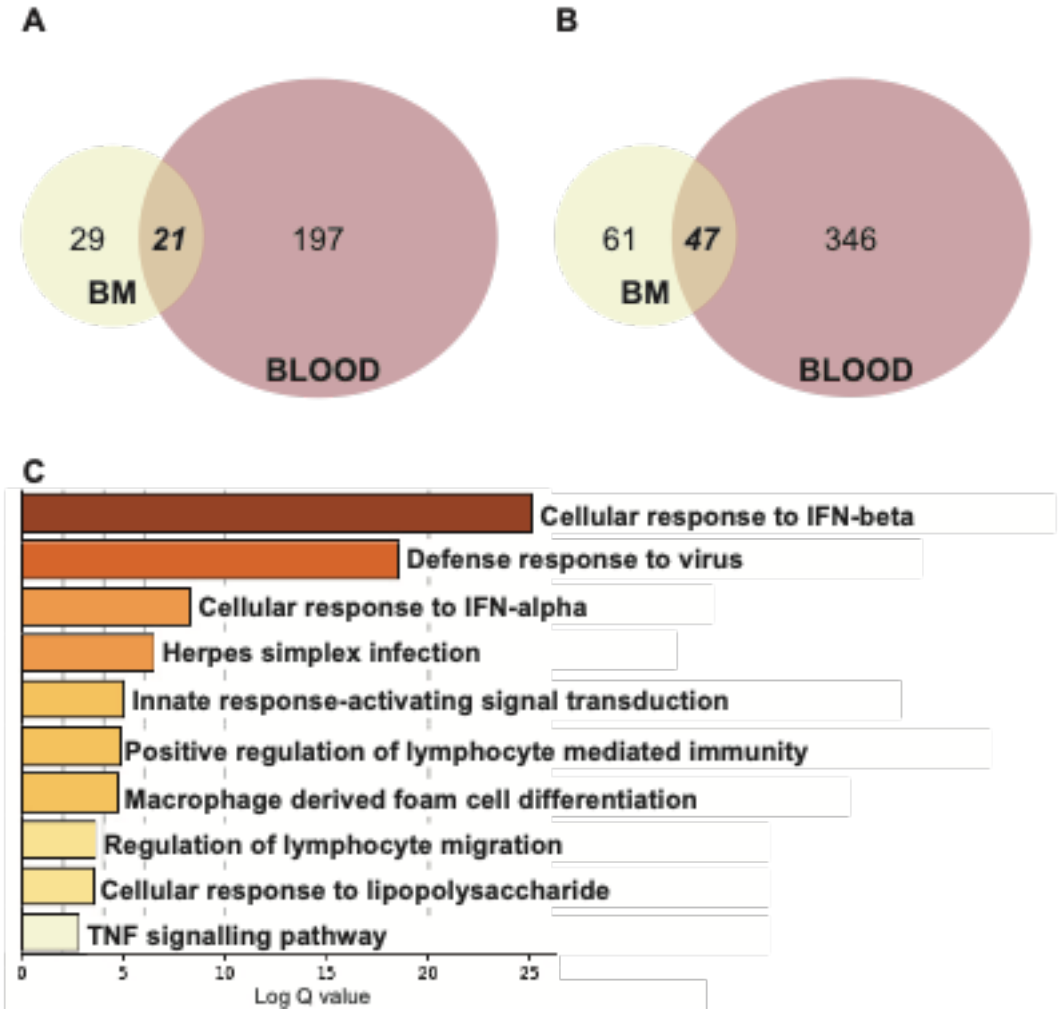

Figure 29 Comparison of DEGs between late cancer and littermate control samples of Ly6c^{high} blood and Ly6c^{high}BM Mo in C57BL/6 mice *(A-B) Venn diagram for DEGs in BM (cream) and blood (red) (A) Genes up-regulated in cancer (B) Genes down-regulated in cancer (C) Pathways for 47 shared down-regulated genes. Log q.values are plotted, and each bar coloured according to the log q.value on a scale of 0 to 30, represented with graduating intensity from cream to dark brown. Gene Ontology or KEGG terms are annotated.*

5.4 **Validation of C57BL/6 RNAseq results**

For validation by qPCR, it was noted that LFCs were very modest and the material available for qPCR was limited. Therefore, just two genes were chosen initially. *Gcnt2* was a gene that was amongst the highest up-regulated genes. There was evidence of it playing a role in cancer cell detachment, adhesion and migration, as well as epithelial to mesenchymal transition (Zhang et al. 2011). Expression of *Gcnt2* by breast cancer cells was driven by TGF-β1 (Zhang et al. 2011). However, there was no evidence for this gene playing a role in Mo function. Hence it was identified as a novel candidate gene. Having chosen a gene that was up-regulated, it was decided to validate a down-regulated gene. A number of genes that had the highest LFC were lowly expressed and so *Lpl* was chosen as having a high LFC while still having adequate expression levels (Figure 25). Using qPCR, it was possible to validate that *Gcnt2* was up-regulated and *Lpl* down-regulated in mice bearing late stage tumours compared with littermate controls (Figure 30).

It was then thought that validating more functionally relevant genes would be useful. For this *Ifit3*, *Stat1* and *Cxcl10* were all chosen. Unfortunately, the efficiency for the primers designed was less than 90% (for primer details see Appendix 9.1.2.). An additional 2 primers for *Stat1* were trialled but with little success. Recognising that low LFC and low levels of expression may hinder validation of these genes by qPCR, this approach was abandoned. A

preference to both validating using protein levels of other markers and to conduct functional assays also contributed to this decision.

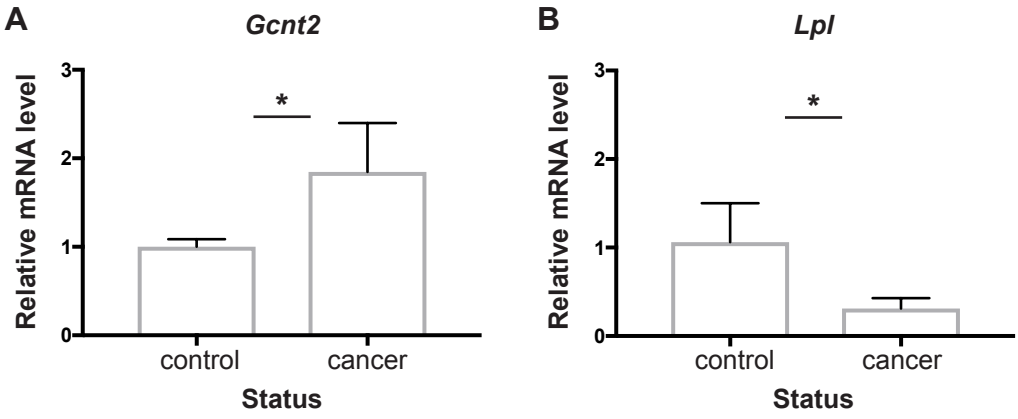

Figure 30 qPCR mRNA levels of Gcnt2 and Lpl in Ly6c^{high} blood Mo from C57BL/6 mice with late cancer versus littermate controls *(A) Gcnt2 (B) Lpl. The relative mRNA expression has been calculated using delta-delta CT method. SDHA was used as the control gene. *p value <0.05, unpaired t-test on the CT values. Experiment was conducted in n=6 (3 cancer).*

The decision was taken to try and assess MHCII by flow cytometry. Levels of MHCII expression in controls were comparable with previous assessment of MHCII expression undertaken in the Jenkins lab (data from Pieter Loewe) on C57BL/6 mice. There was a significant reduction in the frequency of MHCII expressing Mo in the both the BM and the blood (Figure 31).

Finally, to demonstrate functional relevance, the levels of pSTAT1 in response to stimulation with IFN were assessed in cancer and control mice. Sorted

Lyc6^{high} BM Mo were exposed to 10ng or 20ng of IFNγ or PBS. Levels of pSTAT1 were detectable (Figure 32, A). There was an increase in pSTAT when cells were stimulated with 10ng of IFNγ (Figure 32, B). From the initial experiment of just 4 mice, it was not clear if the cancer samples were less responsive at higher levels of IFNγ. Given this, the experiment was repeated. In the second experiment pSTAT1 levels in unstimulated cells were similar to that of stimulated cells from the first experiment. There was a very minimal increase in pSTAT1 levels at 10ng and at 20ng levels were actually lower (Figure 32, C). The staining had worked (Figure 32, D). During both experiments, there had been enough cells to do an FMO for just 2 of 3 exposures in each group. It was decided that unstimulated and 20ng were the priority and therefore these were available for a more accurate comparison. Using these FMOs to subtract the background, it was clear that samples in the second experimental group that had been denoted as unstimulated appeared to have pSTAT1 levels equivalent to stimulated cells from the first group of experiment samples. It may have been that IFNγ was inadvertently added or that the mice were unwell. Nonetheless, at 20ng there was no clear difference in pSTAT1 levels (Figure 32, E). Hence, there was no difference in the pSTAT1 levels in cancer versus control mice proven by stimulating with 10ng or 20ng of IFNγ.

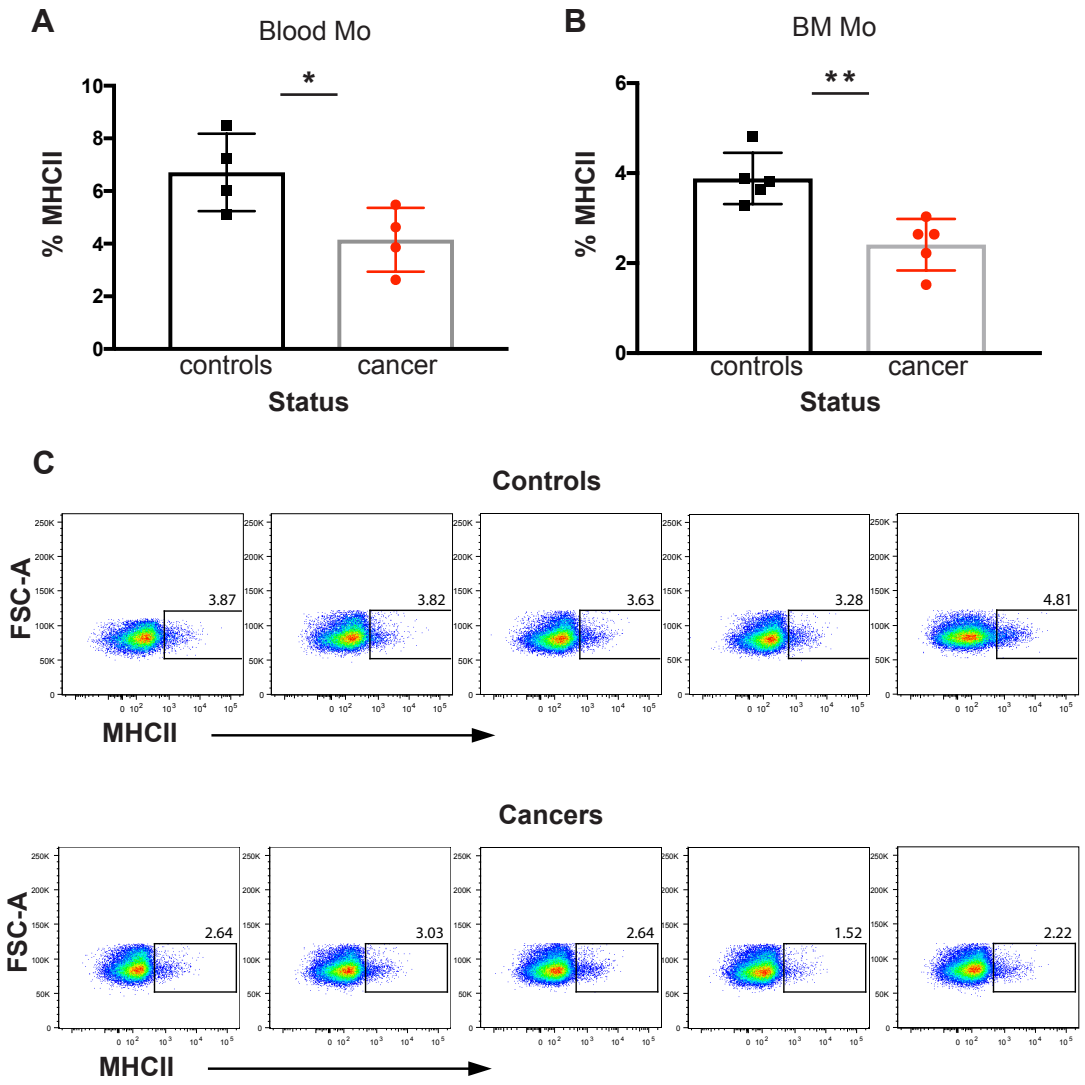

Figure 31 Comparison of MHCII expression on Ly6c^{high} Mo in C57BL/6 mice with late cancer versus littermate controls *(A-B) MHCII+ Ly6c^{high} Mo as a percentage of all Ly6c^{high} in (A) Blood (B) BM (C) Flow cytometry of BM Ly6c^{high} Mo with MHCII (x-axis) against FSC-A (y-axis), gating and frequency of MHCII+ (as a % Ly6c^{high} Mo) cells is shown. * p value <0.05, ** p value <0.01, unpaired t-test. Experiments were conducted in n=8 (4 cancer) and n=10 (5 cancer) for blood and BM respectively.*

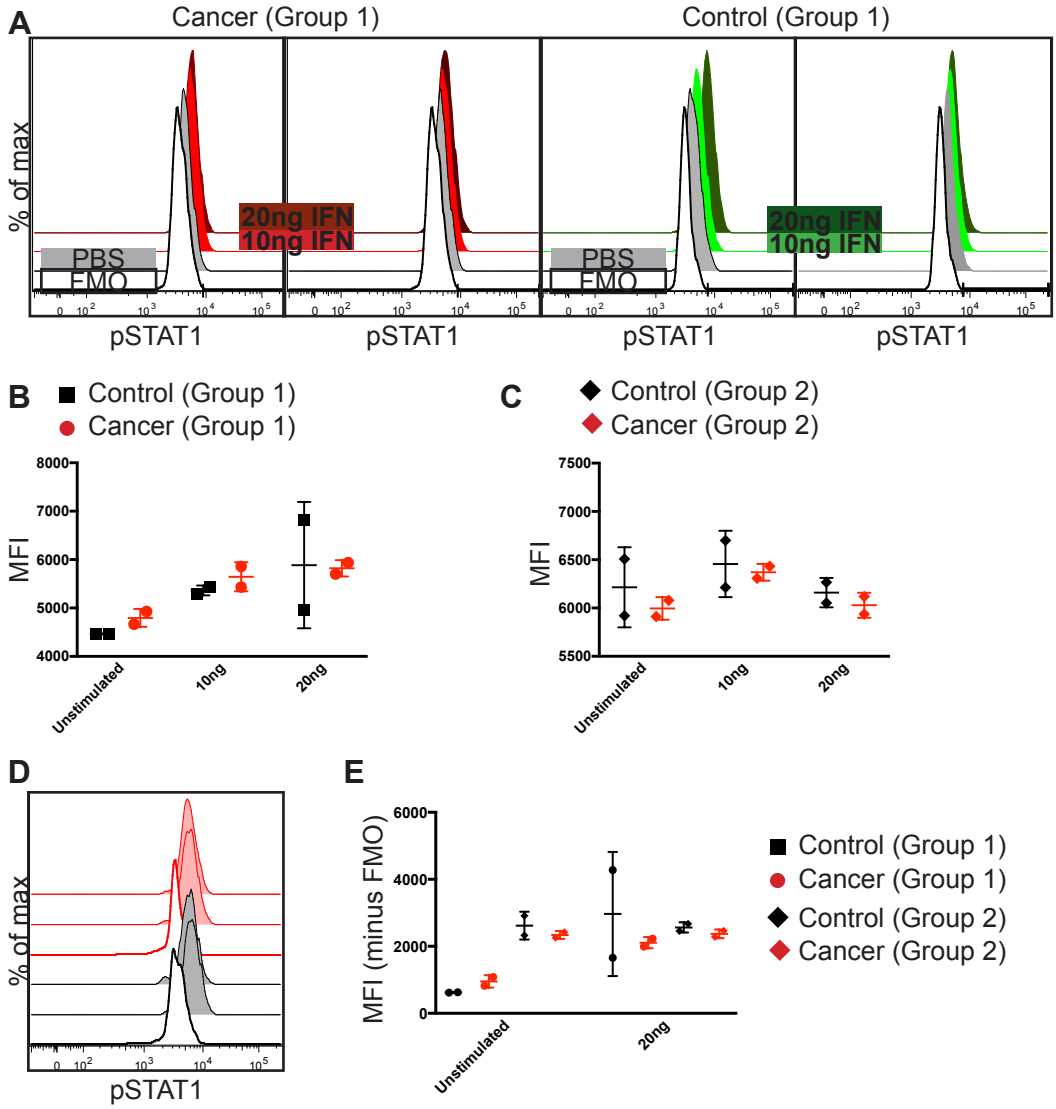

Figure 32 Assessment of pSTAT1 levels by flow cytometry in Ly6c^{high} BM Mo sorted from C57BL/6 mice with late cancer versus controls *(A-C) pSTAT1 levels for each sample in the first experiment (group 1) or second experiment (group 2) exposed to either PBS (unstimulated), 10ng or 20ng of IFNγ. (A) Histograms for group 1. Cancer (red), controls (green). FMO is from a pooled sample for each condition exposed to 20ng IFNγ (B-C) MFI for pSTAT1 (D) Histogram for group 2 exposed to PBS (filled) and FMOs (unfilled). Cancer (red), controls (grey). (E) Overall results showing the MFI of pSTAT1 calculated against FMO for each sample and each condition either unstimulated or exposed to 20ng IFN.*

5.5 **RNAseq of monocytes in FVB PyMT mice**

Throughout the project thus far, all experiments had been undertaken in PyMT mice on a C57BL/6 background. However, as reported in the literature, it was noted that FVB mice had a more aggressive cancer phenotype than C57BL/6 mice (Figure 33). Therefore, this model was characterised for perturbations to Mo to check if they were affected similarly to the C57BL/6 PyMT mice. There was a significant increase in the frequency of blood Mo and Neuts in late tumour bearing FVB mice when compared to controls (Figure 34, A and B respectively). This increase was restricted to the CD11b+ cells (Figure 34, C). There was no increase in the proportion of Ly6c^{high} Mo of the total Mo pool. The fold changes in Mo numbers between control and late stage tumour bearing mice was greater in the FVB than the C57BL/6 mice (Figure 34, D).

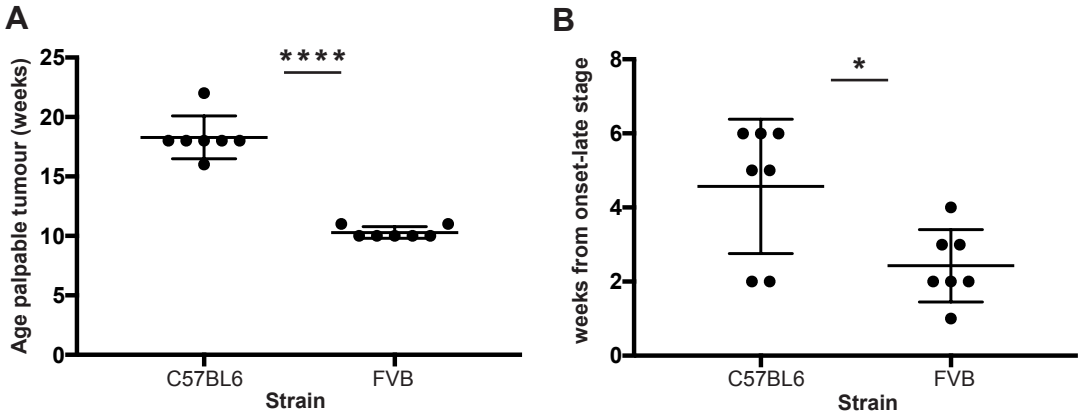

Figure 33 Comparison of tumour development in PyMT+ve mice on a C57BL/6 or FVB background *(A) Age in weeks when tumours first palpable (B) Time in weeks from tumours first palpable to ~20mm size. * p value <0.05, **** p value <0.0001, unpaired t-test. n=14 (7 C57BL/6, 7 FVB).*

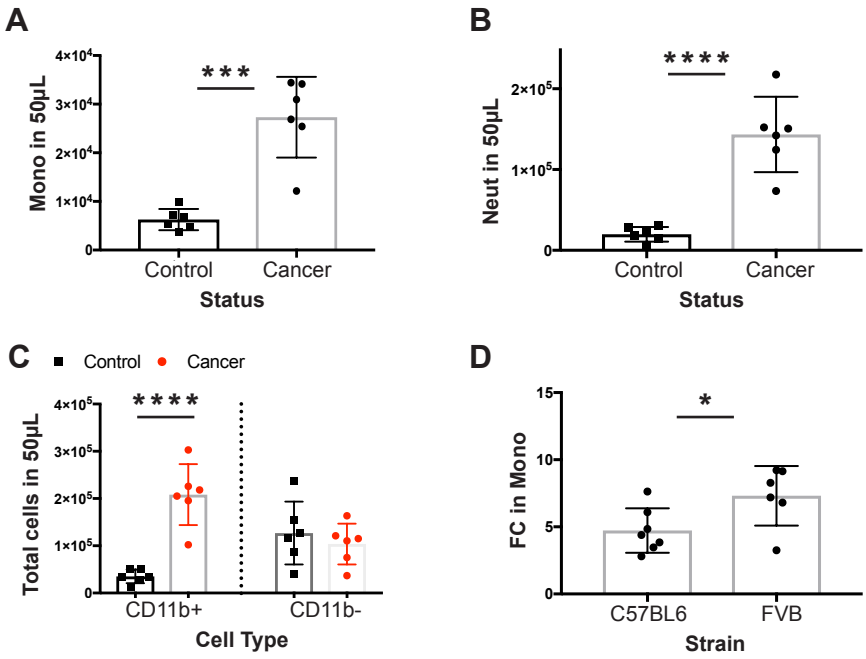

Figure 34 Blood composition in FVB PyMT mice with late cancer or age-matched controls *(A-C) Total cells in 50µl of blood (A) Mo (B) Neuts (C) CD11b+ and CD11b- (D) FC in total Mo in cancer to controls in C57BL/6 or FVB mice. For C, control samples are in black and cancer samples are in red. * p value <0.05, ** p value <0.01, *** p value <0.001, **** p value <0.0001, unpaired t-test. Experiments were conducted in duplicates with littermate and co-housed groups of n=6 (3 PyMT+ve) in each replicate.*

It was hypothesised that transcriptional changes may be stronger in Mo in the FVB mice than had been detected in the C57BL/6 mice. The same protocol was undertaken to sort and undertake RNAseq of Ly6c^{high} blood Mo from FVB late tumour bearing and littermate control mice as had been used for the C57BL/6. On PCA, the cancer and control samples separated out in PC1 (42.86%) but the controls were not tightly clustered (Figure 35, A) By un-supervised hierarchical clustering, 2 cancer and 2 control samples clustered separately, but 1 cancer and 1 control clustered together (Figure 35, B).

There were a total of 466 DEGs when comparing control with cancer, with 267 genes up-regulated in cancer (q.value<0.05). Comparing these 267 genes with the 218 genes of the same criterion in the C57BL/6 dataset, there were 67 DEGs common to both strains (Figure 36, A). A total of 199 genes were down-regulated in cancer (q.value<0.05). Comparing these 199 genes with the 393 genes of the same criterion in the C57BL/6 dataset, there were 51 DEGs commonly down-regulated (Figure 36, B). There were more DEGs in C57BL/6 but sequencing depth was 2-fold to that in FVB samples (Table 3). LFCs were higher in FVB compared to C57BL/6 (Figure 36, C).

	FVB	**BL6**
Mean Seq Depth	$30x10^6$	$67x10^6$
Total DEGs	466	611

Table 3 Mean sequencing depth and total DEGs for Ly6c^{high} blood Mo in C57BL/6 and FVB mice. *Mean seq depth calculated across all 6 samples for each group. Total DEGs with q.value<0.05.*

Up-regulated genes common to both FVB and C57BL/6 were not strongly enriched for in any relevant pathways (pathways with a log q.value>5 were GO:1900027 and GO:0097178 both relating to ruffle assembly). But for the 51 commonly down-regulated genes, IFN responses were again enriched, with a log q.value of 8.5 (GO:0051607 defence response to virus, GO:0098542 defence response to other organism, GO:0009615 response to virus). To assess the relationship of genes and pathways between strains and also the two tissue types, joint pathways analysis was undertaken for all down-

regulated genes (Figure 37). There was a greater enrichment of the pathways in the C57BL/6. This was irrespective to the number of genes having been entered as just 108 genes were entered for the PyMT BM Mo versus 199 for the FVB blood Mo, yet the enrichment was still greater for the BM Mo. The down-regulation of IL-1β was limited to the C57BL/6 mice.

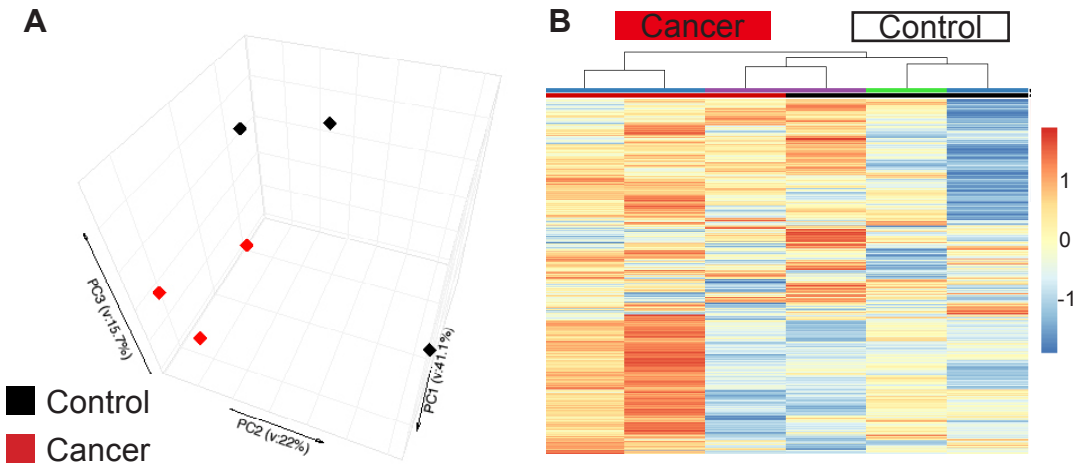

Figure 35 Analysis of RNAseq of Ly6c^{high} blood Mo in FVB mice with late cancer versus littermate controls *(A) PCA of all samples (B) Gene expression heatmap of all genes using non-supervised hierarchical clustering. Samples are arranged horizontally, and sample characteristics are provided in horizontal bars for each column denoting cancer (red) and control (black and the date samples were sorted in purple, blue and green to show the influence of batch effects. Genes are arranged vertically; Red colour within the heatmap indicates up-regulation, and blue colour indicates down regulation based on the tpm z-score (range [-2, 2]). Samples are clustered using complete linkage and Pearson correlation.*

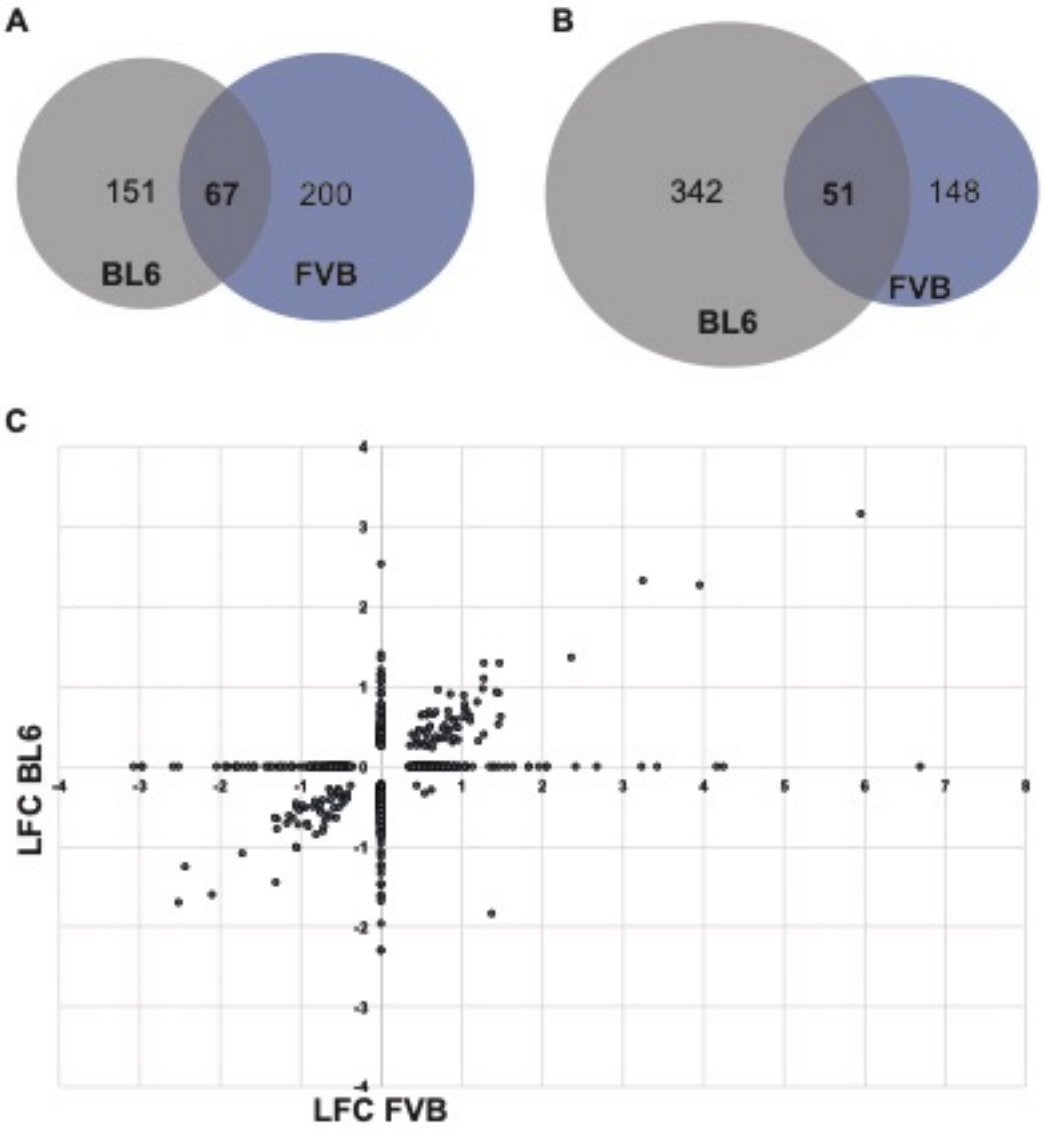

Figure 36 Comparison of DEGs between late cancer and control samples of Ly6c^{high} blood Mo in C57BL/6 and FVB mice *(A-B) Venn diagram for DEGs in C57BL/6 (dark grey) and FVB (dark purple) (A) Genes up-regulated in cancer (B) Genes down-regulated in cancer (C) LFC in FVB (x-axis) and C57BL/6 (BL6) (y-axis) for all DEGs with a q. value<0.05. Each dot represents a gene.*

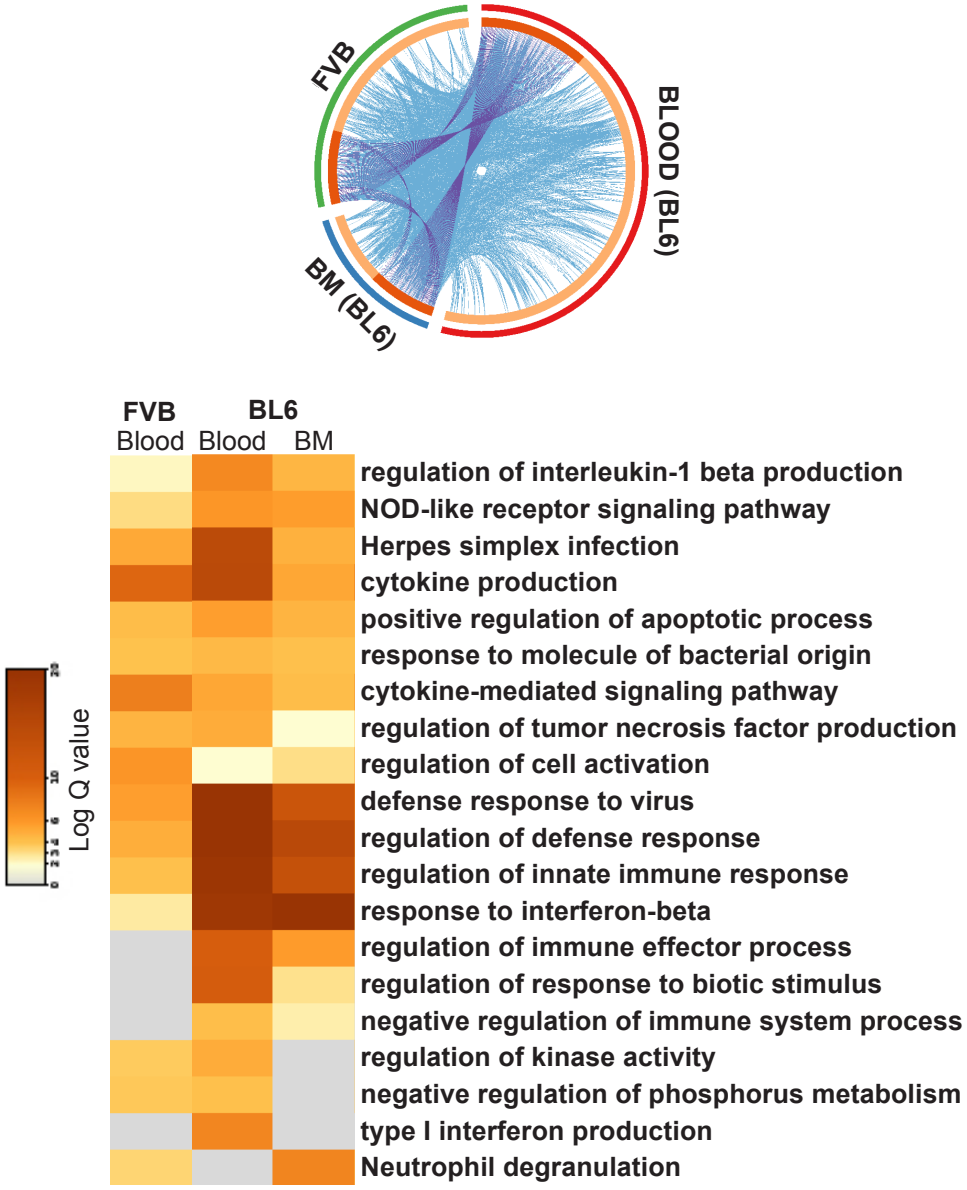

Figure 37 Metascape joint analysis of DEGs down-regulated in the BM and blood of C57BL/6 and the blood of FVB mice*. For each of these analyses, the DEGs produced when contrasting cancer with control have been input for each of the three groups (BL6 blood, BL6 BM, FVB blood). Commonly shared genes and commonly shared pathways are then represented. (A) Circos plot showing commonly enriched genes. The outer arcs represent which DEG gene list is featured. BL6 blood represented by red, BL6 BM*

represented by blue and FVB blood represented by green. The inner arcs reflect whether the genes are common to all 3 (coloured in dark orange) or genes are common to just 2 groups (coloured in light orange). Each occasion that a gene is in common between a group a purple line occurs between where the gene occurs on the respective arcs. Each occasion a gene that belongs to the same enriched ontology term as another gene in another group a blue line occurs between where the gene occurs on the respective arcs. (B) Pathways for down-regulated genes. Each column represents the group of down-regulated genes. Each row represents the Gene Ontology or KEGG terms which are annotated to the right on the heatmap. Log Q.values are plotted, and each bar coloured according to log q.value on a scale of 0 to 20, represented with graduating intensity from cream to dark brown. Gene Ontology or KEGG terms are annotated.

5.6 **Orthologous human and mouse genes**

Having now identified the DEGs in cancer and control mice and the relevant pathways that were altered it was now intended to compare this with the human data set already undertaken by members of the Pollard Lab (Cassetta et al. 2019). As can be seen from the unsupervised clustering in Figure 38, the human cancer samples were quite distinct from the human control samples in this cohort. Pathways that were highly enriched for did not obviously overlap with the pathways observed in any of the mouse analyse (Figure 38, B).

To undertake the comparison a list of 865 DEGs between the breast cancer patient samples and control samples was used (selected using a criterion of absolute LFC>1.5).

There were a total of 7222 and 7653 human orthologues genes in the DEGs for C57BL/6 and FVB respectively. Selecting unique gene names reduced this to 7137 and 7570 for C57BL/6 and FVB respectively. These DEGs were then filtered using a criterion of absolute value of LFC>0.5 as the changes in mouse were more discrete.

Comparing these datasets revealed very few DEGs were common to both mouse and human (Figure 39). The LDTF for Mo, *Jun* was the only gene that was commonly down-regulated in all DEG datasets (Figure 39, B).

To check if there may be common pathways affected, despite a lack in shared genes, joint pathways analysis was undertaken (Figure 40). This revealed some commonly enriched down-regulated pathways, particularly with respect to metabolism, cell differentiation, survival and migration. However, the main pathway that had been highlighted in mice, IFN signalling, was actually up-regulated in human cancer Mo.

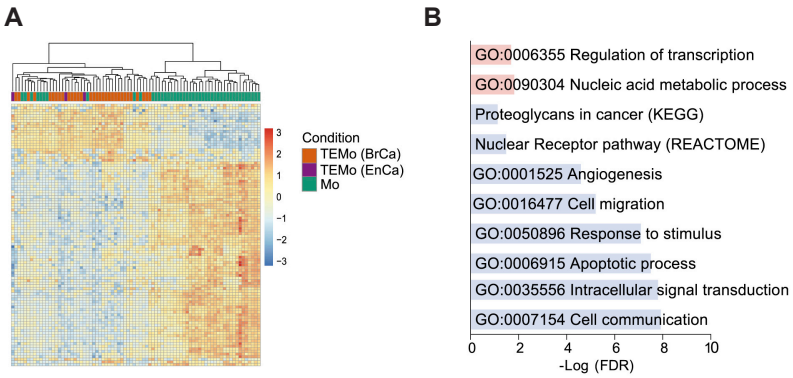

Figure 38 Heatmap and pathways for DEGs of blood Mo between cancer samples and healthy samples in humans. *Both Breast Cancer and Endometrial Cancer samples are included (A) Hierarchical clustering of all differentially expressed genes (DEGs) between Monocytes in Breast cancer (TEMo BrCa) and Endometrial Cancer (TEMo EnCa) and healthy controls (Mo). Expression values are Z score transformed. Samples were clustered using complete linkage and Euclidean distance. B) Gene ontology (GO Hierarchical clustering of all DEGs between Mo and TEMo. Image adapted with permission from Cassetta, L. et al. 2018. Of note, in this paper breast cancer included all subtypes and monocytes were sorted as whole monocytes and not divided into subpopulations.*

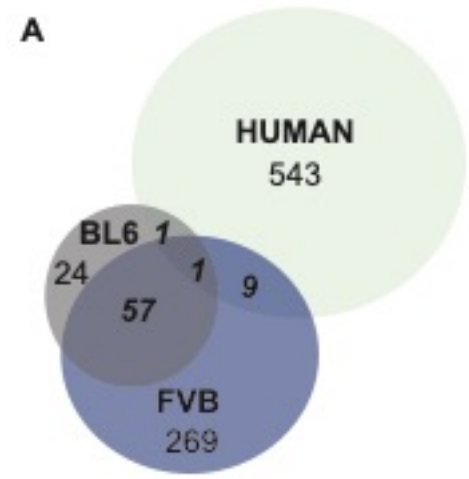

Gene Name	BL6 Log2FC	HUMAN Log2FC
AIG1	*0.55282772*	*1.69*
EGR1	1.14707469	1.85

Gene Name	FVB Log2FC	HUMAN Log2FC
PHOSPHO1	1.55067537	1.51
IFT27	1.16981582	1.54
RGS18	-0.8363791	1.56
NRG1	0.50202031	1.61
AIG1	*0.91406555*	*1.69*
TRAPPC12	0.70059029	1.73
CXCR2	3.43332708	1.96
IPCEF1	1.05291028	2.48
RNASEL	0.58034499	2.59
CD200R1	0.90232089	2.79

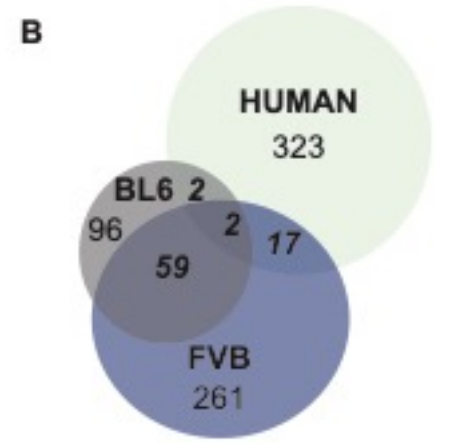

Gene Name	BL6 Log2FC	HUMAN Log2FC
CD69	-0.75	-3.20
JUN	*-0.89*	*-2.66*
EHD1	-0.74	-2.03
STARD4	-0.50	-1.63

Gene Name	FVB Log2FC	HUMAN Log2FC
IRAK2	-0.6283806	-3.02
ATF3	-0.8343716	-2.83
CDKN1A	-0.6121596	-2.68
JUN	*-3.2880353*	*-2.66*
CD83	-1.8356871	-2.32
NR4A1	-0.5934103	-2.23
DDIT3	-0.5418516	-2.23
LMNA	-1.0469356	-2.04
EHD1	-0.8228003	-2.03
THBS1	-0.880316	-1.91
SLC25A37	-0.5614717	-1.88
EMP1	-0.5877802	-1.86
PPP1R15A	-0.6913135	-1.85
PDLIM7	-1.1263603	-1.84
KLRD1	-0.5780911	-1.69
RHOF	-0.8853943	-1.66
TUBB2A	-0.5139839	-1.66
PLK3	-0.6034716	-1.62
IER5	-0.5460374	-1.54

Figure 39 Comparison of DEGs of blood Mo between cancer and controls samples in mouse strains (FVB and C57BL/6) and human *(A) Venn diagram of up-regulated DEGs with list of gene names and LFC values for any in common with human and mouse (B) Venn diagram of down-regulated DEGs with list of gene names and LFC values for any in common with human and mouse.*

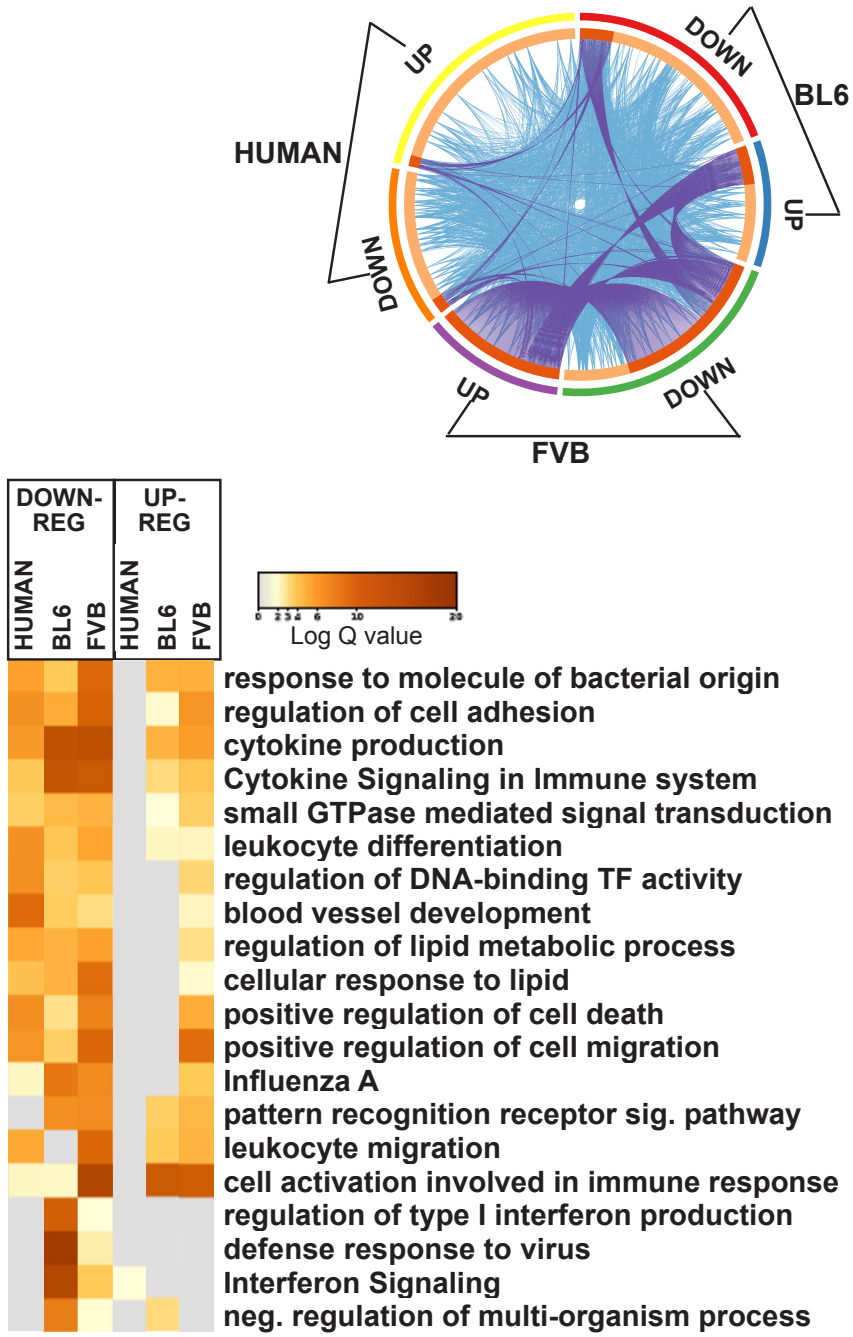

Figure 40 Metascape joint analysis of DEGs blood Mo between cancer and controls samples in mouse strains (FVB and C57BL/6) and human *(A) Circos plot (B) Heatmap of pathways enriched. Up and downregulated genes are annotated for each respective group. All other parameters are as for figure 37 page 137.*

5.7 **Discussion**

Having established that there is a significant pan-Mo expansion as PyMT mice develop mammary gland tumours, it was anticipated that there would be alterations to the transcriptional profiles of Mo. While changes were subtle in terms of the effect size (LFC small and few DEGs), there were a number of interesting findings to discuss, both in terms of individual genes and enriched pathways. Firstly however, it is somewhat unexpected that the effect seemed to be limited to the Ly6c^{high} Mo population, despite the expansion of Mo being across all populations.

An explanation for this could be that only certain Lyc6^{high} Mo are transcriptionally altered. While the majority of Ly6c^{high} cells will go on to die and only a small subset will form Ly6c^{low} Mo, it may be that the Ly6c^{high} Mo that are transcriptionally altered go on to be recruited to tumours. While the recruitment Ly6c^{high} Mo to form TAMs and MAMs is well supported by evidence, it is not known what proportion of Ly6c^{high} Mo fulfil this fate (Arwert et al. 2008; Qian et al. 2011; Kitamura et al. 2015; Movahedi et al. 2010; Bonapace et al. 2014). Alternatively, it may be that the frequency of Lyc6^{low} cells that are transcriptionally altered are not great enough to be detected by bulk RNAseq.

Even in the Ly6c^{high} Mo, both the number of DEGs and the LFCs were modest. While this could be because changes are minimal, it could also be that by bulk RNAseq signatures of subpopulations are diluted. This would be the case for example with regards MHC expression. When validating the alteration to MHCII, MHCII expressing cells accounted for less than 10% of all Ly6c^{high} cells in controls. If this is then a reduction of even 10% to 5%, the remainder of cells that are unaltered would greatly dilute the overall changes observed. To assess this further, scRNAseq can be used. While this was undertaken, no subpopulations were observed. However, just 96 cells were sequenced. A more appropriate method could be a droplet based approach, allowing for many more cells to be assessed (Hwang et al. 2018). However, the biological relevance of such small sub-populations is questionable and potentially negates the need for this.

With regards to individual genes, of those that were altered, *Mrc1* was down-regulated in Ly6c^{high} blood Mo in both strains and in Ly6c^{high} BM Mo in the C57BL/6 mice. While *Mrc1* is up-regulated on so-called alternatively activated macrophages (Jablonski et al. 2015), by flow cytometry levels of Mrc1 are greatly down-regulated on TAMs compared with resident macrophages in the primary tumour (Franklin et al. 2014). However, Mrc1 expression on TAMs has been shown to vary according to TAM subpopulations. Co-expression of Mrc1, Vegfα and Tie-2 corresponds with pro-tumoural, angiogenic TAM populations recruited in response to chemotherapy (Hughes et al. 2015). Mrc1 was also

recently found to be differentially expressed in the metastatic site on pre-MAM and MAM cells, wherein expression was higher than that of resident macrophages but lowest in circulating Mo (Kitamura et al. 2018). Surprisingly, the expression of Mrc1 was independent of CSF1 action (Kitamura et al. 2018). Overall, it seems that levels of Mrc1 are highly dependent on context but may reflect a distinct Mo population.

One of the highest genes up-regulated in FVB mice was *Cxcr2*. While this is an established receptor responsible for Neut recruitment to tumours (Chao et al. 2016), it has recently been proposed that it is required for recruitment of a population of Mo to tissues. In the context of peritoneal inflammation, there was a loss of Ly6c^{high} derived non-resident macrophages in CXCR2$^{-/-}$ mice (Dyer et al. 2017). Macrophages formed from Mo expressing CXCR2 were shown to be involved in the resolution of peritoneal inflammation (Dyer et al. 2017). Thus, it CXCR2 may represent a distinct population of Ly6c^{high} Mo that have anti-inflammatory properties.

It can be more useful to consider genes in functional groups rather than individually. Pathway analysis implied a reduction in immune activation. This may initially seem contradictory to the prior hypothesis that myelopoiesis is being driven by so called pro-inflammatory factors. However, in high stress haematopoiesis, in response to inflammatory signals, immature myeloid cells are produced and released. This is a known phenomenon in cancer and

thought to be a source of both M-MDSCs and PMN-MDSCs (Marvel & Gabrilovich 2015).

The up-regulation of genes associated with proliferation in the Lyc6^{high} BM Mo agrees with the BM BrdU findings in the previous chapter. Down-regulation of immune responses was not only seen on a gene level but also demonstrated by reduced MHCII levels both in the BM and the blood. Collectively this supports the hypothesis that systemic signals acting on the BM lead to stress hematopoiesis and release of Ly6c^{high} Mo that lack a mature functions, such as antigen presentation. While this would need to be functionally verified, if this is the case, Ly6c^{high} Mo in are conditioned in the BM to be pro-tumoural or at least less anti-tumoural.

Aside from the potential reduced antigen presentation capability of Ly6c^{high} Mo in cancer, the production of Mo that are less immune-responsive, in terms of reduced type I and type II IFN signalling would be very fitting with what is already known about IFNs in cancer. The anti-cancer nature of IFN has been known as early as 1969, when Gresser et al showed that the survival of syngeneic cancer cell inoculated mice was improved with the administration of IFN (mixed preparation) (Gresser et al. 1969). Since this time, the role of IFN signalling in cancer has been extensively studied (reviewed in (Parker et al. 2016)). As detailed in Figure 41, IFNs act both directly on the cancer cells, and on the milieu of immune cells present in the microenvironment. Type I IFN

concurrently reverses the immune evasion of cancer cells, promotes T-cell tumour killing and reduces the recruitment of immunosuppressive cells (Parker et al. 2016). Type II IFN has also been shown to induce Mo differentiation into anti-tumoural macrophages rather than TAMs (Duluc et al. 2009; Parker et al. 2016). By modulating the immune cells and also the endothelial cells, the microenvironment is additionally normalised by IFNs (Kammertoens et al. 2017; Glasner et al. 2018; Ivashkiv 2018).

In light of the known actions of IFNs but the limited use due to side-effect and lack of specificity, De Palma and colleagues investigated if IFN therapy could be targeted using Mo. Having previously established that a subset of Tie-2 expressing Mo found both in mice and humans, home to the TME (De Palma et al. 2005; De Palma et al. 2007; Venneri et al. 2007), they used this as a means to achieve targeted therapy. Using a lentivirus expressing mouse *Ifn1a* cDNA from the promoter/enhancer sequences of the *Tie-2* gene and combining this with GFP expression they generated a mouse with inducible *Ifn1a* transgene restricted to Tie-2 expressing cells (De Palma et al. 2008). In the spontaneous PyMT model (FVB background) the results were very promising both with early and late-intervention. There was an increase in T-cell infiltrates and a suggestion of increased cytolytic activity of myeloid cells. In relation particularly to myelopoiesis, the increase in circulating CD11b+ cells observed in the spontaneous PyMT-MMTV FVB tumour bearing mice, was partially attenuated in mice with *IFN1*α Tie-2 cells. It is not clear the mechanism

of this, however. In relation to the findings here, the study by De Palma and colleagues suggests that transcriptional levels of *Ifn1a* in Mo may affect both the kinetics and the subsequent phenotype when Mo differentiate into TAMs.

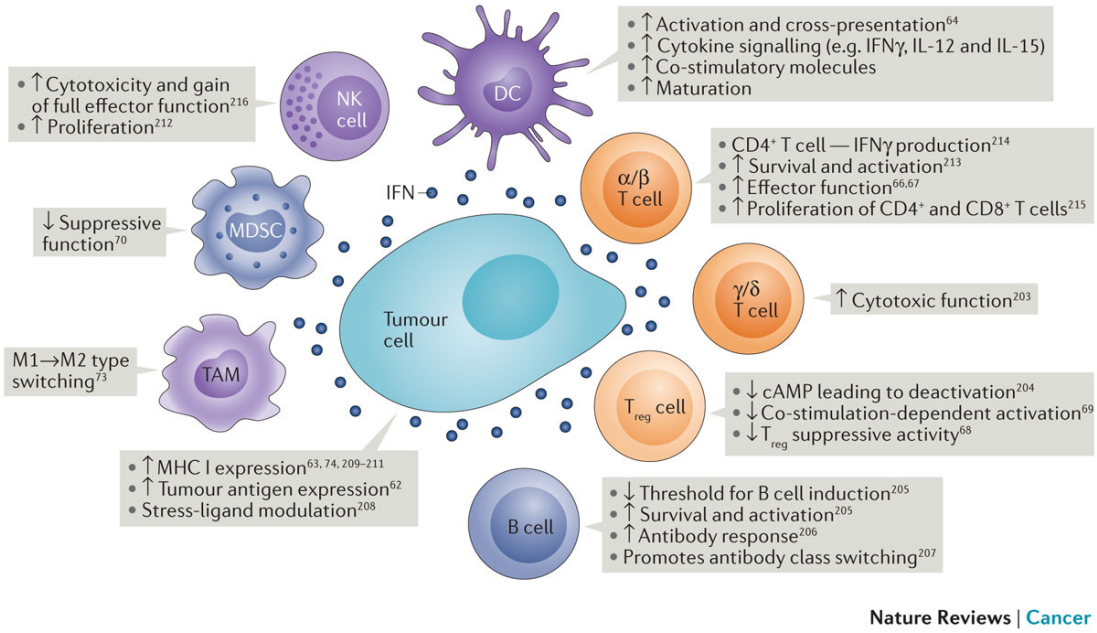

Figure 41 The role of Interferons in cancer. *Both endogenous and exogenous (as a result of IFN therapy) type I and type II IFNs play major roles in activating anticancer immunity (such as promoting the activity of α/β T cells, γ/δ T cells, natural killer (NK) cells and dendritic cells (DCs)), as well as inhibiting the activity of immune-suppressive cells (such as regulatory T (T_{reg}) cells and myeloid-derived suppressor cells (MDSCs)) and the conversion of tumour-associated macrophages (TAMs)). Type I and type II IFNs may also act directly on the tumour cell to improve antigen expression and to upregulate numerous immune-interacting molecules (such as major histocompatibility complex class I (MHC I) and stress ligands recognized by germline-encoded immunoreceptors). Note that although many of these pathways and mechanisms overlap and synergize, the role of B cells in antitumour immunity*

is contentious. In addition to B cells being positively correlated with ovarian cancer outcomes, others suggest that this cell type promotes tumour progression in various mouse models. cAMP, cyclic AMP; IL, interleukin. Image and caption adapted from Parker et al. 2016.

As IFNs are well documented in the literature and the most enriched pathways in cancer featured altered IFN signalling, it was reasonable to assess if IFN signalling in Mo differed in cancer. Unfortunately, the findings were inconclusive. This may be because IFNγ was used. The pathway analysis featured predominantly type I IFN signalling, which acts via IFNα or IFNβ rather than IFNγ (Stark & Darnell 2012; Villarino et al. 2017). IFNγ signals via a type II pathways and, despite having similar nomenclature due to historical context, is distinct from type I IFN responses (Stark & Darnell 2012; Villarino et al. 2017; Parker et al. 2016).

Undertaking further functional work has been considered as well as further profiling of Mo, for example exploring population heterogeneity in the spleen by RNAseq. But this would need to take into account that no orthologous changes have been observed, questioning the clinical relevance of such work. The lack of translation to humans was the main reason that this body of work was not expanded further. In considering the comparisons between mouse and human however, it is worthwhile to highlight the limitations of the evaluation assumed here.

The mice that were sequenced had advanced cancer, whereas human participants had early stage, non-metastatic disease. While the timepoint at which to sequence was chosen when changes were expected to be greatest, it may be that the timepoint was too advanced to compare with the human dataset. Unfortunately, there are no available RNAseq datasets in human Mo with advanced cancer. It is also likely that, if there were, it would be difficult to obtain data that was “off-treatment”. An obvious solution is to re-sequence the mice at a much earlier stage. This is something that is being undertaken and that will permit a more like for like comparison. Another possibility as to why there are no orthologous changes may be because the datasets are not comparable in the way in which they were acquired. The human dataset is taken from whole Mo, whereas the mouse dataset is broken down into two subpopulations.

Nonetheless, undertaking this work in the mouse, conferred a number of benefits. Firstly, it is possible to deduce where cells are being conditioned. Both the RNAseq and the subsequent validation of MHCII expression suggests that the predominant shift in antigen presentation at least occurs within the BM. But that further changes may occur within the blood, as demonstrated by a greater number of DEGs in the blood versus the BM. This is reinforced by the greater enrichment of downstream pathways, such as TNFα production, in the blood but not the BM. Two stage conditioning of immune cells in cancer is described in the field of MDSCs (Marvel & Gabrilovich 2015).

Secondly, the comparison of mouse strains reveals transcriptional profiles of Mo in a setting of resistance in the C57BL/6 versus susceptibility in the FVB. Unfortunately, because the sequencing depth was not matched in the two strains, it is ill informed to draw definite conclusions.

Two arguments could be made. The enrichment of pathways was stronger and more extensive in the C57BL/6 strain. This could be used to argue that in the more resistant C57BL/6 strain, a more coordinated manipulation of the immune system is required. The down-regulation specifically of type I IFN and additionally of IL-1β was restricted to the C57BL/6 mice. This is especially interesting as a recent paper demonstrated that while high levels of IL-1β are required for primary tumour progression, sustained high levels inhibit the formation of secondaries and blocking IL-1β signalling actually potentiates metastases (Castaño et al. 2018). The production of IL-1β by TAMs in the KEP mouse model has been shown to be driven by CCL2 (Kersten et al. 2017). Though in this particular model, blocking CCL2 has no effect on circulating Mo (Kersten et al. 2017). It may be that the differences in pathways found here reflects that different mechanisms are required for tumour progression in the two strains. This would be in keeping with the known difference in both Th and macrophage responses in the two strains (Mills et al, 2000). Contrary to this proposition, the LFCs in FVBs were greater and thus it could be argued that the transcriptional shifts in FVBs are greater. It is reasonable to hypothesise that the FC in genes, including those that were commonly DE in both strains,

are representative of the greater hametopoetic stress in FVB mice. This agrees with the hypothesise that it is the inflammatory context of advanced cancer that drives the transcriptional profiles of Mo observed here.

To conclude this chapter, there are a number of interesting findings in relation to the transcriptional changes that occurred to mouse Mo in late tumour-bearing mice. While the data at current does not conclusively prove that there are no orthologous changes with humans, and it may be worthwhile to undertake further work in mice, there was a lack of evidence to support continued efforts to delineate the transcriptional regulation of Mo using mice. For this reason, it was decided to shift the focus to human samples. This will form the focus of the final results chapter.

Chapter 6 Transcriptional regulation of human monocytes in breast cancer

6.1 Introduction

Initial studies focused on identifying transcriptional signatures in circulating human Mo that could be used for diagnosis and prognosis of cancer (Cassetta et al. 2019; Chittezhath et al. 2014; Hamm et al. 2016). These studies confirmed that circulating Mo were transcriptional distinct in cancer patients, suggesting that transcriptional regulation was altered perhaps systemically within the blood, rather than just on arrival to the TME.

From a therapeutic perspective the importance of understanding transcriptional regulation of Mo was recently highlighted by successful use of HDAC inhibitors targeting myeloid populations in breast cancer mouse models (Guerriero et al. 2017). While the focus of this paper was on reprogramming of TAMs, it was hypothesised that this effect was possibly through reprogramming of the TAM precursors, Ly6c^{high} Mo (Guerriero et al. 2017).

There are many methods used to assess transcriptional regulation. The use of RNAseq can provide some indicators. For example, there may be alterations to genes for TFs and related genes that are known to be regulated by respective TFs. Post-transcriptional focused analysis can also yield further

information (Schmid et al. 2018; Gaidatzis et al. 2015). However, RNAseq cannot reveal epigenetic regulation such as changes to chromatin structure, methylation or acetylation directly of the DNA or indirectly of histones, and the activity of the many regulatory and co-regulatory factors.

An important aspect of transcriptional regulation relates to the binding of TFs, which depends on the availability of binding sites. The accessibility of gene elements can be investigated using both DNA I hypersensitivity assays and the ATACseq method (Elgin 1981; Pipkin 2006; Buenrostro et al. 2013). The latter of which uses a naturally occurring phenomena, the transposase 5 enzyme, which cuts into open areas of DNA. By exaggerating the efficiency of this, and attaching sequencing primers to the enzyme, accessible areas of DNA can be isolated and sequenced (Buenrostro et al. 2013). By using size selection techniques, such as via a simple agarose gel, areas that are closely associated to a nucleosome can be selected for sequencing to reveal which sites are readily (and perhaps differentially) available.

As discussed in the introduction, TF binding alone is not sufficient to regulate transcription. An important factor is the status of histones, which can be assessed using immunoprecipitation techniques with an antibody binding to the protein of interest. By combing this with NGS (ChIPseq), whole genome coverage of binding sites can be elucidated. ChIPseq can also be used to assess binding of transcriptional machinery such as RNA polymerase II. While RNA polymerase II and H3K4me have been used to identify enhancers, both

of these can also be bound to transcriptional elements wherein transcription is either paused or poised (Rada-Iglesias 2017; Chen et al. 2018). Therefore, these methods lack specificity in identifying actively transcribed regions. In contrast, the histone H3K27 is acetylated only post-transcriptionally and has been shown to have greater specificity in identifying active transcription (Creyghton et al. 2010).

Thus, the aim of this final body of work was to use RNAseq, ATACseq and ChIPseq to deduce aspects of transcriptional regulation that are altered in blood Mo in patients with breast cancer.

6.2 Strategy for epigenetic profiling of human blood monocytes in breast cancer

For the first cohort of patients, samples were acquired in January and February 2018. Cancer sample demographics are shown in Table 4. The majority of patients had NST, non-metastatic, grade 2, ER+ cancer. The mean age for cancer and control samples was 64 (range 51-70) and 55 (range 44-72) respectively. Sufficient cells were obtained to process 8 cancer samples and 8 control samples for both RNAseq and ATACseq. Only half the samples had sufficient cells for ChIPseq. The ATACseq data from this cohort was not of good enough quality to allow for analysis and a need for further optimisation was identified. Nonetheless, the RNAseq data was analysed and used to

guide further decision making. For the RNAseq data, an initial exploratory analysis was undertaken using PCA and DE analysis.

On PCA, 4 of the cancer samples clustered separately from the remaining samples (Figure 42, A). To assess why this may be, patient demographics were consulted. However, none of the samples were common in terms of age, histological subtype, grade, lymph node status or receptor status. The details for processing of samples and the analysis files for sorts were inspected. It was noted that there was a significant increase in the proportion of $CD14^{low}$ $CD16^{high}$ Mo (referred to as CD16 Mo hereafter) in some cancer samples. Samples that segregated on PCA, were those which contained a much greater proportion of CD16 Mo (Figure 42, B).

To investigate how much the proportion of CD16 Mo may be contributing, a FANTOM consortium dataset was identified, which compared immune cells from healthy volunteers and included sequencing of $CD14^{high}$ $CD16^{low}$ (here on in referred to as CD14) and CD16 Mo (Schmidl et al. 2014). This enabled comparison of DEGs from comparing cancer versus healthy control Mo with DEGs between the two Mo subsets in healthy human samples.

ID	Age	Type	Grade	LN	ER	PR	HER
CA1	68	NST	2	-	8	5	-
CA2	66	Lob	3	+	8	2	+
CA3	64	NST	2	-	8	8	-
CA4	57	DCIS	2	-	n/a	n/a	n/a
CA5	70	NST	2	-	8	7	-
CA6	70	NST	1	-	8	7	-
CA7	60	Tub	1	-	8	8	-
CA8	51	NST	2	+	8	0	-
CA9	67	Muc	2	-	8	3	-

Table 4 Demographics of human Mo samples from breast cancer patients acquired in January to February 2018. *NST = Non-special type, Lob = Lobular, DCIS = Ductal Carcinoma in Situ, Tub = Tubular, LN = Lymph node status, ER = Oestrogen receptor score; PR = Progesterone score; HER = Herceptin receptor status. The use of n/a signifies not applicable.*

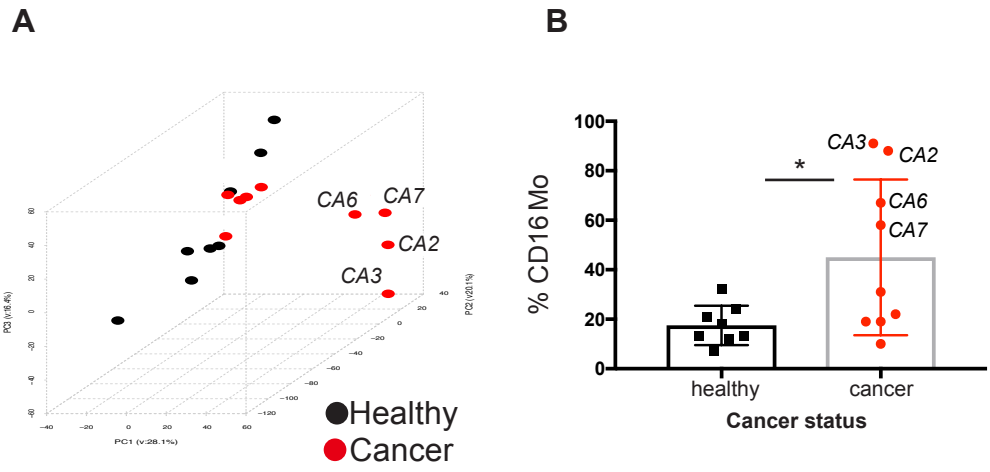

Figure 42 Primary analysis of human blood Mo RNAseq samples acquired in January to February 2018 *(A) PCA of all samples processed for RNAseq (B) Percentage of CD16 Mo as a total of all Mo according to control or cancer sample status. Control samples are indicted in black and cancer in red. Labelled are cancer samples 2,3,6 and 7 which clustered separately to other samples. * p value <0.05 by unpaired t-test.*

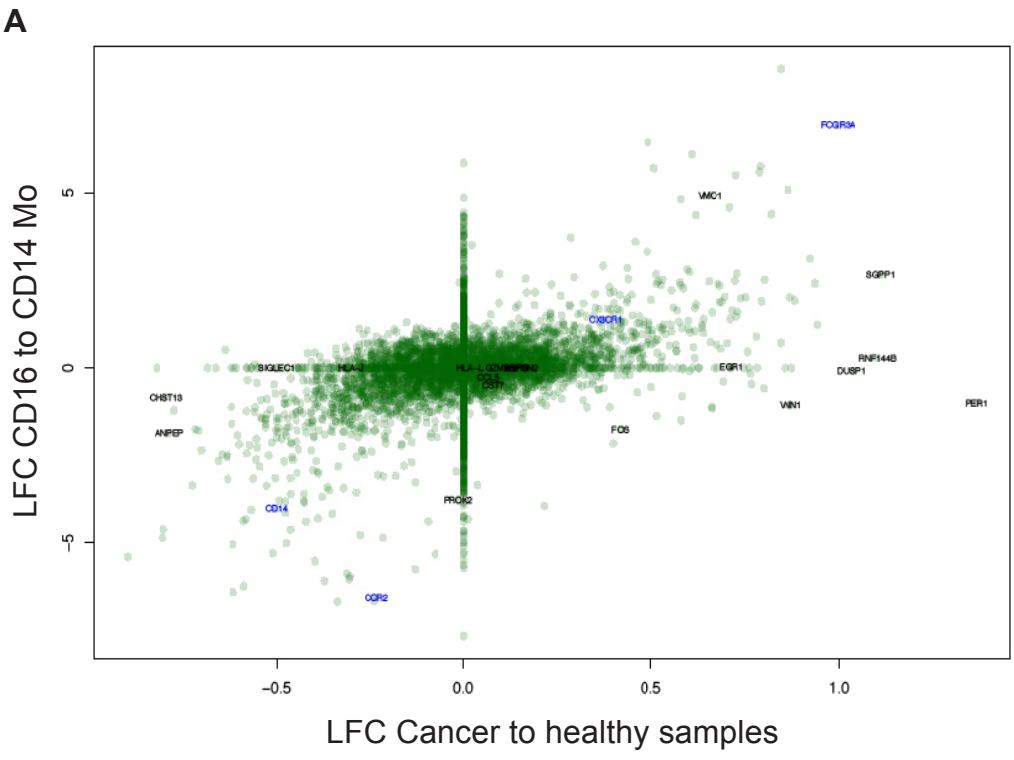

Figure 43 Contribution of ratios of CD16 and CD14 Mo populations in each sample to the DEGs detected *(A) Comparison of LFC in DEGs from two datasets: On the X-axis the data-set comparing cancer and control whole*

Mo and on the Y-axis a data-set generated by comparing CD14 and CD16 from health samples (FANTOM). Genes highlighted are known markers of CD16 and CD14 Mo. Genes in black are those featured in plot (B). Correlation of genes with an absolute LFC>1 was rho 0.78 (Spearman's, p <2.2x10^{-16}) (B) LFC Changes in DEGs when DE modelled for CD16% in each individual sample. Up-regulated genes are shown in red and down-regulated in blue. LFC values are labelled adjacent to corresponding bars.

There were 370 DEGs (q.value<0.05) between the cancer versus healthy control Mo. Plotting the LFC in DEGs in both this and the FANTOM dataset (Figure 43, A) revealed that while there were a number of DEGs unique to each dataset, there was a strong correlation of genes that were DE in both datasets (Spearman's test; rho 0.78, p <2.2x10^{-16}). This suggested that the prominence of CD16 Mo in the cancer samples may be distorting the results. Given this, the percentages of CD16 Mo were built into the analysis. This revealed a number of genes that, without adjustment, were either not shown to be DE or for which the LFC value was lower (Figure 43, B).

The aim of the RNAseq was to be able to correlate findings with Mo epigenetic profiles. As discussed in the introduction, CD14 and CD16 Mo are characterised by common TFs but also have a number of known TFs that are distinct. Little is documented on the ATACseq profiles between the two Mo populations, but it was not unreasonable to suspect that the chromatin conformation may differ. Taking this into account, along with the findings of this preliminary RNAseq analysis, the decision was made that any further

profiling on Mo should be done on the distinct CD14 Mo and CD16 Mo populations, rather than as whole Mo. As this resulted in lower cell yield, the use of ChIPseq was forsaken in the following cohort.

6.3 Transcriptional alterations to human blood monocytes in cancer

Following the decision to profile Mo subsets and the optimisation of techniques (detailed in the Appendix section 9.3.1 Optimising Accessibility of Transposase Assay (ATAC)), the aim was to accrue a small cohort of patients. Samples were accrued from October 2018 to February 2019 on 8 cancer patients and 5 healthy controls. The demographics of all samples collected are detailed in Table 5. Cancer patients were generally older; with a mean age of 58 (range 52-69) and 47 (range 40-60) in cancer and healthy groups respectively. Because sufficient cells for both RNAseq ($25x10^3$ cells) and ATACseq ($50x10^3$ cells) in both Mo populations were not always achieved, there was not a full complement of profiling for each patient (Table 5). Among the samples initially classified as having invasive cancer, there was 1 patient with pure DCIS on finally histology (Table 6). The majority of patients had NST cancer (Table 6). Just 1 patient had grade 3 triple negative breast cancer, representing a high risk for recurrence (Table 6). All patients had confirmed non-metastatic disease (note that for patient CA8 micro-metastasis were detected but that this does not reflect lymph node metastasis by current clinical grading) (Table 6).

In terms of FastQC assessment, all samples were of excellent quality. One RNAseq sample (CA5 CD14) showed a lower correlation with all other samples (<0.9) and clustered separately on PCA (Figure 44, A). This sample was under-sequenced with just $14.5x10^6$ initial reads, a unique mapping rate of 88% and $12.8x10^6$ unique reads. When using normalised transcripts per million (TPM) and checking clustering of samples, this sample again was an outlier (Figure 44, D). It was therefore excluded from further analysis.

Samples clustered predominantly on Mo subtype (Figure 44, A). Visualising CD16 and CD14 Mo samples separately demonstrated that in both subpopulations, healthy controls clustered together (Figure 44, B-C). In the analysis of both Mo subpopulations, CA2, CA7 and CA8 samples clustered with healthy control samples (In PC1 for CD16 Mo and PC2 for CD14 Mo, see Figure 44, B-C). Consulting the clinical information, it was noted that sample CA2 was from a patient with in-situ disease and CA8 from a patient with lobular cancer. There was no clinical explanation for CA7 clustering with the healthy controls. Given this, DE analysis was undertaken including all samples, excluding CA2 or CA8 or both. However, this did not greatly change the DEGs and results are presented inclusive of all samples (a full list of DEGs can be found in the supplementary files).

There was a 7-fold increase in the number of genes up-regulated versus down-regulated in cancer versus healthy control CD16 Mo; 185 genes were up-

regulated while only 27 genes were down-regulated (q.value<0.05) (Figure 45, A). This pattern was true also for CD14 Mo but there were approximately half the number of DEGs in this population; 93 up-regulated and 14 down-regulated genes (q.value<0.05) (Figure 45, B).

There were a number of genes in common to both Mo populations (Figure 46). There were a number of genes commonly up-regulated that indicated towards an activated status of Mo in cancer patients, in particular with regards TNFα and NFkB signalling (Table 7). Despite a gene list of just 28 genes, myeloid activation involved in immune response (GO:0002275) was enriched with a significant Log q.value of 5.66. The gene for the TF, EGR1 was the most up-regulated in both CD14 and CD16 cancer Mo.

Sample ID	Age (years)	Status	CD14 RNA	CD14 ATAC	CD16 RNA	CD16 ATAC
CA1	55	Cancer	✓	✓	✓	✓
CA2	52	Cancer	✓	✓	✓	✓
CA3	53	Cancer	✓	✓	✓	✓
CA4	69	Cancer	✗	✗	✓	✓
CA5	55	Cancer	✓	✗	✓	✓
CA6	55	Cancer	✗	✗	✓	✓
CA7	62	Cancer	✓	✓	✓	✓
CA8	66	Cancer	✓	✗	✓	✗
	Mean 59					
Cn1	44	Healthy	✓	✓	✓	✓
Cn2	60	Healthy	✓	✓	✓	✓
Cn3	40	Healthy	✓	✓	✓	✓
Cn4	44	Healthy	✓	✓	✓	✓
Cn5	46	Healthy	✓	✗	✓	✗
	Mean 47					

Table 5 Demographics and human Mo samples obtained for all sorted samples from October 2018 to February 2019. *✓ = sample, ✗ = no sample obtained.*

Sample ID	Hist. Type	Grade	ER	PR	HER2	LN Status
CA1	NST	2	8	7	Negative	Negative
CA2	DCIS	2	8	0	Negative	Negative
CA3	NST	3	0	0	Positive	Negative
CA4	Tubular	1	8	7	Negative	Negative
CA5	NST	3	0	0	Negative	Negative
CA6	NST	2	8	8	Negative	Negative
CA7	NST	2	8	6	Negative	Negative
CA8	Lobular	2	8	7	Negative	Negative

Table 6 The histological subtypes, grade, receptor status and lymph node status for all cancer patients obtained from October 2018 to February 2019. *Abbreviations are as for Table 4 on page 152.*

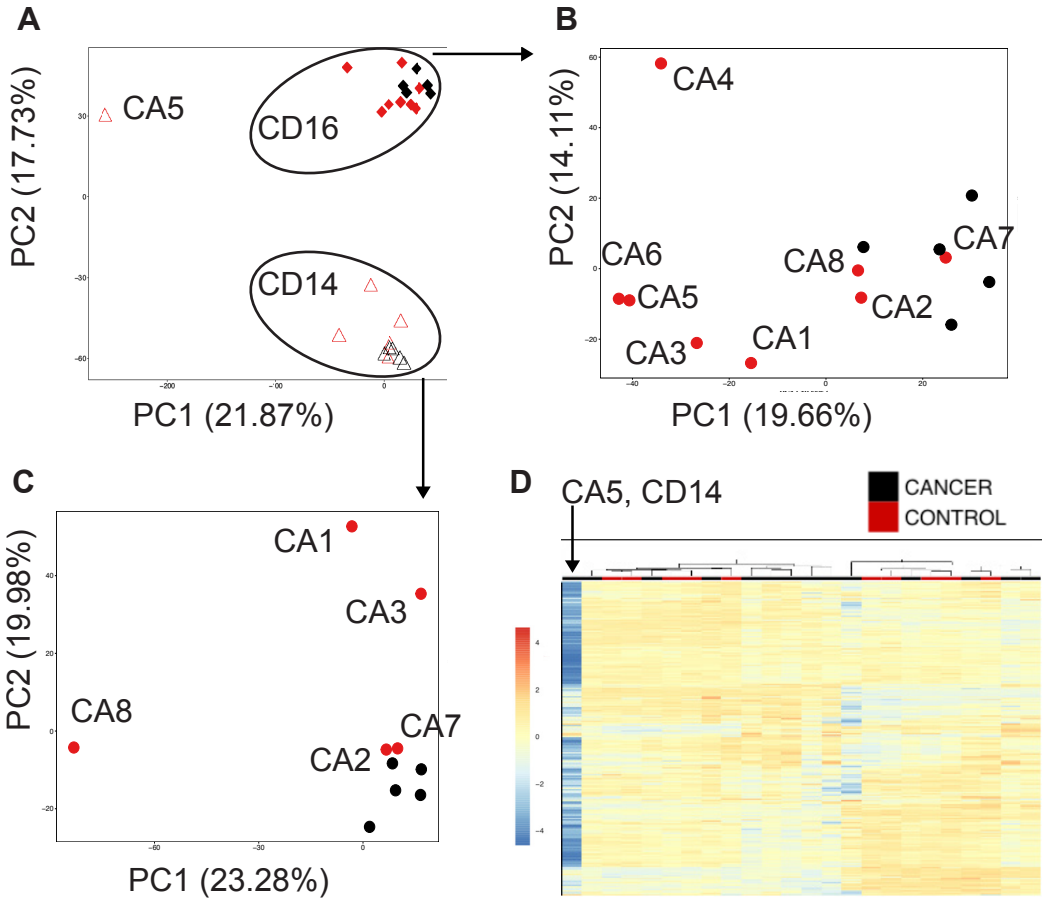

Figure 44 Primary analysis of RNAseq from human Mo samples collected from October 2018 to December 2019 *(A) PCA of all samples, with outlier sample CA5 labelled and clustering by Mo sub-type shown (B) PCA of CD16 Mo samples, with cancer samples labelled (C) PCA of CD14 Mo samples, with cancer samples labelled (D) Gene expression heatmap of all Mo RNAseq samples with unsupervised hierarchical clustering applied to all genes. Samples are arranged horizontally, and sample characteristics are provided in horizontal bars for each column denoting cancer (red) and control (black). Genes are arranged vertically; Red colour within the heatmap indicates up-regulation, and blue colour indicates down regulation based on the tpm z-score (range [-4, 4]). Samples are clustered using complete linkage and Pearson correlation. For (A-C) Control samples are indicted in black and cancer in red.*

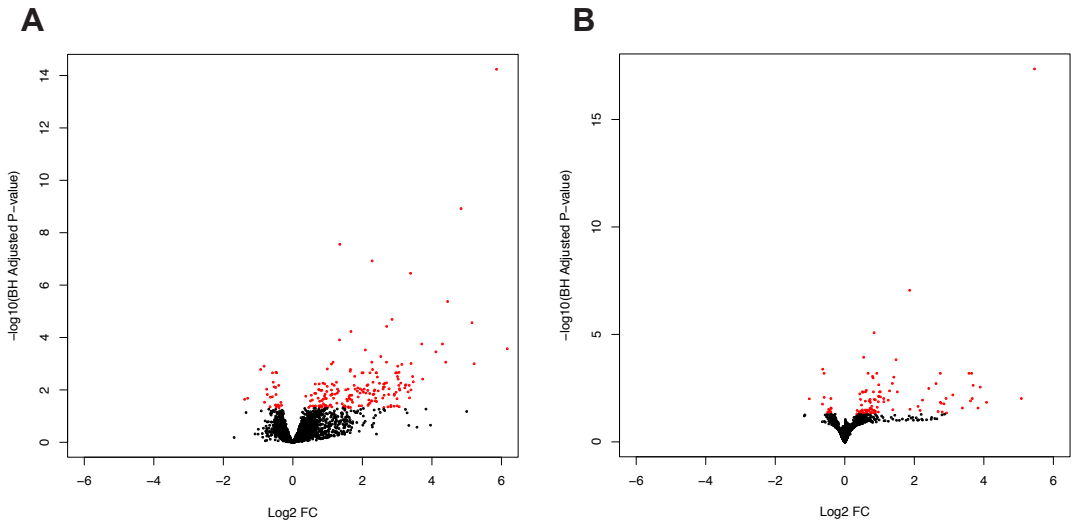

Figure 45 Volcano plots for RNAseq of human samples collected from October 2018 to December 2019 *(A) CD16 Mo samples. A total of 185 up-regulated and 27 down-regulated genes with a q.value<0.05 (B) CD14 Mo samples. A total of 93 up-regulated and 14 down-regulated genes with a q.value<0.05. Genes with a q.value<0.05 are indicted in red.*

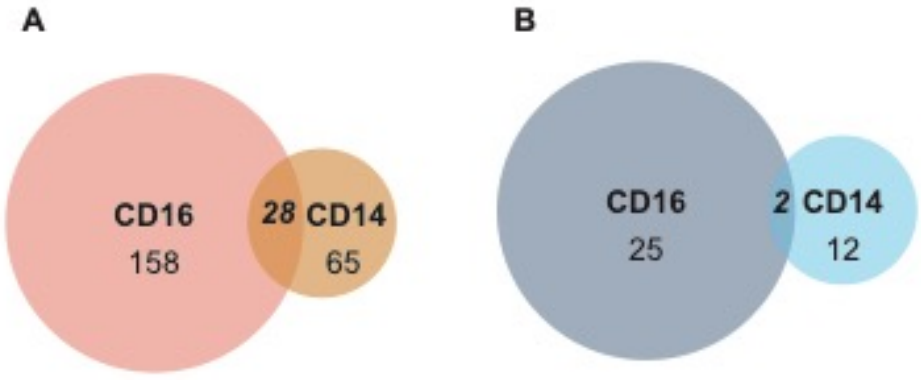

Figure 46 Venn diagram of DEGs in CD16 Mo and CD14 Mo *(A) Up-regulated genes (B) Down-regulated genes. Only genes with a q.value<0.05 included.*

Gene	CD16 LFC	CD14 LFC	Category	Pathway(s)
EGR1	4.8	5.6	Transcription Factor	Diverse, including NFkB
NFKBIA	0.8	1.1	Transcription Factor	NFkB
KLF6	0.7	1.2	Transcription Factor	NFkB
SLC2A3	2.1	1.0	Transporter	NFkB
IRS2	1.6	1.2	Soluble molecule	NFkB
TRIB1	1.1	2.3	Kinase	NFkB
MCL1	0.8	0.9	Anti-apoptotic protein	NFkB
CXCL1	5.2	3.4	Chemokine	NFkB IL2-STAT5
IGF2R	1.5	1.3	Receptor for IGF2	IL2-STAT5
PIM1	0.9	0.8	Enzyme	IL6-JAK-STAT3 IL2-STAT5
ADAM8	1.4	1.1	Transmembrane protein	KRAS signalling
F5	2.6	0.8	Coagulation factor	Complement cascade

Table 7 Selected DEGs common to both CD14 Mo and CD16 Mo in breast cancer versus healthy samples. *For each gene the LFC in each population is given, the category of the protein that the gene codes for and the functional pathways that the protein is involved in.*

Amongst the CD14 Mo there were only 14 genes down-regulated and none were related to each other by a common regulome (STRING analysis and Metascape analysis). A number of down-regulated DEGs were involved in modules or components of transcriptional regulation. This included the gene *SLFN11*, a schlafen family member thought to play a role in dendritic versus macrophage fate in Mo (Liu et al. 2017) and the zinc finger *ZNF644* which has been shown to be a high affinity *EGR1* binding site (Kubosaki et al. 2009). The most strongly down-regulated gene was the metabolic or proliferative gene *BCAT1* (LFC -1.18), which is also known to effect Mo to macrophage differentiation (Papathanassiu et al. 2017).

The amplitude of LFC in the down-regulated genes was modest and far-outweighed by the up-regulation of inflammatory genes. This was reflected in the pathway analysis for up-regulated genes (Figure 47, A). In order to identify potentially important genes, soluble factors, chemokines, transmembrane receptors and TFs relevant to Mo biology were explored. As expected, the majority of changes to ligands and receptors suggested pro-inflammatory phenotypes as did the TFs (Figure 47, B). Genes that were not features in the pathway enrichment included *EGR2* and *FOXO-1* and a number of DEGs are related to increased survival (*MCL-1, ERG1*) and proliferation (*CDKN2D, BTG2, RARA*).

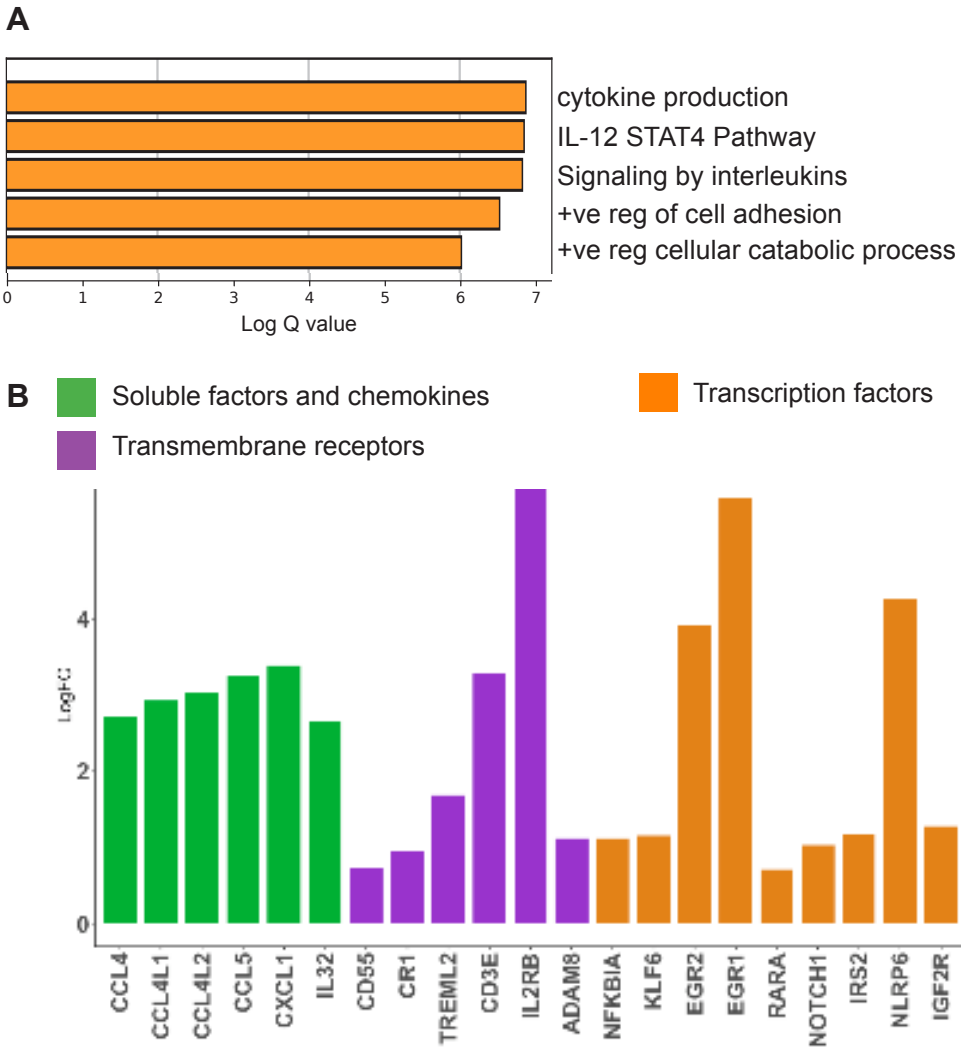

Figure 47 Analysis of DEGs in cancer versus healthy samples in CD14 Mo *(A) Metascape analysis of up-regulated genes. Log Q.values are plotted, and each bar coloured according to value on a scale of 0 to 30, represented with graduating intensity. Gene Ontology or KEGG terms for enriched pathways are annotated. Only pathways with a log q.values>5 are shown (B) Histogram of LFC in DEGs. Genes have been selected and grouped functionally as soluble factors and cytokines (green), transmembrane receptors (purple), and transcription factors (orange).*

With regards to the CD16 Mo, there were a number of relevant pathways significantly up-regulated, including pathways involved in cytokine production and release; migration; IL-10 and 1L-12 signalling; TNF and IFNγ responses (Figure 48, A). The effects of IL-10 are predominantly anti-inflammatory whereas the majority of pathways suggested a pro-inflammatory shift. To further assess if this was a genuine finding, the list of genes that had contributed towards the IL-10 pathway were assessed. The genes listed as hits were *CXCL1*, *CXCL8*, *PTGS2*, *IL1R2*, *CCL3L3* and *CCR2*. Additionally, none of the 39 genes for GO term "positive regulation of interleukin-10 production" (GO:0032733), featured in the CD16 Mo DEGs. Hence the finding of an up-regulation and enrichment in IL-10 was rejected.

In order to further identify potentially important genes, again genes relevant to Mo biology were explored (Figure 48, B). Genes for *CXCL8* and *CXCL1*, and their related receptors *CXCR1*, *CXCR2*, and *IL1R2* were up-regulated. The angiogenic factor *VEGFA* was up-regulated. Both *CXCR3* and *CD83* were down-regulated. Three receptors that are more commonly expressed on CD14 Mo; *CLEC4D*, *CCR2*, *CD163* (Wong et al. 2011) were up-regulated but so was *FCGR3B*. Both *IL7R* and *IGF2R* were up-regulated. Not featured in Figure 48, the extracellular matrix remodelling enzyme, *MMP9* was up-regulated (LFC 2.92), as was *MMP25* (LFC 3.46). Additional to the TFs commonly up-regulated in both Mo populations, TFs such as *ETS2* and *DUSP1* were up-regulated in CD16 Mo.

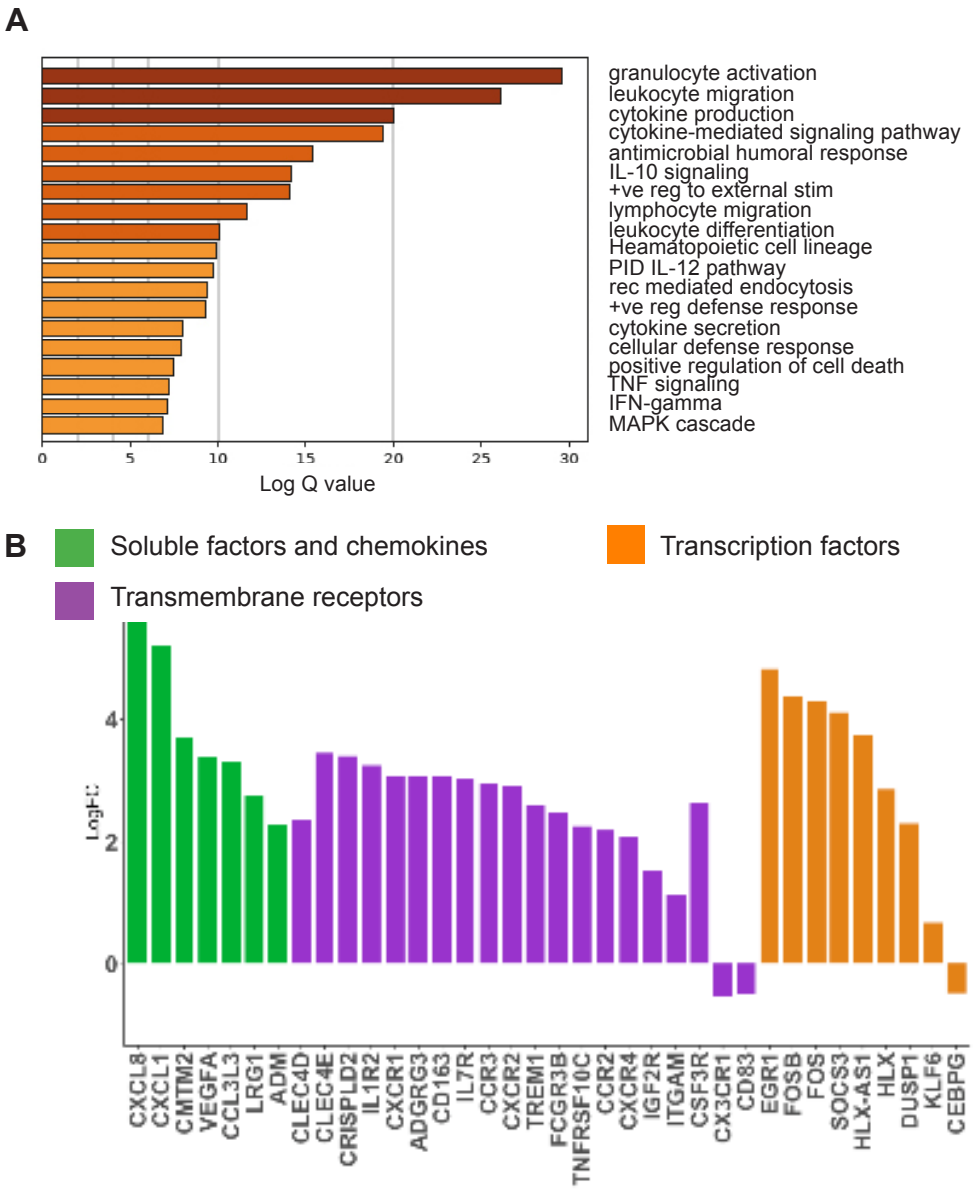

Figure 48 Analysis of DEGs in cancer versus healthy samples in CD16 Mo *(A) Metascape analysis of up-regulated genes. Q.values are plotted, and each bar coloured according to value on a scale of 0 to 30, represented with graduating intensity. Gene Ontology or KEGG terms for enriched pathways are annotated. Only pathways with a q.value>5 are shown (B) Histogram of LFC in DEGs. Genes have been selected and grouped functionally as soluble factors and cytokines (green), transmembrane receptors (purple), and transcription factors (orange).*

6.4 **Chromatin conformation of human monocytes in healthy controls and breast cancer patients**

ATACseq in this second cohort was of good quality with minimal noise. However, some samples were under sequenced and therefore had poor signal (Figure 49). As a further measure, motif enrichment throughout the samples demonstrated the expected motifs for Mo (PU.1, ELF4, SpiB, ETS1).

While deeper sequencing of some samples is required for a comprehensive analysis, a preliminary analysis was undertaken. On PCA, samples clustered by CD14 or CD16 status (Figure 50). It was not clear from PCA if there was a distinct separation of cancer from healthy samples in either the CD14 or CD16 Mo. Further analysis using IDR and DE was undertaken. As predicted by PCA, the most prominent difference was due to Mo subpopulation (Figure 51, A-B). While some cancer samples did cluster, there was no robust DE of tags between cancer and control in either the CD14 or CD16 Mo (Figure 51, C).

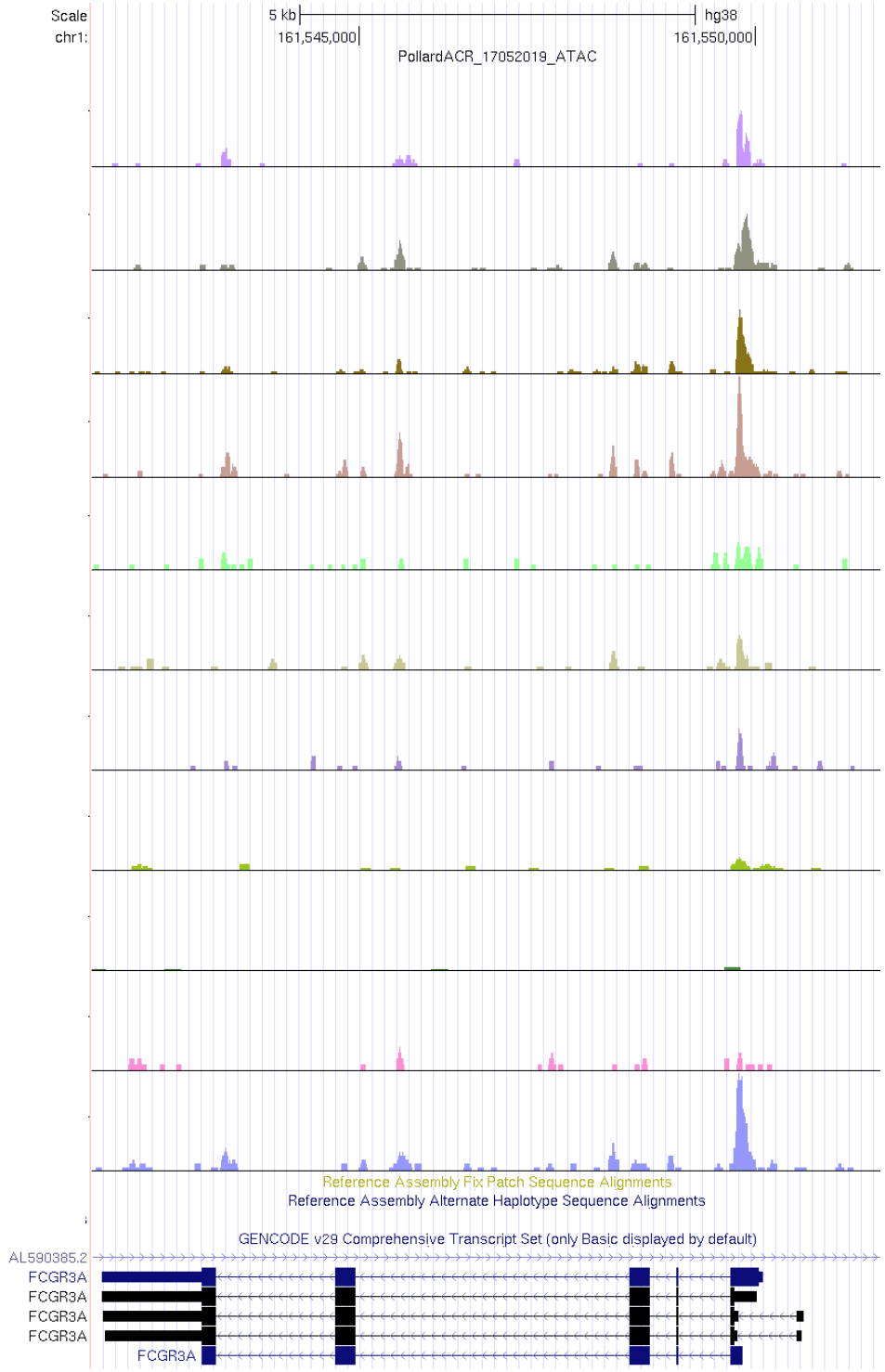

Figure 49 Example browser tracks for samples at the gene for FCGRA.

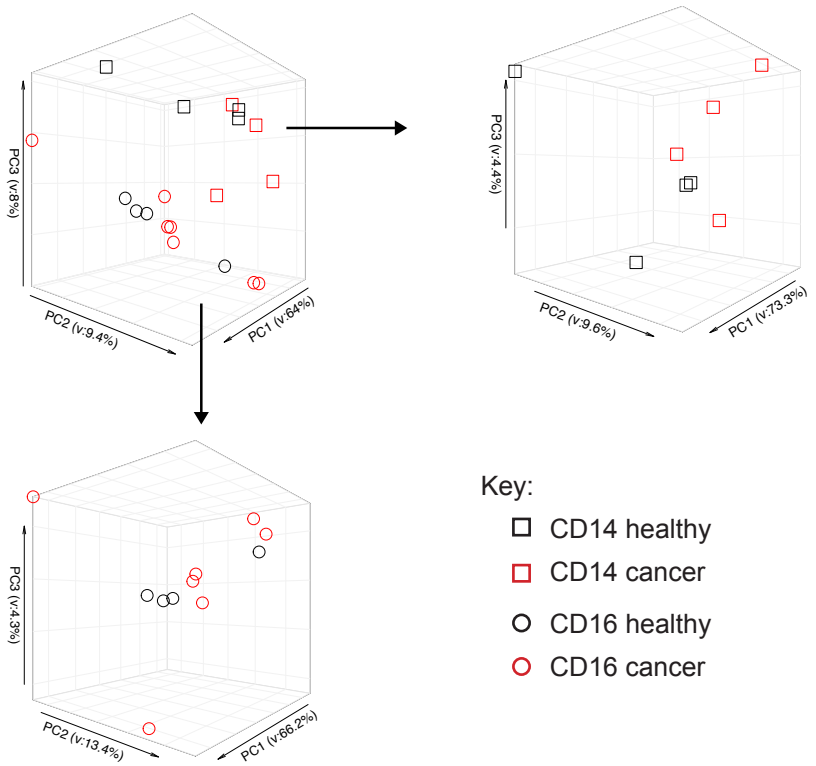

Figure 50 PCA of ATAC samples in healthy and breast cancer samples. *Samples from healthy volunteers are in black and samples from breast cancer patients are in red. CD14 samples squares and CD16 are circles.*

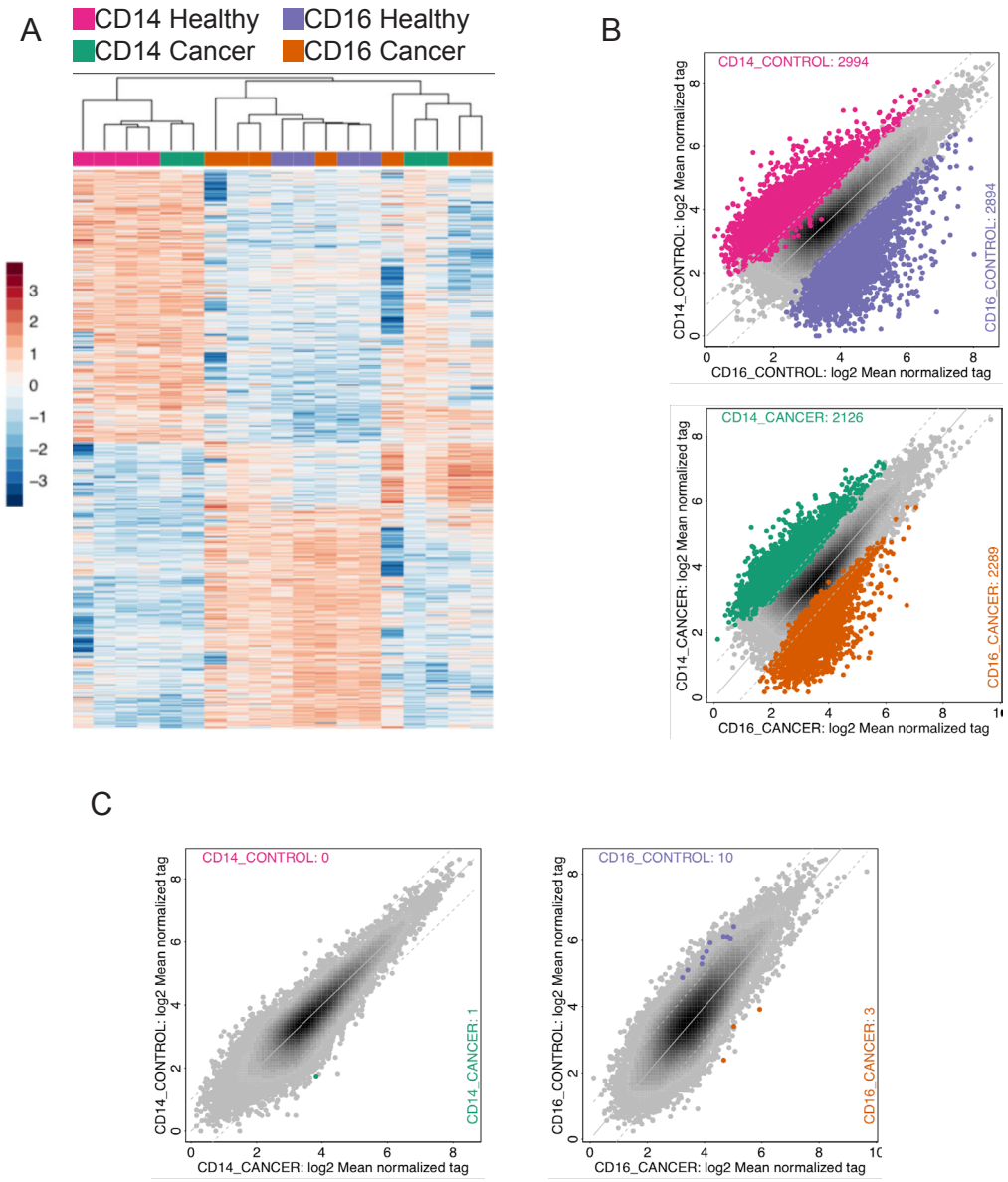

Figure 51 DE of ATAC peaks in cancer versus healthy CD14 and CD16 Mo *(A) Heatmap of normalised tag counts for peaks using non-supervised hierarchical clustering. Each column represents a sample with sample characteristics denoted by coloured bars indicating CD14 healthy (pink), CD14 cancer (green), CD16 healthy (purple) and CD16 cancer (red). Peaks are arranged vertically; Red colour within the heatmap indicates up-regulation, and blue colour indicates down regulation based on the z-score. Samples are clustered using complete linkage and Pearson correlation (B) Pairwise*

comparisons of peaks in CD14 versus CD16 samples for healthy samples (top, labelled control) and cancer samples (bottom) (C) Pairwise comparisons of peaks in cancer versus healthy samples for CD14 samples (left) and CD16 samples (right). Each dot represents the mean normalized tag counts for all samples in each group. Dots that are shaded as per the colours for bars in (A) indicate that the peak is DE between comparator on the x and y-axis (FDR<0.05 and LFC>1).

Returning to the RNAseq data, it was noted that samples CD16 CA1, CD16 CA3, CD16 CA5 and CD16 CA6 clustered away from healthy CD16 Mo (Figure 44, B). Therefore, a supervised approach was used to compare the ATACseq of just these samples with the controls. The IDR reference sets were altered appropriately, and the DE analysis was repeated. The DE of peaks led to clear clustering of cancer and control samples, with the exception of one cancer sample (Figure 52, A). There were over 5000 DE peaks in the cancer and in the control CD16 samples (Figure 52, B). Undertaking motif enrichment of known motifs, the ranking of motifs in cancer and controls were quite different (Figure 52, C). Differential enrichment of motifs of enhancers was evident (Figure 52, D). Further interpretation of these results was not undertaken as this was a bias and very limited analysis. However, given that there were potentially interesting findings, the decision was taken to acquire more samples, re-sequence and then re-analyse. This work is underway and so results are currently unavailable.

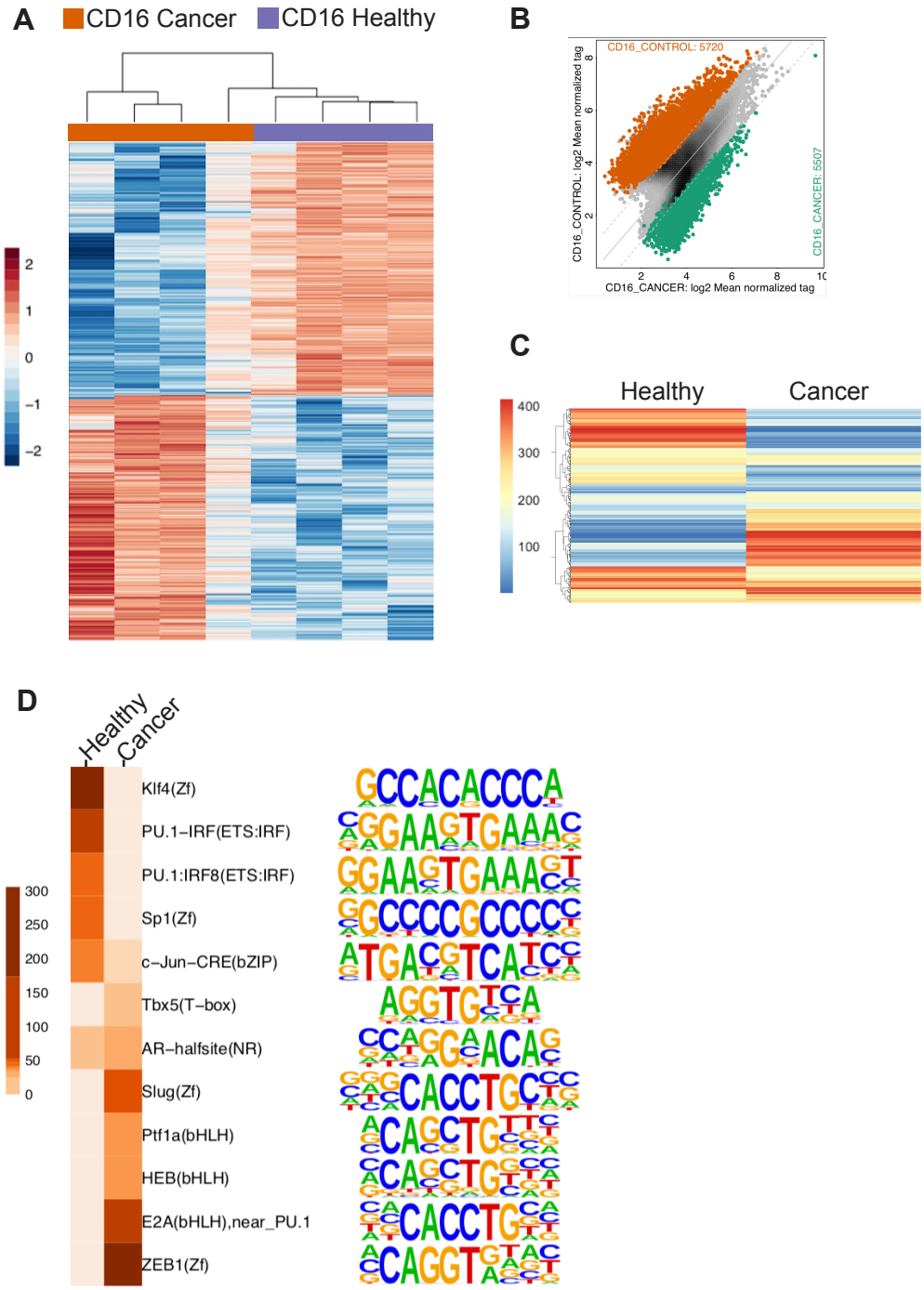

Figure 52 DE and motif enrichment of CD16 ATAC peaks in cancer versus healthy and CD16 Mo using just CA 1, 3, 5, 6. *(A) Heatmap of normalised tag counts for peaks using non-supervised hierarchical clustering. Each column represents a sample with sample characteristics denoted by coloured*

bars indicating CD16 healthy (purple) and CD16 cancer (red). Peaks are arranged vertically; Red colour within the heatmap indicates up-regulation, and blue colour indicates down regulation based on the z-score. Samples are clustered using complete linkage and Pearson correlation (B) Pairwise comparisons of peaks in cancer (green) versus healthy (red). Each dot represents the mean normalized tag counts for all samples in each group in the comparison plotted on the x and y axis. Dots that are shaded as per the colours for bars in (A) indicate that the peak is DE between comparator on the x and y-axis (FDR<0.05 and LFC>1) (C) Heatmap of 415 known motifs indicating the rank value (1 to 415) of each motif in healthy and control samples. Red colour within the heatmap indicates low rank, and blue colour indicates high rank based on a rank of 1 to 415 (D) Heatmap of motifs enriched in healthy and control samples. Each column represents a sample group. Each row represents a motif. Colour ranges from cream to dark brown based on the log q.value of enrichment. The abbreviated motif name is detailed to the right of each row and the Motif is to the right of that. For each group, 6 motifs within the top 15 motifs were selected for the heatmap.

6.5 **Comparison of monocyte subsets with mouse**

As a new gene set had been identified, the mouse data was again assessed for orthologous genes. There were very few genes common to both species (Figure 53). As predicted by the pathways results from both CD14 and CD16 Mo, several of the key TFs were indeed opposite in mouse compared with human. The two S100 calcium binding protein genes *S100A8* and *S100A9* were found to be commonly up-regulated. But, overall, orthologues change robustly linked to functional relevance could not be identified.

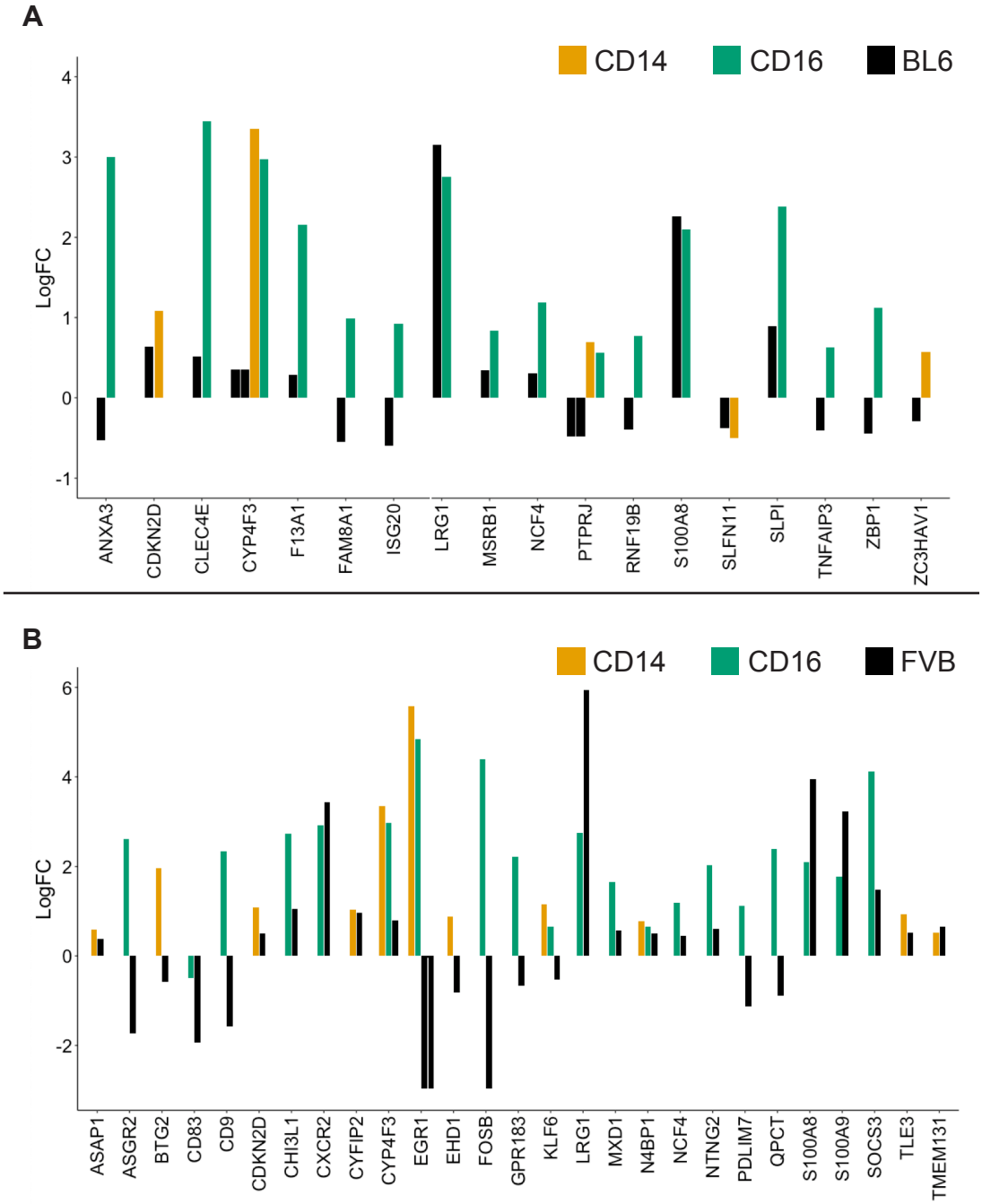

Figure 53 Histogram of LFC in DEGs between cancer and controls in CD14 and CD16 human samples and mouse samples *(A)LFC for human CD14 and CD16 Mo and C57BL/6 (BL6) mouse Mo (B) LFC for human CD14 and CD16 Mo and FVB mouse samples. For each gene the bar represents the LFC in CD14 (ochre) and CD16 (green) human Mo and mouse Mo (black). For mouse, DEGs are from Ly6c^{high} Mo analyses.*

6.6 **Discussion**

The aim of this body of work was to correlate changes on RNAseq with epigenetic changes, to better understand the transcriptional regulation of Mo in cancer. It was proposed that this could be achieved by combining the methods of ATACseq and ChIPseq.

One notable limitation with the data presented here is in obtaining samples from appropriate healthy controls. The prior approach in the lab had been to order blood to be delivered from a blood donor company based in the South of the UK. This was collected in the afternoon and delivered by the following morning. It was not possible to receive the blood on the same day in time to also sort that day. It was felt that this was not appropriate to match the cancer patients and so instead the local blood resource was used. However, as can be observed, the age of women in the healthy control group was generally younger and it was very difficult to identify older healthy controls as volunteers were employees within the QMRI, Edinburgh. Tis has particular implications when studying females with breast cancer as the menopausal status may have differed. This data was not collected and could have implications to the findings here.

Another issue encountered with this body of work was in trying to collect sufficient cells for the desired experiments. Initially, even when collecting

whole Mo, there were insufficient cell numbers for all three techniques. In response to this, ethics were altered to allow the collection of larger blood samples. The initial run of whole Mo was proven by both RNAseq and ATACseq to be a poor approach in understanding the transcriptional changes as there were large differences between the two Mo subpopulations. This meant however that cell numbers for each sample were further reduced. To achieve high quality samples, the aim was to be sorting cells within 2hrs of receiving them and have them sorted and ready for processing within 1hr. This was achieved for all samples but was not going to be possible when sorting much greater numbers, for example as required for ChIPseq. A number of strategies were considered, including bead enrichment or secondary sorting following an initial enrichment step. But overall there was a concern that it would not save enough time and may cause inadvertent stress to the cells. Another consideration was whether to use an inhibitor such as Flavoperidol. However, on further reading, there was evidence that while inhibitors may preserve the mRNA, they may alter the chromatin configuration (Chao & Price 2001).

There are some important observations with regards to the cell sorts. Firstly, while CD16 Mo expanded in cancer, the ratio of CD16 Mo to CD14 Mo was also higher than expected in healthy controls. It was observed that as sorts progressed, the CD14 population diminished. This is perhaps because CD14 Mo are denser than CD16 Mo (Cros et al. 2010). On presenting this work, a

scientist (Dr. Michael Connal Dennedy, NUI Galway) stated that they had encountered the same issue. After a great deal of trial and error, they had opted to use Xantham gum in the FACS buffer. This ensured a higher density buffer and thus kept the CD14 Mo in suspension. The data from these experiments has been requested. It may be that this strategy could be used. However, the effects of Xantham, which may activate Mo, would have to be tested.

With regards to the altered distribution within the Mo population, it is clear that regardless of the density issue, there is an expansion of CD16 Mo in cancer patients. This is in agreement with data from other studies in both colorectal cancer (Saleh et al. 1995) and breast cancer (Feng et al. 2011; Cassetta et al. 2019). To the best of knowledge, the work here is the first time that the two populations have been separately profiled in the context of cancer.

Focusing on the Mo subpopulations individually, there were a number of relevant genes that were up-regulated only in the CD14 Mo population. These included *CCL4* and *CCL5*. CCL5 is predominantly known as both a chemoattractant and modulator in the NFκB pathway. In addition, it is thought to direct Mo differentiation into anti-inflammatory macrophages (Aswad et al. 2017) but has also been shown to stimulate the production of enzymes such as MMP9 (Long et al. 2012). As discussed in detail, there is a great deal of evidence with regards the role of CCL5 in epithelial cancers. Of note, it was

one of the genes identified as up-regulated in Mo from RCC patients (Chittezhath et al. 2014).

CCL4 is known to be produced by Mo and its production can increase in inflammatory conditions such as systemic sclerosis (Carvalheiro et al. 2018). It is generally expressed only at high levels, once cells are activated and is an important chemokine in the recruitment of Mo and other immune cells (Maurer & Stebut 2004). Increased levels of CCL4 have been detected in solid tumours, where it correlates with TAM infiltrates, supporting a role in Mo recruitment in cancer (De la Fuente López et al. 2018). Expression of CCL4 is principally induced via TLR4-MyD88 signalling and depends on the downstream activation of the AP-1-NFκB axis (Kochumon et al. 2018). Thus, its upregulation points to an upregulation in TLR4 and NFκB pathways. This is supported by the finding that *IL-32*, a potentiator of the NFκB pathway (Kim et al. 2005), was also up-regulated in CD14 Mo.

Amongst the genes up-regulated on CD16 Mo, the NFκB induced chemokine gene *CXCL8* had the highest LFC and the NFκB pathway was enriched. As featured in Figure 54, NFκB stimulates the production of a number of factors that prompt angiogenesis (CXCL8), matrix remodeling (MMP9) and chemotaxis (CXCL8 via CXCR1/2) (Gales et al. 2013). In addition, NFκB has anti-apoptotic effects by driving the production of the *BCL-2* family of genes (Gales et al. 2013). Additional to those featured in Figure 54, NFκB promotes

angiogenesis through driving VEGFα pathways, the latter of which can further drive NFκB signalling (Xie et al. 2010; DeNiro et al. 2013). The polarisation of macrophages to a TAM phenotype has also been directly linked to NFκB signalling (Hagemann et al. 2008).

NFκB driven production of factors, such as CXCL8 and VEGFα by circulating Mo in cancer is supported by prior studies. A study of Mo in patients with RCC found up-regulation of *CXCL8* and *VEGFA* in cancer (Chittezhath et al. 2014). This was validated by qPCR and also by increased levels in supernatants from RCC Mo cultures (Chittezhath et al. 2014). Phosphorylated IκBα in RCC Mo was also increased. Up-regulation of *CXCL8* and *VEGFA* was attenuated by both an IKKγ and MyD88 inhibitor, validating that the MyD88-NFκB pathway is essential in the transcriptional changes observed in RCC Mo. Furthermore, Chittezhath et al showed that this was via IL-1R activation. Thus, the up-regulation of receptors for IL-1 in the CD16 Mo here, may suggest that these cells are primed and that there is positive feedback of the NFκB pathway. Signaling may be via IL-1, or via TNF as TRAIL (*TNFSF10*) was also up-regulated. Evidence elsewhere supports the roles of TNFα and IL-1 in NFκB signalling in cancer (Hoesel & J. A. Schmid 2013). TNFα was recently shown to be produced at high levels by both breast cancer cells and TAMs (Cassetta et al. 2019).

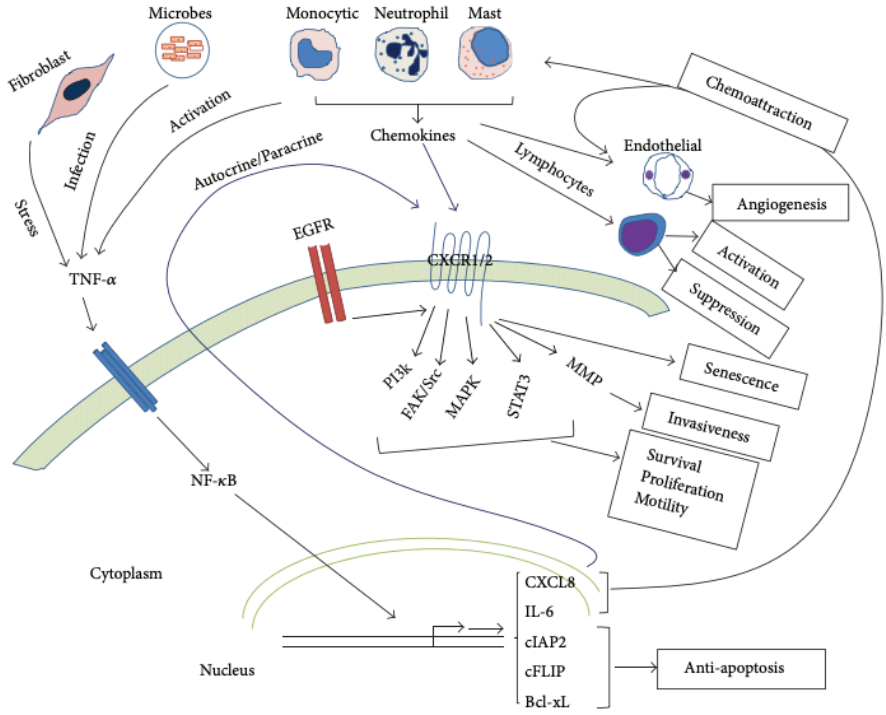

Figure 54 Principal mechanisms of CXCL8 regulation and signalling. *NF-κB activation is initiated primarily by TNFα released by stressed fibroblasts, in response to chronic infection, or by activated leukocytes (monocytes, Neuts, and mast cells). NF-κB is the primary regulator of the chemokines CXCL8 and IL-6, which are potent chemoattractant for leukocytes, especially Neuts. Other major transcriptional targets of NF-κB include the anti-apoptosis proteins, cIAP2, cFLIP, and Bcl-xL. CXCL8 signals through CXCL1 or CXCL2, whereas IL-6 signals through the IL-6 receptor (IL-6R). Leukocytes attracted to the initiated tumour secrete cytokines that drive the tumorigenic process by promoting angiogenesis through endothelial cell proliferation and modulation of lymphocyte responses. CXCL8 directly activates endothelial cells through their CXCR1 or CXCR2 receptors. CXCL8 binds to CXCR1 and CXCR2, and, in cooperation with EGFR signalling, may promote cancer cell survival, proliferation, motility, and invasiveness through the PI3K, MAPK, FAK/Src, STAT3, or MMP pathways. Since tumour cells may also express CXCR1 or CXCR2, CXCL8, in the tumour microenvironment, may signal through both*

paracrine and autocrine mechanisms. Figure and legend used with permission from Gales et al. 2013.

As for the causative factors in cancer that may be driving these changes to Mo, the relevance of CSF1 and other chemokines has been discussed. But, in relation specifically to the human findings and CSF1, CSF1 is known to drive NFκB pathways (Y. Wang et al. 2011; Stanley & Chitu 2014). CSF1 also modulates the survival of Mo and their differentiation to macrophages. Both *CD163* and *CD14* are recognised CSF1 induced genes and were up-regulated on CD16 Mo (Pyonteck et al. 2013).

A key aim was to understand the transcriptional regulation of Mo in breast cancer. On a simplistic level, useful information was obtained with regards alterations to TFs. The most obvious was the upregulation in *NFKB1A* in both Mo subsets. Additionally, both *KLF6* and *ETS2* (*ETS2* in the CD16 Mo only) were up-regulated. These two TFs are both reported to synergistically enhance NFκB signalling (Date et al. 2014; Sweet et al. 1998) . *ETS2* is also known to promote the survival of Mo (Sevilla et al. 1999) and also plays a key role in the angiogenic phenotype of TAMs (Zabuawala et al. 2010). Additionally, *KLF6* has been shown to polarise macrophages to a TAM phenotype (Bi et al. 2016). The most up-regulated TF gene was *ERG1*. The diverse roles of which include potentiating NFκB signalling (Ma et al. 2009) and driving progenitors towards a Mo/macrophage lineage (Nguyen et al. 1993; Krishnaraju et al. 2001). *EGR1* has also been shown to interact with *CSF1R* gene (Bencheikh et al. 2019), an

interaction which dissipates as Mo differentiate into macrophages (Liu et al. 2008). Thus, *EGR1-CSF1R* interactions may be a driving factor in the apparent increased ratio of CD16 Mo to CD14 Mo in cancer patients. This hypothesis is supported by the up-regulation of *NOTCH1* in CD14 Mo as *Notch1* has been shown to drive the differentiation of Lyc6^{high} to Ly6c^{low} Mo and therefore may well have the same action in human Mo (Gamrekelashvili et al. 2017).

Genes for TFs indicative of transcriptional regulation via negative feedback were also up-regulated. As described in the introduction, SOCS3 is one of the transcription factors involved in dampening immune responses. As is DUSP1, which acts to regulate MAPK signalling (Lang et al. 2006). It may be relevant that it is not until the CD16 Mo stage, where the transcriptional changes seem to be more profound, that these regulatory elements are up-regulated.

Crucial in further elucidating the transcriptional changes that were observed, will be investigating the epigenetic alterations to Mo in the context of cancer. While this was an aim of the project, it was only partially completed. There were some clues from very preliminary ATAC analysis undertaken that alterations to the chromatin structure alone may reveal important regulatory elements. It is however well recognised that the use of ATACseq alone is limited. Therefore, a key aim in progressing this body of work will be in optimising and undertaking other methods such as ChIPseq. This may be possible by using refined protocols, enabling the use of much lower inputs (Lorzadeh et al. 2017).

To conclude, the predominant evidence is in favour of NFκB activation throughout the human Mo populations. The CD14 Mo are the precursor to the CD16 Mo (Patel et al. 2017). It would seem that in the context of cancer, NFκB is up-regulated firstly within CD14 Mo. There are a number of indicators that the differentiation of CD14 Mo into CD16 Mo is increased in cancer. This is both in terms of alterations to Mo ratios and with respect to gene expression. It is hypothesised that within the CD16 Mo, the upregulation in NFκB is potentiated further, ultimately resulting in Mo primed to differentiate into pro-tumoural macrophages (Gales et al. 2013; Turner et al. 2014; Joyce & Pollard 2008).

Chapter 7 Summary and future directions

Breast cancer is the most common cancer in women worldwide (25%) and the second most common cancer overall (Antoni et al. 2016). Multiple factors determine the establishment, progression and dissemination of breast cancer cells. The TME is composed of many different cell types, including diverse immune infiltrates (Azizi et al. 2018). The balance of cell types present, and the cross-talk that occurs is crucial in tilting the balance in the favour of cancer.

Because Mo are the source of TAMs and MAMs (Arwert et al. 2018; Joyce & Pollard 2008; Kitamura et al. 2018), they are often portrayed as simply conduits to obtain end cells. Therapies that modulate Mo in cancer, for the most part, focus on reducing Mo recruitment. Re-polarising cell phenotypes tends to focus on cells within the TME (Cassetta & Pollard, 2017). This is based partly on an assumption that cells are polarised once they arrive at the tumour. Conversely, in the field of MDSCs it is well recognised that MDSCs are derived via systemic signals and that conditioning occurs prior to arrival to the solid tumour or metastases (Marvel & Gabrilovich 2015).

The finding that circulating Mo are transcriptionally altered in cancer patients (Chittezhath et al. 2014; Hamm et al. 2016; Cassetta et al. 2019) suggests that Mo are manipulated systemically, perhaps prior to arrival in the TME. By isolating circulating Mo from patients with RCC, a pro-tumoural phenotype has

been demonstrated *in vitro* (Chittezhath et al. 2014). Interestingly, this is not limited to metastatic patients but also patients with early disease (Chittezhath et al. 2014). The studies across colorectal, RCC, breast and endometrial cancer were conducted mainly to develop diagnostic and prognostic tools. Yet, the identification of transcriptional alterations to Mo in cancer raises the question as to whether targeting of Mo transcriptional regulation may be of benefit in therapeutics. In attempting to shift the balance in cancer immune infiltrates, re-polarising cells from pro- to anti-tumoural phenotypes is clearly more beneficial than simply depleting them (Figure 55).

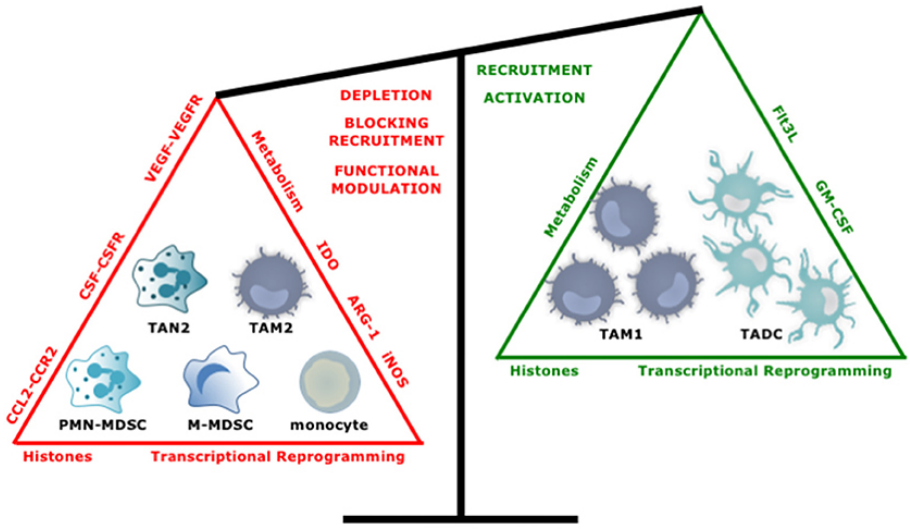

Figure 55 Tipping the balance toward myeloid cells with an antitumor phenotype. *Several approaches have been studied to increase the ratio of anti- over protumour TIMs. These include, depleting or repolarizing tumour-promoting TIMs, and attracting and activating antitumor TIMs. Figure and legend used with permission from Awad, R. M. et al. 2018.*

To begin to work towards the possibility of reprogramming Mo in cancer, having a workable animal model would be advantageous. Additionally, to unpick the transcriptional regulation of Mo in cancer, and having already collected transcriptional data, it would be of benefit to build a profile of epigenetic modifications. To this end, the aim of this thesis work was to define epigenetic regulation in and identify mechanisms of alterations of Mo dynamics and their transcription in the context of breast cancer in mice and humans.

A significant expansion in circulating Mo was evident in mice with late stage PyMT spontaneous tumours. While it was not possible to show alterations to BM progenitors, there is good evidence that cancer can modulate the BM niche (Giles 2016 et al). Thus, the findings here of a monopoesis, driven by the proliferation of Ly6c^{high} Mo in the BM provides an alternative mechanism to the previously described mechanisms of myeloid expansion in breast cancer (Casbon et al. 2015; Castaño et al. 2018). It will be interesting to discover if the BM niche in patients with breast cancer is altered and if so in what way. Obtaining BM samples from patients with breast cancer is problematic as routine biopsy of metastatic lesions is not practiced and even if it were this would not reflect a normal BM niche (Criscitiello et al. 2014).

On a transcriptional level, alterations to mice and human circulating Mo differed greatly. It is the intention to ratify this by repeating RNAseq of mouse Mo at early stage disease. It may be that alternative mouse models are required, as it is known that the immune response to breast cancer varies

greatly (Wellenstein et al. 2019). Nonetheless, in the case that the repeat sequencing fails to reveal useful orthologous, the focus in the immediate future will be on human samples. This is also in line with the advantage that human samples are readily available after progression from PhD to clinical academic training. The background that has been obtained in mouse work is however useful and will expand horizons for post-doctoral research.

Despite the lack of common transcriptional alterations between humans and mice, mechanisms driving the kinetics and transcriptional profile of Mo in cancer may be similar in both species. This is because in both species there was evidence of potentiation of the immune system by pro-inflammatory mediators. In mice, it is hypothesised that the pro-inflammatory systemic signals in cancer lead to altered transcriptional profiles due to the release of immature cells. This is ascribed to the indirect effect of hematopoietic stress, secondary to cancer associated inflammation. In humans, it is hypothesised that pro-inflammatory mediators activate the NFκB pathways, leading to a transcriptional profile that could be described as pro-tumoural (Chittezhath et al. 2014).

The effect in the mouse was greater in the Ly6c^{high}. A limitation of this is that the method of sampling blood does not collect Mo attached to the endothelium. It is therefore too hasty to conclude that in mice the Ly6c^{low} Mo are not important as their main effector function may be amongst those cells that are

actually attached to the endothelium. To correct for this, these cells may need to be studied *in vivo*, however this is outwith the scope of future planned work. This is a consideration when undertaking work in humans and it will be of interest to follow work into the role of these Mo that have a truly "patrolling" phenotype.

The changes observed in the monocytes does raise the question as to what is more important with respect to TAM function; is the phenotype of the circulating Mo or the signals within the TME more or less important than each other? It is likely that both are important. The work conducted here adds to a growing body of evidence that Mo are altered prior to the TME specific signals. Nonetheless, Mo and macrophage phenotype and effector function are extremely plastic and modelled by the tissue environment (Lavin et al, 2014). To investigate how much the circulating Mo phenotype over the TME signals determines ultimate TAM function adoptive transfer could be used. This is limited by the current lack of an appropriate mouse model. In lieu of this, 3D breast cancer models could be used in a more limited capacity. However, this is inferior given that both monocytes and macrophages rapidly lose their tissue specific signatures when in vitro (Gosselin et al. 2014).

In looking forward, there are a number of options to further enhance this body of work. A limitation of the cohort of breast cancer patients that are being collected is that most patients recruited to the trial have low risk disease.

Efforts in the past by colleagues in the Pollard lab had been made to obtain samples from patients with triple negative breast cancer. In response to this, a collaboration has been established with the oncologist and researcher, Dr. Olga Oikonomidou (MRC Institute of Genetics and Molecular Medicine, Edinburgh). This will facilitate the collection of samples from patients with triple negative breast cancer prior to, during and at completion of, neo-adjuvant chemotherapy. This has the benefit of being able to correlate findings with the pathological response rate, thus being able to correlate with response, perhaps revealing potential epigenetic targets for Mo therapy.

To compliment the transcriptomics data, an ambition is to demonstrate differences in cancer Mo on a protein level. A fellow clinical PhD student, Dr Andy Bretherick has worked closely with colleagues at the MRC Institute of Genetics and Molecular Medicine in Edinburgh in optimising pipelines for the processing and analysis of snap frozen peripheral blood monocytes (PBMCs). Discussion is underway to undertake the same methods on Mo from breast cancer patients.

It is postulated that re-programming of Mo occurs due to epigenetic manipulation. Work has begun here to build a cohort of Mo ATACseq samples in cancer patients. The continuation of these efforts will provide a means to answer the question as to whether the chromatin configuration is altered in cancer Mo. To further this, the use of ChIPseq would be extremely beneficial. Collaborators in the lab of Chris Glass, UCSD are working to optimise the input

for this method. In looking forward, and with the aspiration to further expertise, a more ambitious plan in considering the application of proteomics to complement the epigenetics work in Mo. The method of SILAC Nucleosome Affinity Purification (SNAP) provides the protein equivalent to ChIPseq for histones (Bartke et al. 2010). The pursuit of this will be dependent on the results obtained using current strategies.

To conclude, it is proposed that Mo are not simply a conduit in the cancer-immune process. Harnessing the plasticity of Mo by understanding the transcriptional changes in cancer Mo, might be a prelude to developing of novel cancer therapies. Plans for future both in expanding the work commenced in this thesis and taking new approaches, will contribute towards realising this objective.

Chapter 8 References

Akashi, K. et al., 2000. A clonogenic common myeloid progenitor that gives rise to all myeloid lineages. *Nature*, 404(6774), pp.193–197.

Ali, H.R. et al., 2014. Genome-driven integrated classification of breast cancer validated in over 7,500 samples. *Genome biology*, 15(8), p.431.

Allavena, P. et al., 1998. IL-10 prevents the differentiation of monocytes to dendritic cells but promotes their maturation to macrophages. *European Journal of Immunology*, 28(1), pp.359–369.

Ancuta, P. et al., 2009. Transcriptional profiling reveals developmental relationship and distinct biological functions of CD16+ and CD16- monocyte subsets. *BMC Genomics*, 10(1), pp.403–19.

Antoni, S. et al., 2016. Globcan fact sheet cancer. *Bulletin of the World Health Organization*, 94(3), pp.174–184. Available at: http://globocan.iarc.fr/Pages/fact_sheets_cancer.aspx. [accessed 02.02.2019]

Arwert, E.N., Harney, A.S., Entenberg, D., Wang, Y., Sahai, E., Pollard, J.W. & Condeelis, J.S., 2018. A Unidirectional Transition from Migratory to Perivascular Macrophage Is Required for Tumor Cell Intravasation. *CellReports*, 23(5), pp.1239–1248.

Asadzadeh, Z. et al., 2017. The paradox of Th17 cell functions in tumor immunity. *Cellular Immunology*, 322, pp.15–25.

Aswad, M. et al., 2017. CCL5 Promotes Resolution-Phase Macrophage Reprogramming in Concert with the Atypical Chemokine Receptor D6 and Apoptotic Polymorphonuclear Cells. *Journal of immunology,* 199(4), pp.1393–1404.

Auffray, C. et al., 2007. Monitoring of blood vessels and tissues by a population of monocytes with patrolling behavior. *Science*, 317(5838), pp.666–670.

Awad, R.M. et al., 2018. Turn Back the TIMe: Targeting Tumor Infiltrating Myeloid Cells to Revert Cancer Progression. *Frontiers in Immunology*, 9, pp.14–22.

Azizi, E. et al., 2018. Single-Cell Map of Diverse Immune Phenotypes in the Breast Tumor Microenvironment. *Cell*, 174(5), pp.1293–1308.e36.

Ban, Y. et al., 2017. Targeting Autocrine CCL5-CCR5 Axis Reprograms Immunosuppressive Myeloid Cells and Reinvigorates Antitumor Immunity. *Cancer Research*, 77(11), pp.2857–2868.

Bartke, T. et al., 2010. Nucleosome-Interacting Proteins Regulated by DNA and Histone Methylation. *Cell*, 143(3), pp.470–484.

Barter, R.L. & Bin Yu, 2018. Superheat: An R Package for Creating Beautiful and Extendable Heatmaps for Visualizing Complex Data. *Journal of Computational and Graphical Statistics*, 27(4), pp.910-922.

Belge, K.U. et al., 2002. The Proinflammatory CD14+CD16+DR++ Monocytes Are a Major Source of TNF. *The Journal of Immunology*, 168(7), pp.3536–3542.

Bencheikh, L. et al., 2019. Dynamic gene regulation by nuclear colony-stimulating factor 1 receptor in human monocytes and macrophages. *Nature Communications*,10(1), p.1935.

Bergenfelz, C. et al., 2015. Systemic Monocytic-MDSCs Are Generated from Monocytes and Correlate with Disease Progression in Breast Cancer Patients. Public library of Science (*PLoS) ONE*, 10(5), pp.e0127028–23.

Bi, J. et al., 2016. miR-181a Induces Macrophage Polarized to M2 Phenotype and Promotes M2 Macrophage-mediated Tumor Cell Metastasis by Targeting KLF6 and C/EBPα. *Molecular Therapy Nucleic Acids*, 5(Supplement C), p.e368.

Biburger, M. et al., 2011. Monocyte Subsets Responsible for Immunoglobulin G-Dependent Effector Functions in vivo. *Immunity*, 35(6), pp.932–944.

Bittner, J.J., 1936. SOME POSSIBLE EFFECTS OF NURSING ON THE MAMMARY GLAND TUMOR INCIDENCE IN MICE. *Science*, 84(2172), p.162.

Bonapace, L. et al., 2014. Cessation of CCL2 inhibition accelerates breast cancer metastasis by promoting angiogenesis. *Nature*, 515(7525), pp.130–133.

Boyette, L.B. et al., 2017. Phenotype, function, and differentiation potential of human monocyte subsets. Public library of Science (*PLoS) ONE*, 12(4), pp.e0176460–20.

Brandau, S. et al., 2016. Recommendations for myeloid-derived suppressor cell nomenclature and characterization standards. *Nature Communications*, 7, p.12150.

Breton, G.E.L. et al., 2015. Defining human dendritic cell progenitors by multiparametric flow cytometry. *Nature Protocols*, 10(9), pp.1407–1422.

Briseño, C.G. et al., 2016. Distinct Transcriptional Programs Control Cross-Priming in Classical and Monocyte-Derived Dendritic Cells. *CellReports*, 15(11), pp.2462–2474.

Bronte, V. et al., 2016. Recommendations for myeloid-derived suppressor cell nomenclature and characterization standards. *Nature Communications*, 7(1), pp.e12150.

Buenrostro, J.D. et al., 2018. Integrated Single-Cell Analysis Maps the Continuous Regulatory Landscape of Human Hematopoietic Differentiation. *Cell*, 173(6), pp.1535-1548.

Buenrostro, J.D. et al., 2013. Transposition of native chromatin for fast and sensitive epigenomic profiling of open chromatin, DNA-binding proteins and nucleosome position. *Nature Methods*, 10(12), pp.1213–1218.

Campbell, K.R. & Yau, C., 2018. Uncovering pseudotemporal trajectories with covariates from single cell and bulk expression data. *Nature Communications*, 9(1), p.2442.

Cannarile, M.A. et al., 2017. Colony-stimulating factor 1 receptor (CSF1R) inhibitors in cancer therapy. *Journal of Immunotherapy Cancer*, 5(1), p.53.

Carlin, L.M. et al., 2013. Nr4a1-Dependent Ly6Clow Monocytes Monitor Endothelial Cells and Orchestrate Their Disposal. *Cell*, 153(2), pp.362–375.

Carvalheiro, T. et al., 2018. Increased frequencies of circulating CXCL10-, CXCL8- and CCL4-producing monocytes and Siglec-3-expressing myeloid dendritic cells in systemic sclerosis patients. *Inflammation research*, 67(2), pp.169–177.

Casbon, A.-J. et al., 2015. Invasive breast cancer reprograms early myeloid differentiation in the bone marrow to generate immunosuppressive neutrophils. *Proceedings of the National Academy of Sciences (PNAS)*, 112(6), pp.e566–575.

Cassetta, L. & Pollard, J.W., 2017. Repolarizing macrophages improves breast cancer therapy. *Cell Research*, 27(8), pp.963–964.

Cassetta, L. et al., 2019. Human Tumor-Associated Macrophage and Monocyte Transcriptional Landscapes Reveal Cancer-Specific

Reprogramming, Biomarkers, and Therapeutic Targets. *Cancer Cell*, 35(4), pp. 588-602.e10.

Castaño, Z. et al., 2018. IL-1β inflammatory response driven by primary breast cancer prevents metastasis-initiating cell colonization. *Nature Cell Biology*, 20(9), pp.1084-1097.

Chao, S.-H. & Price, D.H., 2001. Flavopiridol Inactivates P-TEFb and Blocks Most RNA Polymerase II Transcription in Vivo. *Journal of Biological Chemistry*, 276(34), pp.31793–31799.

Chao, T., Furth, E.E. & Vonderheide, R.H., 2016. CXCR2-Dependent Accumulation of Tumor-Associated Neutrophils Regulates T-cell Immunity in Pancreatic Ductal Adenocarcinoma. *Cancer Immunology Research*, 4(11), pp.968–982.

Chen, F.X., Smith, E.R. & Shilatifard, A., 2018. Born to run: control of transcription elongation by RNA polymerase II. *Nature Reviews Molecular Cell Biology*, 19(7), pp.464-478.

Chen, L. et al., 2016. Genetic Drivers of Epigenetic and Transcriptional Variation in Human Immune Cells. *Cell*, 167(5), pp.1398–1414.e24.

Chen, T. & Dent, S.Y.R., 2013. Chromatin modifiers and remodellers: regulators of cellular differentiation. *Nature Reviews Genetics*, 15(2), pp.93–106.

Chen, X. et al., 2009. The NF-κB Factor RelB and Histone H3 Lysine Methyltransferase G9a Directly Interact to Generate Epigenetic Silencing in Endotoxin Tolerance. *Journal of Biological Chemistry*, 284(41), pp.27857–27865.

Chittezhath, M. et al., 2014. Molecular Profiling Reveals a Tumor-Promoting Phenotype of Monocytes and Macrophages in Human Cancer Progression. *Immunity*, 41(5), pp.815–829.

Chung, S. et al., 2014. Distinct role of FoxO1 in M-CSF- and GM-CSF-differentiated macrophages contributes LPS-mediated IL-10: implication in hyperglycemia. *Journal of Leukocyte Biology*, 97(2), pp.327–339.

Ciampricotti, M. et al., 2012. Chemotherapy response of spontaneous mammary tumors is independent of the adaptive immune system. *Nature Medicine*, 18(3), pp.344–6.

Clappaert, E.J. et al., 2018. Diamonds in the Rough: Harnessing Tumor-Associated Myeloid Cells for Cancer Therapy. *Frontiers in Immunology*, 9, pp.646–20.

Coffelt, S.B. et al., 2015. IL-17-producing γδ T cells and neutrophils conspire to promote breast cancer metastasis. *Nature Publishing Group*, 522(7556), pp.345–348.

Cole, J. et al., 2016. The therapeutic potential of epigenetic manipulation during infectious diseases. *Pharmacology and Therapeutics*, 167, pp.85-99.

Corces, M.R. et al., 2016. Lineage-specific and single-cell chromatin accessibility charts human hematopoiesis and leukemia evolution. *Nature Genetics*, 48(10), pp.1193–1203.

Corces, M.R. et al., 2017. Omni-ATAC-seq: Improved ATAC-seq protocol. *Nature Methods*, 14(10), pp.959-962.

Cortés, M. et al., 2017. Tumor-associated macrophages (TAMs) depend on ZEB1 for their cancer-promoting roles. *The EMBO Journal*, 36(22), pp.3336–3355.

Cowell, C.F. et al., 2013. Progression from ductal carcinoma in situ to invasive breast cancer: Revisited. *Molecular Oncology*, 7(5), pp.859–869.

Crawford, K. et al., 1999. Circulating CD2+ monocytes are dendritic cells. *The Journal of Immunology*, 163(11), pp.5920–5928.

Creyghton, M.P., the, A.C.P.O.2010, 2010. Histone H3K27ac separates active from poised enhancers and predicts developmental state. *Proceedings of the National Academy of Sciences (PNAS)*, 107(50), pp.21931–21936.

Criscitiello, C. et al., 2014. Biopsy confirmation of metastatic sites in breast cancer patients: clinical impact and future perspectives. *Breast Cancer Research*, 16(2), p.205.

Cros, J. et al., 2010. Human CD14dim Monocytes Patrol and Sense Nucleic Acids and Viruses via TLR7 and TLR8 Receptors. *Immunity*, 33(3), pp.375–386.

Crown, S.E. et al., 2006. Heterodimerization of CCR2 chemokines and regulation by glycosaminoglycan binding. *Journal of Biological Chemistry*, 281(35), pp.25438–25446.

C.R.U.K. Breast Cancer Statistics. *www.cancerresearchuk.orghealth-professionalcancer-statisticsstatistics-by-cancer-typebreast-cancerheading-Three*. [Visited on 02.02.2019]

Curtis, C. et al., 2012. The genomic and transcriptomic architecture of 2,000 breast tumours reveals novel subgroups. *Nature*, 486(7403), pp.346–352.

Dai, X. et al., 2015. Breast cancer intrinsic subtype classification, clinical use and future trends. *American Journal of Cancer Research*, 5(10), pp.2929–2943.

Darnell, J.E., Kerr, I.M. & Stark, G.R., 1994. Jak-STAT pathways and transcriptional activation in response to IFNs and other extracellular signaling proteins. *Science*, 264(5164), pp.1415–1421.

Date, D. et al., 2014. Kruppel-like transcription factor 6 regulates inflammatory macrophage polarization. *Journal of Biological Chemistry*, 289(15), pp.10318–10329.

De Palma, M. et al., 2007. Tie2-expressing monocytes: regulation of tumor angiogenesis and therapeutic implications. *Trends in Immunology*, 28(12), pp.519–524.

De Palma, M. et al., 2008. Tumor-targeted interferon-alpha delivery by Tie2-expressing monocytes inhibits tumor growth and metastasis. *Cancer Cell*, 14(4), pp.299–311.

De Palma, M., et al., 2005. Tie2 identifies a hematopoietic lineage of proangiogenic monocytes required for tumor vessel formation and a mesenchymal population of pericyte progenitors. *Cancer Cell*, 8(3), pp.211–226.

De La Fuente López, M. et al., 2018. The relationship between chemokines CCL2, CCL3, and CCL4 with the tumor microenvironment and tumor-associated macrophage markers in colorectal cancer. *Tumor Biology*, 40(11), pp.e101042831881005–12.

de la Fuente, de, M.A. et al., 1997. CD84 leukocyte antigen is a new member of the Ig superfamily. *Blood*, 90(6), pp.2398–2405.

de Ruiter, J.R., Wessels, L.F.A. & Jonkers, J., 2018. Mouse models in the era of large human tumour sequencing studies. *Open Biology*, 8(8), pp.180080–16.

de Visser, K.E., Eichten, A. & Coussens, L.M., 2006. Paradoxical roles of the immune system during cancer development. *Nature Reviews Cancer*, 6(1), pp.24–37.

de Vlaeminck, Y. et al., 2016. Cancer-Associated Myeloid Regulatory Cells. *Frontiers in Immunology*, 7(10), pp.286–9.

DeNardo, D.G. et al., 2011. Leukocyte complexity predicts breast cancer survival and functionally regulates response to chemotherapy. *Cancer Discovery*, 1(1), pp.54–67.

DeNiro, M. et al., 2013. The Nexus between VEGF and NFκB Orchestrates a Hypoxia-Independent Neovasculogenesis. Public library of Science (*PLoS) ONE*, 8(3), pp.e59021–17.

Dobin, A. et al., 2013. STAR: ultrafast universal RNA-seq aligner. *Bioinformatics*, 29(1), pp.15–21.

Donnard, E. et al., 2018. Comparative Analysis of Immune Cells Reveals a Conserved Regulatory Lexicon. *Cell Systems*, 6(3), pp.381–394.e7.

Doornebal, C.W. et al., 2013. A preclinical mouse model of invasive lobular breast cancer metastasis. *Cancer Research*, 73(1), pp.353–363.

Dorrington, M.G. & Fraser, I.D.C., 2019. NF-κB Signaling in Macrophages: Dynamics, Crosstalk, and Signal Integration. *Frontiers in Immunology*, 10, pp.921–12.

Dougan, M., Dranoff, G. & Dougan, S.K., 2019. GM-CSF, IL-3, and IL-5 Family of Cytokines: Regulators of Inflammation. *Immunity*, 50(4), pp.796–811.

Doyle, A.G. et al., 1994. Interleukin-13 alters the activation state of murine macrophages in vitro: Comparison with interleukin-4 and interferon-γ. *European Journal of Immunology*, 24(6), pp.1441–1445.

Drews-Elger, K. et al., 2014. Infiltrating S100A8+ myeloid cells promote metastatic spread of human breast cancer and predict poor clinical outcome. *Breast Cancer Research and Treatment*, 148(1), pp.41–59.

Duluc, D. et al., 2009. Interferon-γ reverses the immunosuppressive and protumoral properties and prevents the generation of human tumor-associated macrophages. *International Journal of Cancer*, 125(2), pp.367–373.

Duncan, S.A. et al., 2017. SOCS Proteins as Regulators of Inflammatory Responses Induced by Bacterial Infections: A Review. *Frontiers in Microbiology*, 8, pp.410–15.

Dyer, D.P. et al., 2017. CXCR2 deficient mice display macrophage-dependent exaggerated acute inflammatory responses. *Scientific Reports*, pp.1–11.

Elgin, S.C., 1981. DNAase I-hypersensitive sites of chromatin. *Cell*, 27(3Pt2), pp.413–415.

Elston, C.W. & Ellis, I.O., 1991. Pathological prognostic factors in breast cancer. I. The value of histological grade in breast cancer: experience from a large study with long-term follow-up. *Histopathology*, 19(5), pp.403–410.

Ernst, J. et al., 2011. Mapping and analysis of chromatin state dynamics in nine human cell types. *Nature*, 473(7345), pp.43–49.

Ewels, P. et al., 2016. MultiQC: summarize analysis results for multiple tools and samples in a single report. *Bioinformatics*, 32(19), pp.3047–3048.

Farmaki, E. et al., 2016. A CCL8 gradient drives breast cancer cell dissemination. 35(49), pp.6309–6318.

Babraham Bioinformatics, 2010. *FastQC: a quality control tool for high throughput sequence data [Internet].* Available at https://www.bioinformatics.babraham.ac.uk/projects/fastqc/ [downloaded 07.07.2017]

Feng, A.L. et al., 2011. CD16+ monocytes in breast cancer patients: expanded by monocyte chemoattractant protein-1 and may be useful for early diagnosis. *Clinical and Experimental Immunology*, 164(1), pp.57–65.

Fogg, D.K., 2006. A Clonogenic Bone Marrow Progenitor Specific for Macrophages and Dendritic Cells. *Science*, 311(5757), pp.83–87.

Foulds, L., 1954. The Experimental Study of Tumor Progression: A Review. *Cancer Research*, 14(5), p.327.

Franklin, R.A. et al., 2014. The cellular and molecular origin of tumor-associated macrophages. *Science*, 344(6186), pp.921–925.

Gabrilovich, D.I., 2017. Myeloid-Derived Suppressor Cells. *Cancer Immunology Research*, 5(1), pp.3–8.

Gaidatzis, D. et al., 2015. Analysis of intronic and exonic reads in RNA-seq data characterizes transcriptional and post-transcriptional regulation. *Nature Biotechnology*, 33(7), pp.722-729.

Gales, D. et al., 2013. The Chemokine CXCL8 in Carcinogenesis and Drug Response. *International Scholary Research Notices Oncology*, 2013, p.e859154.

Gamrekelashvili, J. et al., 2017. Regulation of monocyte cell fate by blood vessels mediated by Notch signalling. *Nature Communications*, 7, p.e12597.

Geissmann, F., Jung, S. & Littman, D.R., 2003. Blood Monocytes Consist of Two Principal Subsets with Distinct Migratory Properties. *Immunity*, 19(1), pp.71–82.

Giles, A.J. et al., 2016. Activation of Hematopoietic Stem/Progenitor Cells Promotes Immunosuppression Within the Pre–metastatic Niche. *Cancer Research*, 76(6), pp.1335–1347.

Glasner, A. et al., 2018. NKp46 Receptor-Mediated Interferon-γ Production by Natural Killer Cells Increases Fibronectin 1 to Alter Tumor Architecture and Control Metastasis. *Immunity*, 48(2), pp.396–398.

Golovkina, T.V., Dudley, J.P. & Ross, S.R., 1998. B and T cells are required for mouse mammary tumor virus spread within the mammary gland. *The Journal of Immunology*, 161(5), pp.2375–2382.

Gosselin, D. et al., 2014. Environment Drives Selection and Function of Enhancers Controlling Tissue-Specific Macrophage Identities. *Cell,* 159**,** pp. 1327–1340.

Greaves, M. & Maley, C.C., 2012. Clonal evolution in cancer. *Nature*, 481(7381), pp.306–313.

Gresser, I. et al., 1969. Increased survival in mice inoculated with tumor cells and treated with interferon preparations. *Proceedings of the National Academy of Sciences (PNAS)*, 63(1), pp.51–57.

Guerriero, J.L. et al., 2017. Class IIa HDAC inhibition reduces breast tumours and metastases through anti-tumour macrophages. *Nature*, 543(7645), pp.428–432.

Hagemann, T. et al., 2008. “Re-educating” tumor-associated macrophages by targeting NF-κB. *The Journal of Experimental Medicine*, 205(6), pp.1261–1268.

Halama, N. et al., 2016. Tumoral Immune Cell Exploitation in Colorectal Cancer Metastases Can Be Targeted Effectively by Anti-CCR5 Therapy in Cancer Patients. *Cancer Cell*, 29(4), pp.587–601.

Hamm, A. et al., 2016. Tumour-educated circulating monocytes are powerful candidate biomarkers for diagnosis and disease follow-up of colorectal cancer. *Gut*, 65(6), pp.990–1000.

Hamers, A.A.J. et al., 2019. Human Monocyte Heterogeneity as Revealed by High-Dimensional Mass Cytometry. *Arteriosclerosis, thrombosis, and vascular biology*, 39(1), pp.25–36.

Hamon, P. et al., 2017. CX3CR1-dependent endothelial margination modulates Ly6Chigh monocyte systemic deployment upon inflammation in mice. *Blood*, 129(10), pp.1296–1307.

Hanahan, D. & Weinberg, R.A., 2000. The hallmarks of cancer. *Cell*, 100(1), pp.57–70.

Hanahan, D. & Weinberg, R.A., 2011. Hallmarks of Cancer: The Next Generation. *Cell*, 144(5), pp.646–674.

Hanna, R.N. et al., 2015. Patrolling monocytes control tumor metastasis to the lung. *Science*, 350(6263), pp.985–990.

Harrington, L.E. et al., 2005. Interleukin 17–producing CD4+ effector T cells develop via a lineage distinct from the T helper type 1 and 2 lineages. *Nature Immunology*, 6(11), pp.1123–1132.

Hayat, M.J. et al., 2007. Cancer Statistics, Trends, and Multiple Primary Cancer Analyses from the Surveillance, Epidemiology, and End Results (SEER) Program. *The Oncologist*, 12(1), pp.20–37.

Heinz, S. et al., 2013. Effect of natural genetic variation on enhancer selection and function. *Nature Publishing Group*, 503(7477), pp.487–492.

Heinz, S. et al., 2010. Simple Combinations of Lineage-Determining Transcription Factors Prime cis-Regulatory Elements Required for Macrophage and B Cell Identities. *Molecular Cell*, 38(4), pp.576–589.

Heinz, S. et al., 2015. The selection and function of cell type-specific enhancers. *Nature Publishing Group*, 16(3), pp.144–154.

Hettinger, J. et al., 2013. Origin of monocytes and macrophages in a committed progenitor. *Nature Immunology*, 14(8), pp.821–830.

Hildebrand, D. et al., 2018. The Interplay of Notch Signaling and STAT3 in TLR-Activated Human Primary Monocytes. *Frontiers in Cellular and Infection Microbiology*, 8, pp.e1002341–12.

Hirano, T., Ishihara, K. & Hibi, M., 2000. Roles of STAT3 in mediating the cell growth, differentiation and survival signals relayed through the IL-6 family of cytokine receptors. *Oncogene*, 19(21), pp.2548–2556.

Hnisz, D. et al., 2013. Super-Enhancers in the Control of Cell Identity and Disease. *Cell*, 155(4), pp.934–947.

Hoesel, B. & Schmid, J.A., 2013. The complexity of NF-kB signaling in inflammation and cancer. *Molecular Cancer*, 12(1), p.e86.

Hon, J.D.C. et al., 2016. Review Article Breast cancer molecular subtypes: from TNBC to QNBC. *American Journal of Cancer Research*, 6(9), pp.1864–1872.

Honvo-Houeto, E. & Truchet, S., 2015. Indirect Immunofluorescence on Frozen Sections of Mouse Mammary Gland. doi:10.3791/53179 [Accessed on 2nd May 2016]

Hu, Z. et al., 2006. The molecular portraits of breast tumors are conserved across microarray platforms. *BMC Genomics*, 7(1), p.e96.

Hughes, R. et al., 2015. Perivascular M2 Macrophages Stimulate Tumor Relapse after Chemotherapy. *Cancer Research*, 75(17), pp.3479–3491.

Hwang, B., Lee, J.H. & Bang, D., 2018. Single-cell RNA sequencing technologies and bioinformatics pipelines. *Experimental & Molecular Medicine*, 50(8), p.e96.

Ingersoll, M.A. et al., 2010. Comparison of gene expression profiles between human and mouse monocyte subsets. *Blood*, 115(3), pp.e10–19.

Ivashkiv, L.B., 2018. IFNγ: signalling, epigenetics and roles in immunity, metabolism, disease and cancer immunotherapy. *Nature Reviews Immunology*, 18(9), pp.545–548.

Jablonski, K.A. et al., 2015. Novel Markers to Delineate Murine M1 and M2 Macrophages. Public library of Science (*PLoS) ONE*, 10(12), pp.e0145342–25.

Javeed, N. et al., 2017. Immunosuppressive CD14HLA-DR monocytes are elevated in pancreatic cancer and ``primed´´ by tumor-derived exosomes. *OncoImmunology*, 6(1), p.e1252013.

Joyce, J.A. & Pollard, J.W., 2008. Microenvironmental regulation of metastasis. *Nature Reviews Cancer*, 9(4), pp.239–252.

Jung, K. et al., 2017. Ly6Clo monocytes drive immunosuppression and confer resistance to anti-VEGFR2 cancer therapy. *Journal of Clinical Investigation*, 127(8), pp.3039–3051.

Kammertoens, T. et al., 2017. Tumour ischaemia by interferon-γ resembles physiological blood vessel regression. *Nature*, 545(7652), pp.98–102.

Kawamura, S. et al., 2017. Identification of a Human Clonogenic Progenitor with Strict Monocyte Differentiation Potential: A Counterpart of Mouse cMoPs. *Immunity*, 46(5), pp.835–848.e4.

Kent, W.J. et al., 2002. The Human Genome Browser at UCSC. *Genome Research*, 12(6), pp.996–1006.

Kersten, K. et al., 2017. Mammary tumor-derived CCL2 enhances pro-metastatic systemic inflammation through upregulation of IL1β in tumor-associated macrophages. *OncoImmunology*, 6(8), pp.1–14.

Kim, J. & Bae, J.-S., 2016. Review Article Tumor-Associated Macrophages and Neutrophils in Tumor Microenvironment. *Mediators of Inflammation*, 2016, p.e6058147.

Kim, S.-H. et al., 2005. Interleukin-32. *Immunity*, 22(1), pp.131–142.

Kitamura, T. et al., 2018. Monocytes Differentiate to Immune Suppressive Precursors of Metastasis-Associated Macrophages in Mouse Models of Metastatic Breast Cancer. *Frontiers in Immunology*, 8, pp.69–14.

Kitamura, T., Qian, B.-Z. & Pollard, J.W., 2015. Immune cell promotion of metastasis. *Nature Publishing Group*, 15(2), pp.73–86.

Kitamura, T., Qian, B.-Z., Soong, D., et al., 2015. CCL2-induced chemokine cascade promotes breast cancer metastasis by enhancing retention of metastasis-associated macrophages. *The Journal of Experimental Medicine*, 212(7), pp.1043–1059.

Papathanassiu, A.E. et al., 2017. BCAT1 controls metabolic reprogramming in activated human macrophages and is associated with inflammatory diseases. *Nature Communications*, 8, p.e16040.

Kochumon, S. et al., 2018. Palmitate Activates CCL4 Expression in Human Monocytic Cells via TLR4/MyD88 Dependent Activation of NF-κB/MAPK/PI3K Signaling Systems. *Cellular Physiology and Biochemistry*, 46(3), pp.953–964.

Krämer, A. et al., 2013. Causal analysis approaches in Ingenuity Pathway Analysis. *Bioinformatics,* 30(4), pp.523–530.

Krishnaraju, K., Hoffman, B. & Liebermann, D.A., 2001. Early growth response gene 1 stimulates development of hematopoietic progenitor cells along the macrophage lineage at the expense of the granulocyte and erythroid lineages. *Blood*, 97(5), pp.1298–1305.

Kubosaki, A. et al., 2009. Genome-wide investigation of in vivo EGR-1 binding sites in monocytic differentiation. *Genome biology*, 10(4), p.R41.

Kurotaki, D. et al., 2013. Essential role of the IRF8-KLF4 transcription factor cascade in murine monocyte differentiation. *Blood*, 121(10), pp.1839–1849.

Kurotaki, D. et al., 2014. IRF8 inhibits C/EBPα activity to restrain mononuclear phagocyte progenitors from differentiating into neutrophils. *Nature Communications*, 5(1), pp.3764–15.

Kurotaki, D. et al., 2018. Transcription Factor IRF8 Governs Enhancer Landscape Dynamics in Mononuclear Phagocyte Progenitors. *CellReports*, 22(10), pp.2628–2641.

Lafont, V., 2014. Plasticity of γδ T cells: impact on the anti-tumor response. *Frontiers in Immunology*, pp.1–13.

Lang, R., Hammer, M. & Mages, J., 2006. DUSP Meet Immunology: Dual Specificity MAPK Phosphatases in Control of the Inflammatory Response. *The Journal of Immunology*, 177(11), pp.7497–7504.

Langmead, B. & Salzberg, S.L., 2012. Fast gapped-read alignment with Bowtie 2. *Nature Methods*, 9(4), pp.357–359.

Lapko, N. et al., 2017. Long-term Monocyte Dysfunction after Sepsis in Humanized Mice Is Related to Persisted Activation of Macrophage-Colony Stimulation Factor (M-CSF) and Demethylation of PU.1, and It Can Be Reversed by Blocking M-CSF In Vitro or by Transplanting Naïve Autologous Stem Cells In Vivo. *Frontiers in Immunology*, 8, pp.463–12.

Lara-Astiaso, D. et al., 2014. Chromatin state dynamics during blood formation. *Science*, 345(6199), pp.943–949.

Lasitschka, F. et al., 2017. Human monocytes downregulate innate response receptors following exposure to the microbial metabolite n-butyrate. *Immunity, Inflammation and Disease*, 5(4), pp.480–492.

Lavin, Y. et al., 2014. Tissue-Resident Macrophage Enhancer Landscapes Are Shaped by the Local Microenvironment. *Cell*, 159(6), pp.1312–1326.

Läubli, H., Spanaus, K.-S. & Borsig, L., 2009. Selectin-mediated activation of endothelial cells induces expression of CCL5 and promotes metastasis through recruitment of monocytes. *Blood*, 114(20), pp.4583–4591.

Leoni, F. & Fossati, G., 2005. The Histone Deacetylase Inhibitor ITF2357 Reduces Production of Pro-Inflammatory Cytokines In Vitro and Systemic Inflammation In Vivo. *Molecular Medicine*, 11(1-12), pp.1–15.

Leoni, F. et al., 2002. The antitumor histone deacetylase inhibitor suberoylanilide hydroxamic acid exhibits antiinflammatory properties via suppression of cytokines. *Proceedings of the National Academy of Sciences (PNAS)*, 99(5), pp.2995–3000.

Lessard, A.-J. et al., 2017. Triggering of NOD2 Receptor Converts Inflammatory Ly6Chigh into Ly6Clow Monocytes with Patrolling Properties. *CellReports*, 20(8), pp.1830–1843.

Leuschner, F. et al., 2012. Rapid monocyte kinetics in acute myocardial infarction are sustained by extramedullary monocytopoiesis. *The Journal of Experimental Medicine*, 209(1), pp.123–137.

Li, Q. et al., 2011. Measuring reproducibility of high-throughput experiments. *The Annals of Applied Statistics*, 5(3), pp.1752–1779.

Li, Y. et al., 2008. Role of the Histone H3 Lysine 4 Methyltransferase, SET7/9, in the Regulation of NF-κB-dependent Inflammatory Genes. *Journal of Biological Chemistry*, 283(39), pp.26771–26781.

Lifsted, T. et al., 1998. Identification of inbred mouse strains harboring genetic modifiers of mammary tumor age of onset and metastatic progression. *International Journal of Cancer*, 77(4), pp.640–644.

Lin, E.Y. et al., 2001. Colony-stimulating factor 1 promotes progression of mammary tumors to malignancy. *The Journal of Experimental Medicine*, 193(6), pp.727–740.

Lin, E.Y. et al., 2006. Macrophages regulate the angiogenic switch in a mouse model of breast cancer. *Cancer Research*, 66(23), pp.11238–11246.

Lin, E.Y. et al., 2003. Progression to Malignancy in the Polyoma Middle T Oncoprotein Mouse Breast Cancer Model Provides a Reliable Model for Human Diseases. *The American Journal of Pathology*, 163(5), pp.2113–2126.

Lin, E.Y. et al., 2002. The macrophage growth factor CSF-1 in mammary gland development and tumor progression. *Journal of Mammary Gland Biology and Neoplasia*, 7(2), pp.147–162.

Liu, F. et al., 2017. The Schlafen family: complex roles in different cell types and virus replication. *Cell Biology International*, 42(1), pp.2–8.

Liu, H. et al., 2008. Transcriptional diversity during monocyte to macrophage differentiation. *Immunology Letters*, 117(1), pp.70–80.

Liu, Y.-Z. et al., 2016. RNA-sequencing study of peripheral blood monocytes in chronic periodontitis. *Gene*, 581(2), pp.152–160.

Long, H. et al., 2012. Autocrine CCL5 Signaling Promotes Invasion and Migration of CD133 +Ovarian Cancer Stem-Like Cells via NF-κB-Mediated MMP-9 Upregulation. *StemCells,* 30, 2309–2319.

Lorzadeh, A. et al., 2017. Generation of Native Chromatin Immunoprecipitation Sequencing Libraries for Nucleosome Density Analysis [online]. *Journal of Visualized Experiments*, doi: 10.3791/56085.

Love, M.I., Huber, W. & Anders, S., 2014. Moderated estimation of fold change and dispersion for RNA-seq data with DESeq2. *Genome biology*, 15(12), p.550.

Ma, J. et al., 2009. Targeted Knockdown of EGR-1 Inhibits IL-8 Production and IL-8-mediated Invasion of Prostate Cancer Cells through Suppressing EGR-1/NF-κB Synergy. *Journal of Biological Chemistry*, 284(50), pp.34600–34606.

Mantovani, A. et al., 2004. The chemokine system in diverse forms of macrophage activation and polarization. *Trends in Immunology*, 25(12), pp.677–686.

Mantovani, A. et al., 2017. Tumour-associated macrophages as treatment targets in oncology. *Nature Reviews Clinical Oncology*, 14(7), pp.399-416.

Martinez, M. & Moon, E.K., 2019. CAR T Cells for Solid Tumors: New Strategies for Finding, Infiltrating, and Surviving in the Tumor Microenvironment. *Frontiers in Immunology*, 10, pp.139–21.

Marvel, D. & Gabrilovich, D.I., 2015. Myeloid-derived suppressor cells in the tumor microenvironment: expect the unexpected. *Journal of Clinical Investigation*, 125(9), pp.3356–3364.

Maurer, M. & Stebut, von, E., 2004. Macrophage inflammatory protein-1. *The International Journal of Biochemistry & Cell Biology*, 36(10), pp.1882–1886.

Micalizzi, D.S., Maheswaran, S. & Haber, D.A., 2017. A conduit to metastasis: circulating tumor cell biology. *Genes & Development*, 31(18), pp.1827–1840.

Morita, C.T. et al., 1995. Direct presentation of nonpeptide prenyl pyrophosphate antigens to human γδ T cells. *Immunity*, 3(4), pp.495–507.

Morrow, E.S., Roseweir, A. & Edwards, J., 2019. The role of gamma delta T lymphocytes in breast cancer: a review. *Translational Research*, 203, pp.88–96.

Mills, C.D. et al., 2000. M-1/M-2 Macrophages and the Th1/Th2 Paradigm. *The Journal of Immunology*, 164(12), pp.6166–6173.

Motulsky, H.J. & Brown, R.E., 2006. Detecting outliers when fitting data with nonlinear regression - a new method based on robust nonlinear regression and the false discovery rate. *BMC bioinformatics*, 7, p.e123.

Movahedi, K. et al., 2010. Different Tumor Microenvironments Contain Functionally Distinct Subsets of Macrophages Derived from Ly6C(high) Monocytes. *Cancer Research*, 70(14), pp.5728–5739.

Mukherjee, R. et al., 2015. Non-Classical monocytes display inflammatory features: Validation in Sepsis and Systemic Lupus Erythematous. *Scientific Reports*, 5(1), p.e13886.

Muller, W.J. et al., 1988. Single-step induction of mammary adenocarcinoma in transgenic mice bearing the activated c-neu oncogene. *Cell*, 54(1), pp.105–115.

Murdoch, C. et al., 2007. Expression of Tie-2 by Human Monocytes and Their Responses to Angiopoietin-2. *The Journal of Immunology*, 178(11), pp.7405–7411.

Murphy, J.M. & Young, I.G., 2006. IL-3, IL-5, and GM-CSF Signaling: Crystal Structure of the Human Beta-Common Receptor. *Vitamins & Hormones, 74, pp.1-30.*

Murray, P.J. et al., 2014. Macrophage Activation and Polarization: Nomenclature and Experimental Guidelines. *Immunity*, 41(1), pp.14–20.

Naik, S.H. et al., 2013. Diverse and heritable lineage imprinting of early haematopoietic progenitors. *Nature*, 496(7444), pp.229–232.

Nelson, A.C., Machado, H.L. & Schwertfeger, K.L., 2018. Breaking through to the Other Side: Microenvironment Contributions to DCIS Initiation and Progression. *Journal of mammary Gland Biology Neoplasia, 23(4),* pp.207-221.

Nelson, C.M. & Bissell, M.J., 2006. Of Extracellular Matrix, Scaffolds, and Signaling: Tissue Architecture Regulates Development, Homeostasis, and Cancer. *Annual Review of Cell and Developmental Biology*, 22(1), pp.287–309.

Nguyen, H.Q., Hoffman-Liebermann, B. & Liebermann, D.A., 1993. The zinc finger transcription factor Egr-1 is essential for and restricts differentiation along the macrophage lineage. *Cell*, 72(2), pp.197–209.

Nie, Y. et al., 2019. Breast Phyllodes Tumors Recruit and Repolarize Tumor-Associated Macrophages via Secreting CCL5 to Promote Malignant Progression, Which Can Be Inhibited by CCR5 Inhibition Therapy. *Clinical Cancer Research*, 25(13), pp.3873–3886.

Notta, F. et al., 2016. Distinct routes of lineage development reshape the human blood hierarchy across ontogeny. *Science*, 351(6269), pp.aab2116.

Noy, R. & Pollard, J.W., 2014. Tumor-Associated Macrophages: From Mechanisms to Therapy. *Immunity*, 41(1), pp.49–61.

Ostrand-Rosenberg, S., 2008. Immune surveillance: a balance between protumor and antitumor immunity. *Current opinion in genetics & development*, 18(1), pp.11–18.

Ouzounova, M. et al., 2017. Monocytic and granulocytic myeloid derived suppressor cells differentially regulate spatiotemporal tumour plasticity during metastatic cascade. *Nature Communications*, 8, p.e14979.

Park, H. et al., 2005. A distinct lineage of CD4 T cells regulates tissue inflammation by producing interleukin 17. *Nature Immunology*, 6(11), pp.1133–1141.

Parker, B.S., Rautela, J. & Hertzog, P.J., 2016. Antitumour actions of interferons: implications for cancer therapy. *Nature Reviews Cancer*, 16(3), pp.131–144.

Passeri, D. et al., 2006. Btg2 Enhances Retinoic Acid-Induced Differentiation by Modulating Histone H4 Methylation and Acetylation. *Molecular and Cellular Biology*, 26(13), pp.5023–5032.

Passlick, B., Flieger, D. & Ziegler-Heitbrock, L., 1989. Identification and Characterization of a Novel Monocyte Subpopulation in Human Peripheral Blood. *Blood*, 74(7), pp.2527–2534.

Patel, A.A. et al., 2017. The fate and lifespan of human monocyte subsets in steady state and systemic inflammation. *The Journal of Experimental Medicine*, 214(7), pp.1913–1923.

Perou, C.M. et al., 2000. Molecular portraits of human breast tumours. *Nature*, 406(6797), pp.747–752.

Piehler, A.P. et al., 2010. Gene expression results in lipopolysaccharide-stimulated monocytes depend significantly on the choice of reference genes. *BMC immunology*, 11(1), pp.21–13.

Pipkin, M.E., 2006. A reliable method to display authentic DNase I hypersensitive sites at long-ranges in single-copy genes from large genomes. *Nucleic acids research*, 34(4), p.e34.

Plebanek, M.P. et al., 2017. Pre-metastatic cancer exosomes induce immune surveillance by patrolling monocytes at the metastatic niche. *Nature Communications*, 8(1), p.e1319.

Pucci, F. et al., 2009. A distinguishing gene signature shared by tumor-infiltrating Tie2-expressing monocytes, blood “resident” monocytes, and embryonic macrophages suggests common functions and developmental relationships. *Blood*, 114(4), pp.901–914.

Pyonteck, S.M. et al., 2013. CSF-1R inhibition alters macrophage polarization and blocks glioma progression. *Nature Medicine*, 19(10), pp.1264–1272.

Qian, B.-Z et al., 2009. A distinct macrophage population mediates metastatic breast cancer cell extravasation, establishment and growth. Public library of Science (*PLoS) ONE*, 4(8), p.e6562.

Qian, B.-Z. & Pollard, J.W., 2010. Macrophage Diversity Enhances Tumor Progression and Metastasis. *Cell*, 141(1), pp.39–51.

Qian, B.-Z. et al., 2011. CCL2 recruits inflammatory monocytes to facilitate breast-tumour metastasis. *Nature*, 475(7355), pp.222–225.

Qiao, Y. et al., 2016. IFN-γ Induces Histone 3 Lysine 27 Trimethylation in a Small Subset of Promoters to Stably Silence Gene Expression in Human Macrophages. *Cell Reports*, 16(12), pp.3121–3129.

Rada-Iglesias, A., 2017. Is H3K4me1 at enhancers correlative or causative? *Nature Genetics*, 50(1), pp.4–5.

Rakha, E.A. et al., 2008. Prognostic significance of Nottingham histologic grade in invasive breast carcinoma. *Journal of clinical oncology*, 26(19), pp.3153–3158.

Ravdin, P.M. et al., 2001. Computer program to assist in making decisions about adjuvant therapy for women with early breast cancer. *Journal of clinical oncology*, 19(4), pp.980–991.

Reimand, J. et al., 2007. g:Profiler—a web-based toolset for functional profiling of gene lists from large-scale experiments. *Nucleic acids research*, 35(2), pp.W193–W200.

Reuss, F.U. & Coffin, J.M., 1995. Stimulation of mouse mammary tumor virus superantigen expression by an intragenic enhancer. *Proceedings of the National Academy of Sciences (PNAS)*, 92(20), pp.9293–9297.

Richards, D.M., Hettinger, J. & Feuerer, M., 2012. Monocytes and Macrophages in Cancer: Development and Functions. *Cancer Microenvironment*, 6(2), pp.179–191.

Richardsen, E. et al., 2015. Macrophage-colony stimulating factor (CSF1) predicts breast cancer progression and mortality. *Anticancer research*, 35(2), pp.865–874.

Rico, D. et al., 2017. Comparative analysis of neutrophil and monocyte epigenomes [online]. *bioRxiv,* 237784. doi: https://doi.org/10.1101/237784.

Roca Suarez, A.A. et al., 2018. Viral manipulation of STAT3: Evade, exploit, and injure. Public library of Science (*PLoS) Pathogens*, 14(3), pp.e1006839–21.

Rodero, M.P. et al., 2013. Control of Both Myeloid Cell Infiltration and Angiogenesis by CCR1 Promotes Liver Cancer Metastasis Development in Mice. *Neoplasia*, 15(6), pp.641–648.

Saleh, M.N. et al., 1995. CD16+ monocytes in patients with cancer: spontaneous elevation and pharmacologic induction by recombinant human macrophage colony-stimulating factor. *Blood*, 85(10), pp.2910–2917.

Schmid, M., Tudek, A. & Jensen, T.H., 2018. Simultaneous Measurement of Transcriptional and Post-transcriptional Parameters by 3′ End RNA-Seq. *CellReports*, 24(9), pp.2468–2478.e4.

Schmidl, C. et al., 2014. Transcription and enhancer profiling in human monocyte subsets. *Blood*, 123(17), pp.e90–99.

Scholl, S.M. et al., 1994. Anti-colony-stimulating factor-1 antibody staining in primary breast adenocarcinomas correlates with marked inflammatory cell infiltrates and prognosis. *Journal of the National Cancer Institute*, 86(2), pp.120–126.

Schönheit, J. et al., 2013. PU.1 Level-Directed Chromatin Structure Remodeling at the Irf8 Gene Drives Dendritic Cell Commitment. *CellReports*, 3(5), pp.1617–1628.

Senichkin, V.V. et al., 2019. Molecular Comprehension of Mcl-1: From Gene Structure to Cancer Therapy. *Trends in Cell Biology*, 29(7), pp.549–562.

Serbina, N.V. & Pamer, E.G., 2006. Monocyte emigration from bone marrow during bacterial infection requires signals mediated by chemokine receptor CCR2. *Nature Immunology*, 7(3), pp.311–317.

Serbina, N.V. et al., 2009. Distinct responses of human monocyte subsets to Aspergillus fumigatus conidia. *Journal of immunology*, 183(4), pp.2678–2687.

Sevilla, L. et al., 1999. The Ets2 Transcription Factor Inhibits Apoptosis Induced by Colony-Stimulating Factor 1 Deprivation of Macrophages through a Bcl-xL-Dependent Mechanism. *Molecular and Cellular Biology*, 19(4), pp.2624–2634.

Schade, B. et al., 2009. PTEN-Deficiency in a Luminal MMTV-ERBB-2 Mouse model results in dramatic acceleration of Mammary Tumorigenesis and Metastasis. *Journal of Biological Chemistry*, 284(28), pp.19018-26.

Shah, S.P. et al., 2012. The clonal and mutational evolution spectrum of primary triple-negative breast cancers. *Nature*, 486(7403), pp.395–399.

Shalova, I.N. et al., 2015. Human Monocytes Undergo Functional Re-programming during Sepsis Mediated by Hypoxia-Inducible Factor-1&alpha. *Immunity*, 42(3), pp.484–498.

Shi, C. & Pamer, E.G., 2011. Monocyte recruitment during infection and inflammation. *Nature Reviews Immunology*, 11(11), pp.762–774.

Shi, L. et al., 2015. Monocyte enhancers are highly altered in systemic lupus erythematosus. *Epigenomics*, 7(6), pp.921–935.

Shultz, L.D. et al., 2005. Human Lymphoid and Myeloid Cell Development in NOD/LtSz-scid IL2R null Mice Engrafted with Mobilized Human Hemopoietic Stem Cells. *The Journal of Immunology*, 174(10), pp.6477–6489.

Singletary, S.E., Greene, F.L.Breast Task Force, 2003. Revision of breast cancer staging: the 6th edition of the TNM Classification. *Seminars in surgical oncology*, 21(1), pp.53–59.

Skrzeczyńska-Moncznik, J. et al., 2008. Peripheral Blood CD14 high CD16 +Monocytes are Main Producers of IL-10. *Scandinavian Journal of Immunology*, 67(2), pp.152–159.

Song, X. et al., 2016. Cancer Cell-derived Exosomes Induce Mitogen-activated Protein Kinase-dependent Monocyte Survival by Transport of Functional Receptor Tyrosine Kinases. *Journal of Biological Chemistry*, 291(16), pp.8453–8464.

Stanley, E.R. & Chitu, V., 2014. CSF-1 Receptor Signaling in Myeloid Cells. *Cold Spring Harbor Perspectives in Biology*, 6(6), pp.a021857–a021857.

Stansfield, B.K. & Ingram D.A., 2015. Clinical significance of monocyte heterogeneity. *Clinical Translational Medicine*, 14(4)p.e5.

Stark, G.R. & Darnell, J.E., 2012. The JAK-STAT Pathway at Twenty. *Immunity*, 36(4), pp.503–514.

Stein, M. et al., 1992. Interleukin 4 potently enhances murine macrophage mannose receptor activity: a marker of alternative immunologic macrophage activation. *The Journal of Experimental Medicine*, 176(1), pp.287–292.

Sumagin, R. et al., 2010. LFA-1 and Mac-1 Define Characteristically Different Intralumenal Crawling and Emigration Patterns for Monocytes and Neutrophils In Situ. *The Journal of Immunology*, 185(11), pp.7057–7066.

Sweet, M.J., Stacey, K.J. & Ross, I.L., 1998. Involvement of Ets, rel and Sp1-like proteins in lipopolysaccharide-mediated activation of the HIV-1 LTR in macrophages. *Journal of Inflammation*, 48(2), pp.67–83.

Swirski, F.K. et al., 2009. Identification of splenic reservoir monocytes and their deployment to inflammatory sites. *Science*, 325(5940), pp.612–616.

Sørlie, T. et al., 2001. Gene expression patterns of breast carcinomas distinguish tumor subclasses with clinical implications. *Proceedings of the National Academy of Sciences (PNAS)*, 98(19), pp.10869–10874.

Talreja, J. et al., 2017. RNA-sequencing Identifies Novel Pathways in Sarcoidosis Monocytes. *Scientific Reports*, 7(1), pp.1446–10.

The FANTOM Consortium et al., 2014. An atlas of active enhancers across human cell types and tissues. *Nature*, 507(7493), pp.455–461.

Thomas, G.D. et al., 2016. Deleting an Nr4a1 Super-Enhancer Subdomain Ablates Ly6C low Monocytes while Preserving Macrophage Gene Function. *Immunity*, 45(5), pp.975–987.

Tlsty, T.D. & Coussens, L.M., 2006. Tumor Stroma and Regulation of Cancer Development. *Annual Review of Pathology: Mechanisms of Disease*, 1(1), pp.119–150.

Todd, J.H. et al., 1987. Confirmation of a prognostic index in primary breast cancer. *British Journal of Cancer*, 56(4), pp.489–492.

Tripathi, S. et al., 2015. Meta- and Orthogonal Integration of Influenza "OMICs" Data Defines a Role for UBR4 in Virus Budding. *Cell Host & Microbe*, 18(6), pp.723–735.

Turner, M.D. et al., 2014. Cytokines and chemokines: At the crossroads of cell signalling and inflammatory disease. *BBA - Molecular Cell Research*, 1843(11), pp.2563–2582.

Turrini, R. et al., 2017. TIE-2 expressing monocytes in human cancers. *OncoImmunology*, 6(4), p.e1303585.

Ueno, T. et al., 2000. Significance of macrophage chemoattractant protein-1 in macrophage recruitment, angiogenesis, and survival in human breast cancer. *Clinical Cancer Research*, 6(8), pp.3282–3289.

Valls, F.A. et al., 2019. VEGFR1+ Metastasis-Associated Macrophages Contribute to Metastatic Angiogenesis and Influence Colorectal Cancer Patient Outcome. *Clinical Cancer Research*.

Veglia, F., Perego, M. & Gabrilovich, D., 2018. Myeloid-derived suppressor cells coming of age. *Nature Immunology*, 19(2), pp.108–119.

Venneri, M.A. et al., 2007. Identification of proangiogenic TIE2-expressing monocytes (TEMs) in human peripheral blood and cancer. *Blood*, 109(12), pp.5276–5285.

Veremeyko, T. et al., 2018. Early Growth Response Gene-2 Is Essential for M1 and M2 Macrophage Activation and Plasticity by Modulation of the Transcription Factor CEBPβ. *Frontiers in Immunology*, 9, pp.514–23.

Verreck, F. A. W. et al., 2004. Human IL-23-producing type 1 macrophages promote but IL-10-producing type 2 macrophages subvert immunity to (myco)bacteria. *Proceedings of the National Academy of Sciences (PNAS)*, 101(13), pp4560–65.

Villani, A. et al., 2017. Single-cell RNA-seq reveals new types of human blood dendritic cells, monocytes, and progenitors. *Science*, 356(6335), pp.eaah4573–14.

Villarino, A.V., Kanno, Y. & O'Shea, J.J., 2017. Mechanisms and consequences of Jak–STAT signaling in the immune system. *Nature Immunology*, 18(4), pp.374–384.

Vogel, G. et al., 2018. Functional characterization and phenotypic monitoring of human hematopoietic stem cell expansion and differentiation of monocytes and macrophages by whole-cell mass spectrometry. *Stem Cell Research*, 26(C), pp.47–54.

Wagner, K.U. et al., 1997. Cre-mediated gene deletion in the mammary gland. *Nucleic acids research*, 25(21), pp.4323–4330.

Walsh, J.C. et al., 2002. Cooperative and antagonistic interplay between PU.1 and GATA-2 in the specification of myeloid cell fates. *Immunity*, 17(5), pp.665–676.

Wang, S. et al., 2019. A dynamic and integrated epigenetic program at distal regions orchestrates transcriptional responses to VEGFA. *Genome Research*, 29(2), pp.193–207.

Wang, Y. et al., 2011. M-CSF Induces Monocyte Survival by Activating NF-κB p65 Phosphorylation at Ser276 via Protein Kinase. Public library of Science (*PLoS) ONE*, 6(12), pp.e28081–15.

Wang, Y. et al., 2014. Transcriptional repression of CDKN2D by PML/RARα contributes to the altered proliferation and differentiation block of acute promyelocytic leukemia cells. *Cell Death and Disease,* 5(10), p.e1431.

Weiterer, S. et al., 2015. Sepsis Induces Specific Changes in Histone Modification Patterns in Human Monocytes. Public library of Science (*PLoS) ONE*, 10(3), pp.e0121748–13.

Wellenstein, M.D. et al., 2019. Loss of p53 triggers WNT-dependent systemic inflammation to drive breast cancer metastasis. *Nature Publishing Group*, pp.1–26.

Wellings, S.R. & Jensen, H.M., 1973. On the origin and progression of ductal carcinoma in the human breast. *Journal of the National Cancer Institute*, 50(5), pp.1111–1118.

Wierda, R.J. et al., 2012. Epigenetic control of CCR5 transcript levels in immune cells and modulation by small molecules inhibitors. *Journal of Cellular and Molecular Medicine*, 16(8), pp.1866–1877.

Wiśnik, E., Płoszaj, T. & Robaszkiewicz, A., 2017. Downregulation of PARP1 transcription by promoter-associated E2F4-RBL2-HDAC1-BRM complex contributes to repression of pluripotency stem cell factors in human monocytes. *Scientific Reports*, 7(1), p.e9483.

Wong, K.L. et al., 2011. Gene expression profiling reveals the defining features of the classical, intermediate, and nonclassical human monocyte subsets. *Blood*, 118(5), pp.e16–31.

Wu, L. et al., 2017. Ascites-derived IL-6 and IL-10 synergistically expand CD14+HLA-DR-/low myeloid-derived suppressor cells in ovarian cancer patients. *Oncotarget*, 8(44), pp.76843–76856.

Wyckoff, J.B. et al., 2007. Direct visualization of macrophage-assisted tumor cell intravasation in mammary tumors. *Cancer Research*, 67(6), pp.2649–2656.

Xie, T.X. et al., 2010. Constitutive NF-κB activity regulates the expression of VEGF and IL-8 and tumor angiogenesis of human glioblastoma. *Oncology reports*, 23, pp.725–723.

Yang, J. et al., 2010. Reversible methylation of promoter-bound STAT3 by histone-modifying enzymes. *Proceedings of the National Academy of Sciences (PNAS)*, 107(50), pp.21499–21504.

Yona, S. et al., 2013. Fate Mapping Reveals Origins and Dynamics of Monocytes and Tissue Macrophages under Homeostasis. *Immunity*, 38(1), pp.79–91.

Zabuawala, T. et al., 2010. An Ets2-Driven Transcriptional Program in Tumor-Associated Macrophages Promotes Tumor Metastasis. *Cancer Research*, 70(4), pp.1323–1333.

Zawada, A.M. et al., 2011. SuperSAGE evidence for CD14++CD16+ monocytes as a third monocyte subset. *Blood*, 118(12), pp.e50–e61.

Zhang, H. et al., 2011. Engagement of I-Branching -1, 6-N-Acetylglucosaminyltransferase 2 in Breast Cancer Metastasis and TGF- Signaling. *Cancer Research*, 71(14), pp.4846–4856.

Zhang, Y. et al., 2012. A novel role of hematopoietic CCL5 in promoting triple-negative mammary tumor progression by regulating generation of myeloid-derived suppressor cells. *Cell Research*, 23(3), pp.394–408.

Zhao, F. et al., 2012. S100A9 a new marker for monocytic human myeloid-derived suppressor cells. *Immunology*, 136(2), pp.176–183.

Zhao, X. et al., 2017. Prognostic significance of tumor-associated macrophages in breast cancer: a meta-analysis of the literature. *Oncotarget*, 8(18), pp.30576–30586.

Zhou, Y. et al., 2019. Metascape provides a biologist-oriented resource for the analysis of systems-level datasets. *Nature Communications*, 10(1), p.e1523.

Zhu, Y. et al., 2014. CSF1/CSF1R blockade reprograms tumor-infiltrating macrophages and improves response to T-cell checkpoint immunotherapy in pancreatic cancer models. *Cancer Research*, 74(18), pp.5057–5069.

Chapter 9 Appendix

9.1 Reagents

9.1.1 Flow cytometry antibodies (mouse)

BLOCK and LIVE/DEAD STAINS				
	Antibody	**Clone**	**Company**	**CatNo**
N/A	CD16/32	93	Biolegend	101320
Blood PyMT Kinetic				
	Antibody	**Clone**	**Company**	**CatNo**
FITC	45.2	104	Biolegend	109806
PE	Treml4	16 e 5	Biolegend	143303
PeCy7	Cd11b	M1/70	Biolegend	101216
APC	CD115	Afs98	Biolegend	135510
Pac blue	Cd3	17A2	Biolegend	100214
Pac blue	CD19	6d5	Biolegend	115523
BV421	Siglec F	E50-2440	BD Horizon	562681
AF700	Ly6c	hk1.4	Biolegend	128024
BV510	Ly6g	1a8	Biolegend	127633
DAPI for live/dead				
BM (Analysis and sorts)				
	Antibody	**Clone**	**Company**	**CatNo**
PE CF594	CD135	A2F10.1	BD Horizon	562537
PE	Sca1	D7	Biolegend	108107
PeCy7	CD117	2b8	Biolegend	105814
APC	CD115	Afs98	Biolegend	135510
AF700	Ly6c	hk1.4	Biolegend	128024
BV510	Ly6g	1a8	Biolegend	127633
BV650	CD11b	M1/70	Biolegend	101259
BV711	CD127	A7R34	Biolegend	135035
Pac blue	Cd3	17A2	Biolegend	100214
Pac blue	CD19	6d5	Biolegend	115523
Pac blue	NK1.1	PK136	Biolegend	108722
Pac blue	Ly6g	1A8	Biolegend	127612
Pac blue	Ter119	ter-119	Biolegend	116232
BV421	Siglec F	E50-2440	BD Horizon	562681
APCCy7	CD11c	N418	Biolegend	117324
DAPI for live/dead				

BrdU panel (blood)				
	Antibody	**Clone**	**Company**	**CatNo**
PE	Treml4	16 e 5	Biolegend	143303
PeCy7	Cd11b	M1/70	Biolegend	101216
APC	CD115	Afs98	Biolegend	135510
PB	Ly6c	HK1.4	Biolegend	128014
Biotin	CD3	17A2	Biolegend	100244
Biotin	CD19	6d5	Biolegend	115504
Biotin	Ly6g	1a8	Biolegend	127604
Biotin	SiglecF		macs	130-101-861
BV650	streptavadin		Biolegend	405232
EF780 for live/dead				
BrdU (BM)				
	Antibody	**Clone**	**Company**	**CatNo**
PE	Sca1	D7	Biolegend	108107
PeCy7	CD117	2b8	Biolegend	105814
APC	CD115	Afs98	Biolegend	135510
AF700	Ly6c	hk1.4	Biolegend	128024
BV650	CD11b	M1/70	Biolegend	101259
BV711	CD127	A7R34	Biolegend	135035
Pac blue	Cd3	17A2	Biolegend	100214
Pac blue	CD19	6d5	Biolegend	115523
Pac blue	NK1.1	PK136	Biolegend	108722
Pac blue	Ly6g	1A8	Biolegend	127612
Pac blue	Ter119	ter-119	Biolegend	116232
BV421	Siglec F	E50-2440	BD Horizon	562681
Zombie Aqua for live/dead			Biolegend	423102
Blood sort mouse				
	Antibody	**Clone**	**Company**	**CatNo**
FITC	45.2	104	Biolegend	109806
PE	Treml4	16 e 5	Biolegend	143303
PeCy7	Cd11b	M1/70	Biolegend	101216
APC	CD115	Afs98	Biolegend	135510
Pac blue	Cd3	17A2	Biolegend	100214
Pac blue	CD19	6d5	Biolegend	115523
BV421	Siglec F	E50-2440	BD Horizon	562681
BV711	Ly6c	hk1.4	Biolegend	128037
AF700	Ly6g	1A8	Biolegend	127622
DAPI for live/dead				

Extended BM progenitors panel				
	Antibody	**Clone**	**Company**	**CatNo**
FITC	CD34	RAM	BD Pharmingen	553733
APC Cy7	CD48	HM48-1	Biolgened	103432
PE CF594	CD135	A2F10.1	BD Horizon	562537
Perp Cp5.5	CD16/32	93	Biolegend	101324
BV711	CD127	A7R34	Biolegend	135035
BV650	CD150	TC15-12F12.2	Biolegend	115932
PE	Sca1	D7	Biolegend	108107
PeCy7	CD117	2b8	Biolegend	105814
APC	CD115	Afs98	Biolegend	135510
Pac blue	Cd11b	M1/70	Biolegend	101224
Pac blue	Ly6c	hk1.4	Biolegend	128014
Pac blue	Cd3	17A2	Biolegend	100214
Pac blue	CD19	6d5	Biolegend	115523
Pac blue	NK1.1	PK136	Biolegend	108722
Pac blue	Ly6g	1A8	Biolegend	127612
Pac blue	Ter119	ter-119	Biolegend	116232
DAPI for live/dead				
pSTAT1				
	Antibody	**Clone**	**Company**	**CatNo**
AF488	anti-STAT1 Phospho	A15158B	Biolegend	686410
PE	Treml4	16 e 5	Biolegend	143303
PeCy7	Cd11b	M1/70	Biolegend	101216
APC	CD115	Afs98	Biolegend	135510
PB	Ly6c	HK1.4	Biolegend	128014
Biotin	CD3	17A2	Biolegend	100244
Biotin	CD19	6d5	Biolegend	115504
Biotin	Ly6g	1a8	Biolegend	127604
Biotin	SiglecF		macs	130-101-861
BV650	streptavadin		Biolegend	405232
EF780 for live/dead			eBioscience	65-0865-14
MHCII Blood				
	Antibody	**Clone**	**Company**	**CatNo**
AF700	MHCII	M5/114.15.2	Biolgened	107622
Antibodies as used for BrdU(blood)				
MHCII BM				
	Antibody	**Clone**	**Company**	**CatNo**
APCCy7	MHCII	M5/114.15.2	Biolgened	107628
Antibodies as used for BM sorts excluding CD11c on APCCy7				

9.1.2 Flow cytometry antibodies (human)

	Antigen	Clone	Company	CatNo
PE Texas Red	**CD45**	HI30	ThermoFisher	MHCD4517
BV 711	**CD3**	OKT3	Biolegend	317328
BV 711	**CD56**	HCD56	Biolegend	318336
BV 711	**CD19**	HIB19	Biolegend	302246
BV 605	**CD11b**	ICRF44	Biolegend	301332
BV 510	**CD14**	M5E2	Biolegend	301842
BV650	**HLA-DR**	L243	Biolegend	307650
EF450	**CD16**	eBIOCB16	eBioscience	48-0168-42

9.1.3 Primers for qPCR

Gene	Forward	Reverse	Tm	Eff.	(R^2)
LPL	GAAAGGGCTCTGCCTGAGTT	TAGGGCATCTGAGAGCGAGT	78	92	0.987
IFIT2	TTTGAGAAGGAATGCACCAGAA	GCAGCACAGAGTTGAGAGGTT	78	79	0.988
CXCL10	ATGACGGGCCAGTGAGAATG	TCGTGGCAATGATCTCAACAC	78	89	0.992
STAT1	GAACGCGCTCTGCTCAA	TGCGAATAATATCTGGGAAAGTAA	-	-	-
STAT1	GGAAGCGAAGGCAGCAGAG	CTGCAACAATGGTGAACCACG	-	-	-
STAT1	CTCGTGGAGTGGAAGCGAAG	TGCAACAATGGTGAACCACG	82	88	1
SDHA	TGTTCCGTGTGGGGAGTGTA	TCCAAACCATTCCCCTGTCG	75	97	1
GCNT2	CTACGCGGGAAAGTTTTCGC	GTAGAGGTTGGGCAGGCTTA	78	100	0.991

Table 8 Primers used for qPCR. Tm = melting temperature, Eff. = efficiency, R^2= correlation coefficient.

9.1.4 General reagents

- Flow cytometry staining buffer (0.5% w/vBSA in DPBS)
  - BSA (Sigma, Cat No A1470)
  - DPBS- (Life Technologies, Cat No 14190169)

- Red blood cell lysis buffer for blood (Biolegend, Cat No 420301)
- Red blood cell lysis buffer for BM (MERCK, Cat No 11814389001)

- 0.5M EDTA (Fisher Scientific, Cat No 11836714)

9.2 Detailed protocols

9.2.1 Quantification of blood cells

Blood collection

1. 10µl EDTA to pipette then adjust to 50µl
2. Make a superficial oblique cut in the end of the lateral vein
3. Collect 50µl total (40µl blood) by pipetting droplets from the tail
4. Place sample in eppendorph and onto ice
5. Apply pressure with a gauze to the tail and ensure bleeding has stopped
6. Record procedure as per guidelines in animal unit
   Return to laboratory to process samples

Sample preparation for flow cytometry

7. Make up RBC lysis buffer 1:10 (dilute with H_2O)
8. Transfer exactly 40µl to a 15ml falcon tube ensuring you maintain correct labelling
9. Add 400µl of RBC to each sample and briefly vortex to ensure fully mixed
10. After 5 mins add 5mls FACS buffer and centrifuge at 300g for 5 mins
11. Discard supernatant and resuspend in 400µl RBC lysis buffer
12. After 5 mins add 5mls FACS buffer and centrifuge at 300g for 5 mins
13. Discard supernatant and re-suspend pellet. NOTE: 96 well plates can only take 200µl of volume so discard and leave tube inverted on paper towel to absorb supernatant around the top of the tube then invert and re-suspend
14. Plate re-suspended pellets onto 96 well FACS plate. NOTE: leave an empty cell between each sample to ensure no cross-contamination
15. Add FACS buffer ~100ul/well (depending on volume of re-suspended pellet) centrifuge at 300g for 5 mins
16. Re-suspend in 20µl block (1 in 200 of CD16/32 block in FACS buffer). Leave for 15 mins in the dark on ice
17. Make-up master mix (See Table 1)
18. Add the 30L antibody master mix to each sample
19. Incubate on ice for 30mins protected from the light
20. While incubating antibody, make up compensation beads
21. Add 100µl of FACS buffer and centrifuge at 300g for 5 mins
22. Discard supernatant, resuspend and add 100µl of FACS buffer and centrifuge at 300g for 5 mins (completing two washes)
23. Re-suspend pellet and Add 1:1000 of BV650 stain to each sample well and leave 20 mins in the dark on ice
24. Add 100µl of FACS buffer and centrifuge at 300g for 5 mins
25. Discard supernatant, resuspend in 150µl FACS buffer and filter through blue top filter into FACS tube
26. Use an additional 150µl FACS buffer to wash cell and filter to make to a total volume of 300µl
27. At the flow cytometer, add 7AA D 10µl per sample 2-5 mins before acquiring sample and prior to acquiring sample, add 50µl of counting beads to sample and vortex. NOTE: the beads need vortexing well prior to use for each sample

9.2.2 Processing BM for quantification and sorting by flow cytometry

Obtain BM

1. Sacrifice mice by cervical dislocation (or CO2 if also collecting blood)
2. Spray with 70% ethanol to sterilise outer coat
3. Sterilise surgical tools – forceps, scalpel and scissors with 70% ethanol
4. Pinch skin on back, snip and then pull it off to expose the flesh underneath
5. Strip away muscle to expose the leg bone
6. Separate the rest of the lower leg (tibia/femur bones) from the femur but make sure to keep it attached to the body
7. Cut away the muscles and ligaments, then dislocate the femur from the pubis bone
8. Cut at the base of the femur to separate it from the body and place in bijoux containing medium then onto ice
   Return to laboratory to process samples in a sterile hood

Sample preparation for flow cytometry

9. Place sample in the lid of petri dish and keep on ice
10. Take the femur and cut the femoral head and very distal aspect of femur
11. Flush BM into the base of the petri dish (on ice) with RPMI medium 10ml until all marrow is flushed (none should look translucent)
12. Repeat for all bones using the same 10mls
13. Remove the needle and agitate sample in syringe/against petri to break up clumps of marrow
14. Filter sample using yellow filter into 15ml falcon
15. Centrifuge at 400g 5mins 4˚C
16. Re-suspend in 3ml RBC lysis for 3 mins
17. Add 8mls FACS buffer
18. Centrifuge at 400g 5mins 4˚C.
19. Discard the supernatant and tip upside down in rack with a paper lining to absorb
20. Re-suspend by flicking the bottom of the falcon and make up to 1ml
21. Count cells and aliquot out desired amount for each sample
    1. For quantification recommend $10x10^6$ cells
    2. CFU assays and RNAseq recommend $25x10^6$ and proceed with volumes below
22. Centrifuge at 400g 5mins 4˚C
23. While spinning, make up block 1:00 in FACS buffer
24. Re-suspend (total volume will be 100µl)
25. Add the 100µl of block master mix to each sample and transfer to FACS tube via blue top filter
26. Leave for 15 mins on ice in the dark
27. While blocking, make up master mix for staining
28. After 15 mins, add 300µl of master mix to each sample
29. Incubate on ice for 30mins protected from the light
30. While incubating antibody, make up compensation beads
31. After 30 mins, add 3ml FACS buffer to each sample
32. Centrifuge at 400g for 5 mins
33. Re-suspend in 0.5ml of FACS buffer (300µl for quantification)
34. Filter through blue top FACS tube
35. Prior to running, run a small amount of each sample to check gating and homogenous staining
36. Prior to flow cytometry analysis add 10µl of 7AAD as live/dead OR for sorting, add 1:200 DAPI as live/dead stain

- For quantification Immediately prior to acquiring sample, add 50µl of counting beads to sample and vortex. NOTE: the beads need vortexing well prior to use for each sample
- For CFU assay Sort progenitors into the polypropolene tubes (ref352063) coated with 50% HI FCS in PBS
- For RNA seq sort $100x10^6$ cells into LowBind DNA/RNA free 1.5ml eppendrophs

9.2.3 BrdU BM by flow cytometry

Additional reagents

- Live/dead stain Zombie Aqua™ Fixable Viability Kit (Biolgened, Cat No 423102
- Ebioscience FoxP3-staining-buffer-set (eBioscience, Cat No 00-5523)
- DNase –I (Stock at 1mg/ml in D-PBS in 300ul Aliquots, Sigma Aldrich, Cat No D5025)
- Dulbecco's PBS (Sigma Aldrich Cat No D8537)
- 0.42M MgCl2
- Anti-BrDU-antibody (Alexa Fluor® 488 anti-BrdU Antibody, EBioScience, Cat No 364106)
- Aluminium-foil
- DNase-solution (30ul DNase-stock [in -80] + 960ul D-PBS + 10ul MgCl2)

Sample preparation for flow cytometry

1. Harvest bone marrow, lyse and count as per protocol 2 steps 1-21
2. Aliquot out 10 million cells for each sample
3. Centrifuge at 400g 5mins at 4˚C
4. Discard the supernatant
5. Re-suspend in 100µl of live/dead aqua stain (1:100)
6. Leave at RT for 10 mins in the dark
7. Add 100µl of block (1:100 in FACS buffer)
8. Leave for 15 mins on ice in the dark
9. Make up Antibody MM and add 300µl to each sample
10. Incubate on ice for 30mins protected from the light
11. Add FACS buffer 5mls
12. Centrifuge at 400g 5mins at 4˚C
13. Re-suspend in 125ul/sample Fixation-Permeabilisation buffer (1part Fix – 3 parts Fix Diluent)
14. At this point take a pooled sample from the benign and the control that will be used for the BrdU control
15. Incubate for 1 hr at RT in the dark
16. Add perm wash buffer (made up 1:10 with H_20)
17. Centrifuge at 400g 5mins at 4˚C
18. Add the DNase 100µl or PBS 100µl to the BrdU control samples, mix and incubate for 30 mins at 37˚C wrapped in foil
19. Add perm wash
20. Centrifuge at 400g 5mins at 4˚C
21. Re-suspend in perm wash/BrdU 80µl (MM of 755 Perm wash + 50µl BrdU for both blood and BM made-up) and incubate at RT for 30 mins in the dark
22. Wash once with Perm wash buffer and re-suspend cells in FACS-buffer TV 500µl
23. When acquiring on flow cytometer, ensure that cells are on scale – fixation of cells will alter cell morphology and voltages will need to be adjusted accordingly

9.2.4 BrdU blood

Additional reagents

- Fixable Viability Dye eFluor™ 780 (eBioscience, Cat No 65-0865-18)
- Ebioscience FoxP3-staining-buffer-set (eBioscience, Cat No 00-5523)
- DNase –I (Stock at 1mg/ml in D-PBS in 300ul Aliquots, Sigma Aldrich, Cat No D5025)
- Dulbecco's PBS (Sigma Aldrich, Cat No D8537)
- 0.42M MgCl2
- Anti-BrDU-antibody (Alexa Fluor 488 anti-BrdU Antibody, EBioScience, Cat No 364106)
- Aluminium-foil
- DNase-solution (30ul DNase-stock + 960ul D-PBS + 10ul MgCl2)

Sample preparation for flow cytometry

1. Process 40µl of tail vein blood as per protocol 1 from steps 1-15
2. Re-suspend in Fix viability dye MM 10µl /sample (1:1000 in PBS NOT FACS BUFFER)
3. Incubate for 10 mins at RT in the dark
4. Add in 10µl block (1:100 in FACS buffer) and incubate on ice for 15 mins
5. Add 80µl of surface staining MM (stain in 100µl total volume)
6. Incubate for 30mins on ice in the dark
7. Add 100µl FACS buffer to wash
8. Centrifuge at 400g at 4˚C for 5 mins
9. Discard supernatant
10. Re-suspend in 100µl of BV650 streptavadin (1:1000 in FACS buffer) for 20mins on ice in the dark
11. Add 100µl FACS buffer
12. Centrifuge at 400g at 4˚C for 5 mins
13. Discard supernatant
14. Re-suspend in 100ul/well Fixation-Permeabilisation buffer (1part Fix – 3 parts Fix Diluent)
15. Incubate at RT in the dark 1 hr
16. Add 100µl perm wash to each well
17. At this point take a pooled sample from the benign and the control that will be used for the BrdU control
18. Centrifuge at 400g for 5 mins
19. Discard and resuspend in 100µl DNase or 100µl of PBS for BrdU controls
20. Incubate for 30min at 37ºC wrapped in aluminium foil
21. Add 100µl perm wash to each well
22. Centrifuge at 400g for 5 mins
23. Add 2.5ul* of anti-BrDU (FITC) antibody to all the samples and make up to a total of 40ul/well with perm wash and incubate at RT for 30min.
24. Add 100µl perm wash to each well
25. Centrifuge at 400g for 5 mins
26. Add 100µl perm wash to each well
27. Centrifuge at 400g for 5 mins
28. Re-suspend cells in FACS-buffer 300µl and analyse of flow cytometer

9.2.5 Bone marrow colony forming unit assays

You will need an incubator set at 37ºC 5% and CO_2 >= 95% humidity. All procedures should be carried out in a sterile hood.

Additional reagents

- Methocult media (MethoCult™ GF M3534, StemCellTM Technologies)
- Iscove's Modified Dulbecco's Medium (IMDM) (ThermoFisherScientifc, Cat No 12440053)

Equipment

- Falcon™ Round-Bottom Polystyrene Tubes (Falcon 352058, product code 10100151)
- 35mm petri dish (2 per mouse as will want to do duplicates of each sample)
- 15cm dish (1 per 6 plated samples)
- 5ml syringe
- 18G blunt ended needle

Assay setup

1. Using a 5 ml syringe with a 18G blunt ended needle, dispense 3 ml of Methocult into sterile 5ml FACS tubes (Falcon, 352058) for each pair of duplicates. Do not fully void syringe e.g. measure from 4 ml to 1 ml. This is best done on the morning of the experiment or while the sort is being done as you will want to work quickly once cells are ready. The Methocult can be aliquoted out into tubes with 3ml each and then stored at -20˚C.
2. Take the sorted cells and spin down at 500g for 5 mins at 4˚C
3. Remove supernatant and resuspend to ensure desired cell number in 300µl of Iscove's Modified Dulbecco's Medium (IMDM).
4. Add the 300µl of cells at desired concentration
5. Seal tube and vortex vigorously to mix
6. Leave for bubbles to rise whilst preparing plates. ~ 5 mins
7. Prepare plates (35mm) and carefully label on the side not the top of the lid as this will obscure view when counting if on the top. For each sample, it is best to do a duplicate. You also must include a 35mm plate containing just PBS in the centre of the 15cm plate. You can fit up to six plates per dish.
8. Draw up 1ml of the cell mix, then expel back in the tube to remove air Repeat if needed. Leave in top of tube and perform for next tube
    1. Return to first, any new bubbles should have risen, and draw up 2.4ml or more
    2. Lift lid to 35 mm dish, still covering from above, and dispense 1.1 ml to the two dishes, not fully voiding syringe as before.
    3. Gently tilt dish to spread Methocult mix evenly across.
    4. Repeat for each sample.
    5. Incubate the plates at 37ºC 5% CO_2 >= 95% humidity. For GF M3434 incubate for 10-14 days.

9.2.6 Cytospin and staining of colonies for morphological assessment

Additional equipment

- Shandon Cytospin II
- Thermo Scientific™ Double Cytology Funnel with White Filter Cards (Product Code.15211886)
- Slides and coverslips

Additional Reagents

- Rapid Romanowsky Stain Solution A, B, C, (TCS Biosceinces Ltd; Cat#HS705)

Cytospins

1. Label the frosted end of the glass slide with pencil
2. Insert the slide into a cytoclip
3. Align filter paper to the glass slide with the absorbent surface touching the slide
4. Slide a cytofunnel into the clip (on top of the slide with filter paper)
5. Ensure the circle is aligned with the cytofunnel
6. Gently fasten the clip
7. Prime the slide with 50ul of PBS
8. Spin down for 1min at 500rpm (50x10) using the Shandon Cytospin II
9. Load cells (20-100ul volumes only) and centrifuge for 5min at 500rpm
10. Carefully unload the cytoclips
11. Let the slides dry for 1h or O/N
12. Prepare 4x 50ml falcon tubes with respectively Rapid Romanowsky Stain Solution A, B, C, (TCS Biosceinces Ltd; Cat#HS705) and water
13. Transfer the slide with cells (one by one) to the solutions as indicated
14. Remove excess water
15. Let the slides dry for 1h or O/N
16. Mount the slides with coverslips using a drop of Entellan mounting medium

#	Reagent	Time
1	**Solution A**	30 sec
2	**Solution B**	15 sec
3	**Solution C**	2 mins
4	**Water**	Until clean

9.2.7 Sorting of mouse blood monocytes for RNAseq

Harvesting blood

1. Take up just over 100µl of EDTA into 1ml syringe, prime the needle and ensure have just 100µl of EDTA in the syringe
2. Place mice in CO_2 chamber for 5 mins
3. Spray mouse with 70% ethanol
4. Lift the chest with forceps and cut open by cutting the sternum (careful not to disrupt the vasculature) and the left hemi-diaphragm. By holding the sternum up with the forceps in you left had you should be able to visualise the left ventricle into which you insert the needle
5. Gently aspirate (you should achieve 800-1000µl per mouse)
6. Place into falcon and place sample straight onto ice.

Sample preparation for flow cytometry

7. Split samples into two 500µl of blood as lyses more effectively
8. Per sample, Add RBC lysis buffer (x10 of total volume of blood) to sample and immediately vortex to ensure all is mixed and homogenous
9. Leave on ice for 5 mins
10. Add FACS buffer to top up falcon to 15ml

Note: If any clot seen at this stage you must remove it using 1ml stripette

11. Centrifuge at 400g for 5 mins at 4˚C
12. Discard supernatant and re-suspend
13. Add RBC lysis again, mix well and leave on ice for 5 mins
14. Top up to 15mls with FACS buffer
15. Centrifuge at 400g for 5 mins at 4˚C
16. Discard supernatant
17. Pool back together again in FACS tube
18. Centrifuge at 400g for 5 mins at 4˚C
19. While centrifuging, make up the block 1:100
20. Discard supernatant and invert to discard fully.
21. Re-suspend so will all be in same volume (100µl)
22. Add 100µl block solution per sample (block now 1:200)
23. Leave for 15 mins on ice in the dark
24. While blocking, make up FACS antibody master mix
25. Add 300µl of antibody master mix to each sample tube
26. Incubate on ice for 30mins protected from the light
27. Top up with 3mls FACS buffer
28. Centrifuge at 400g for 5 mins 4˚C
29. While centrifuging, prime each filter tube with 100µl FACS buffer to wet the filter
30. Discard supernatant
31. Re-suspend and filter through blue top tube
32. Take to FACS on ice
33. Proceed to sort using blood panel with DAPI (1:200) for live/dead
34. Sort $25x10^3$ cells into a BSA coated low-retention 2ml Eppendorf if proceeding to RNAseq

9.2.8 Sorting of human blood monocytes for seq

1. Collect blood (10ml) in EDTA tubes and keep on ice
2. Transfer blood up to 20mls in a 50ml Flacon tube
3. Add 1X RBC Lysis Buffer to make up to 50mls, mix well and incubate on ice for 5-10 mins. You must keep checking and inverting the sample to check - it should go a clearer slightly browner/darker colour.
4. Centrifuge for 5 mins at 500g and 4˚c. Discard the supernatant by gently pouring off and re-suspend the pellet.
5. Transfer to 15ml falcon tube and top up to 5mls with FACS buffer
6. Centrifuge for 5 mins at 500g and 4˚c
7. Discard supernatant* and re-suspend in block so have total volume 1ml
   *here you should have a nice white pellet - if you don't then you must repeat RBC lysis.
8. Count the cells and record total number of cells, you will adjust the master mix to fully saturate staining
11. Once the block has been on for 30 mins, add the master mix of stain*
12. Incubate for 30min on ice in the dark
13. Top up with 4ml of staining buffer and centrifuge for 5 mins at 500 rcf and 4˚C
14. Re-suspend the pellet in 0.5ml staining buffer
15. Sort cells into LoBind DNA/RNA free 1.5ml eppendorphs coated in 2% w/vBSA in DPBS and proceed to process for RNAseq.

9.2.9 Hoescht staining of monocytes

Additional reagents

- Loading medium
  - DMEM, high glucose 10% FBS
  - HEPES buffer, 10mM
- Reserpine (Sigma, Cat No R0875-1G FW=608.69)
  Stock concentration = 5mM = 1000X
  Working concentration = 5µM Preparation of 5mM Reserepine:
  Dissolve 30 mg in 10 ml DMSO → filter sterilize → aliquot → store in freezer

- Hoechst 3334 (Invitrogen/Moleculr Probes, Cat No H3570)
  Stock conc = 10 mg/ml in water = 667X
  Working conc = 15 µg/ml

- Propidium Iodide (PI)
  Stock = 1 mg/ml = 200X
  Working conc = 5 µg/ml

Hoechst loading of cells

1. Proceed through steps 1-21 of protocol 5.
2. Adjust the concentration to 2 million total cells/ml with loading medium. Lower cell densities are OK.
3. Add Hoechst (final concentration = 15 ug/ml) and Reserpine (final concentration = 5 μM). Hoechst is actively pumped out of cells by the ABC transporter, ABCG2. Reserpine selectively inhibits ABCG2, thereby preventing the cells from pumping Hoechst out.
4. Incubate cells in the dark for 30 mins at 37°. This step "loads" Hoechst into the cells.
5. Optional antibody stain. Procced with steps 22-28 of protocol 5.
6. Add PI (final concentration = 5 ng/ml).
7. Keep cells on ice and in the dark until sorting/analysis.
8. For sorting on the fusion, use the 100 μm nozzle.
    - Hoechst is excited with the UV laser.
    - Can use the gating strategy for monocytes and sort into a 96 well imaging plate with PFA
    - Expect approximately 25-50% of the cells to be dead.
9. Image plate using and DAPI capable filter set. I used the Carl Zeiss Axio200 inverted microscope equipped with 20x objective lens. Light was filtered using a Zeiss standard DAPI filter set. Check each well for the presence of a cell or more than one cell.

9.2.10 Preparing dUTP RNA-seq libraries

NOTE Samples were transported on dry ice to UCSD where RNAseq libraries were prepared by A Robinson or Claudia Han. The following protocol includes recommended stop points and it is recommended that the total protocol is undertaken in 2-3 days.

Buffers

DTBB (2x)

20mM Tris-HCl (pH 7.5)
1M LiCl
2mM EDTA
1% lithium dodecyl sulfate
0.1% Triton X-100
*add final 10mM DTT if polyA directly from cells

Washing buffer 1

10mM Tris-HCl (pH 7.5)
0.15M LiCl
1mM EDTA
0.1% lithium dodecyl sulfate
0.1% Triton X-100

Washing buffer 2

10mM Tris-HCl (pH 7.5)
0.15M NaCl
1mM EDTA

Note

5X SSIII first-strand buffer [250mM Tris-HCl (pH 8.3), 375mM KCl, 15mM MgCl2] contains Mg2+ which is utilized for RNA fragmentation (at 2x concentration = 30mM).

DAY 1

* use 0.05-1µg starting material (total RNA)

** heat PCR machine lid 5°C above inc. temp. Do NOT use 100°C (but for final PCR)

*** increasing PEG particularly at step 2.3 allows recovery of fragments <75nt

1 RNA extraction and precipitation

1.1 Dissolve cells in 375µl Trizol LS (3x total vol), vortex well (10 mins+); freeze or continue

1.2 Add 150 µL dH2O+0.05%Tween (dH2OT) and the required volume of CHCl3 (trizol/5), really shake and vortex (should look milky pink)

1.3 Centrifuge for 10min at 15,000 at 4˚C

1.4 While centrifuging prepare transfer tubes

1.5 Transfer supernatant to fresh tube. If disrupt at all then centrifuge again.

1.6 Check the amount of supernatant

1.7 Calculate 1/10 vol 3M NaOAc of supernatant

1.8 **Add** GlycoBlue (15mg/ml) for each sample

1.9 **Add 1/10 of total supernatant vol NaOAc + glycol blue to each sample**

1.10 Ensure that this is well mixed so RNA is salted

1.11 Add 1 volume Isopropanol to each sample

1.12 **ENSURE THAT THIS IS WELL MIXED AND CHECK VISUALLY THEN QUICK SPIN**

1.13 Precipitate 20 mins or O/N at -20˚C

1.14 Centrifuge >25mins @max speed at 4˚C

1.15 ONCE SPIN FINISHED RETURN TO PRECIP RNA – Check all the pellets are good.

1.16 Suction off the Isopropanol and then remove the last bit with the P1000filter + gel load tip

1.17 Add 500µl ETOH 75% to each sample

1.18 Bang so pellet loosens to release any phenol

1.19 Quick centrifuge

1.20 Using p1000 take off the ETOH

1.21 Centrifuge (table-top) then ALL the ETHO away with the P1000/gel tip combo

1.22 Open and leave to dry for 3 mins. Dry pellet can be stored at -80.

1.23 Add 50µl TET to each sample, re-suspend, centrifuge (table-top) and transfer to PCR tubes using low retention tip OR can freeze at -80˚C (not -20 or will oxidise)

DAY 2

START HERE IF ALREADY HAVE FROZEN PELLET (re-suspend in 50µl TET)

2. Poly A tail selection

Prepare oligo(dT)25 Dynabeads (NEB S1419S) as follows:

2.1. *Allow beads to equilibrate to room temp for ~15 mins, mix well, then wash with DBTT.*

2.2. *Use an appropriate amount of oligo(dT)25 Dynabeads (**10 µL per 1ug total RNA**)*
**we added 10µl even though didn't know exact amount.*

*____ µL beads * _____ samples = _____ µL*

Vol 1x DBTT = same volume as beads (just dilute 2x DBTT using H_20

Vol 2x DBTT = 50µl x number samples =

2.3. Collect the beads on a magnet, remove supernatant and wash 2x with ~1 vol 1xDTBB

2.4. Re-suspend in 50µL 2x DTBB per sample. They are now ready to use.

2.5. Add to the PCR lids ready to put into the samples

2.6. Add the correct amount of beads to each sample (1:1 so 50µl) which is in 50µl TET already

PolyAA selection:

2.7. *Heat to 65°C for 2 mins [Lid: 70°C].*

2.8. *Incubate for 5-10 mins at RT on rotator set at 2. *(could also use shaker)*

2.9. *Spin down so all sample off lid.*

2.10. *Collect on magnet 2 mins, remove supernatant*

2.11. *1x wash with 200 µL of RNA washing buffer 1.*

2.12. *1X wash with RNA washing buffer 2.*

2.13. *Spin and ensure you have removed ALL*

2.14. ***IF ROUND 2 STOP AND GO TO STEP 4. DON'T ELUTE.***

3. Elution and detachment round 1

3.1. Elute the mRNA by adding 50 µL of TET (beads still in the mix)

3.2. Shake tray hard up and down to mix then centrifuge (table-top) to get off lid

3.3. Incubation at 80°C for 2 mins [Lid 85°C], quick vortex then place on ice IMEDIATELY [detaches at 80˚C and will reattach at 48˚C so minimize time in binding conditions]

2.1. Once cooled, transfer supernatant to new chilled PCR strip (low reten tips)

USE MAGNET SO DON'T TAKE THE BEADS WITH YOU BUT KEEP BEADS

2.2. Wash beads 1x 200 µL TET

2.3. Wash beads 1x 200 µL 2x DTBB

2.4. Re-suspend in 50 µL 2x DTBB

2.5. Transfer washed beads back to the respective RNA supernatant.

2.6. Repeat steps 2.7 to 2.14 and after washing buffer 2 has been added and washed and removed

4. Fragmentation

4.1. Calculate amount of fragmentation mix needed:

FRAGMENTATION MM	1x(µl)	Total sample
5x First strand buffer*	10	
100mM DTT	2.5	
dH_20 + 0.05%Tween	12.5	
TOTAL VOLUME	25µl	

*MUST HAVE Mg^{2+}

You will need 15µl for the wash (with 15µl water to make 2x into 1x)

So 15µl x number samples = µl

TAKE AMOUNT TO NEW TUBE, Add this to the same volume of H_20 and mix well

4.2. To each lid add 30 µL of prechilled 1x SuperScript III first-strand buffer you have just made with H2O

ONCE ADDED THROW AWAY TO PREVENT ACCIDENT

4.3. Mix well and centrifuge (table-top). Remove using magnet.

4.4. To new lids add 10 µL of Fragmentation MM x2 **NOT DILUTED!**

4.5. Re-suspend and centrifuge (table-top).

4.6. Incubate at 94°C for 10 mins* to fragment the mRNA and immediately place on ice (zfrag programme)

4.7. Once cooled, remove the beads and transfer the samples to new PCR tubes using low retention tips

While incubating you can make up your MM but don't add enzymes until ready

5. First-Strand cDNA Synthesis – work on ice with lids etc so enzymes stay at -4˚C.

Primer MM	1x (µl)	Total samples
Random primer (3µg/µl)	0.5	
Oligo dT (50µM)	0.5	
Superase-IN (round cooler)	0.5	
	1.5	

5.1. Quick centrifuge (table-top) to samples and onto ice

5.2. Add Primer MM 1.5 µL to 10 µL fragmented mRNA in 2x RT buffer

5.3. Incubate at 50˚C 1 min. Quick centrifuge (table-top) and place on ice

5.4. RT MM to each lid and add to each sample then start RT reaction

Reverse transcriptase MM	1x (µl)	Total samples
dH_20	6	
Actinomycin D	0.1	
100mM DTT	1	
dNTPs (10mM)	1	
Superscript III Enzyme	0.5	
	8.6µl	

RT reaction

i. 25˚C 10 mins

ii. 50˚C 50 mins

5.5. Add 36 µL of RNAClean XP to each reaction (13% final) and mix well and centrifuge (table-top).

5.6. Add 36 µL 100% isopropanol and mix thoroughly

5.7. Incubate mixture 10-15 mins at room temp

5.8. Pipette off mix using magnet so beads remain

5.9. Wash 2x with 200 µL of 80% ethanol made with dH2O+T

5.10. Spin down, remove residual EtOH

5.11. AIR DRY UNTIL YOU GET THE RING

5.12. Elute with 10µl warm TET into lids (1xstrip then back onto hot block)

5.13. Transfer supernatant to new PCR tube to remove beads

Second-Strand Synthesis with dUTP

5.14. Make up MM:

2nd Strand MM	1x (µl)	Total samples
dH_20	1.2	
10x Blue buffer	1.5	
dUTP	0.1	
dUTP mix	1	
RNase H	0.2	
DNA Pol I (10U/µl)	1	
	5	

5.15. Add 5 µL of the 2nd Strand master mix to each 10 µL of RNA/cDNA. Incubate at 16°C for 2+h or O/N.

6. DsDNA End Repair

dsDNA Repair MM	1x	Total Samples
dH_2O+T	2.64	
10x T4 DNA Ligase Buffer	0.5	
10mM **dNTP** mix	1.0	
T4 PNK	0.3	
10mM ATP	0.5	
Klenow Fragments	0.06	
	5 µl	

6.1. Add 5 µL of the Repair MM to 15 µL of the dsDNA.

6.2. Incubate at 20°C for 30 mins, then place on ice.

6.3. Add beads in 30µl MNaCL/PEG. Mix well and centrifuge (table-top).

6.4. Add 30 µL 100% Isopropanol.

6.5. Incubate at RT for 10–15 mins and then repeat usually pipette off and then wash with ETOHx2 and centrifuge to get rid of all the ETOH. Air dry beads.

6.6. Elute with 16.1 µL warm TET. Keep Speedbeads in solution with DNA.

7. dA-Tailing

dA Tailing MM	1x	Total samples
dH_2O+T	10 µl	
NEB 2	3 µl	
10mM **dATP** mix	0.6 µl	
Klenow Exo-	0.3 µl	
	13.9 µl	

7.1. Add 13.9 µL of dA Tailing master mix to each sample

7.2. Incubate at 37°C for 30 mins, place on ice.

7.3. Make up mix of 45 µL 20% PEG8000/2.5M NaCl per sample.

7.4. Add and Vortex well. Spin.

7.5. Add 45uL 100% Isopropanol. Mix well and centrifuge (table-top).

7.6. Incubate at RT for 10–15 mins.

7.7. Collect 2-3 mins on magnet and pipette off PEG supernatant.

7.8. Wash x 2 with ETOH, centrifuge (table-top), remove all ETOH and air dry.

7.9. Elute with 13.7µL warm TET. Keep Speedbeads in solution with DNA.

8. Y-Shape Adapter Ligation

NOTE – IMPORTANT THAT THIS IS DONE AT 21˚C as this is optimal for Ligase action in this buffer

Ligation MM	1x	Total samples
2x Rabid Ligase Buffer	15 μl	
1% Tween	0.3 μl	
Rapid Ligase	0.5 μl	
	15.8 μl	

8.1. Add 15.8 µL of Ligation MM for each sample into the PCR strip lid on ice.

8.2. **Add 0.5 µL unique barcode ds-adapter per "lid well". **** BE VERY VERY CAREFUL YOU GET THE RIGHT WAY AROUND – USE THE WHOLE TO GET THE LID RIGHT!!!! Use 1:50**

8.3. PlacePCR strip lid on tube w. respective sample DNA

8.4. Incubate at RT for 15 mins+, then place on ice.

8.5. Add7µL 20% PEG8000/2.5M NaCl.

8.6. Mix well by vortexing, centrifuge (table-top) briefly.

8.7. Incubte at RT for 10–15 mins.

8.8. Collet 2-3 mins on magnet and pipette off PEG supernatant. and then repeat usually pipette off and then wash with ETOH. Air dry beads- they get a ring when ready so check!

9. UDG Second Strand Digest

9.1. Make master mix TET and UDG:

	(µl)	total
TET	14	
UDG	1	
	15	

9.2. **Elute beads with 15µl MM and proceed with UDG digest**

9.3. Incubate at 37°C for 30 mins

10. Amplification & Library Prep.

PCR MM	1x	Total
5M Betaine	3 µl	
5x Q Buffer	5 µl	
10mM dNTP mix	1 µl	
100mM Primer 1GA	0.25 µl	
100mM Primer 1GB	0.25 µl	
Q5 Polymerase	0.5 µl	
	10 µl	

10.1. add 10 µL PCR MM

10.2. Cycle:

1) 98°C for 3 mins
2) 98°C for 45 sec
3) 60°C for 30 sec
4) 72°C for 30 sec
Repeat 2-4 4x
(5 total)
5) 72°C for 3 mins

Place PCR reactions on ice.

12. **qPCR**

12.1. Prepare qPCR plate with qPCR MM

12.2. Add 1.5µL pre-amplified PCR product

12.3. Run qPCR

12.4. Add calculated number of cycles and amplify

qPCR	1x	Total
2xKappa	5µl	
Primer 1GA	0.25µl	
Primer 1GB	0.25µl	
dH_20	3µl	
	8.5µl	

To determine additional required cycles:

number of cycles on curve minus 4

(usually around 11-12, try to stay <15)

Note: If sample was frozen, add some new polymerase (2µL 2xQ5 MM and 2µL dH2O)

13. Purification of amplified cDNA and gel size selection

13.1. Aliquot desired amount of beads

2µl x no samples = µl total volume beads

13.2. Take away TET

13.3. Add 25µlxNo.samples NaCL 5M to beads and thoroughly salt/mix/. Spin.

13.4. Add same volume PEG 40% (a bit extra as very viscous)

13.5. Clean up reaction by adding 1.5x total volume of reaction µL Speedbeads in 20%

PEG8000/2.5M NaCl eg if no qPCR you should have 25µl so need 37.5µl beads per

sample or if did qPCR you have 23.5 so add 35µl.

13.6. Mix well by vortexing, centrifuge (table-top) briefly. Incubate at RT for 10–15 mins.

13.7. Collect 2-3 mins on magnet and pipette off PEG supernatant.

13.8. Wash 2x with 200µL of 80% ethanol made with dH2O+T.

13.9. Spin down, remove residual EtOH.

13.10. Air-dry the beads 5 mins

13.11. Elute with 14µl Gel loading dye. Keep Speedbeads in solution with DNA.

13.12. Collect beads w. magnet and load on a 10% Acrylamide 1x TBE gel.

13.13. Run @80V till all dye in gel, then ~140V (180V if in a rush).

13.14. Stop when Cyanol [~120 bp] ~1cm before running off.

13.15. Prepare a shredder tubes (0.22G needle 0.5ml tube) into 1.5ml tube.

13.16. Stain gel 3µl CyberGold into TBE in tray prior to placing gel in.

13.17. Cut out 200-375 bp and place in 0.5ml tube. (23bp + adapter 125 = 150)

13.18. Shredder gel fragments- centrifuge max 3 mins turn 180˚ if not All through

13.19. 150µ gel EB (1M LiCl, 0.1% LDS, 1mM EDTA, 5mM TrisHCl pH ~8.0) and vortex, centrifuge (table-top) and onto shaker >4hr max 48hrs.

13.20. Repeat zymo kit purification **BUT**

a. Add 700µl DNA binding buffer (5x ay 750 would overflow!)

b. Centrifuge 900g 4mins (varies – check all elute through and then can increase up to 10k)

c. Discard or will fill up too much

d. Wash with 200µl wash buffer* 10k 1 min

*check has ETOH added and don't use ETOH

e. After wash and centrifuge (table-top), flick to discard the dry bit left in the filter tube

f. Wash with 200µl wash buffer 10k 1 min

g. Discard, centrifuge at 18k 1 min to dry out

h. Leave with cap open to dry 2-5 mins

i. <u>ELUTE WITH seqTET* (pH 8 denatures the DNA prior to sequencing) – ensure that the seqTET is warm.</u>

j. Spin at 15-18k for 2 mins (make sure is at RT)

**You can elute 1x 20µl but 15% higher yield if do 2z10µl elutions.*

14. Quantify using qBIT.

Buffer = 198 x No samples (+2)µl

Dye = (No samples =2) µl

Add 190 to standards 1 and 2

Add 198 to all others

Add 10µl standards and add 2µl sample so total volume 200µl

Vortex and **flick out any bubble** and proceed to measure. (NB record $1/10^{th}$ a unit is /ml)

9.2.11 RT-qPCR validation of genes

Reagents

- SuperScript™ VILO™ (ThermoFisherScientifc, Cat No11754050)
  - 5X VILOTM Reaction Mix
  - 10X VILOTM Reaction Mix
- SYBR Green™ (ThermoFisherScientifc, Cat No 4385610)

Making cDNA

To make cDNA from RNA (RNA should already have been extracted and quantified as detailed in methods)

1. Make up master mix:

	X1	total
5X VILO™ Reaction Mix	4µl	
10X VILO™ Reaction Mix	2µl	

2. To PCR tubes add 6µl of the MM above and up to 14µl of RNA (max 2.5ng), if less than 14µl of RNA then make up to 20µl with DEPC-water.

3. Run RT-PCR cycles:

   - 25˚C for 25mins
   - 42 ˚C for 60 mins
   - 85 ˚C for 5 mins
   - Plate can be held at 4 ˚C until ready to proceed

Plate MM and DNA

1. Make up master mix for primers and controls:

	X1	total
SYBR Green™	10	
Forward primer (10μM)	0.4	
Reverse primer (10μM)	0.4	
DPEC-water	4.2	

2. Aliquot out 15μl to each well and then add 5μl of cDNA

   For each gene you need triplicate wells for each sample and 2 samples with no DNA but 5μl H_20 to check for any contamination

3. Cover plate
4. Vortex
5. Centrifuge using pulse for ~1min to 500g
6. Take plate to the qPCR machine ready for running qPCR

9.2.12 Preparation of ATACseq samples and libraries

Cell Preparation

1. Collect 50x10^3 cells by FACS
2. Spin down cells at 500g for 5 mins at 4ºC.
3. Take off nearly all of supernatant -50µl can be left
4. Gently pipette to resuspend the cell pellet in 50µl of ice-cold Lysis Buffer.
5. Spin down immediately at 500g for 10 min a 4ºC.
6. Discard the supernatant, and immediately continue to transposition reaction.

Transposition Reaction and Purification

1. Leave cell pellet on ice and make the transposition reaction MM:

MM	**1X**	**5X**	**10X**	**15X**	**20X**
Tagment DNA Buffer	25µl	125µl	250µl	375µl	500µl
Tagment DNA enzyme I	2.5µl	12.5µl	25µl	37.5µl	50µl
Nuclease Free H2O	22.5µl	112.5µl	225µl	337.5µl	450µl

2. Gently pipette to re-suspend nuclei in the transposition reaction mix.
3. Incubate the transposition reaction at 37ºC for 30 min.
4. Immediately purify using a Zymo Research ChIP DNA Clean and Concentrator Kit.

Zymo ChIP DNA Clean & Concentrator

CHECK CENTRIFUGE AS NEED IT AT ROOM TEMP FOR ELUTION

1. Add x5 volume of DNA binding buffer (250µl) to each sample, mix, vortex and quickly centrifuge (table-top).
2. Transfer to column and centrifuge at 10k 1min room temp
3. Wash x 2 with 200µl wash buffer* 10k 30" min

   *Check has ETOH. Do not wash with ETOH like beads!
4. Discard, centrifuge at 18k 1 min to dry out
5. Open and leave to dry fully and transfer to elution tubes
5. Elute transposed DNA 8µl Elution Buffer (preheat to 70˚C)
6. Spin at 15-18k for ~2 minutes –ROOM TEMP
7. Repeat elution (final total volume of 16µl)

STOP FREEZE SAMPLE AT -20˚C ready for shipping

PCR Amplification

1. To amplify transposed DNA fragments, create MM:

PCR MM	**1X**	**X**
10 µM Nextera Primer 1* [**no** Barcode]	6.25µl	
10x SYBER Green	3µl	
NEBNext High-Fidelity 2x PCR MM	25µl	
	34.25µl	

2. Transfer 10µl of DNA into PCR tube
3. Add 34.25µl of PCR MM to each sample
4. Add 6.25µl of 10µM Nextera Primer 2 [**with** Barcode] to each sample (DIFFERENT BARCODED PRIMER PER SAMPLE!)
5. Set program as follows:
   (1) 72˚C 5 min
   (2) 98˚C 30 sec
   (3) 98˚C 10 sec
   (4) 63˚C 30 sec
   (5) 72˚C 1 min
   (6) Repeat steps 3 – 5, for 3 cycles **total**
   (7) Hold at 4˚C
6. In order to reduce GC and size bias in PCR amplification, the PCR reaction is monitored using qPCR to stop amplification prior to saturation. To run a qPCR side reaction, combine the following MM:

qPCR MM	1X	X
Nuclease Free H2O	3.15µl	
10µM Nextera Primer 1* [no barcode]	0.625µl	
10x SYBR Green I	0.6µl	
NEBNext High-Fidelity 2x PCR MM	5µl	
	9.375µl	

7. Transfer 5µl of PCR amplified DNA (3-cycles) into PCR tube.
8. Add 9.375µl of qPCR MM.
9. Add 0.625µl of 10µM Nextera Primer 2 [barcode] to each sample.
10. Run on qPCR program as follows:
    (1) 98˚C 30 sec
    (2) 98˚C 10 sec
    (3) 63˚C 30 sec
    (4) 72˚C 1 min
    (5) Repeat steps 2 – 4, for 19 cycles
11. To determine the number of additional cycles needed for the remaining 45µl PCR reaction: plot Rn vs Cycle in **linear**, set RF threshold to 5000 and calculate the cycle # that corresponds to ¼ of max fluorescent intensity.
12. Run the remaining 45µl PCR reaction for the correct # of cycles. Program as follows:
    (1) 98˚C 30 sec
    (2) 98˚C 10 sec
    (3) 63˚C 30 sec
    (4) 72˚C 1 min
    (5) Repeat steps 2 -4, for **x** cycles (**x** is ~6 additional cycles)

(6) Hold at 4˚C

13. Purify amplified library using Zymo ChIP & DNA Clean up.
14. Elute the purified library in 20µl Elution Buffer.
15. Add 5µl 5xTBE loading buffer and load on 12-well 10% TBE gel. Use 0.25-0.5µl ladder (25bp) diluted in 5µl 5xTBE loading buffer.
16. Run at 70V until DNA enters gel then increase to 140V for ~1 hr.
17. Stain gel in 10ml 1x TBE with SYBRGold diluted 1:10,000 (1µl).
18. Cut gel between 175 – 225 bp markers (or ~150 – 250 bp) into a 0.5ml LowBind tube perforated 3 times with a 22G needle.
19. Shred gel by centrifuging at max speed for 2 min at RT into 1.5 ml LowBind tube.
20. Add 150µl Diffusion Buffer to gel in 1.5 ml tube and shake at RT for 45 min.
21. Transfer to filter columns using wide-bore tips and centrifuge at max speed for 2 min.
22. Purify DNA (~140µl) with Zymo DNA Clean and Concentrator columns.
23. Elute in 15µl Elution Buffer into 1.5 ml LoBind tubes.
24. Quantitate with QuBit and store at -20^{o}C prior to sequencing (yield ~ 0.25 ng/ µl).

9.3 Optimisation of protocols

9.3.1 Optimising Accessibility of Transposase Assay (ATAC)

When this project was initially established, the proposal was that ATAC could be undertaken on nuclei isolated from sorted Mo and then frozen down. This was a protocol that had been optimised by Sascha Duttke at the Glass lab in University of California San Diego (UCSD) but was optimised for much greater cell numbers than we could achieve (10-fold). The following reagents and buffers were used:

1. Swelling Buffer
    - 500ml Ultrapure water
    - 5ml of 1M Tris/HCl pH 7.5 (10mM final)
    - 1ml of 1M $MgCl_2$ (final 2mM)
    - 1.5ml of 1M $CaCl_2$ (final 3mM)
    - 10% Glycerol
2. Freezing buffer (50ml)
    - 27.5ml Ultrapure water
    - 20ml of glycerol (final 40 %)
    - 250µl 1M $MgCl_2$ (final 5mM)
    - 10µl of 0.5M EDTA (final 0.1mM)
    - 1.25ml Tris/HCl pH 7.5
    - 1.25ml Tris/HCl pH 8
3. Lysis buffer
    - Swelling buffer + 0.2% IPEGAL CA630 detergent
4. Wash buffer
    - Lysis buffer + 0.1% IPEGAL CA630 detergent

FACS isolated Mo were centrifuge at 700g 4°C for 5 mins the supernatant was removed, and ice-cold Swelling Buffer was added to the cells for 5 mins on ice. Cells were then centrifuged at 400g at 4°C for 10 mins. Supernatant was then removed, and cells were re-suspended in the swelling buffer. Lysis buffer (1:1 with swelling Buffer) was then added and finally the wash

buffer was added, and cells left on ice for 5 mins. Cells were then centrifuged at 600g 4°C for 7 mins. Supernatant was removed and cells were then re-suspended in 500µl of freezing buffer and then centrifuged at 900g 4°C for 6 mins. Supernatant was then removed, and nuclei were re-suspended in 20µl freezing buffer and snap-frozen in liquid nitrogen for shipping.

There was some trial and error with optimising the volumes to suit the cell numbers that were being used. Additionally, on checking samples under the microscope, nuclei were not intact. The purpose of the swelling buffer is to swell the cellular membrane, the detergent then inserts and the cellular membrane bursts isolating the nuclei which are accessible but intact. Therefore, we used four human control samples to test different conditions: Lysis buffer with 0.1% or 0.2% IPEGAL detergent and wash buffer with 0.05% or 0.1% IPEGAL detergent. These samples were sent to be processed at UCSD. The quality of the samples was inadequate and there was a concern that the ATAC reaction needed to be undertaken on freshly isolated cells.

Subsequently, time was spent isolating Mo and testing differing lysis buffers to obtain good quality nuclei (Figure 56). These experiments were undertaken at UCSD while RNAseq, ChIPseq and relevant bioinformatics techniques were also being acquired. From these experiments it was agreed that 0.06% IPEGAL 630 was to be used for subsequent samples.

The protocol was also refined to reduce centrifugation steps and cell loss. A total of $150x10^3$ Mo were isolated and centrifuged at 300g at 4˚C for 10 mins. All the supernatant was removed, and cells were re-suspended in 500µl swelling buffer and left on ice for 5 mins. A total of 500µl of 0.12% IPEGAL 630 was added dropwise while vortexing the sample to obtain a final concentration of 0.06% IPEGAL 630. The sample was then centrifuged at 600g at 4˚C for 5 mins. Samples were then immediately processed with the tagmentation enzyme as detailed in the methods. Four samples were processed using this concentration, were amplified and run onto gels to check the process. From this, it was decided to proceed with this protocol.

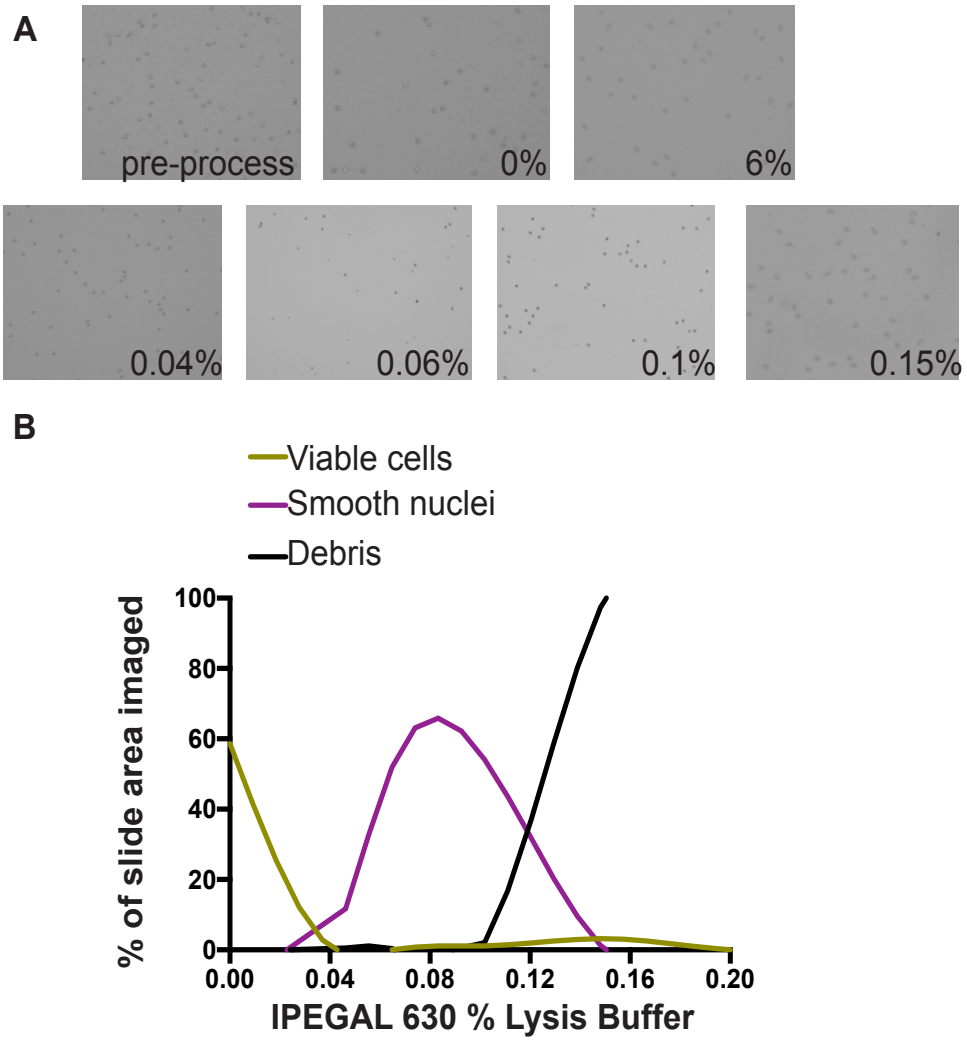

Figure 56 Optimisation of IPEGAL 630 detergent concentrations *(A) Microscope images of samples to demonstrate intact cells, smooth nuclei and debris obtained at increasing concentrations of IPEGAL 630. An unprocessed, 0% processed and 6% IPEGAL 630 samples were used as controls. (B) Plot of the percentage of viable cells, smooth nuclei and debris obtained at differing concentrations of IPEGAL 630 detergent.*

In this first cohort of patients, a total of 16 samples (8 cancer, 8 healthy controls) of whole Mo were collected alongside RNAseq and ChIPseq samples. Unfortunately, ATAC samples were of poor quality and it was felt that further optimisation was required. At this stage, work was undertaken with Nathaneal Spann at UCSD whom is a expert in ATACseq methods is. A refined ATAC protocol had been published (Corces et al. 2017) and so the decision was made to try a variation of this with the following buffer conditions:

1. 10mM Tris-HCl (pH 7.5), 10mM NaCl, 10mM MgCl2, 0.1% Tween20
2. Solution 1 with 0.01% digitonin
3. 10mM Tris-HCl (pH 7.5), 10mM NaCl, 10mM MgCl2, 0.1% Tween20 0.1% Igepal CA-630 with 0.025% digitonin

During the acquisition of the initial 16 samples, it was also realised that the cell input that could be obtained was limited and so it was also desirable to assess what the lowest possible input. Samples were obtained by using red cell lysis, FACS and then the immediate tagmentation reaction was undertaken as detailed in the methods. These samples were then sent to UCSD to be amplified and sequenced. The samples were then quality checked and browser tracks inspected for peaks and the level of noise. [Tracks can be inspected directly at the UCSC browser with the following URL: http://homer.ucsd.edu/hubs//LysisBufferOptomisation_ATAC/hub.txt]

From this trial, it was decided that the minimum input was $50x10^3$ cells and that samples were optimal (high ratio of tags within peaks indicating both peaks and minimal noise) was 1achieved with the 10mM Tris-HCl (pH 7.5), 10mM NaCl, 10mM MgCl2, 0.1% Tween20 Solution 1 with 0.01% digitonin (Figure 57). These conditions were therefore chosen to proceed with in the final cohort of patients.

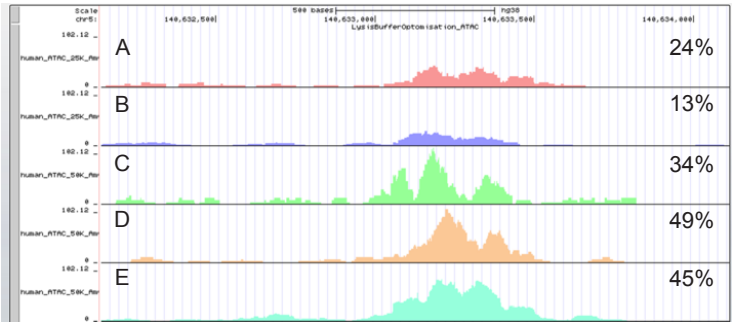

Figure 57 UCSC Browser tracks for optimising lysis buffer for ATAC of human Mo *(A) 25x10^{3}cell input, Lysis buffer 2. (B) 25x10^{3}cell input, Lysis buffer 3 (C-E) 50x10^{3}cell input, Lysis buffer 1,2, and 3. For each track the percentage of tags that occur within peaks are given. Lysis buffers 1. 10mM Tris-HCl (pH 7.5), 10mM NaCl, 10mM MgCl2, 0.1% Tween20 2. As for 1 but with 0.01% Digitonin 3. 10mM Tris-HCl (pH 7.5), 10mM NaCl, 10mM MgCl2, 0.1% Tween20 0.1% Igepal CA-630 with 0.025% digitonin.*

Chapter 10 Supplementary files

10.1.1 S1_MOUSE_ C57BL/6_BLOOD_DEGs.xls

10.1.2 S2_MOUSE_ C57BL/6_BM.xls

10.1.3 S3_MOUSE(FVB)_BLOOD_DEGs.xls

10.1.4 S4_HUMAN(ALL_SAMPLES)_BLOOD_DEGs.xls

10.1.5 S5_HUMAN(CA_1_3_5_6)_DEGs_Motif.xls